AN INVESTIGATION INTO THE MOLECULAR MECHANISMS INDUCED BY DERIVATIVES OF NATURAL PRODUCTS IN OESOPHAGEAL CANCER

Nelusha Shunmoogam-Gounden

Thesis presented for the degree of

DOCTOR OF PHILOSOPHY

in the Department of

Clinical Laboratory Sciences

Division of

Medical Biochemistry

UNIVERSITY OF CAPE TOWN

Supervised by

Associate Professor Denver Hendricks

April 2014

ACKNOWLEDGEMENTS

I wish to express my great appreciation to many people, too numerous to name individually, and a very special thank you to the following people:

Firstly, Associate Professor Denver T. Hendricks, for supervising this project and sharing his brilliant scientific insights and expertise. His love for teaching and mentorship has been an enormous inspiration. After the years of toil it takes to bring a PhD project to completion, I extend my sincerest gratitude and appreciation to him for the encouragement and motivation along the way, and especially for nurturing my ambitions as scientific researcher.

Professor Kelly Chibale, Dr Renate Hans and Dr Aman Mahajan, for providing the compounds that formed the basis of this research project. Many thanks for the excellent work in the Department of Chemistry (University of Cape Town) and for the valuable discussions.

Associate Professor Virna Leaner, for her guidance and untiring support throughout the duration of this project. Her enthusiasm for science will always be admired.

Dr Amanda Skepu, Dr Abram Madiehe and Professor Jasper Rees, for being instrumental in the development of my career in science. Great teachers are never forgotten!

Mr Ronald Dreyer, for assistance with flow cytometry; Mrs Susan Cooper, for assistance with fluorescent and confocal microscopy; Mr Mohamed Jaffer, for assistance with transmission electron microscopy and Professor Ed Sturrock, for use of the fluorescent spectrophotometer.

National Research Foundation/Deutscher Akademischer Austausch Dienst (NRF/DAAD) and scholarships from the University of Cape Town, for financial assistance.

Mrs Hajira Guzgay and Mr Robert Samuels, for keeping the laboratory running smoothly and for providing a family environment at work. Many thanks for all the hard work and caring.

Past and present members of the Cancer Research Group, especially: Dr Nina Holderness-Parker, Miss Hapiloe Maranyane, Miss Erin Strydom, Miss Cherise Dunn and Miss Alicia Chi, an enormous thank you for the constructive suggestions during laboratory meetings, strong friendships and for making the laboratory a warm and happy place to work in.

Extra special thanks to Dr Widaad Zemanay, Dr Pauline van der Watt, Dr Kate Hadley and Dr Lotte Angus for their expert advice, assistance with experimental protocols and superb mentorship. Their dedication, hard work and zest for science have been a great inspiration.

Mrs Cleo Groenewald and Mrs Asheena Pillay, unconditional friendships are rare – a heartfelt thank you.

Dr Luke Esau, for his unwavering support, constant encouragement and genuine friendship. Many thanks for the interest in my work, valuable discussions and contribution of ideas. I am very grateful to have had a "lab-partner" that is second to none.

Mr Mahendra Shunmoogam and Mr Kiran Shunmoogam, for being exceptional brothers and an endless source of motivation.

Mr Devanathan Shunmoogam and Mrs Gonapathi Shunmoogam, my parents, for their love, never-ending support and for always believing in me, and also for encouraging the pursuit of intellectual enlightenment.

Finally, Dr Ronald Gounden, for everything. His role in the completion of this project has been a significant one, and I am extremely grateful for his unfaltering love, support and understanding.

This thesis is dedicated to my grandparents and my parents –
the hardships you endured and the sacrifices you made allowed me to pursue my dreams, and
for this I am eternally grateful

TABLE OF CONTENTS

ABBREVIATIONS

A1	Bcl-2-related gene A1
AD	Adenocarcinoma
ADP	Adenosine diphosphate
AIF	Apoptosis inducing factor
AKT	AK (refers to a mouse strain) Thymoma
AMBRA1	Activating molecule in Beclin-1-regulated autophagy
AMP	Adenosine monophosphate
AMPK	AMP -activated protein
Apaf-1	Apoptotic protease activating factor 1
ART	Artesunate
ATF6	Activating transcription factor 6
ATG	Autophagy-related-genes
ATM	Ataxia telangiectasia
ATP	Adenosine triphosphate
Bad	Bcl-2 agonist of cell death
Bak	Bcl-2 agonist killer 1
Bax	Bcl-2 associated x protein
BC	Before Christ
BCA	Bicinchoninic acid
Bcl-2	B-cell lymphoma-2
Bcl-w	Bcl-2 like 2 protein
Bcl-xL	Bcl-2-related gene, long isoform
Bid	BH3 interacting domain death agonist
Bif 1	Bax-interacting factor 1
Bik	Bcl-2-interacting killer
Bim	Bcl-2 interacting mediator of cell death
BH	Bcl-2 homology
Bok	Bcl-2 ovarian killer
Bp	Base pairs
BSA	Bovine serum albumin
CAD	Caspase-activated DNAse

CaMKKβ	Calcium-activated calmodulin-dependent kinase kinase-beta
CARD	Caspase activation and recruitment domain
Caspases	Cysteinyl-aspartate-cleaving proteases
cDNA	Complementary DNA
c-FLIP	FLICE inhibitory protein
CHOP	C/EBP homologous protein
CI	Confidence intervals
CMA	Chaperone-mediated autophagy
Co.	Corporation
COX-2	Cyclooxygenase-2
C_T	Cycle threshold
CYLD	Cylindromatosis 1
DαG	Donkey anti-goat
DAPI	4',6-diamidino-2-phenylindole dihydrochloride
DAPk	Death-associated protein kinase
DCFDA	2',7'-dichloro-fluorescein diacetate
DED	Death effector domain
DEPC	Diethylpyrocarbonate
DHA	Dihydroartemisinin
DISC	Death-inducing signaling complex
DMEM	Dulbecco's Modified Eagle Medium
DMSO	Dimethyl sulphoxide
DNA	Deoxyribonucleic acid
dNTPs	Deoxynucleoside triphosphate
dTMP	Deoxythymidine monophosphate
dTTP	Deoxythymidine triphosphate
DR3	Death receptor 3
DR4	Death receptor 4
DR5	Death receptor 5
EDTA	Ethylene diamine tetra acetic acid
EGFR	Epidermal growth factor receptor
eIF2α	eukaryotic initiation factor 2 alpha
ER	Endoplasmic reticulum

ERK	Extracellular-signal-related kinase
FACS	Fluorescence activated cell sorting
FADD	FAS-associated death domain
FAS	Fatty acid synthetase
FASL	FAS ligand
FBS	Foetal bovine serum
FdUMP	Fluorodeoxyuridine monophosphate
FIP200	The focal adhesion kinase family-interacting protein of 200kDa
FLICE	FADD-like ICE
GAPDH	Glyceraldehyde-3-phosphate dehydrogenase
GαM	Goat anti-mouse
GαR	Goat anti-rabbit
GTP	guanosine-5'-triphosphate
GusB	*β-glucoronidase*
γ-H2AX	Phosphorylated histone protein H2A variant
h	Hour
HDGC	Hereditary Diffuse Gastric Cancer
HIV/AIDS	Human immunodeficiency virus/acquired immunodeficiency syndrome
HPV	Human papillomavirus
Hrk	Harakiri
HtrA2/Omi	High temperature requirement/Omi stress regulated endoprotease
hVps34	Human Vacuolar protein sorting 34
IAP	Inhibitor of apoptosis proteins
IARC	International Agency for Research on Cancer
IC_{50}	50% inhibitory concentration
ICAD	Inhibitor of caspase-activated DNAse
ICE	Interleukin 1β converting enzyme
IKK	Inhibitor of NFκB kinase
IL-2	Interleukin-2
ION/TPA	Ionomycin/12-*o*-tetradecanoylphorbol-13-acetate
IRE1	Inositol requiring enzyme 1
JNK	c-Jun-N-terminal kinase
kDa	kiloDaltons

KR buffer	Krebs-Ringer buffer
LAA	L-Ascorbic acid
LAMP	Lysosome-associated membrane protein
LC3	Microtubule-associated protein 1 light chain 3
LDH	Lactate dehydrogenase
LM-PCD	Lysosomal mediated- programmed cell death
M	Molar
3-MA	3-Methyladenine
MAPK	Mitogen activated protein kinase
Mcl	Myeloid cell leukemia 1
MEK	Mitogen-activated protein kinase kinase
min	Minute
mg	Milligram
ml	Millilitre
mLST8	mammalian lethal with sec-thirteen protein 8
MnSOD	Manganese superoxide dismutatase
MOMP	Mitochondrial outer membrane permeabilisation
MOPS	3-[N-morpholino] propanesulphuric acid
mRNA	Messenger ribonucleic acid
mTOR	Mammalian target of Rapamycin
mTORC1	mTOR complex 1
mTORC2	mTOR complex 2
MTT	3-[4,5-dimethylthiazol-2-yl]-2,5-diphenyltetrazolium bromide
MWM	Molecular weight marker
NA	Not Active
NAC	*N*-acetyl-L-cysteine
NCCD	Nomenclature Committee on Cell Death
NCI	National Cancer Institute
Nec-1	Necrostatin-1
NEMO	NFκB essential modulator
NFκB	Nuclear factor kappa-light-chain-enhancer of activated B cells
nm	Nanometer
Noxa	Phorbol-12-myristate-13-acetate-induced protein 1

NR	Neutral red
NRU	Neutral red uptake
OC	Oesophageal cancer
OD	Optical density
O/N	Overnight
OSCC	Oesophageal squamous cell carcinoma
PARP	Poly (ADP-ribose) polymerase
PAS	Phagophore assembly site
PBS	Phosphate buffered saline
PCD	Programmed cell death
PE	Phosphatidylethanolamine
PERK	Protein kinase R-like ER kinase
PI	Propidium iodide
PI3K	Phosphatidylinositol 3-kinase
PIP	Phosphatidylinositol-phosphate
PIP_2	Phosphatidylinositol 4,5-bisphosphate
PIP_3	Phosphatidylinositol-3,4,5-triphosphate
pJNK	Phosphorylated JNK
PRAS40	Proline rich AKT substrate of 40kDa
PTEN	Phosphatase and tensin homolog deleted on chromosome 10
PUMA	P53 up-regulated modulator of apoptosis
RAPTOR	Regulatory associated protein of mTOR
Rheb	Ras Homolog Enriched in Brain
RIP1	Receptor-interacting protein 1
RIP3	Receptor-interacting protein 3
RIPA	Radioimmunoprecipitation assay buffer
RNA	Ribonucleic acid
ROS	Reactive oxygen species
RPM	Revolutions per minute
RT-PCR	Reverse transcription polymerase chain reaction
Rubicon	RUN domain and cysteine-rich domain containing beclin-1-interacting protein
s	Second
SD	Standard deviation

SDS-PAGE	Sodium dodecyl sulphate- polyacrylamide gel electrophoresis
SEM	Standard error of the mean
siRNA	Small interfering RNA
Smac/ DIABLO	Second mitochondria-derived activator of caspases/ Direct IAP-binding protein with low pI
SQSTM1	p62/sequestosome 1
SP	SP600125
TAK1	Transforming growth factor-β-activating kinase 1
TB	Tuberculosis
tBid	Truncated Bid
TBS-T	Tris buffered saline with 0.1% Tween-20
TCM	Traditional Chinese Medicine
TEMED	N,N,N-Tetramethyl-ethylene diamine
TEMPOL	4-hydroxy-2,2,6,6- tetra-ethylpiperidine 1-oxyl
TRADD	TNFR type-1-associated DEATH domain protein
TRAF	TNF receptor associated factors
Trolox	6-hydroxy-2,5,7,8-tetramethylchroman-2-carboxylic acid
TNF	Tumour necrosis factor
TNF-α	Tumour necrosis factor-alpha
TNFR	Tumour necrosis factor receptor
TOR	Target of Rapamycin
TPA	12-*o*-tetradecanoylphorbol-13-acetate
TRAIL	TNF-related apoptosis-inducing ligand
TRAIL-R1	TNF-related apoptosis inducing ligand-Receptor 1
TRAIL-R2	TNF-related apoptosis inducing ligand-Receptor 2
TSC	Tumour sclerosis complex
TUNEL	Terminal deoxynucleotidyl transferase-mediated 2'-deoxyuridine 5'-triphosphate nick end-labelling
U	Unit
Ubl	Ubiquitin-like
UCT	University of Cape Town
ULK1 and -2	Unc-51-like kinase 1 and -2
UPR	Unfolded Protein Response
USA	United States of America

USD	United States Dollars
UVRAG	Ultraviolet irradiation resistant-associated gene
V	Volts
VEGF	Vascular endothelial growth factor
Vps	Vacuolar protein sorting
WHO	World Health Organisation
XIAP	X-linked mammalian inhibitor of apoptosis protein
µl	Microlitre
µg	Microgram
µM	Micromolar

ABSTRACT

Current chemotherapies for oesophageal cancer display poor efficacy and tolerability, highlighting an unmet need for novel chemotherapeutic agents. Artemisinin derivatives, currently used to treat malaria, were recently shown to possess potent anticancer activity. This study investigated the potential of two first generation artemisinin derivatives (artesunate and dihydroartemisinin), together with novel artemisinin hybrid compounds, as cancer chemotherapeutic agents and explored the mechanism of action in oesophageal cancer.

Artesunate and dihydroartemisinin including seventeen other artemisinin derivatives were screened against oesophageal cancer cells using the 3-[4,5-dimethylthiazol-2-yl]-2,5-diphenyltetrazolium bromide (MTT) assay and GraphPad Prism Software to calculate IC_{50} (50% inhibitory concentration) values. Novel halogenated artemisinin-isatin hybrid compounds displayed the best activity against oesophageal cancer cells, and were more potent than artesunate and dihydroartemisinin in a small panel of oesophageal, breast and cervical cancer cell lines tested. The novel derivatives induced a G0/G1 cell cycle arrest whilst the parental compounds induced a G2/M block of the cell cycle, using flow cytometry. This suggested a different mechanism of action for the novel compounds. Dihydroartemisinin and the most active novel hybrid, EXP57EA, were investigated to understand their molecular mechanisms of action in oesophageal cancer.

The results indicated that dihydroartemisinin induced apoptosis (based on poly (ADP-ribose) polymerase cleavage analysis and caspase-3/7 activation) while EXP57EA induced autophagy (based on LC3-II and Beclin 1 expression and transmission electron microscopy analysis). Both compounds significantly increased reactive oxygen species (ROS) production in oesophageal cancer cells, shown using a fluorescent probe (2',7'-dichloro-fluorescein diacetate) to measure intracellular ROS production. However, different types of ROS were implicated in the activation of downstream signalling pathways. Dihydroartemisinin-induced ROS resulted in deoxyribonucleic acid (DNA) damage, G2/M cell cycle arrest and apoptosis, which could all be blocked with the ROS scavenger, *N*-acetyl-L-cysteine. However, EXP57EA induced the production of superoxide, based on the observation that the superoxide-specific ROS scavenger, 4-hydroxy-2,2,6,6- tetra-ethylpiperidine 1-oxyl (TEMPOL), blocked ROS production, autophagy and cell death.

Taken together, the results of this study indicate that EXP57EA may have potential as an effective cancer chemotherapeutic agent that is more active than, and employs a mechanism of action different to, the parental compound, dihydroartemisinin, thus warranting further investigation.

CHAPTER 1:

LITERATURE REVIEW

1.1 Oesophageal Cancer

1.1.1 Introduction

South Africa is heavily burdened with a wide range of communicable diseases particularly HIV/AIDS (Human immunodeficiency virus/acquired immunodeficiency syndrome) and TB (Tuberculosis), extracting a heavy mortality toll on the country. According to a recent report by the World Health Organisation (WHO), HIV/AIDS and TB prevalence in South Africa is 11 087 per 100 000 and 768 per 100 000, respectively (WHO, 2013). Understandably, major efforts are dedicated to research for treatment and prevention of these communicable diseases. With this attention focussed on the devastating effects of HIV/AIDS and TB in South Africa, it has recently become apparent that non-communicable diseases, such as cancer, also present a significant burden on the health complex of the country. In addition, once the delivery of highly effective antiretroviral treatment becomes commonplace in the public health sector, it is predicted that deaths from HIV/AIDS should decrease resulting in a rise in life expectancy of South Africans, together with a rise in cancer (Mayosi et al., 2009; McCormack and Schüz, 2012).

The IARC (International Agency for Research on Cancer) reported 542 000 deaths from cancer and 715 000 new cancer cases in Africa for 2008, and estimations dictate that these alarming figures will double by 2030 (Ferlay et al., 2010; McCormack and Schüz, 2012). This represents a significant health challenge considering that Africa is a high risk area for a variety of cancers, including oesophageal cancer (OC) in South Africa. OC is characterised by malignant tumours that develop in the epithelium of the oesophagus, and this type of cancer poses a formidable threat as it is usually asymptomatic and therefore diagnosed at a very late stage. The prognosis for patients with OC is very poor, and South Africa currently ranks as one on the top five countries with the highest age-standardised death rate (18.2 per 100 000) due to OC (Chai and Jamal, 2012). Therefore there is a significant demand to unravel the molecular circuitry maintaining the biologic properties of OC cells and to thoroughly investigate better and highly effective treatment options in order to combat this disease.

1.1.2 Description of OC

The aetiology of OC differs by cell type, and can be categorised into two main forms: adenocarcinoma (AD) and oesophageal squamous cell carcinoma (OSCC). Despite both types displaying characteristic male predominance and being included jointly in therapeutic and prognostic clinical studies (Pennathur et al., 2008), AD and OSCC are by no means similar. They have clear differences including causes, epidemiology and originating cells (Bandla et al., 2012). Of the two types of epithelial tumours, adenocarcinoma (AD) arises from columnar epithelial cells and occurs mostly within the distal third of the oesophagus (Figure 1.1). Factors influencing this disease include chronic reflux, obesity and Barrett's oesophagus (Stein et al., 2005). There has been a remarkable increase in AD in first world

countries over the past fifty years, with the greatest upsurge observed in the United States of America (Demeester, 2009; Simard et al., 2012). In contrast, oesophageal squamous cell carcinoma (OSCC), which develops from squamous epithelium in the proximal oesophagus, predominates in developing countries and is of particular relevance to South Africa where an unusually high occurrence is observed in certain areas. Hence, this study is directed toward squamous cell carcinoma and is explored in further detail below.

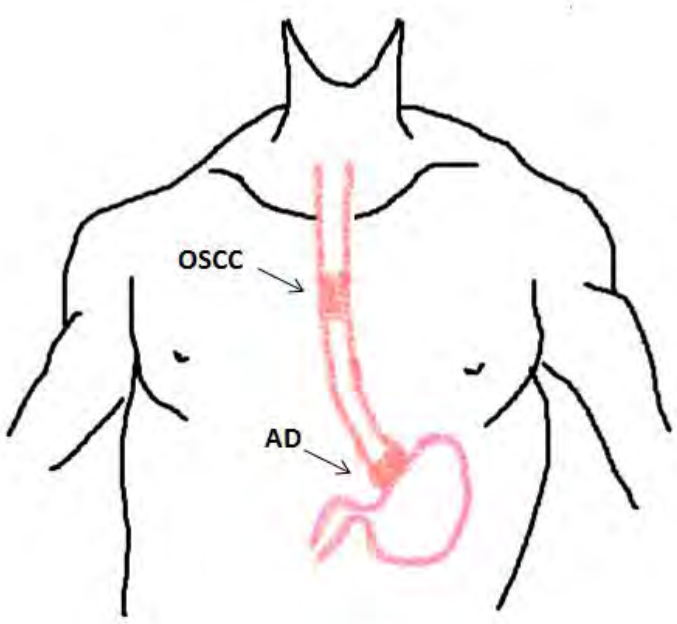

Figure 1.1: Diagram showing the location of the two main types of oesophageal cancer. Oesophageal squamous cell carcinoma near the proximal third of the oesophagus; and adenocarcinoma near the distal third of the oesophagus.

1.1.3 Epidemiology of OSCC

OC has displayed one of the most remarkable epidemiological shifts that has been documented, where AD was a disease that was not widely known in the 1950's and has become one of the greatest rising cancers in the Western world (Demeester, 2009). Yet, despite this profound change, OSCC still accounts for the majority of oesophageal cancer

diagnoses worldwide. This is mostly due to the high prevalence of this disease in Asian and African countries (Mawhinney and Glasgow, 2012). As illustrated in Figure 1.2, the incidence of OSCC varies widely geographically; where Southern and Eastern Africa as well as Eastern Asia have the highest incidence rates in the world, and Western and Middle Africa have the lowest rates in the world (Chai and Jamal, 2012). The disease is frequently two to four times more common among males than females, and in South Africa OSCC affects mostly the black population, especially in the high risk former Transkei region of the Eastern Cape Province (Hendricks and Parker, 2002; Jemal et al., 2011; Pacella-Norman et al., 2002; Somdyala et al., 2003).

A variety of risk factors have been implicated in the aetiology of OSCC. Smoking and alcohol consumption are important contributors to the disease in most parts of the world, but in developing countries nutritional deficiencies, drinking beverages at high temperatures, chewing tobacco and betel nut, consuming food contaminated with fungal mycotoxins and diets rich in nitrosamines have also been identified as important risk factors for the disease (Griffin and Wahed, 2011; Jemal et al., 2011; Sewram et al., 2003; Stoner and Gupta, 2001). In addition, a number of studies have implicated Human papillomavirus (HPV) in the pathogenesis of OSCC (Eslick, 2010; Löfdahl et al., 2012; Matsha et al., 2002, 2007; Togawa et al., 1994). Furthermore, agents that irritate the oesophagus such as lye, high-starch foods and radiation have been associated with the development of OSCC (Layke and Lopez, 2006). Other risk factors include disorders characterised by chronic inflammation and stasis, such as achalasia, previous head and neck cancer, Plummer-Vinson syndrome (oesophageal webs associated with iron deficiency anaemia), Tylosis (an autosomal-dominant genetic disorder characterised by hyperkeratosis of the palms and soles) and HDGC (Hereditary Diffuse Gastric Cancer) (Elton, 2005; Lao-Sirieix et al., 2010; Layke and Lopez, 2006). Interestingly,

inflammation has recently been described as one of the newly recognised hallmarks of cancer as it is thought to contribute to the genesis of cancer by supplying bioactive molecules, such as growth factors, survival factors and proangiogenic factors, to the tumour microenvironment, and this adds to the complexity of the disease (Hanahan and Weinberg, 2011).

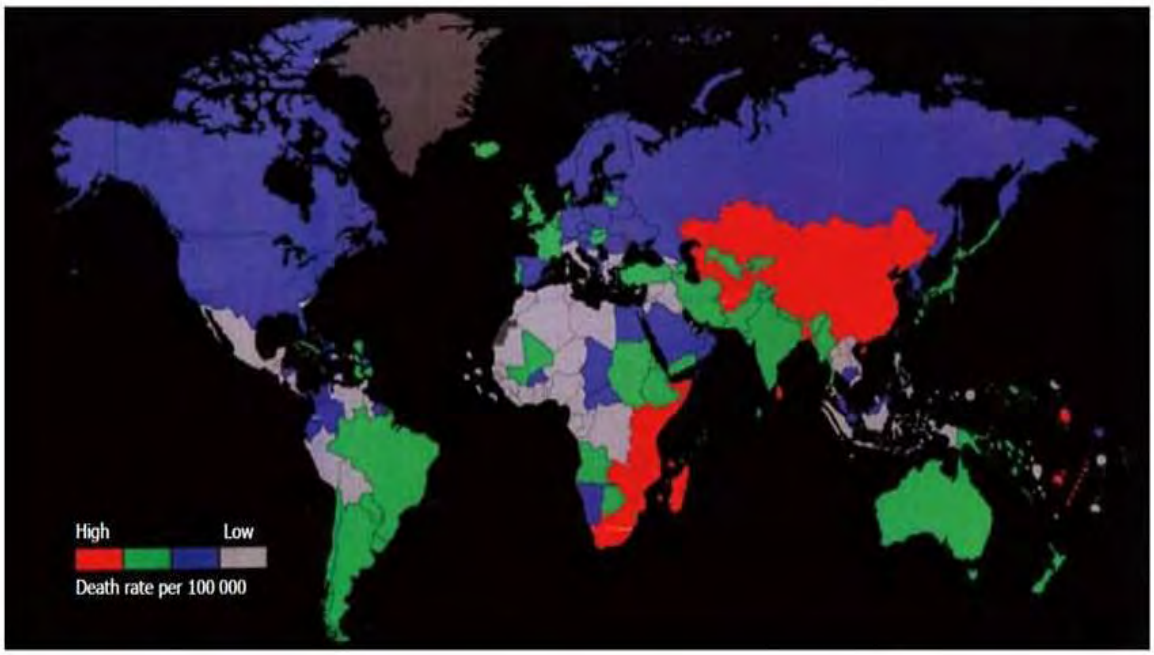

Figure 1.2: Global distribution of oesophageal squamous cell carcinoma. Red indicates the regions with the highest incidence rates in the world, including Southern and Eastern Africa as well as Eastern Asia. The regions coloured in grey, such as Western and Middle Africa, indicate the lowest incidence rates in the world (Image reproduced from Chai and Jamal, 2012).

1.1.4 Treatment

The multiple modes of oesophageal cancer treatment involves surgery, chemotherapy and radiotherapy (Kranzfelder et al., 2010). Surgical removal of the oesophagus is the standard treatment for patients with excisable OC (if detected at an early stage), but most patients present with an advanced stage of disease. Therefore surgery alone as a treatment option is

limited because metastasis would have already occurred at the first diagnosis (Ilson, 2008; Lv, 2009). As a result, radiotherapy and chemotherapy are frequently used in combination, either as neoadjuvant (preoperative) therapy or adjuvant (postoperative) therapy, to try to improve patient survival outcomes. However, these approaches have had little effect on improving prognosis and survival of OC patients, and the 5-year overall survival rate remains between 5 and 15% (Scarpa et al., 2011).

A number of cytotoxic drugs and drug combinations have been tested in various clinical trials for efficacy against OC and are currently being used to treat OC. The drugs most commonly used in the chemotherapeutic regimens to treat OC patients include cisplatin and 5-fluorouracil. Cisplatin is an alkylating-like platinum compound whereas 5-fluorouracil is a pyrimidine analogue of the antimetabolite class of anticancer drugs. Cisplatin forms adducts (in the *cis* configuration, hence the name cisplatin) with DNA (deoxyribonucleic acid) resulting in the inhibition of DNA synthesis and repair. This is a result of the disruption of the three-dimensional structure of DNA caused by the platinum adducts. Cisplatin ultimately induces apoptosis via the intrinsic apoptotic pathway (to be discussed in more detail later) (Desoize and Madoulet, 2002). Ototoxicity (damage to ears associated with hearing loss) and anosmia (inability to smell) are some of the side effects associated with cisplatin treatment. However, the major side effect patients experience is nephrotoxicity. Other side effects include sensory peripheral neuropathy, optic neuritis, cortical blindness and seizures (SAMF, 2010).

The antimetabolite 5-fluorouracil (a uracil analogue with a fluorine atom at the 5' carbon of the pyrimidine ring) inhibits thymidilate synthase which leads to the inhibition of DNA

synthesis and repair. When 5-fluorouracil is metabolized in the cell it forms fluorodeoxyuridine monophosphate (FdUMP) which tightly binds thymidilate synthase and prevents the formation of thymidilate, an important precursor for deoxythymidine monophosphate (dTMP). Therefore dTMP and dTTP (deoxythymidine triphosphate) become depleted and DNA synthesis and repair is inhibited (Kunz et al., 2009). Furthermore, 5-fluorouracil can be incorporated into RNA as a false nucleotide and in so doing disrupt many cellular processes (Longley et al., 2003). Patients treated with 5-fluorouracil experience side effects such as cardiotoxicity, diarrhoea, stomatitis (infection around mouth), hand-foot syndrome and skin rashes (SAMF, 2010). Mucositis and myelosuppression have also been reported in cisplatin/5-fluorouracil combination treatments (Ilson, 2008). These significant adverse effects associated with the cisplatin/5-fluorouracil chemotherapy limit the tolerability in patients suffering from OC.

Recent interest in cancer treatment has focussed on targeted agents. Several molecular pathways have been investigated to identify potential targets in oesophageal cancer and these include cyclin-dependent kinases, NFκB (nuclear factor kappa-light-chain-enhancer of activated B cells), matrix metalloproteinases, COX-2 (cyclooxygenase-2), c-MET (a proto-oncogene), mTOR (mammalian Target of Rapamycin), EGFR (epidermal growth factor receptor) and VEGF (vascular endothelial growth factor). The latter two currently appear to be the most promising targets (Boone et al., 2008; Campbell, 2010; Tew et al., 2005; Villaflor et al., 2012).

EGFR, a member of the human epidermal growth factor receptor family, plays an important role in cell differentiation, proliferation and survival. Overexpression of EGFR proteins may

occur in 30 - 90% of OSCC tissue and is associated with increased aggressiveness of the disease as well as poor prognosis (Lin and Papadopoulos, 2007). EGFR tyrosine kinase inhibitors (erlotinib, gefitinib and lapatinib) and anti-EGFR monoclonal antibodies (cetuximab, panitumumab and matuzumab) are the two most developed EGFR-targeting strategies (Lin and Papadopoulos, 2007; Syrigos et al., 2008; Villaflor et al., 2012).

The small molecule tyrosine kinase inhibitors targeting EGFR have limited monotherapy efficacy with low response rates thus triggering the investigation into the typical OC multimodal therapy. Combination of tyrosine kinase inhibitors with other drugs displayed limited further benefit with a response rate of 51.5%, 5.5 months progression free survival and only 11 months overall survival (Wainberg et al., 2011). As a result, this approach has mostly been abandoned (Boland and Burtness, 2013). Radiation and erlotinib combination treatment yielded a clinical complete response rate of 46% and phase III study of chemoradiation with or without erlotinib is ongoing (Boland and Burtness, 2013). Cetuximab, a monoclonal antibody targeting EGFR, used in monotherapy also displayed limited activity with response rates ranging from 3 - 6% but when used in combination with other drugs response rates of 51 - 62% were observed (Boland and Burtness, 2013). However, it was reported that the median progression free survival (5.7 months) and overall survival (10 months) were not significantly different to historical controls (Boland and Burtness, 2013). In addition, grade III/IV nonhaematologic toxicity occurred in 70% of patients (Boland and Burtness, 2013).

Metastasis of oesophageal cancer is associated with angiogenesis, which is one of the hallmarks of cancer (Hanahan and Weinberg, 2000, 2011). During this process a complex

interplay between several angiogenic growth factors, receptors and signalling molecules is deployed for the development of new blood vessels that allow cancer cells to thrive and opportunistically metastasize (Hanahan and Weinberg, 2000, 2011). The VEGF family of proteins are the main players in the process, and VEGF-A and VEGF-C were reported to be frequently overexpressed in OC (Syrigos et al., 2008). Therefore strategies targeting this family of proteins are highly attractive, and similar to the situation in EGFR targeted therapy, the anti-VEGF monoclonal antibodies (bevacizumab) and the VEGF (multi-target) tyrosine kinase inhibitors (vandetatanib, sorafenib and sunitinib) are the most developed (Syrigos et al., 2008). Despite various ongoing phase-II and phase-III clinical trials employing these targeted therapies with and without the conventional multimodal OC therapy, the reported results reflect poor response rates (2.6 - 46%) coupled with serious side-effects (oesophageal fistula formation and fatal gastrointestinal haemorrhage), especially in patients who present with multiple comorbidities (Bang et al., 2011; Boland and Burtness, 2013; Campbell, 2010; Schmitt et al., 2012; Villaflor et al., 2012).

As mentioned before, despite recent advances and the use of the above-mentioned therapies for oesophageal cancer, the 5-year mortality rate remains unacceptably high at 80 - 90% (Ilson, 2008). Therefore it is important to develop more effective chemotherapeutic agents with fewer side-effects for the treatment of this disease. One of the goals of developing effective chemotherapeutic agents is the production of agents capable of targeting and killing cancer cells without affecting normal cells. Research in developing novel agents capable of triggering cell death pathways in cancer cells may provide improved alternatives to current chemotherapeutic agents against OC.

1.2 Cell Death Pathways

1.2.1 Introduction

Programmed cell death (PCD) plays a significant role in normal development as well as in disease. Extensive research underpinned the in-depth characterisation of necrosis and apoptosis, originally the main two cell death mechanisms identified, which have fundamental differences in morphology and biochemistry. There are, however, other recently characterised cell death pathways that are coming to the fore that include autophagy, necroptosis, paraptosis, pyroptosis, pyronecrosis, lysosomal mediated-programmed cell death (LM-PCD), mitotic catastrophe and entosis (Kreuzaler and Watson, 2012; Kroemer et al., 2009).

Evasion of cell death is one of the hallmarks of cancer, as described by Hanahan and Weinberg, since cancer cells have developed mechanisms to avoid cell death (Hanahan and Weinberg, 2000, 2011). Apoptosis has been the main PCD pathway implicated since it is known that some of the mechanisms employed by cancer cells to avoid cell death include upregulating the expression of antiapoptotic members and downregulating the expression of proapoptotic members (Hanahan and Weinberg, 2011), and many chemotherapeutic agents have been directed at inducing this type of cell death (Lockshin and Zakeri, 2004). However, it is clear that more evidence is required to elucidate the role of other cell death pathways, such as autophagy, as promising killing mechanisms activated by cancer chemotherapeutic agents.

1.2.2 Apoptosis

1.2.2.1 Description and Function

Since its official description by Kerr et al. in 1972, apoptosis has received a great deal of attention from molecular and cell biologists the world over. The word 'apoptosis' is of Greek origin and is used to describe "falling off" of leaves from trees or petals from flowers and aptly portrays the type of cell death that is characterised by cells breaking away from or losing contact with surrounding cells (Kerr et al., 1972). Other morphological features of apoptosis include cell shrinkage, chromatin condensation (pyknosis) and nuclear fragmentation (karyorrhexis), blebbing of the plasma membrane and ultimately disintegration into apoptotic bodies (Hockenbery, 1995; Kaufmann and Hengartner, 2001; Saikumar et al., 1999).

Apoptosis is a tightly regulated, energy-dependent process that occurs during adult tissue homeostasis, development and disease (Hockenbery, 1995; Kerr et al., 1972). It performs a significant function that complements (but has an opposite role to) mitosis to maintain homeostasis. In adult humans, approximately ten billion cells are synthesised every day to account for those undergoing apoptosis (Elmore, 2007). A. Glucksman was one of the earliest researchers to implicate cell death in development and since then many studies have confirmed the importance of programmed cell death in development (Glucksman, 1951). Studies performed in different cell types and species indicated that RNA and protein synthesis were essential for this type of cell death to occur, and that inhibiting any of these two processes blocked apoptosis, and consequently some developmental processes like metamorphosis in model systems (Lockshin and Williams, 1964; Tata, 1966). These pioneering studies proved that cell death required the expression of endogenous genes and

that apoptosis had important physiological roles in development. Indeed, apoptosis must be tightly regulated as insufficient or excessive cell death may result in pathology such as developmental faults, neurodegenerative diseases (including Parkinson's disease, Alzheimer's disease and Huntington's disease), autoimmune diseases and cancer (Elmore, 2007; Hotchkiss et al., 2009; Nicholson, 2000).

The management of over-produced cells, a frequent occurrence in many tissues and organs, by programmed cell death is critical for maintaining optimal cell numbers (Jacobson et al., 1997). Examples include the excess of neurons and oligodendrocytes produced in the vertebrate nervous system and oocytes produced in human females which are removed by apoptosis (Fuchs and Steller, 2011; Jacobson et al., 1997). Apoptosis plays an important role in the elimination of cells in response to viral infection, cells containing damaged DNA that is not sufficiently repaired or that display cell-cycle irregularities (Fuchs and Steller, 2011). Apoptosis is critically important for the death of mutated cells and thus plays a vital role in the prevention of cancer. When mutated cells destined to die develop mechanisms to evade programmed cell death pathways a window to tumourigenesis is opened (Green and Evan, 2002; Hanahan and Weinberg, 2000, 2011).

1.2.2.2 The Apoptosis Pathway

Apoptosis is a highly complex cellular pathway (made up of various sub-pathways) that can be induced by either extracellular or intracellular signals. Groundbreaking discoveries in apoptosis research that contributed the elucidation of this pathway include the identification of the anti-apoptotic *bcl-2* gene by Vaux and colleagues (Vaux et al., 1988) followed by the

characterisation of the Bcl-2 family (consisting of pro-apoptotic and anti-apoptotic members) of proteins, as well as the identification of the key destructive enzymes called the caspases (cysteinyl-aspartate-cleaving proteases) (Lockshin and Zakeri, 2001; Yuan et al., 1993).

In humans, fourteen caspases have been identified and characterised (Duprez et al., 2009; Shi, 2002), and they exist as zymogens or procaspases within the cell that once activated, result in the cleavage of proteins at aspartic acid residues. The caspases are the main mediators of apoptosis and are grouped into the initiator caspases (caspase-2, -8, -9, -10 and -12) and executioner or effector caspases (caspase-3, -6 and -7) (Hengartner, 2000; Thornberry et al., 1997). The initiator procaspases are present as monomers in the cell and when an apoptotic signal is triggered, dimers are formed which are activated by oligomerisation with adaptor molecules (Boatright and Salvesen, 2003). The activated initiator caspases cleave the executioner procaspases (dimers) into activated executioner caspases (monomers), which are in turn responsible for the cleavage of a large variety of substrates ultimately responsible for the demise of the cell (Boatright and Salvesen, 2003; Elmore, 2007; Green, 2000).

The key pathways identified according to the type of initiator caspase activated are the intrinsic or mitochondrial apoptotic pathway (caspase-9), the extrinsic or death receptor apoptotic pathway (caspase-8), the ER stress pathway (caspase-12) and the perforin/granzyme B pathway (caspase-10) (Assunção Guimarães and Linden, 2004; Elmore, 2007; Hayashi et al., 2005; Thornberry et al., 1997).

1.2.2.2.1 Intrinsic pathway

The intrinsic apoptotic pathway is mainly activated by stimuli that could reflect exposure of cells to a noxious environment that could lead to irreparable cellular damage. These stimuli include increased intracellular reactive oxygen species (ROS), DNA damage, decrease in growth factors, ionising radiation, chemotherapeutic drugs and mitochondrial damage (Boatright and Salvesen, 2003; Hotchkiss et al., 2009). The death signal is accompanied by the selective permeabilisation of the mitochondria orchestrated by the Bcl-2 (B-cell lymphoma-2) family of pro- and anti-apoptotic members.

The family members are grouped according to structure and function into anti-apoptotic and pro-apoptotic members. The anti-apoptotic members (Table 1.1) contain four Bcl-2 homology (BH) domains (BH1-4). The pro-apoptotic members (Table 1.1) are further divided into effectors, with multiple BH domains (BH1-4), and BH3-only members with only one BH domain (BH3) (Chipuk et al., 2010). The effectors, Bax, Bak, and Bok (refer to Table 1.1 for full names), are the main positive regulators of apoptosis and are usually present on the mitochondrial outer membrane or in the cytoplasm (Green, 2000; Hengartner, 2000). The BH3-only family members are further characterised into "sensitisers and/or derepressors" (Bad, Noxa, Bik, Hrk, PUMA) and "direct activators" (Bid and Bim) (Table 1.1) (Chipuk et al., 2010). The former group is able to bind and inhibit anti-apoptotic Bcl-2 family members only whereas the latter group interacts with both the anti-apoptotic and pro-apoptotic (effectors), and can directly stimulate Bax and Bak homo-oligomerisation and activation thus promoting mitochondrial outer membrane permeabilisation (MOMP).

Table 1.1: The Bcl-2 family of anti-apoptotic and pro-apoptotic members, including their abbreviations and full names.

Anti-apoptotic		**Pro-apoptotic**	
Bcl-2	B-cell lymphoma-2	Bax	Bcl-2 associated x protein
A1	Bcl-2-related gene A1	Bak	Bcl-2 agonist killer 1
Bcl-w	Bcl-2 like 2 protein	Bok	Bcl-2 ovarian killer
Bcl-xL	Bcl-2-related gene, long isoform	Bad	Bcl-2 agonist of cell death
Mcl-1	Myeloid cell leukemia 1	Bid	BH3 interacting domain death agonist
		Bim	Bcl-2 interacting mediator of cell death
		Bik	Bcl-2-interacting killer
		Hrk	Harakiri
		Noxa	Phorbol-12-myristate-13-acetate-induced protein 1
		PUMA	P53 up-regulated modulator of apoptosis

MOMP induces the release of the mitochondrial protein cytochrome c, one of the key regulators of the intrinsic apoptotic pathway, into the cytoplasm where it binds Apaf-1 (Apoptotic protease activating factor 1), the cytoplasmic adaptor protein. Apaf-1 then forms a complex with cytochrome c, attracting procaspase-9 and ATP molecules, resulting in the formation of the apoptosome (Figure 1.3). The initiator caspase, procaspase-9, contains a N-terminal CARD (caspase activation and recruitment domain) domain that facilitates binding and association with Apaf-1 (Hengartner, 2000). Procaspase-9, a monomer, is activated by dimerisation and conformational changes once in contact with Apaf-1 in the apoptosome (Boatright and Salvesen, 2003; Zimmermann and Green, 2001). Caspase-9 is responsible for the cleavage and activation of procaspase-3 into mature caspase-3, which is the ultimate executioner of apoptosis by virtue of its role in cleaving a wide range of substrates critical for cellular function.

During homeostasis the anti-apoptotic Bcl-2 family members (such as Bcl-2 and Bcl-xL) prevent unwanted cell death by antagonising the pro-apoptotic effector proteins (Bax and Bad) and preventing the release of cytochrome c from the mitochondria. In the presence of a death signal, the BH-3 only pro-apoptotic proteins (such as Bim and PUMA) are responsible for binding and inhibiting the anti-apoptotic proteins resulting in the liberation of Bax and Bak, which are able to facilitate the release of cytochrome c upon activation and induction of MOMP (Figure 1.3).

Other proteins released from the mitochondria include Smac/DIABLO (Second mitochondria-derived activator of caspases/Direct IAP-binding protein with low pI), HtrA2/Omi (High temperature requirement/Omi stress regulated endoprotease) and AIF (Apoptosis inducing factor) (involved in early DNA fragmentation and chromatin condensation after translocation to the nucleus) (Elmore, 2007). Smac/DIABLO and HtrA2/Omi function by inhibiting the IAPs (Inhibitor of apoptosis proteins), such as XIAP (X-linked mammalian inhibitor of apoptosis protein), cIAP1, cIAP2 and survivin, which are deployed in the cell to prevent the activation of caspase-3 (Figure 1.3) (Green, 2000; Hengartner, 2000), thus constituting a complex system that controls apoptosis.

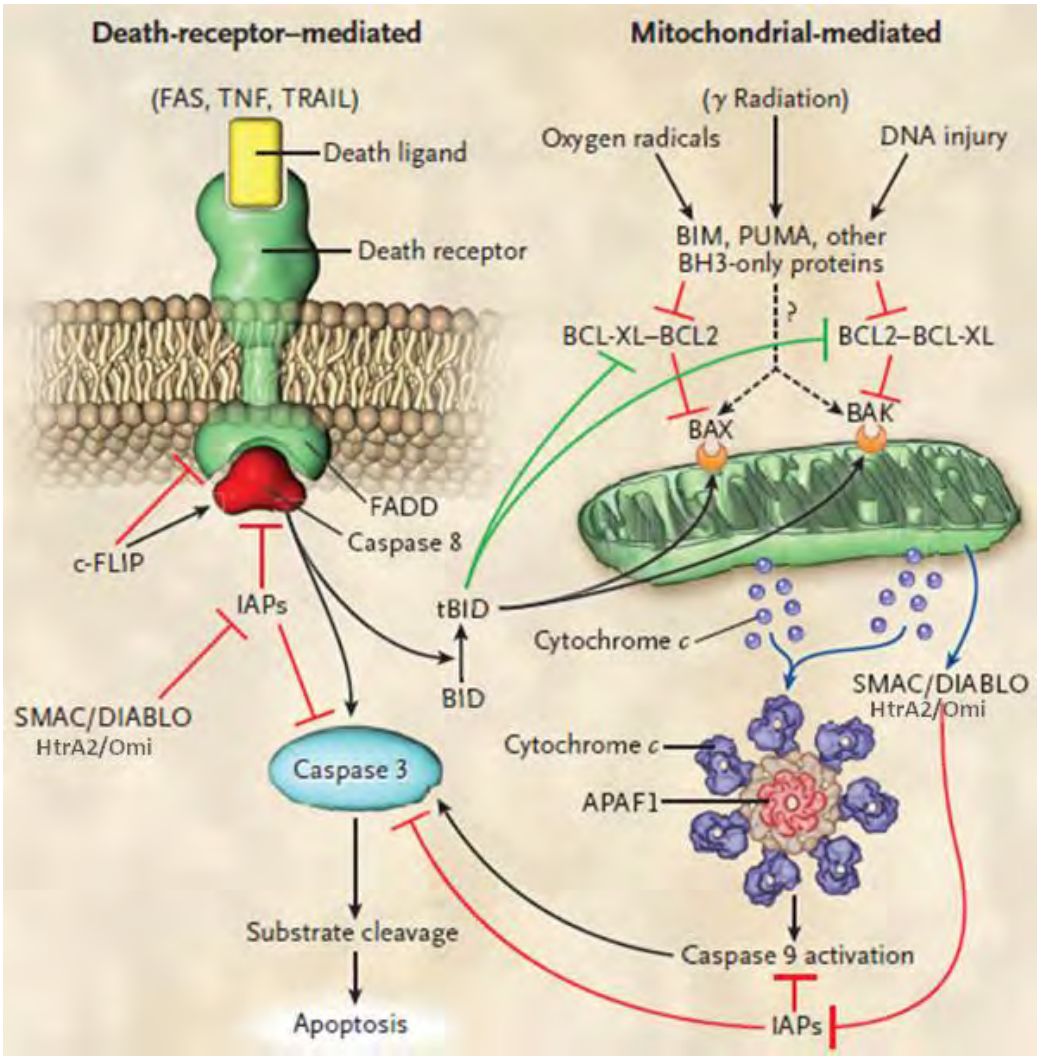

Figure 1.3: The extrinsic and intrinsic pathways of apoptosis. The intrinsic (mitochondria mediated) and the extrinsic (death-receptor mediated) pathways are the two main pathways of apoptosis. The intrinsic pathway is mediated by the Bcl-2 family of anti-apoptotic (Bcl-2 and Bcl-xL) and pro-apoptotic proteins (Bax and Bak). Stimuli such as γ radiation and ROS cause pro-apoptotic BH3 only proteins (such as Bim and PUMA) to inhibit anti-apoptotic Bcl-2 and Bcl-xL, allowing Bax and Bak to promote MOMP resulting in the release of cytochrome c. This leads to the activation of caspase-9, which then activates caspase-3 The extrinsic pathway is mediated by the activation of death receptors by binding of extracellular ligands (such as FAS, TNF and TRAIL), allowing recruitment of adaptor proteins (such as FADD). FADD recruits caspase-8, ultimately activating caspase-3. (Image reproduced from Hotchkiss et al., 2009).

1.2.2.2.2 Extrinsic pathway

The extrinsic or death receptor pathway of apoptosis mainly functions to eliminate unwanted cells during development, immune system function and immune-surveillance (including immune-system-mediated tumour elimination) (Boatright and Salvesen, 2003). This apoptotic pathway relies on the binding of extracellular ligands to the death receptors of the TNFR (Tumour necrosis factor receptor) family including FAS (Fatty acid synthetase) or CD95, TNFR1 (Tumour necrosis factor receptor 1), DR3 (Death receptor 3), DR4 (Death receptor 4) or TRAIL-R1 (TNF-related apoptosis inducing ligand-Receptor 1) and DR5 (Death receptor 5) or TRAIL-R2 (TNF-related apoptosis inducing ligand-Receptor 2) (Elmore, 2007; Zimmermann and Green, 2001).

The extrinsic pathway is best described by the FAS/FASL (FAS ligand) model where upon ligand binding, the receptors aggregate in a trimeric manner facilitating the recruitment of adaptor proteins such as FADD (FAS-associated death domain). FADD recruits procaspase-8 molecules (initiator caspase), forming a death-inducing signalling complex (DISC), via interaction with the zymogen's N-terminal death effector domain (DED). This allows activation of caspase-8. Depending on its concentration, c-FLIP (FLICE inhibitory protein) can inhibit or support binding of FADD to caspase-8 (Hotchkiss et al., 2009). Activated caspase-8 cleaves and activates caspase-3 in addition to Bid, the connector of the intrinsic and extrinsic apoptotic pathways. Truncated Bid (tBid) translocates to the mitochondria in order to activate Bax and Bax which promotes MOMP and cytochrome c release ultimately resulting in caspase-3 activation (Figure 1.3) (Boatright and Salvesen, 2003). As this description illustrates, activation of apoptosis by the extrinsic pathway is frequently associated with activation of the intrinsic pathway as a result of Bid cleavage by caspase-8.

As mentioned earlier, caspase-3 has a large number of substrates, and their cleavage ultimately results in the execution of cell death. For example, caspase-3 activates CAD (Caspase-activated DNAse), a DNAse that is normally attached to an inhibitory subunit, ICAD (Inhibitor of Caspase-activated DNAse), that is present in cells. Cleavage of the inhibitory subunit, ICAD, allows the release of the catalytic subunit, CAD, that in turn cleaves genomic DNA between nucleosomes generating DNA fragments with lengths of approximately 180 base pairs (bp) (Hengartner, 2000; Wyllie, 1980). This feature has been used as a generally accepted method to detect apoptosis by analysing DNA ladders using electrophoresis or to demonstrate TUNEL (Terminal deoxynucleotidyl transferase-mediated 2'-deoxyuridine 5'-triphosphate nick end-labelling) staining of nuclei using histochemical approaches.

DNA fragmentation assays were among the first biochemical assays used to characterise apoptosis (Wyllie, 1980) and over the years numerous methods to detect apoptosis have been established. These include Caspase-3/7 activity, Annexin V staining (based on the binding of labelled Annexin V to phosphatidylserine, which translocates from the inner leaflet of the plasma membrane to the outer part during apoptosis) and PARP (poly (ADP-ribose) polymerase cleavage. PARP is a 116 kilo Dalton (kDa) nuclear enzyme responsible for DNA repair, and is cleaved into 89 kDa and 24 kDa fragments by caspase-3 (and caspase-7) during apoptotic cell death (Boulares et al., 1999; Germain et al., 1999). Western blot analysis to determine the expression of the 89 kDa cleaved fragment of PARP is a widely employed biochemical assay for apoptosis. These methods used to detect apoptosis not only added to the further understanding of the apoptotic pathway but also facilitated the elucidation of various signalling pathways involved in the induction of apoptosis.

1.2.3 Autophagy

1.2.3.1 Description and Function

Autophagy is an important cellular pathway, and it has seen a substantial surge in publications in the past two decades despite being discovered in the 1960's by Christian de Duve (De Duve and Wattiaux, 1966; Klionsky, 2008). The term "autophagy" comes from the Greek words "auto" (self) and "phagy" (to eat) and literally means "to eat oneself". Indeed autophagy works hand-in-hand with lysosomes as the cell's main pathway responsible for turnover of long-lived proteins and damaged or old cytoplasmic organelles. This is especially true for those too large for degradation by the proteosome, another important protein degradation system employed by the cell for the degradation of short-lived proteins. Autophagy occurs constitutively in the cell at a basal level to maintain homeostasis by ensuring "quality control" of important proteins and organelles (Yang and Klionsky, 2010a). This pathway is activated in response to stress including starvation, oxidative stress, accumulation of misfolded proteins, hormonal signalling, irradiation and treatment with chemical compounds (Meijer and Codogno, 2004).

Three distinct types of autophagy have been classified according to the different methods of cargo to lysosome delivery: macroautophagy, micro-autophagy and chaperone-mediated autophagy (CMA). CMA involves the specific degradation of proteins containing a specific KFERQ-like motif. Tagged proteins are directly translocated through the lysosomal membrane facilitated by LAMP (lysosome-associated membrane protein) type 2A (Dice, 2007; Kaushik et al., 2008). Interestingly, CMA has not been characterised in yeast, yet this type of autophagy has been characterised in all higher eukaryotes (Chen and Klionsky, 2011). The lysosomal membrane directly engulfs parts of the cytosol in cells undergoing

microautophagy (Mortimore et al., 1988; Müller et al., 2000), a process which is not well understood in mammalian cells. Macroautophagy is evolutionarily well conserved and is the main pathway involved in the turnover of cytoplasmic constituents (Klionsky and Emr, 2000). For the sake of simplicity, macroautophagy will be referred to as autophagy hereafter.

Autophagy plays a role in normal development, senescence, microbial invasion, immunity and defence as well as in disease states that include cancer, myopathies, neurodegeneration, gastrointestinal disorders and heart and liver diseases (Baehrecke, 2003; Chen and Klionsky, 2011; Klionsky and Emr, 2000). One of its main functions is to facilitate cell survival during times of stress, particularly starvation. Nutrient deprivation can activate autophagy to break down cytoplasmic constituents that can be sacrificed in order to produce new proteins or ATP essential for cell survival. Uncontrolled or excessive autophagy can result in autophagic cell death, previously known as Type II programmed cell death (Clarke, 1990; Galluzzi et al., 2012; Klionsky and Emr, 2000; Kroemer et al., 2009; Maiuri et al., 2007), a pathway that was subjected to intense debate and scrutiny (Clarke and Puyal, 2012; Edinger and Thompson, 2004; Gozuacik and Kimchi, 2004, 2007; Kroemer and Levine, 2008; Kroemer et al., 2009; Levine and Yuan, 2005; Li et al., 2009b; Shen et al., 2012; Tsujimoto and Shimizu, 2005). This is mostly due to the paradoxical roles of autophagy in cell survival and in cell death, as well as in cancer (discussed further in Section 1.2.3.4).

Autophagic cell death is thought to occur by excessive autophagic activity that results in a cell "eating" itself (Gozuacik and Kimchi, 2004), however it was proposed that this type of cell death mostly occurs in cells where apoptosis is compromised since apoptosis is perceived as the preferred cell death pathway (Levine and Yuan, 2005; Lockshin and Zakeri, 2004).

There are a number of reports that demonstrated that autophagy directly caused cell death when apoptosis was blocked (Shimizu et al., 2004; Xavier et al., 2013; Yu et al., 2004), suggesting that autophagy has a causative role in cell death in cells exposed to harsh stimuli. Shimizu and colleagues demonstrated this by treating *Bax*$^{-/-}$*Bak*$^{-/-}$ mouse embryonic fibroblasts with etoposide or staurosporine, which resulted in cell death together with a significant increase in autophagic vacuoles (Shimizu et al., 2004). Furthermore, they showed a reduction in autophagy and cell death by treating cells with a pharmacological autophagy inhibitor as well as using siRNA (small interfering RNA) directed at essential autophagy genes (Shimizu et al., 2004).

Interestingly, autophagy can occur in the absence of apoptosis and it can also occur at the same time as apoptosis (Codogno and Meijer, 2005). This has been evidenced by studies that demonstrated the ability of promising anticancer agents (such as histone deacetylase inhibitors (sodium butyrate and suberoylanilide hydroxamic acid) and 2-methoxyestradiol) to activate both autophagy and apoptosis resulting in cell death (Kim et al., 2012; Lorin et al., 2009; Shao et al., 2004; Wong et al., 2010; Zhang et al., 2013). Numerous reports have shown that anticancer compounds (including temozolomide and soybean B-group triperpenoid saponins) can induce autophagic cell death independently of apoptosis in cancer cells (Ellington et al., 2006; Huang et al., 2011b; Kanzawa et al., 2004; Li and Johnson, 2012; Li et al., 2009a; Shinojima et al., 2007; Wang et al., 2012). In addition, studies have demonstrated that compounds that cause oxidative stress stimulate ROS-mediated signalling pathways that activate the autophagic cell death pathway in cancer cells (Chen et al., 2008; Duan et al., 2011; Eom et al., 2010; Gong et al., 2012; Son et al., 2011; Xie et al., 2011), also to be discussed further in Section 1.2.3.4.

Considering the substantial body of evidence demonstrating the ability of a variety of anticancer compounds to induce autophagy as the main cell death pathway employed by cancer cells, it is difficult to dispute that autophagy causes cell death. However, conflicting views have been put forward questioning the existence of autophagic cell death, and there has been uncertainty regarding the precise function of autophagy in cell death, and whether cell death occurred "by" autophagy or "with" autophagy (Kroemer and Levine, 2008; Levine and Yuan, 2005; Shen et al., 2012). According to specific guidelines set out by the Nomenclature Committee on Cell Death (NCCD), the term "autophagic cell death" can only be used once the following criteria have been met: firstly, cell death must be inhibited when cells are treated with pharmacological agents known to block autophagy; secondly, inhibition of autophagy by genetically targeting two or more essential autophagy mediators must suppress cell death (Galluzzi et al., 2012). An additional criterion has been put forward, recommending that the term autophagic cell death should only be used when the above two criteria are met independently of other cell death pathways such as apoptosis or necrosis (Clarke and Puyal, 2012; Shen et al., 2012). In light of the controversy surrounding autophagic cell death, these recommendations were clearly put forward to assist cell death researchers in making meaningful conclusions regarding autophagic cell death.

The morphology of a cell undergoing autophagic cell death differs substantially from that of a cell undergoing apoptosis. While apoptosis results in nuclear degradation, the nucleus of an autophagic cell remains intact until the late stages of the process. In addition, autophagy is characterised by the presence of many vesicles within the cell that range from tiny autophagosomes (double-membrane) to relatively large autophagolysosomes (single-membrane) that are not observed in apoptosis. However, similarities do exist in the molecular regulation of apoptosis and autophagy where key players in the apoptotic program such as

Bcl-2 and Bax are involved in cross-talk with important autophagy regulatory proteins (Maiuri et al., 2007). Moreover, the lysosomes play a key role in the removal of cells undergoing cell death via both pathways. During apoptosis the lysosomes of the phagocytes and neighbouring cells take responsibility for disposal of the dead cell whereas cells undergoing death by autophagy employ their own lysosomes that fuse with the autophagosomes (to generate autophagolysosomes) to self-digest (Gozuacik and Kimchi, 2004).

Autophagy has made an explosive impact on the literature in the recent years. One of the main reasons for this was the discovery of the autophagy-related (ATG) genes that were first characterised in yeast (Matsuura et al., 1997). Presently, a total of thirty five ATG genes have been characterised in the yeast model with at least seventeen orthologues identified in eukaryotes (Chen and Klionsky, 2011). These genes have made a significant contribution to the understanding of the molecular regulation of autophagy and formation of the double membraned autophagosomes central to the process. The yeast model system was ideal to study autophagy because it contains a single phagophore assembly site (PAS), the only site where the autophagosome is produced, situated close to the vacuole (mammalian lysosome) for degradation (He and Klionsky, 2009). The nomenclature and pathway differs slightly compared to higher eukaryotes and for the purposes of this study the mammalian molecular pathway of autophagy (macroautophagy) will be discussed below.

1.2.3.2 The Autophagy Pathway

The autophagic process involves very distinct stages where specific regulatory proteins interact and allow progression to the next stage. The main stages include: initiation of preautophagosomal structure, elongation of autophagosomal membrane, maturation of autophagosome and autophagosome-lysosome fusion. Unlike in yeast, the initiation of the preautophagosomal isolation membrane (phagophore) can occur at several sites within the mammalian cell and structures such as the ER, Golgi apparatus and mitochondrial outer membrane have been implicated in this process, although no conclusive evidence is available (He and Klionsky, 2009; Juhasz and Neufeld, 2006; Yang and Klionsky, 2010b).

The formation of the autophagosome involve very intricate interactions between various proteins (often referred to as the 'core machinery') resulting in a completed double-membrane vesicle that fuses with lysosomes forming autophagolysosomes or autolysosomes for degradation of the organelles and cytoplasmic constituents contained within the autophagosome (Xie and Klionsky, 2007). Four important core complexes involved in this process are: (1) ULK1/2 (Uncoordinated-51-like kinase-1 or -2)-Atg13-Atg101-FIP200 (the focal adhesion kinase family-interacting protein of 200kDa) complex, (2) the class III PI3K (phosphatidylinositol 3-kinase) complexes, (3) the Atg12 complex and the Atg8 complex, representing two ubiquitin-like conjugation systems and (4) Atg9, which cycles between the phagophore and other structures and is essential for formation of the autophagosome (Yang and Klionsky, 2010b; Yorimitsu and Klionsky, 2005).

The mammalian Target of Rapamycin (mTOR) has a key function in the regulation of autophagy (Jung et al., 2010). In the presence of sufficient nutrients, mTOR inhibits autophagy by associating with and inhibiting (by phosphorylation) ULK-1 or ULK-2 (mammalian homologs of Atg1 and collectively referred to ULK1/2) and Atg13 (inactivated by hyperphosphorylation) (Figure 1.4). ULK1/2-Atg13-FIP200 forms a stable complex in cells irrespective of nutrient conditions (He and Klionsky, 2009). Starvation or chemical inhibition of mTOR results in its disassociation from ULK1/2 (Figure 1.4). ULK1/2 is then activated by a conformational change, and in turn phosphorylates and activates Atg13 and FIP200 (Atg17) (activated by hyperphosphorylation), forming an active complex (Figure 1.4). In addition, a recently identified Atg-13 binding protein, Atg101, was also found to be part of this complex necessary for the assembly of the preautophagosome during the induction of autophagy (Chen and Klionsky, 2011; Hosokawa et al., 2009; Jung et al., 2009; Mercer et al., 2009).

Mammalian cells have three types of PI3K, Class I, II and III PI3K, with Class I and Class III implicated in the control of autophagy. Class I members negatively regulate autophagy of which AKT (AK (refers to a mouse strain) Thymoma) is an example (Chen and Klionsky, 2011; Ellington et al., 2006). The Class III PI3K, hVps34 (human Vacuolar protein sorting 34), positively regulates autophagy (Chen and Klionsky, 2011) and forms part of three important complexes together with Beclin 1 (Atg6 or Vps 30, a coiled-coil, myosin-like Bcl-2-interacting protein) and p150 (Vps 15 or phosphoinositide-3-kinase regulatory subunit 4, a myristoylated kinase) that are essential for the formation of the preautophagosomal structure (Figure 1.5) (Chen and Klionsky, 2011). The Atg14L complex consisting of the core components (hVps34, Beclin 1 and p150) associated with Atg14L (yeast Atg14-like or Barkor) and AMBRA 1 (activating molecule in Beclin 1-regulated autophagy), and the

UVRAG (ultraviolet irradiation resistant-associated gene) complex made up of the core components associated with Bif 1 (Bax-interacting factor 1) and UVRAG positively regulate autophagy (Figure 1.5).

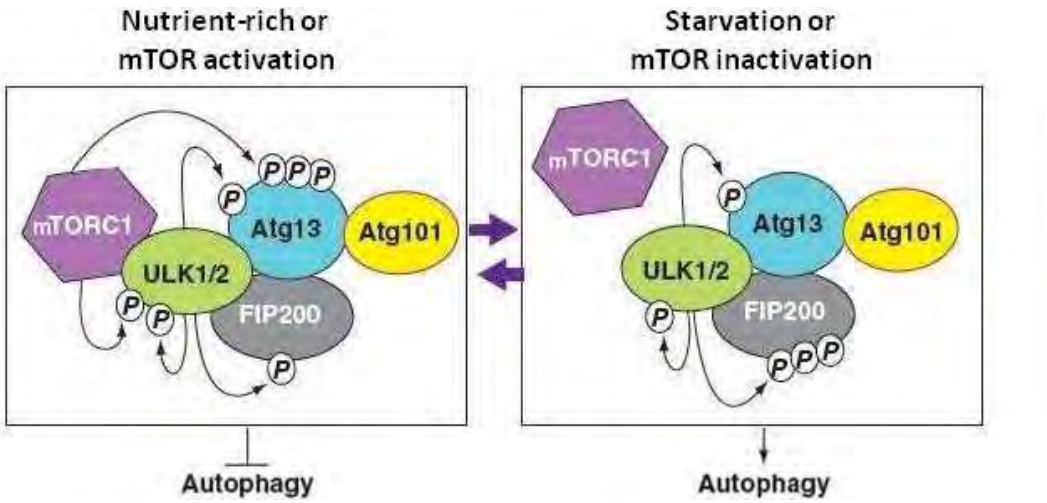

Figure 1.4: mTOR regulation of autophagy during nutrient-rich and starvation conditions. During nutrient-rich conditions mTOR associates with and phosphorylates ULK1/2 resulting in the hyperphosphorylation and inactivation of Atg13, thus inhibiting autophagy. During starvation or chemical inhibition, mTOR dissociates from ULK1/2 which undergoes a conformational change and is activated by autophosphorylation resulting in hypophosphorylation of Atg13 and hyperphosphorylation of FIP200 thus activating autophagy. (Image reproduced from Chen and Klionsky, 2011).

In contrast, the Rubicon (RUN domain and cysteine-rich domain containing Beclin 1-interacting protein) complex (Figure 1.5) - where Rubicon interacts with the Class III PI3K core components and UVRAG - has an inhibitory role on autophagy (Chen and Klionsky, 2011; He and Klionsky, 2009; Kuppusamy et al., 2011; Matsunaga et al., 2009; Yang and Klionsky, 2010a). Another inhibitor of this process is Bcl-2 (from the ER) that binds to Beclin 1 at the BH3 domain (Beclin 1 is a BH3-only family member) preventing Beclin 1 from forming the PI3K complexes necessary for autophagy induction (He and Levine, 2010).

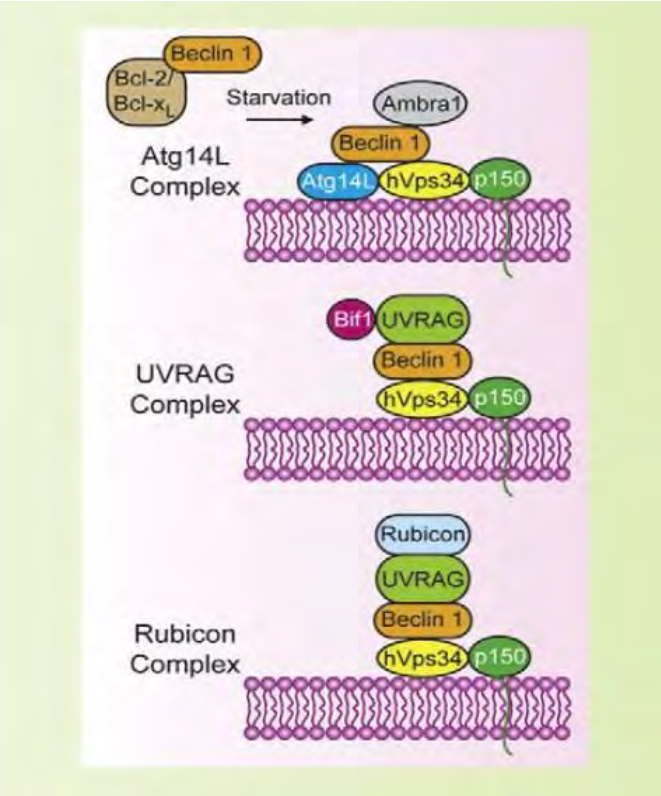

Figure 1.5: Class III PI3K complexes essential for the formation of the preautophagosomal structure. PI3K Class III, hVps34, together with Beclin 1 and p150 can exist as multiple complexes that associate with different partners: Ambra 1, Atg14L, Bif 1, UVRAG and Rubicon. The Ambra 1-Atg14L and Bif 1-UVRAG complexes activate autophagy whereas the Rubicon-UVRAG complex inhibits autophagy (Image reproduced from Yang and Klionsky, 2010b).

The Class III PI3K complexes play an important role in the formation of the preautophagosomal structure or phagophore, to which two strongly interdependent ubiquitin-like systems are recruited (Ohsumi, 2001). The first is the Atg12-Atg5-Atg16 system where Atg12 represents an ubiquitin-like (Ubl) protein. Atg12 is activated by Atg7 (which acts as an E1 activating enzyme) and then transferred to Atg10 (playing the role of the E2 conjugating enzyme) that facilitates the binding of Atg12 to Atg5 via covalent linkage of an internal lysine on Atg5. The Atg12-Atg5 conjugates interact with Atg16, allowing self-

oligomerisation (of Atg16) to form a tetramic complex with Atg12-Atg5. The Atg16-Atg12-Atg5 complex attaches to the phagophore (via Atg16) enabling the elongation process (Yang and Klionsky, 2010a) (Figure 1.6).

The second essential Ubl system employed for the expansion of the preautophagosome is Atg8-PE (phosphatidylethanolamine). Atg8 or LC3 (Microtubule-associated protein 1 light chain 3), the second Ubl protein, is cleaved by the cysteine-protease Atg4, exposing a C-terminal glycine residue thus generating LC3-I. This is recognised by Atg7 (E1 activating enzyme) which activates and transfers LC3-I to Atg3 (E2 conjugating enzyme) (Figure 1.6). The first Ubl system (Atg16-Atg12-Atg5) facilitates the second system by conjugating LC3-I to PE, via an amide bond, producing a lipidated form of LC3 called LC3-II (Yang and Klionsky, 2010a). In this way, LC3 is responsible for controlling the expansion of the autophagosome by recruiting lipid molecules (Knævelsrud and Simonsen, 2012; Xie et al., 2008). LC3-II is extensively used in biochemical assays for autophagy as it is found on both the inner and outer autophagosome membrane and is directly associated with the autophagosome, which form randomly throughout the cytoplasm (Jahreiss et al., 2008; Kabeya et al., 2000).

An adaptor protein called sequestosome-1 (SQSTM 1) or p62, also bound by LC3-II, functions to aid the degradation of ubiquitinated protein aggregates via autophagy. During the autophagic process p62/SQSTM 1 is degraded, but accumulates during autophagy inhibition (Mathew et al., 2009; Moscat and Diaz-Meco, 2009). Thus levels of p62/SQSTM 1 is also used in biochemical assays monitoring autophagy (Klionsky et al., 2009). Once the completed autophagosome fuses with the lysosome the LC3-II on the outer membrane is

cleaved and delipidated by Atg4 and returned to the cytoplasm to be recycled while the LC3-II on the inner autophagosomal membrane is degraded with the rest of the cargo (He and Klionsky, 2009).

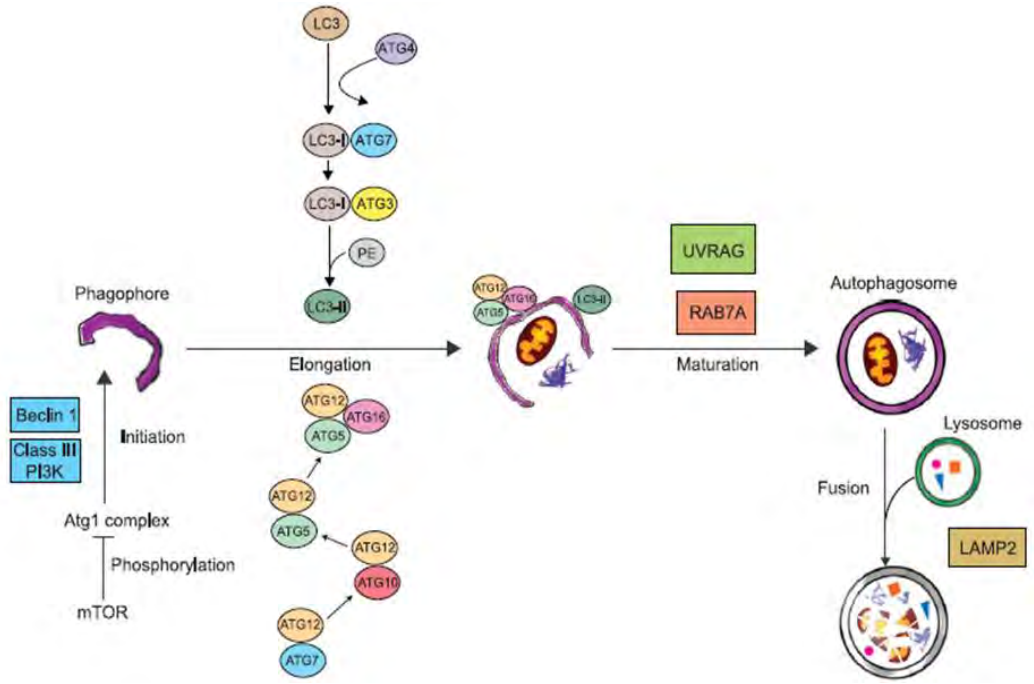

Figure 1.6: The pathways regulating autophagy. During the initiation phase of autophagy the Class III PI3K complexes, including Beclin 1, play a pivotal role in the recruitment of two ubiquitin-like conjugation systems: the Atg12-Atg5-Atg16 system and LC3-PE system. Both systems function together to elongate the autophagosome resulting in a mature autophagosome. The maturation of autophagosomes and fusion with lysosomes is facilitated by UVRAG, RAB7A and LAMP-2. Autophagosomes fused with lysosomes are called autolysosomes, and contain acidic hydrolases from the lysosomes that are responsible for the degradation of the contents of the autophagosome (Image reproduced from Liu and Ryan, 2012).

The fusion of the autophagosome to the lysosome is made possible by LAMP-2 (lysosome-associated membrane protein-2), a lysosomal membrane protein and the small GTP (guanosine-5'-triphosphate) binding protein RAB7A (Jäger et al., 2004; Liu and Ryan, 2012; Tanaka et al., 2000). UVRAG, apart from its function in autophagosome initiation, activates

RAB7A thereby controlling autophagosome maturation (Liu and Ryan, 2012). Fusion of the autophagosome to the lysosome results in a single-membrane autolysosome, where the inner membrane of the autophagosome attaches to the lysosome releasing its contents (Figure 1.6). The lysosome contains acidic hydrolases (cathepsin B, D and L) responsible for breakdown of the material contained within the autophagosome (Tanida et al., 2005). The amino acids, fatty acids and nucleosides produced can be reused by the cell to maintain energy production and protein synthesis required for cell survival, especially during stressful conditions such as starvation (Wirawan et al., 2012). If the autophagic process is excessive, cell death occurs (Kroemer et al., 2009).

1.2.3.3 Autophagy in Cancer

Autophagy has been frequently referred to as a "double-edged sword" because of its paradoxical roles in both cell survival and cell death of cancer cells (Apel et al., 2009; Shintani and Klionsky, 2004). Many studies have implicated autophagy as a tumour suppressor mechanism whereas others have demonstrated its tumourigenic role in cancer. The diverse roles of autophagy in tumour suppression and as a promoter of tumourigenesis will be explored further below.

Beclin 1 provided the first evidence that autophagy had tumour suppressive functions. Initial studies demonstrated that allelic *BECN1* (gene encoding Beclin 1) deletion was repeatedly detected in ovarian, breast and prostate human cancers (Eccles et al., 1990; Futreal et al., 1992; Gao et al., 1995; Russell et al., 1990; Saito et al., 1993). Liang and colleagues reported that overexpression of Beclin 1 induced autophagy and inhibited tumourigenesis in human breast carcinoma cell lines (Liang et al., 1999). In addition, later studies demonstrated a high

incidence of spontaneously occurring tumours as well as promotion of tumourigenesis in mice with Beclin 1 mutations confirming the tumour suppressing function of Beclin 1 (Qu et al., 2003; Yue et al., 2003). Furthermore, decreased expression or alterations of several other essential autophagy regulatory proteins (including LC3-II, Atg5, Atg12 UVRAG, Bif-1) have been observed in a wide variety of human tumours (such as brain, colon, gastric and prostate) thus supporting the notion that tumour suppression is achieved by various components of the autophagic pathway (Huang et al., 2010; Liang et al., 2006; Liu and Ryan, 2012; Takahashi et al., 2007). In addition, autophagy is responsible for degrading p62/SQSTM 1, which is implicated in the promotion of tumourigenesis and is often upregulated in cancer cells (Mathew et al., 2009; Moscat and Diaz-Meco, 2009).

In order to understand the role of autophagy in cancer cell survival and cancer cell death, various hypotheses have been suggested, mainly that the stages of tumour development are important factors in determining whether autophagy is pro-death or pro-survival. Some authors hold that autophagy is important for the survival of cancer cells during the initial stages of tumour formation, since the mutated cells trying to proliferate in a distressed environment with limited nutrients enter a state of dormancy, thus depending on autophagy as a survival mechanism (Liu and Ryan, 2012). Yet, others propose that autophagy limits the growth of tumours in the early stages of tumourigenesis by removing damaged proteins and organelles that contribute to tumourigenesis (Karantza-Wadsworth et al., 2007). This includes mitochondria that produce high levels of reactive oxygen species contributing to increased DNA damage that could result in cancer development (Jin, 2006; Karantza-Wadsworth et al., 2007). Furthermore, other studies demonstrate that autophagy promotes cancer cell survival at the late stages of cancer (Fung et al., 2008; Kenific et al., 2010). Cancer cells are under increased metabolic stress due to increased cell proliferation, and the cells at the core of

tumours are prone to starvation and/or hypoxia due to poor blood perfusion. Thus, in this scenario, autophagy represents an attractive survival mechanism (Chen and Karantza, 2011; Mathew et al., 2007).

Studies have also implicated autophagy as a survival mechanism employed by various cancer cells during treatment with a number of anticancer agents (including cisplatin, trastuzumab and camptothecin) (Chen and Karantza, 2011; Eskelinen, 2011; Liu et al., 2011). Paradoxically, other anticancer agents (including arsenic trioxide and temozolomide) have been shown to induce autophagic cell death (Kanzawa et al., 2004; Li and Johnson, 2012). Interestingly certain anticancer agents such as bortezomib and tamoxifen have been shown to induce autophagic cell death in some cancer cell model systems (Bursch et al., 1996; Li and Johnson, 2012), yet in other model systems inhibition of autophagy sensitized cultured cancer cells to treatment with the same agents (in this case bortezomib and tamoxifen) (Fels et al., 2008; Schoenlein et al., 2009).

Taken together, it is evident that cancer chemotherapeutic agents can either increase autophagy or decrease autophagy in cancer cells. Furthermore, increased autophagy by cancer therapeutics can have a pro-survival or a pro-death effect on cancer cells. Understandably, the role of autophagy in cancer is a complex one. It would appear that the cell death and cell survival functions of autophagy in cancer are context-, tissue-, and cell-specific. Moreover, several cancer-associated signalling pathways, both divergent and convergent, have been characterised to regulate autophagy. Some of the main signalling networks will be discussed below.

As mentioned earlier, mTOR plays a key regulatory role in autophagy. Mammalian cells have two mTOR complexes: mTORC1 (mTOR complex 1) and mTORC2 (mTORC2). mTORC1 consists of mTOR, mLST8 (mammalian lethal with sec-thirteen protein 8), PRAS40 (Proline rich AKT substrate of 40kDa) and RAPTOR (regulatory associated protein of mTOR), and it is the main complex involved in autophagy regulation (Guertin and Sabatini, 2007; Jung et al., 2010). An important inhibitory pathway of autophagy regulated by Class I PI3K members and mTOR is referred to as the PI3K-AKT-mTOR pathway (Chen and Karantza-Wadsworth, 2009). This pathway, activated by nutrients, growth factors and insulin, involves the phosphorylation of phosphatidylinositol-phosphate (PIP) forming phosphatidylinositol-3,4-biphosphate, and phosphatidylinositol-4,5-biphosphate ($PIP_{2)}$ and also forming phosphatidylinositol-3,4,5-triphosphate (PIP_3) by Class I PI3K enzymes. This allows the activation of AKT, which inhibits the TSC1/2 (Tuberous sclerosis factor 1 and 2, harmartin and tuberin, respectively) stable complex by phosphorylation of TSC2 (Manning et al., 2002). The inhibition of TSC1/2 results in the activation of Rheb (Ras Homolog Enriched in Brain) that is able to activate mTOR, which inhibits autophagy (Figure 1.7). The tumour suppressor, PTEN (Phosphatase and tensin homolog deleted on chromosome 10), functions in this pathway by hydrolysing and dephosphorylating PIP_3 therefore resulting in the inhibition of AKT and ultimately the inhibition of mTOR resulting in activation of autophagy (Figure 1.7) (Esclatine et al., 2009).

Abnormal activation of the PI3K-AKT-mTOR axis is frequently observed in cancer and may be caused by loss of PTEN function, loss of TSC1/2 function, increased activity or mutation of Class I PI3K proteins, overexpression of AKT, constitutive activation of tyrosine kinase growth factor receptors and carcinogen exposure (Chen and Karantza-Wadsworth, 2009). The deregulation and increased activation of the PI3K-AKT-mTOR pathway inhibits autophagy

and is therefore believed to play a role in increased tumourigenesis (Chen and Karantza, 2011). In addition, this pathway induces cell growth and proliferation, both critical for tumourigenesis. Given this content, inhibitors of the Class I PI3K members, AKT and mTOR are thought to represent good potential anticancer agents as has been demonstrated by a number of reports (Chen and Karantza-Wadsworth, 2009; Crazzolara et al., 2009; Tanemura et al., 2009).

In contrast to the PI3K-AKT-mTOR pathway, the AMPK-mTOR signalling pathway is involved in the induction of autophagy (Meley et al., 2006). AMPK (Adenosine monophosphate-activated protein) is mainly activated by the tumour suppressor LKB1 (a serine/threonine kinase gene defective in Peutz–Jeghers syndrome) in response to a decrease in energy levels, starvation and oxygen deprivation (Woods et al., 2003). These metabolic stress conditions result in a reduction of ATP with a concomitant increase in the AMP/ATP ratio thus activating LKB1 (Shaw et al., 2004). LKB1 activates AMPK by phosphorylation on threonine 172, triggering a cascade that ultimately induces autophagy (Figure 1.7). AMPK activates the TSC1/2 complex resulting in mTOR inhibition via inactivation of Rheb. AMPK can employ a TSC-independent mechanism of autophagy induction by directly inhibiting mTORC1 by means of RAPTOR phosphorylation.

A recent study demonstrated that the LKB1-AMPK pathway can induce autophagy independently of mTOR via phosphorylation of $p27^{KIP}$ and cell cycle arrest (Liang et al., 2007). Furthermore, LKB1 independent mechanisms of AMPK activation have been identified that are involved in the regulation of autophagy. Recently, a study showed that epithelial cells treated with the cytokine TRAIL was shown to activate TAK1 (transforming

growth factor-β-activating kinase 1), a protein that is capable of directly activating AMPK (Herrero-Martín et al., 2009). Most recently, studies demonstrated the ability of AMPK to directly activate autophagy via direct phosphorylation of ULK1, a process independent of both LKB1 and mTOR signalling (Lee et al., 2010).

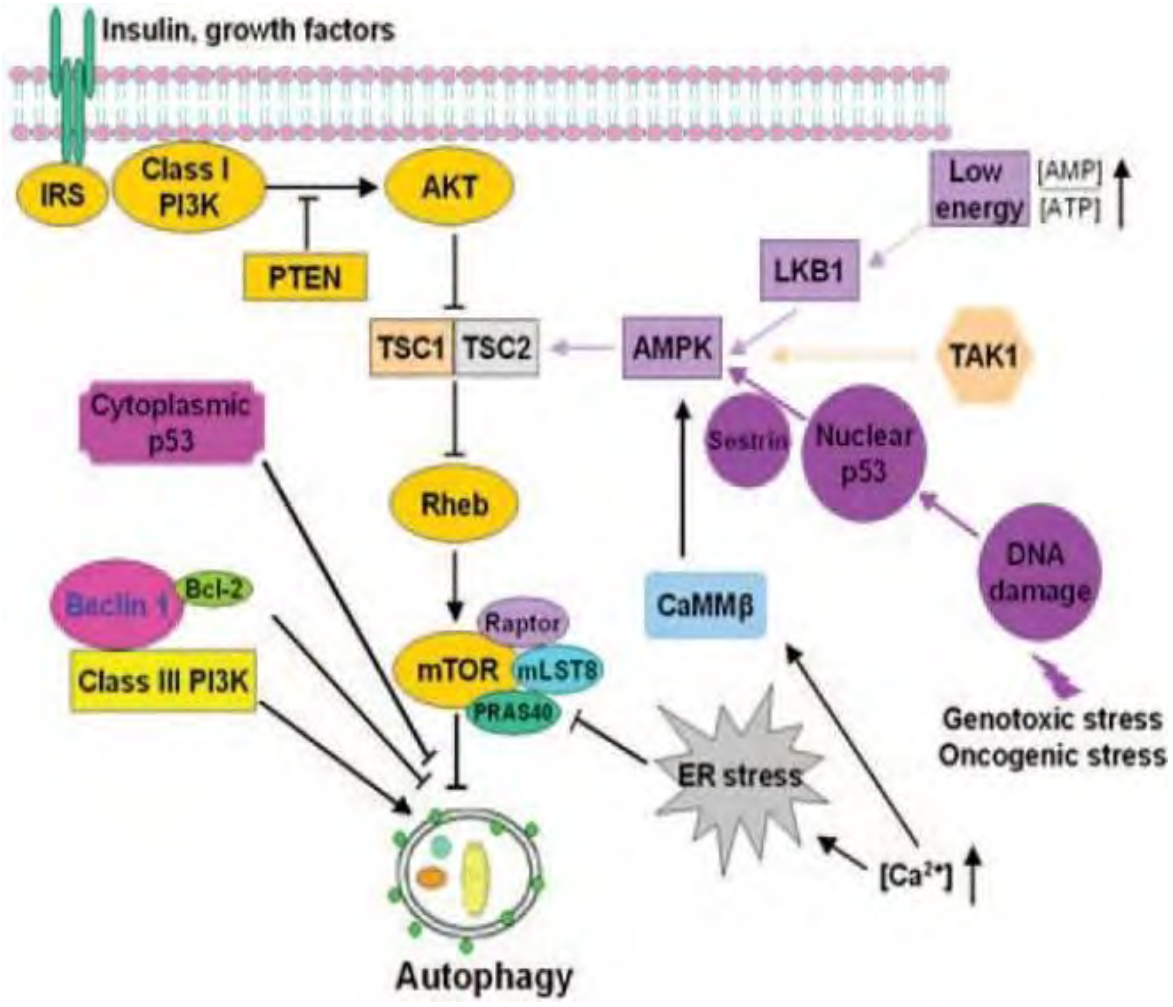

Figure 1.7: The molecular regulation of autophagy illustrating the upstream control of AMPK and mTOR. The PI3K-AKT-mTOR axis inhibits autophagy whereas the Class III PI3K complexed with Beclin 1 activates autophagy. Bcl-2 complexed with Beclin 1 inhibits Beclin 1 functions in the induction of autophagy. AMPK upregulates autophagy via TSC1/2 inhibition of the mTORC1 complex and can be activated by LKB1, nuclear p53, TAK1 and calcium. Calcium release is linked to ER stress, which plays a role in the activation of autophagy (Image reproduced from Chen and Karantza, 2011).

Calcium is another important regulator of AMPK that is independent of LKB1. Various stress conditions result in calcium release into the cytoplasm allowing the phosphorylation and activation of CaMKKβ (calcium-activated calmodulin-dependent kinase kinase-β), an activator of AMPK and autophagy (Figure 1.7) (Høyer-Hansen and Jäättelä, 2007; Høyer-Hansen et al., 2007). The ER is the main intracellular storage facility for calcium, and the ER stress pathway is one of the main pathways involved in calcium-mediated AMPK-induced autophagy.

Apart from being the main storage site of calcium, the ER is important for protein folding and posttranslational modifications, biosynthesis of steroids, cholesterol and lipids, cell signalling pathways mediated by calcium and drug detoxification in mammalian cells (Rutkowski and Kaufman, 2007; Verfaillie et al., 2009). ER stress can be induced by a variety of factors including an accumulation of unfolded proteins, severe decrease in glucose, hypoxia, oxidative stress and loss of calcium homeostasis (Rutkowski and Kaufman, 2004, 2007). The UPR (Unfolded Protein Response) is induced by ER stress to ease the stress on the ER by upregulation of protein folding and degradation pathways and inhibition of protein synthesis. Severe ER stress can result in cell death mostly by apoptosis, however autophagy has also been implicated in this process (Høyer-Hansen and Jäättelä, 2007).

The UPR is facilitated by three ER stress sensors: PERK (Protein kinase R-like ER kinase), IRE1 (inositol requiring enzyme 1) and ATF6 (activating transcription factor 6) (Verfaillie et al., 2009). PERK is involved in the autophagic pathway by phosphorylation of eIF2α (eukaryotic initiation factor 2 alpha) which increases the transcription of *ATG12* and plays a role in LC3 conversion (Kouroku et al., 2007). Additionally, IRE1 induces autophagy by

activating JNK (c-Jun N-terminal kinase), an important regulator in autophagy (Ogata et al., 2006). Activation of JNK plays an important role in Beclin 1 activity as it phosphorylates Bcl-2 releasing Beclin 1 from its inhibitory complex (He and Levine, 2010). Similarly, DAPk (death-associated protein kinase) can be activated by increased levels of calcium resulting in the phosphorylation of Beclin 1, hindering the Beclin 1-Bcl-2 complex and allowing Beclin 1 to activate autophagy (He and Klionsky, 2009; Zalckvar et al., 2009).

JNK activation plays a further role in autophagy regulation as it is involved in the transcriptional regulation of Beclin 1 via c-Jun, its target transcriptional factor (Li et al., 2009a; Park et al., 2009). In addition, JNK-induced autophagy can be controlled by ROS, important signalling molecules involved in cancer and in the autophagic process (Huang et al., 2011a).The ERK1/2 (extracellular-signal-related kinase 1 or 2) pathway, another MAPK pathway, can also be activated by ROS to stimulate autophagy (Cagnol and Chambard, 2010). ROS regulation of autophagy encompasses a number of signalling pathways in addition to the JNK and ERK pathways such as the AMPK and p53 (a key tumour suppressor that is mutated in many types of cancer) signalling pathways (Huang et al., 2011a; Li et al., 2012; Scherz-Shouval and Elazar, 2011).

Initial studies implicating ROS in the autophagic pathway were performed by Schval and colleagues who demonstrated that ROS inhibited Atg4 thus preventing LC3 inhibition and promoting autophagy (Scherz-Shouval and Elazar, 2007). High levels of ROS can also activate AMPK via LKB1 directly or indirectly via ER stress and calcium signalling (Høyer-Hansen et al., 2007; Li et al., 2012; Son et al., 2011). ROS activation of p53 is important for cell cycle arrest and apoptosis, and interestingly for autophagy as well. Nuclear activation of

p53 by ROS stimulates the transcription of important autophagy regulatory proteins including AMPK, sestrin, TSC2, PTEN and DRAM (damage-regulated autophagy modulator) (Chen and Debnath, 2010; Chen and Karantza, 2011; Li et al., 2012). DRAM, a new p53 target, was recently identified as a specific positive regulator of autophagy (Crighton et al., 2007). In contrast, cytoplasmic activation of p53 is involved in the inhibition of autophagy thus demonstrating the opposing roles of p53 in autophagy (Chen and Debnath, 2010).

Given the information discussed above, it is clear that numerous links between autophagy and signalling pathways involved in cancer have emerged. Furthermore, the role of autophagy in tumourigenesis, tumour suppression and cancer treatment is complex as autophagy can function in cancer cell survival, cancer cell death and resistance of cancer cells to chemotherapeutic agents. Moreover, a large number of anticancer compounds have been shown to induce autophagic cell death in a variety of cancer cell lines, demonstrating that autophagy has potential as a promising target for chemotherapeutic agents. However, it is evident that the cell death and cell survival functions of autophagy in cancer are context-, tissue-, and cell-specific. Ongoing research should provide valuable information on how autophagy can be manipulated to offer the best possible outcomes in the treatment of cancer.

1.2.4 Necrosis

1.2.4.1 A Brief Introduction to Necrosis

Necrosis is synonymous with ‘accidental cell death’, just as apoptosis is synonymous with ‘programmed cell death’ (a concept that is undergoing a profound transformation as more programmed cell death pathways are being elucidated) (Kroemer et al., 2009). The word

‘necrosis’ is derived from the Greek word ‘nekros’ meaning corpse but this cell death mechanism goes by other names including oncosis (from the Greek ‘oncos’ for swelling) and oncotic necrosis (Hotchkiss et al., 2009; Proskuryakov et al., 2003). Recently, it has been reported that necrosis can also be ‘programmed’ and more names have been added to the lexicon such as necroptosis, programmed necrosis, necrotic cell death and Type III cell death (Galluzzi and Kroemer, 2008; McCall, 2010).

Classical (accidental) necrosis is a process that does not rely on strict genetic control and requires minimal energy, which cells undergo upon a wide variety of stimuli. Necrosis has been shown to occur in response to severe physiological changes such as hypoxia, abrupt anoxia, ischemia, hypoglycaemia, toxin exposure, reactive oxygen species, extreme changes in temperature/pH and nutrient withdrawal (Kroemer et al., 1998; Syntichaki and Tavernarakis, 2002). In contrast to apoptosis, there is little evidence implicating classical necrosis in development but plenty of evidence implicating its involvement in disease. It has a significant role in Alzheimer’s disease, Huntington’s disease, Parkinson’s disease, Creutzfeldt-Jakob disease, amyotrophic lateral sclerosis, muscular dystrophy, diabetes and epilepsy (McCall, 2010; Proskuryakov et al., 2003; Syntichaki and Tavernarakis, 2002).

Necrosis can occur as primary necrosis (necrosis in the absence of apoptosis) or secondary necrosis (necrosis after the onset of apoptosis) (Kroemer et al., 1998). The main characteristics of necrosis include widespread swelling of the cell (hence the name oncosis), swelling of several cellular organelles (including the mitochondria), clumping and random degradation of nuclear DNA and loss of plasma membrane integrity (Assunção Guimarães and Linden, 2004; Syntichaki and Tavernarakis, 2002). The breakdown of the plasma

membrane results in the release of intracellular contents and pro-inflammatory molecules into the local environment around the dying cell that induces an immune response and attracts immune cells ultimately causing inflammation, a key characteristic of necrosis (Edinger and Thompson, 2004).

1.2.4.2 The Programmed Necrosis Pathway

Necroptosis is the name given to programmed necrosis (Degterev et al., 2005; Galluzzi and Kroemer, 2008; Golstein and Kroemer, 2007). This type of cell death demonstrates necrotic morphology and, interestingly, relies on the stimulation of the same ligands involved in death-receptor mediated apoptosis such as TNF-α, FASL and TRAIL (Holler et al., 2000; Vercammen et al., 1998). In addition, caspase-8 was shown to play an important regulatory role in this cell death pathway and demonstrated a link between apoptosis and necroptosis (Holler et al., 2000; Varfolomeev et al., 1998). Other key regulatory proteins involved in necroptosis include RIP1 (Receptor-interacting protein 1), RIP3 (Receptor-interacting protein 3) and CYLD (cylindromatosis 1) (Figure 1.8) (Degterev et al., 2005, 2008; Hitomi et al., 2008; Zhang et al., 2009) .

The induction of necroptosis can be mediated by a wide variety of molecules including reactive oxygen species and calcium, and is thought to have functions in mediating neuronal excitotoxicity and stimulating the immune system in response to viral infections (Christofferson and Yuan, 2010; Duprez et al., 2009). The molecular regulation of necroptosis is best described using the TNF-α/TNFR model (Figure 1.8). The binding of the ligand, TNF-α, to its receptor, TNFR, in the absence of apoptosis inhibitors or apoptosis-

defective conditions, results in the intracellular assembly of complex I. This complex consists of TRADD (TNFR type-1-associated DEATH domain protein), TRAF (TNF receptor associated factors), RIP1 and cIAPI. cIAPI is responsible for the ubiquitination of RIP1, which then allows NEMO (NFκB essential modulator) to be recruited to form part of the IKK (inhibitor of NFκB kinase) complex that activates NFκB, and a pro-survival pathway. However, it is not completely understood how the transition from complex I to complex IIa occurs (Yuan and Kroemer, 2010). RIP1 dissociates from complex 1 and joins complex IIa together with caspase-8 and FADD. Caspase-8 is then able to proteolytically cleave and inactivate RIP1 resulting in the initiation of the caspase-dependent death receptor apoptotic pathway (Figure 1.8) (Christofferson and Yuan, 2010; Yuan and Kroemer, 2010).

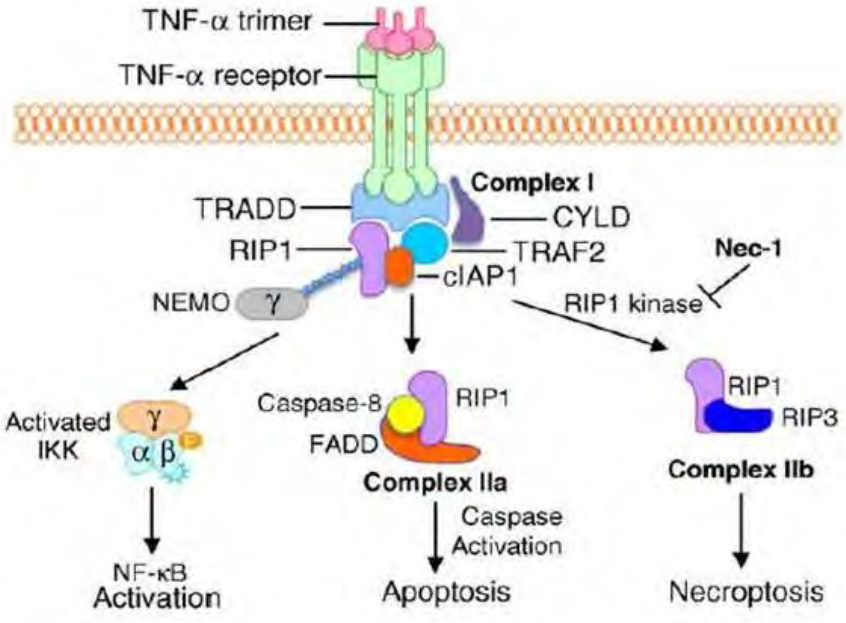

Figure 1.8: An illustration of the molecular regulation of necroptosis showing the role of RIP1 in NF-kB activation, apoptosis and programmed necrosis. TNFα stimulates TNFR resulting in an intracellular complex including TRADD, TRAF2, RIP1 and cIAP1. cIAP1 ubiquitinates RIP1 allowing NEMO to be recruited for NF-κβ activation. When apoptosis is not compromised, RIP1 forms a stable complex with FADD and caspase-8 (Complex IIa) that can activate apoptosis. When apoptosis is compromised, RIP1 forms a stable complex with RIP3 (Complex IIb) that activates necroptosis. Nec-1 can inhibit the kinase activity of RIP1 and necroptosis. (Image reproduced from Christofferson and Yuan, 2010).

In contrast, in the presence of apoptosis inhibitors or when apoptosis is compromised complex IIb is formed, facilitated by CYLD deubiquitination of RIP1, which is thought to be a key process involved in the regulation of necroptosis (Christofferson and Yuan, 2010). Nec-1 (necrostatin-1) can inhibit RIP1, which is required for the formation of complex IIb with RIP3 (Degterev et al., 2005; Hitomi et al., 2008). The interaction between RIP1 and RIP3 is important for the induction of necroptosis (Duprez et al., 2009). Many studies involved in the characterisation of necroptosis were performed in models where apoptosis was inhibited, suggesting that this mechanism of cell death could represent a compensatory pathway when cell death is necessary. Interestingly, it is also suggested that necroptosis and autophagy may function in concert, since autophagic vacuoles are often observed in cells undergoing necroptosis proposing that autophagy may precede necroptosis in some cell types (Christofferson and Yuan, 2010). However, more research is needed in order to fully understand the role of necroptosis in the armamentarium of the cell's death pathways.

Section 1.2 described some of the programmed cell death pathways employed by cells to execute homeostasis, development and survival. When these pathways are deregulated, cancer ensues. Of note, cells have a variety of tightly coordinated death pathways at their disposal, and an in-depth understanding of these pathways in cancer cells as well as clever manipulation of these pathways by anticancer compounds may lead to an increase in ammunition for use in the war against cancer.

1.3 Cancer Drug Development

1.3.1 Introduction

Many drugs currently used for the treatment of cancer are known to offer a minimal increase in overall survival, are coupled with serious side effects and are expensive (Gupta et al., 2013). Therefore, there is a significant need for the development of novel anticancer compounds. Novel chemotherapeutic agents targeted at cancer cells frequently elicit their effect by inducing cell death by modulating the highly regulated cell death pathways described previously (Section 1.2). Generally, most drug development programmes choose to target apoptosis although this probably reflected a poor understanding of the role of other programmed cell death pathways such as autophagy and programmed necrosis, and their potential as cancer therapeutic targets. Cancer cells often develop resistance to chemotherapeutic agents; therefore developing agents that exploit more than one cell death pathway may prove beneficial in the pursuit of eradicating cancer cells.

The development of cytotoxic compounds represents a significant thrust of cancer drug discovery and remains an important focus area in many research institutions. Natural products have made a significant contribution to our current arsenal of therapeutic agents and research continues in the search for more promising anticancer agents from nature's sources. Considering the advancement of technologies in all fields of research and development, it is not surprising that novel drug development strategies have surfaced. Small molecule targeted therapies and nanotechnology are presently exciting fields in cancer drug development. In addition, medicinal chemistry approaches have been forthcoming in the crusade against

cancer by not only introducing novel hybrid compounds but by also going back to old drugs used to treat non-cancer related diseases with the aim of repurposing them to treat cancer.

1.3.2 Approaches to Improve Anticancer Drug Development

1.3.2.1 Drug repurposing

Repurposing, repositioning, reprofiling or redirecting are some of the terms used to describe the process that searches for new uses for drugs already in the market (Ashburn and Thor, 2004). This is an ingenious venture considering that the drug discovery process is long and arduous involving many steps from the discovery process (screening and identification) to the preclinical phase (in vitro and in vivo testing) and finally, the clinical development stage (clinical trials in human beings). This entire process can take close to twenty years (Padhy and Gupta, 2011). In addition, the cost of bringing a new drug into the market is another major factor that contributes to the interest in repurposing old drugs. It has been estimated that in developed countries the average cost of producing one new drug is 1.24 billion USD (United States Dollars) (Padhy and Gupta, 2011). Time and cost factors are significantly reduced in repurposed drugs since a large amount of data is available at the onset with regard to safety and pharmokinetics (Tobinick, 2009). Moreover, many different diseases share common molecular pathways resulting in the observation of secondary indications in a large percentage of currently approved drugs (Boguski et al., 2009). It is therefore not surprising that a number of successful drugs have already been repurposed to treat different ailments, and a recent estimate indicates that 65% of repurposed compounds reach the market from Phase III clinical trials (Gupta et al., 2013).

The serendipitous discovery of the angina drug, sildenafil, as a treatment for erectile dysfunction led to the production of the extremely popular drug Viagra® by Pfizer, representing a successful example of drug repurposing that has stimulated interest in the pharmaceutical industry (Novac, 2013). Other examples of repurposed drugs include amantadine (influenza), colchicine (gout) and propranolol (hypertension) now used to for Parkinson's disease, recurrent pericarditis and migraine prophylaxis, respectively (Bidabadi and Mashouf, 2010; Padhy and Gupta, 2011). In addition, zidovudine, paclitaxel, methotrexate and miltefosine, part of the arsenal against cancer, are now used in the treatment of HIV/AIDS, restenosis, rheumatoid arthritis and visceral leishmaniasis, respectively (Ashburn and Thor, 2004; Novac, 2013; Padhy and Gupta, 2011).

Not surprisingly, numerous drugs used for a variety of non-cancerous diseases are now being used for or investigated as anticancer agents (Gupta et al., 2013). Thalidomide was initially used to treat nausea during pregnancy but was withdrawn due to its teratogenic effects (Mcbride, 1961). Further investigation demonstrated its valuable anticancer characteristics and it is now used to treat multiple myeloma (Boguski et al., 2009). Aspirin, valproic acid, statins, metformin and celecoxib are additional examples of drugs originally indicated for a variety of diseases that are now repurposed as anticancer agents (Gupta et al., 2013). The antimalarial, chloroquine, has also been repurposed as a potential treatment for cancer and was shown to induce cell death in a variety of cancer cell lines, including breast, lung and colon cancer (Jiang et al., 2008; Solomon and Lee, 2009; Zheng et al., 2009). Interestingly, another antimalarial compound, artemisinin, has recently also displayed promising anticancer properties, which represents the basis for this research project.

1.3.2.2 Artemisinins: from antimalarial to anticancer agents

Artemisinin is a compound isolated from a Chinese herbal plant (*Artemisia annua*, also known as sweet wormwood) that has been used for many years in Traditional Chinese Medicine (TCM). The first recorded use of the plant dates as far back as the third century BC (Before Christ) to treat fever and chills. Much later in the late 1960's, the Chinese government embarked on a search for new antimalarial drugs from TCM and this led to the discovery of artemisinin or *qinghaosu* (Klayman, 1985). Artemisinin displayed low solubility in oil and water, poor bioavailability and a short half life in vivo (Crespo-Ortiz and Wei, 2012), therefore many derivatives such as dihydroartemisinin, artemether, arteether and artesunate (collectively called the artemisinins) were developed (Figure 1.9). The artemisinins are commonly used to treat malaria and the World Health Organisation recommends artemisinin combination therapies as the first-line treatment of uncomplicated malaria to prevent to development of resistance (Kokwaro et al., 2007). In Africa, artemether/lumefantrine and amodiaquine/artesunate are the two main artemisinin combination therapies in use (Kokwaro et al., 2007; SAMF, 2010). Recently the artemisinins were found to be effective against cancer cells (Lai and Singh, 1995), and therefore represents an example of good candidates for repurposing.

Artemisinin is a sesquiterpene lactone that contains an endoperoxide bridge (C-O-O-C) and is the parent compound to several first generation derivatives: the reduced lactol dihydroartemisinin (DHA) (in vivo metabolite of some artemisinin derivatives) and the semisynthetic derivatives (artemether, arteether, artesunate and artelinate) are the ethers or esters of the lactol (Figure 1.9). The water-soluble artesunate (ART) was shown to have significant pharmacokinetic advantages over the lipid-soluble derivatives (artemether and

arteether) in addition to being less toxic (Haynes and Krishna, 2004). Many second-generation derivatives of artemisinin have also been synthesized, all of which contain the endoperoxide bridge. This bridge is located in the trioxane pharmacophore (a six-membered ring containing three oxygen atoms) (Figure1.9), and is essential for artemisinin activity as an antimalarial agent (Olliaro et al., 2001). An artemisinin derivative designed without the endoperoxide bridge, deoxyartemisinin, had no antimalarial activity demonstrating that the peroxide structure is crucial for the pharmacological activity of the artemisinins (Klayman, 1985; Neill and Posner, 2004). One of the proposed antimalarial mechanisms of action of the artemisinins is the iron-mediated cleavage of the endoperoxide bridge generating ROS and carbon-centred radical molecules that causes extensive protein damage and ultimately death of the malaria parasites (Meshnick, 2002; Olliaro et al., 2001).

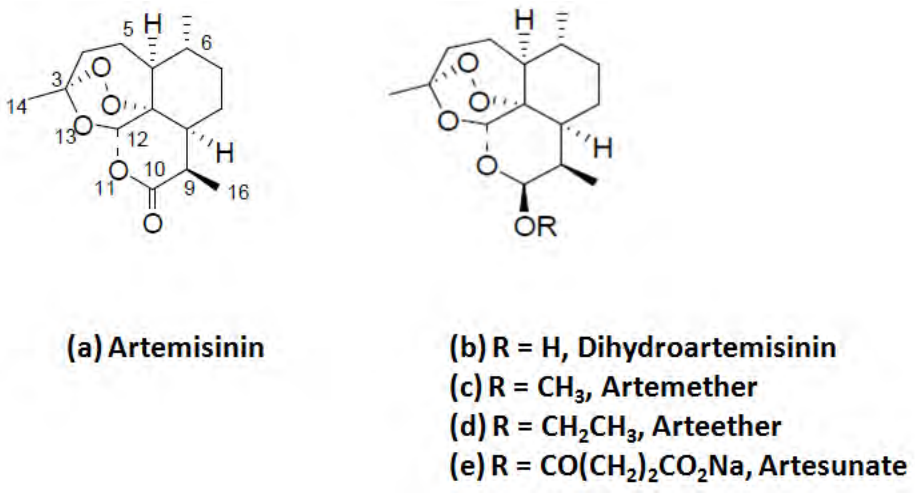

Figure 1.9: Chemical structures of artemisinin (a) and the first generation derivatives (b-e).

As previously mentioned, artemisinin derivatives have displayed potent anticancer activity, both in vitro and in vivo (Crespo-Ortiz and Wei, 2012; Dell'Eva et al., 2004; Hou et al., 2008; Ji et al., 2011; Morrissey et al., 2010; Singh and Lai, 2004). ART showed strong anticancer activity against 55 human cancer cell lines, including leukaemia, colon cancer, melanomas, breast, ovarian, prostate, central nervous system and renal cancer cell lines, in

the Developmental Therapeutics Program of the National Cancer Institute (NCI), United States of America (USA) (Efferth et al., 2001). The mechanism of action of artemisinins as anticancer agents is proposed to be similar to the action as antimalarial agents. Most cancer cells have high rates of iron intake (via transferrin receptors) and this facilitates the cleavage of the artemisinin endoperoxide bridge generating ROS which are toxic to cells at high concentrations (Lai and Singh, 2006). Furthermore, the different rates of iron metabolism between cancerous and normal cells can be associated with the high selectivity of artemisinins to cancer cells relative to normal cells (Oh et al., 2009). This observation holds promise for the future of the artemisinins in cancer chemotherapy.

The endoperoxide bridge of the artemisinins represent the active moiety of the compound, and it leads to an increase of ROS within cancer cells. In a study where leukaemia cells were treated with ART, a rapid increase in ROS was observed, which was completely blocked by the antioxidant, *N*-acetyl-L-cysteine (NAC) (Efferth et al., 2007). It was further demonstrated that treatment with NAC not only completely blocked ROS production but also inhibited ART-induced apoptosis (via the intrinsic mitochondrial pathway) which was initially shown in the same cell line. It was therefore suggested that ART induced the accumulation of ROS resulting in the initiation of apoptosis in the cancer cells (Efferth et al., 2007). Anthracyclines, well-known cancer drugs, also produce ROS but are also associated with cardiotoxicity (Rajagopalan et al., 1988). Interestingly, artemisinins are currently used to treat malaria and have not revealed cardiotoxicity or any other significant side effects (Crespo-Ortiz and Wei, 2012).

Studies performed to examine the effects of artemisinins on DNA damage showed that cancer cells treated with ART caused both single and double-strand breaks in DNA, and the authors proposed that the DNA damage observed after ART-treatment may be a result of oxidative stress induced by the compound (Li et al., 2008). Other studies have revealed that artemisinin derivatives induced growth arrest involving changes in the expression and activity of different components of the cell cycle. Leukaemia, lung carcinoma, pancreatic cancer and liver cancer cell lines treated with ART or DHA were shown to induce G1-phase cell cycle arrest (Chen et al., 2010a; Hou et al., 2008; Li et al., 2001). However, DHA has been reported to induce a G2/M cell cycle arrest in various cancer cells including osteosarcoma and ovarian cancer cells (Ji et al., 2011; Jiao et al., 2007). It can be speculated that the artemisinins-induced increase in ROS production is linked to the DNA damage observed, leading to cell cycle arrest and ultimately apoptosis of cancer cells.

Efferth and colleagues used leukaemic T cells as a model system and showed that artesunate induced the cells to undergo apoptosis via the intrinsic mitochondrial pathway. This was demonstrated by the release of cytochrome c from the mitochondria after cells were treated with artesunate followed by the activation of caspase-9, a key component of the intrinsic pathway (Efferth et al., 2007). Ovarian cancer cells treated with DHA led to decreased levels of anti-apoptotic proteins, Bcl-2 and Bcl-xL, and increased levels of pro-apoptotic proteins, Bax and Bad (Jiao et al., 2007). Additionally, human lung adenocarcinoma ASTC-a-I cells treated with DHA showed an induction of caspase-3, the key effector caspase which mediates many of the cellular events observed in apoptosis (Lu et al., 2009).

A panel of chemoresistant neuroblastoma cell lines treated with artesunate exhibited increased levels of caspase-3 as well as an enhanced number of cells in the sub-G1 phase of the cell cycle, indicative of apoptosis (Michaelis et al., 2010). HepG2 cells (liver cancer cells) exposed to ART or DHA displayed a dose-dependent reduction in the level of Bcl-2 protein with a corresponding increase in the level of Bax (Hou et al., 2008). A study performed by Singh and Lai showed that apoptosis was the primary mode of cell death in Molt-4 human lymphoblastoid leukaemia cells treated with the artemisinin derivatives (Singh and Lai, 2004). Taken together, it is evident that apoptosis is the predominant form of cell death employed by these compounds in a wide variety of cancer cell lines.

Many studies were performed to further elucidate the mechanism of action of artemisinin derivatives in cancer cells, and have gone on to show that artemisinin derivatives not only induce apoptosis and increase ROS production, but also inhibit angiogenesis and alter various signalling pathways involved in the proliferative, metastatic and invasive properties of cancer cells (Chen et al., 2010a; Crespo-Ortiz and Wei, 2012; Efferth et al., 2004; Konkimalla et al., 2009; Zhou et al., 2007). Some of these findings will be explored briefly.

Pancreatic cancer cells, BxPC-3 and AsPC-1 cells, treated with DHA and subjected to cell cycle analysis also demonstrated a G1-phase cell cycle arrest as well as NFκB inactivation (Chen et al., 2010a). NFκB has been associated with cell proliferation, invasion, angiogenesis, metastasis as well as suppression of apoptosis in cancer cells. The transcription factor is known to promote the growth of pancreatic cancer cells and Chen and colleagues found that DHA inhibited Bcl-2 and cyclin D1 in these cells in addition to NFκB inactivation (Chen et al., 2010a). Therefore, it was suggested that DHA induced cell cycle arrest and

apoptosis in pancreatic cancer cells as a result of inhibition of NFκB signalling (Chen et al., 2010a).

Other signalling pathways implicated in the anticancer activity of artemisinins include the Wnt/β-catenin pathway. Colorectal cancer cells treated with artesunate displayed a strong inhibition of the hyperactive Wnt/ß-catenin pathway, which is an important pathway for survival, proliferation and migration in many tissues (Li et al., 2007). Furthermore, studies have demonstrated the ability of ART and DHA to inhibit angiogenesis by downregulation of VEGF (Chen et al., 2003; Zhou et al., 2007), and inhibition of proliferation, movement and tube formation in human umbilical vein endothelial cell (Chen et al., 2003). Moreover, ART reduced angiogenesis in an in vivo experiment involving vascularisation of Matrigel plugs injected subcutaneously into mice (Dell'Eva et al., 2004). These studies, along with the numerous others, point to the artemisinins as attractive cancer chemotherapeutic drug candidates.

In addition to its antimalarial and anticancer properties, artemisinins also displayed evidence of antifungal and antiviral activity (Efferth et al., 2008; Galal et al., 2005; Romero et al., 2005). Therefore it represents a promising family of compounds that has great potential for repurposing. Although artemisinin derivatives have been shown to have anticancer effects and have been studied extensively in a wide variety of cancer cell lines such as breast cancer (Lai and Singh, 1995; Lai et al., 2005; Nakase et al., 2008; Singh and Lai, 2001; Tin et al., 2012), ovarian cancer (Chen et al., 2009a; Jiao et al., 2007), pancreatic cancer (Chen et al., 2010a; Du et al., 2010; Wang et al., 2010), prostate cancer (Huang et al., 2008; Morrissey et al., 2010; Nakase et al., 2009; Willoughby et al., 2009) and lung cancer (Lu et al., 2009; Mu

et al., 2008; Sadava et al., 2002; Zhao et al., 2011), the role of artemisinin derivatives in oesophageal cancer cells and the molecular mechanisms involved are not well known. It is therefore imperative that studies are performed to fully understand the effects of the artemisinins in oesophageal cancer, considering that it is one of the top ten most common types of cancer in the world with a poor overall response to current chemotherapeutic agents.

1.3.2.3 Rationale for design of novel compounds used in this study

Combination drug therapy is used in a wide variety of diseases, an approach that partners two or more drugs to increase the therapeutic effect and prevent resistance. In addition, this strategy reduces adverse side effects by allowing lower doses of each agent to be used. The treatment of OC frequently involves the use of cisplatin and 5-fluorouracil in combination, two drugs with differing structures and mechanisms of action. Another well known example, as mentioned above, is artesunate and amodiaquine that is used together to treat malaria in most African countries. An alternative approach based on this strategy of combination drug therapy is hybridization, a medicinal chemistry 'tool' that fuses two active drugs to produce a molecule with more potent activity than the parent compounds (Decker, 2011).

The development of hybrid molecules is a very useful drug discovery technique that aims to produce novel compounds with improved biological functions. Using one drug that contains the active moiety of a combination of drugs is a highly beneficial treatment option as this approach may involve lower drug doses and fewer side effects. The use of drug hybridization has been investigated quite broadly in the search for antimalarial, antibacterial and anticancer agents, as well agents that treat neurodegenerative disorders (Decker, 2011). Natural products

have been the main source of anticancer drugs in the past and hybrid drug design incorporating natural products has been a major focus area for many medicinal chemists (reviewed by Tietze et al., 2003; Decker, 2011). Of note, hybridizing compounds with artemisinin has produced several interesting new compounds that show good activity as antimalarial and anticancer agents (Lai et al., 2013).

One example is the DHA-quinine hybrids that have been reported that have more potent in vitro activity against the malaria parasite, *Plasmodium falciparum*, than the parent compounds alone (Walsh et al., 2007). Quinine, a natural product from the bark of the *Cinchona* tree, has been used for many years in the treatment of malaria and it is the structural basis from which chloroquine and mefloquine were designed. Chalcones are also natural products found abundantly in plants and are part of the flavanoid family. These compounds too have been hybridized with artemisinins by two different research groups who demonstrated that the hybrids displayed greater toxicity to cancer cells than the parent compounds alone (Ixe et al., 2011; Yang et al., 2009), thus achieving the objectives of hybrid compounds. The artemisinins are compounds with promising anticancer activity, largely due to the endoperoxide bridge, and therefore serve as excellent candidates for the synthesis of hybrid compounds with improved biological functions, as demonstrated above.

On the basis of these considerations and promising results achieved with artemisinins as both antimalarial and anticancer agents, this study undertook to investigate a series of novel artemisinin hybrid compounds designed and synthesized by the Department of Chemistry at the University of Cape Town. These compounds, to the best of our knowledge, have not been investigated for their biological effects against oesophageal cancer. Current oesophageal

cancer chemotherapy is limited by the development of resistance and adverse side effects, as described in Section 1.1.4. Therefore the investigation of more effective anticancer agents is required to circumvent these limitations. Considering that a large number of chemotherapeutic agents in current use were sought from natural sources, this study aimed to investigate the potential of compounds obtained from natural products that exploited innovative medicinal chemistry approaches to improve biological function.

1.4 Aim and Objectives

1.4.1 Aim:

Investigate the potential of artemisinin derivatives as chemotherapeutic agents and determine the mechanism of action in cultured oesophageal cancer cells.

1.4.2 Objectives:

- To determine the effect of artemisinin derivatives in an oesophageal cancer cell culture model.
- To investigate the cell death pathways activated by the artemisinin derivatives in oesophageal cancer cells.
- To identify signalling pathways that may contribute to anticancer activity

CHAPTER 2:

INVESTIGATING THE ANTICANCER POTENTIAL OF ARTEMISININ DERIVATIVES

2.1 Introduction

Currently, some of the key drivers associated with the extensive, worldwide search for novel chemotherapeutic agents are the serious side effects often accompanying cancer chemotherapy and the observation that cancer cells frequently develop resistance in response to therapy. Natural product drug discovery has in the past, and continues to be a significant source of new drugs, and this together with various medicinal chemistry approaches, such as the synthesis of hybrid compounds and repurposing "old" drugs, may increase the development of new lead anticancer agents with lower costs and in shorter time periods.

Artemisinin has been cited as one of the best examples of natural product drug discovery and development for its role as an antimalarial, according to a recent review by Cragg and Newman (Cragg and Newman, 2013). In addition, it is also a spectacular example of drug repurposing as many studies have demonstrated its anticancer properties, as discussed in Section 1.3.2.2. This study took advantage of artemisinin's repurposing potential by employing its reduction product, dihydroartemisinin (DHA), to form hybrid compounds with various other compounds in order to enhance anticancer activity. Colleagues from the Department of Chemistry at the University of Cape Town designed and synthesized novel

hybrid compounds by linking, in this case, artemisinin to other compounds to produce novel hybrid compounds. The work presented in this chapter explores the anticancer potential of these compounds in an oesophageal cancer cell culture model.

The MTT assay and GraphPad Prism software were (50% inhibitory concentration) employed to perform dose response curves and calculate IC_{50} values. The most active compounds were selected for further investigations including testing in a variety of cancer cell lines such as cervical, breast and liver cancer. Two non-cancerous cell types were also included to determine if the compounds displayed reduced activity against normal cells compared to cancer cells. Furthermore, the ability of the compounds to disturb the cell cycle was also analysed. The results discussed in this chapter provided initial evidence that the novel hybrid compounds are promising anticancer agents.

2.2 Results

2.2.1 The effect of a library of artemisinin derivatives on the proliferation of oesophageal squamous carcinoma cell lines

A total of twenty compounds were screened to determine their effect on cell proliferation. This panel of compounds included three first generation artemisinin derivatives, ART, DHA and artemether. The remaining sixteen compounds, with the exception of isatin (1*H*-indole-2,3-dione), were novel artemisinin hybrid compounds designed and synthesized by the Department of Chemistry at the University of Cape Town. The effects of the compounds were tested in an oesophageal cancer cell line (WHCO1) that has routinely been used as a model oesophageal cancer cell line in our laboratory (Stringer et al., 2013; Sunassee et al., 2013; Whibley et al., 2005, 2007). To determine the effect of the compounds on cell viability and proliferation, the MTT assay was performed. The IC_{50} values and 95% confidence intervals (CI) were calculated using GraphPad Prism version 5.00 for Windows, GraphPad Software, which generated IC_{50} curves, and each experiment was performed at least twice (Figure 2.1). IC_{50} is the minimum compound concentration required for 50% inhibition of cell growth. Table 2.1 shows the IC_{50} values obtained for the panel of 20 compounds tested in the WHCO1 cell lines and Figure 2.1 shows the dose-response curves obtained for ART and DHA.

ART was the most active first generation derivative yielding an IC_{50} value of 13.4 μM and artemether was completely inactive. DHA, the in vivo metabolite of some artemisinin derivatives (including ART), displayed a slightly higher IC_{50} value (20.0 μM) than ART in

WHCO1 cells (Figure 2.1). The novel compounds tested included three compounds that were completely inactive (Dihyate, EXP62A, EXP39) and one compound (EXP66B) that was insoluble (Table 2.1). The remaining twelve novel compounds yielded IC_{50} values ranging from 3.5 µM (EXP57EA) to 45.3 µM (EXP66A). The most active compounds (EXP57A, EXP57EA and EXP57FA), marked with an asterisk in Table 2.1, were chosen for further analysis together with the first generation derivatives, ART and DHA (Figure 2.2). Isatin, one of the natural product scaffolds used in the synthesis of the artemisinin hybrids that was included in this study, was completely inactive.

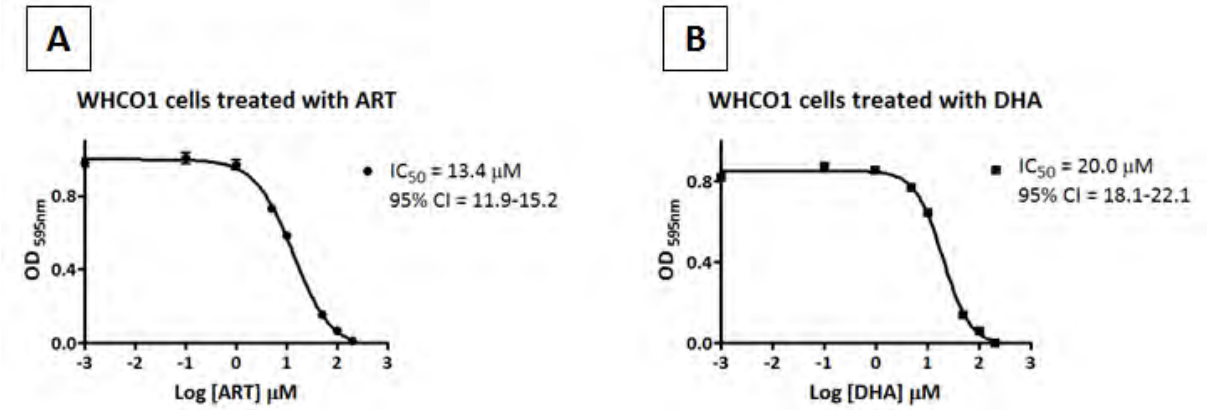

Figure 2.1: IC_{50} curves demonstrating sensitivity of WHCO1 cells to ART and DHA. WHCO1 cells were seeded at a density of 3000 cells per well in 96-well plates and were treated with a range of concentrations of ART (**A**) and DHA (**B**) to determine the IC_{50} values. Cells were incubated with ART and DHA for 48 h followed by the MTT assay. The absorbance was read using a multi-plate reader at 595 nm and data was analysed using GraphPad Prism software. Each point was performed in triplicate and error bars represent the mean ±SD. The experiments were independently repeated at least three times.

The most active novel compounds yielded IC_{50} values lower than that observed for the first generation derivatives (Table 2.1). The novel compounds chosen for further analysis (EXP57A, EXP57EA and EXP57FA) were artemisinin-isatin hybrids that were structurally identical except for the substitution of the different halogen side groups (Figure 2.2 B.1 - B.3).

Table 2.1: IC_{50} values for a panel of compounds tested in WHCO1 cells.

The MTT assay and GraphPad Prism software were used to calculate IC_{50} values and 95 % confidence intervals (CI) for a panel of 20 compounds consisting of the natural product scaffold isatin, 3 first generation artemisinin derivatives (ART, DHA and artemether) and 16 novel artemisinin hybrid compounds against WHCO1 cells. Cells were seeded in triplicate and each experiment was performed at least twice.

Compound	IC_{50} [µM]	95% CI
*ART	13.4	11.9 - 15.2
*DHA	20.0	18.1 – 22.1
Artemether	Inactive	
Dihyate	Inactive	
AJ19	14.7	12.9 - 16.6
AJ38	31.0	25.0 - 38.3
AJ2DH1	17.6	12.2 - 25.5
*EXP57A	6.6	5.3 – 8.1
EXP57BA	13.0	9.3 - 18.2
EXP57CC	25.9	14.7 - 45.6
EXP57D	12.7	9.5 - 17.1
*EXP57EA	3.5	2.4 – 5.1
*EXP57FA	10.0	7.8 - 12.9
EXP61C	39.1	35.5 - 43.1
EXP62A	Inactive	
EXP66A	45.3	31.6 - 64.9
EXP66B	Insoluble	Insoluble
EXP66C	44.1	39.3 - 49.6
EXP39	Inactive	
Isatin	Inactive	

**** Compounds chosen for further investigations***

The compound, EXP57EA, with an iodine group occupying the side chain was the most active with an IC_{50} value of 3.5 μM. Interestingly, isatin was completely inactive against WHCO1 cells but when fused with artemisinin, the hybrid compounds displayed lower IC_{50} values than either DHA (used in the synthesis of the artemisinin-isatin hybrids) or isatin.

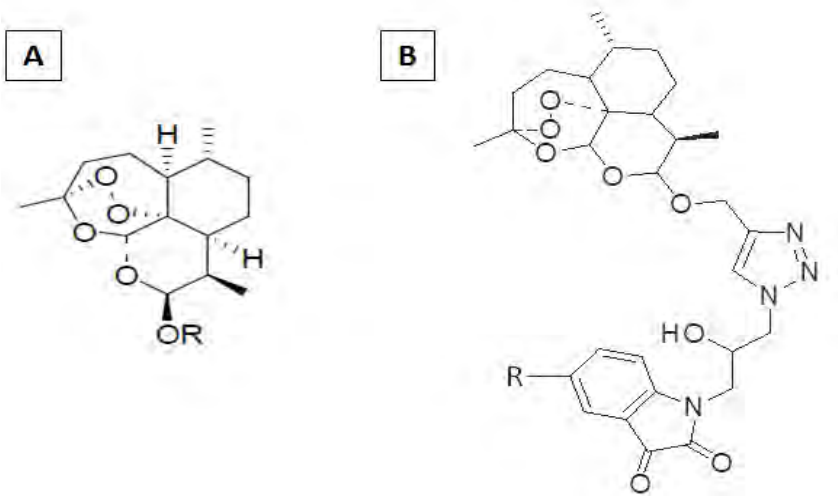

(A) First generation derivatives
(A.1) R = $CO(CH_2)_2CO_2Na$, ART

(A.2) R = H, DHA

(B) Novel artemisinin derivatives
(B.1) R = Cl, EXP57A

(B.2) R = I, EXP57EA

(B.3) R = Br, EXP57FA

Figure 2.2: Structure of artemisinin derivatives selected for further investigation. (**A**) The structures of the first generation derivatives ART (**A.1**) and DHA (**A.2**) are illustrated, (**B**) represents the novel artemisinin derivatives chosen for further investigation (**B.1**) – (**B.3**).

2.2.2 The effect of selected artemisinin derivatives on a broad panel of cancer cell lines

The artemisinin-isatin hybrids together with the parent compound, DHA, and another first generation artemisinin, ART, were tested against a number of cell lines, following the promising results obtained in the initial screens against WHCO1 cells. The cancer cell lines tested included six oesophageal cancer, three cervical cancer, three breast cancer cell lines as well as one liver cancer and one neuroblastoma cell line. As control cells, we routinely used human skin fibroblasts - DMB and FG^0 cells.

The three artemisinin-isatin hybrid compounds were more active than the first generation derivatives in all six oesophageal cancer cell lines tested. The OC cell lines were more sensitive to EXP57EA (average IC_{50} value across OC cell lines = 4.4 μM) than the other compounds EXP57A and EXP57FA (average IC_{50} values = 7.8 μM and 10.7 μM, respectively), suggesting that the iodine side chain conferred higher activity than the compounds containing the other side chains. As observed in WHCO1 cells, the other five OC cell lines treated with isatin were completely unaffected by this compound and continued proliferation at all treatment concentrations (Table 2.2).

Testing the selected panel of compounds against cervical cancer and breast cancer cell lines as well as a liver cancer and neuroblastoma cell lines, demonstrated that the artemisinin-isatin hybrids were more active than ART and DHA, as observed in the panel of OC cell lines (Table 2.2 and 2.3). A similar observation was made in the cervical, breast, liver and neuroblastoma cell lines regarding their response to isatin, where no IC_{50} values could be calculated due to inactivity (Table 2.3). In general, the cervical, breast, liver and neuroblastoma cell lines tested were less sensitive to the artemisinin derivatives than the OC cell lines. Furthermore, no IC_{50} values could be calculated for MDA-MB-231 cells treated with ART and DHA since this highly metastatic breast cancer cell line was completely insensitive to the first generation artemisinin derivatives. Following suit, the T47D breast cancer cell line displayed high IC_{50} values for ART and DHA (87.9 μM and 78.5 μM, respectively), compared to the MCF7 cell line (33.7 μM and 36.2 μM, respectively).

Table 2.2: IC_{50} values of selected compounds in a panel of oesophageal cancer cell lines.

The IC_{50} values (and 95 % CI) obtained for the selected artemisinin derivatives and isatin against six oesophageal cancer cell lines, three of South African origin (WHCO1, WHCO5 and WHCO6) and three of Japanese origin (KYSE30, KYSE150 and KYSE180). The MTT assay and GraphPad software were used to calculate IC_{50} values and 95 % CI.

	IC_{50} values in µM (95% CI)					
	ART	**DHA**	**EXP57A**	**EXP57EA**	**EXP57FA**	**ISATIN**
WHCO1	13.4	20.0	6.6	3.5	10.0	NA
WHCO5	30.1	26.9	10.0	6.0	15.0	NA
WHCO6	20.5	16.5	7.8	4.1	9.6	NA
KYSE30	17.3	14.6	8.3	3.7	13.0	NA
KYSE150	28.9	27.9	6.3	4.2	5.3	NA
KYSE180	13.8	18.3	7.7	4.7	11.1	NA

**NA = Not active at the highest concentration (200µM) tested*

The cervical cancer cell line, SiHa, also displayed decreased sensitivity to ART (82.2 µM) and DHA (77.4 µM) compared to the OC cell lines, where the average IC_{50} value calculated for both compounds was 20.7 µM. In fact, in the small panel of 3 cervical cancer cell lines examined, this cell line was most resistant to the first generation artemisinin derivatives. Similar activity profiles were observed for the CaSki and HeLa cell lines as well as for the HepG2 liver cancer cell line and the SK-N-SH neuroblastoma cell line. In summary, all the cell lines tested were more sensitive to the novel artemisinin-isatin hybrid compounds than the first generation artemisinin derivatives. Furthermore, isatin was completely inactive against all cancer cell lines tested here.

Table 2.3: IC_{50} values of selected compounds in a broad panel of cancer cell lines.

The IC_{50} values (and 95 % CI) obtained for the selected artemisinin derivatives and isatin against three cervical cancer cell lines (CaSki, HeLa and SiHa), three breast cancer cell lines (MCF7, MDA-MB-231 and T47D), a liver cancer cell line (HepG2) and a neuroblastoma cell line (SK-N-SH). The MTT assay and GraphPad Prism software were used to calculate IC_{50} values and 95 % CI.

	IC_{50} values in µM (95% CI)					
	ART	**DHA**	**EXP57A**	**EXP57EA**	**EXP57FA**	**ISATIN**
CaSki	32.9	39.4	14.3	14.4	16.3	NA
HeLa	28.3	21.4	13.0	13.0	15.8	NA
SiHa	82.2	77.4	19.0	18.0	18.5	NA
MCF7	33.7	36.2	21.7	13.0	27.9	NA
MDA-	NA	NA	26.3	16.9	22.3	NA
T47D	87.9	78.5	8.7	8.4	11.7	NA
HepG2	48.5	45.2	22.8	21.0	19.8	NA
SK-N-SH	36.9	40.3	21.7	22.0	17.7	NA

**NA = Not active at the highest concentration (200µM) tested*

We next tested the activity of the artemisinin hybrids against normal cultured fibroblasts compared to an oesophageal cancer cell line. In this study, cultured fibroblasts were used as a model for normal cultured cells considering that it is difficult to culture normal epithelial cells and since the immortalized normal epithelial cells typically used in this context may not reflect normal biology (Allen et al., 2005; Fenton and Hord, 2006; Haglund et al., 2012; Kroemer et al., 2009; Zang et al., 2012).

The first generation derivatives, ART and DHA, were nearly ten-fold and five-fold more effective at killing OC cells compared to DMB and FG^0 cells, respectively (Figure 2.3 A). However the novel compounds, EXP57A, EXP57EA and EXP57FA, were only between five-fold and two-fold more active in killing OC cells compared to normal fibroblasts (Figure 2.3 B). These results indicate that the novel artemisinin hybrid compounds were four to five times more active than the first generation artemisinin derivatives, and that they still retained some selectivity to cancer cells compared to normal cells albeit less so than the first generation derivatives.

We continued to explore the activity of the novel artemisinin hybrid compounds because of the increased activity displayed by these compounds in a variety of cancer cell lines, and the observation that these novel artemisinin hybrids also blocked the proliferation of cells that were shown to be insensitive or resistant to the first generation artemisinin derivatives.

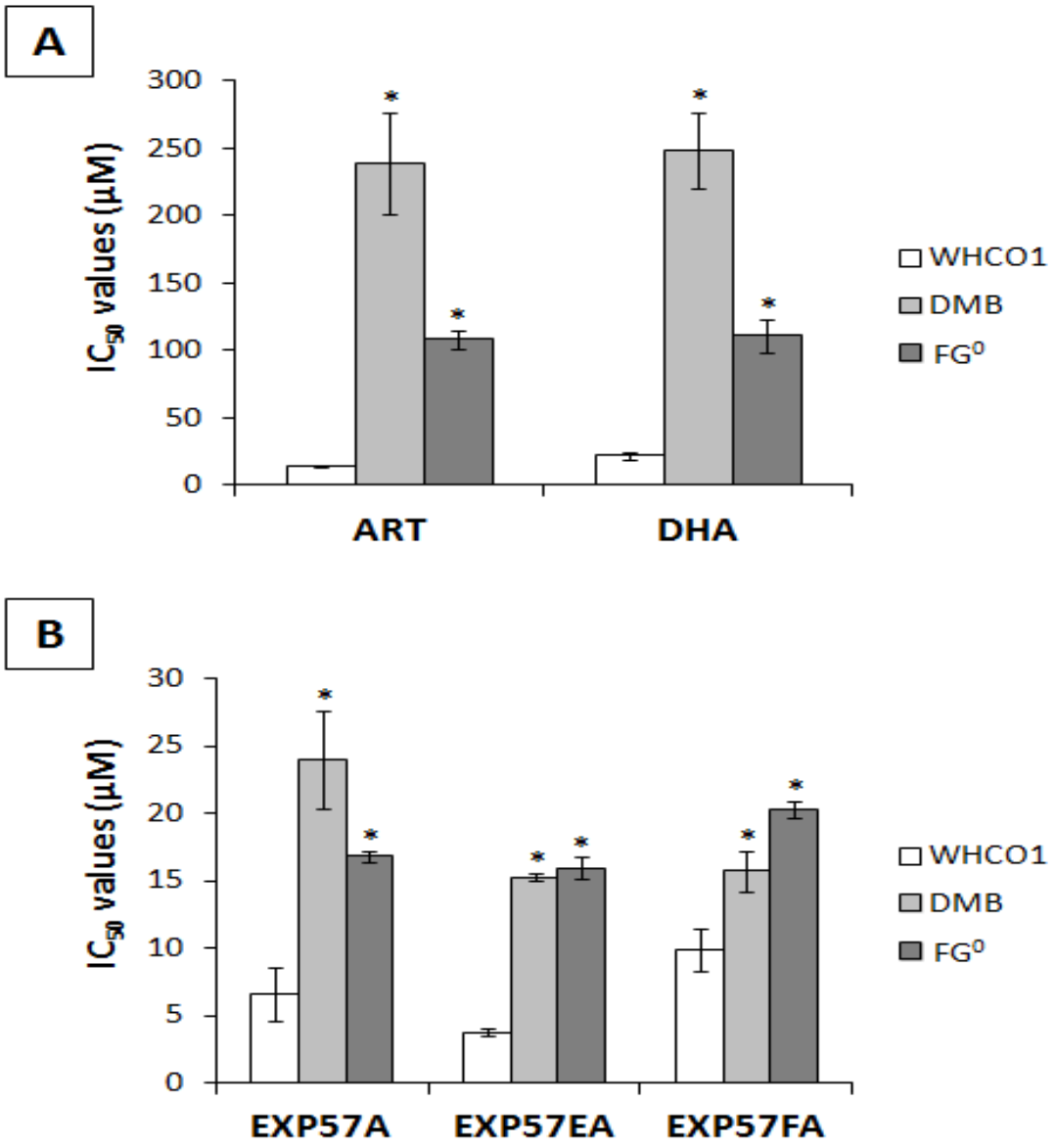

Figure 2.3: The effects artemisinin derivatives on fibroblast cells versus the oesophageal cancer cell line – WHCO1. WHCO1, DMB and FG^0 cells cultured in 96-well plates were treated with a range of either the first generation derivatives, ART and DHA **(A)**, or the novel artemisinin-isatin hybrids, EXP57A, EXP57EA or EXP57FA **(B)** followed by the MTT assay. The IC_{50} values were calculated using GraphPad Prism software and analysed based on 3 experiments. The error bars represent the mean ±SD. * $P<0.05$ compared with WHCO1-treated cells.

2.2.3 Investigating the growth inhibitory effects of artemisinin derivatives

A growth curve of cells treated with and without artemisinin derivatives was carried out over a period of 4 days (Figure 2.4). Cells were seeded at 1500 cells per well in quadruplicate in 96-well plates and allowed to settle overnight. This was followed by treatment with three concentrations of the indicated compound close to the IC_{50} value of each compound, for the indicated time, followed by the MTT assay. Cells treated with the vehicle, dimethyl sulphoxide (DMSO), only were included as the control and were represented by the dotted line in Figure 2.4 (A-E).

The effects of the novel artemisinin hybrid compounds can already be observed at the 24-hour time point for all concentrations tested. This effect on cell number was maintained up to the last time point tested (96 hours) (Figure 2.4 C-E). A similar observation was recorded for ART and DHA (Figure 2.4 A and B). The novel compound EXP57EA, at 12 μM, displayed a cell number lower than the cell number plated at the 24 hour time point, suggesting a cytotoxic effect.

To determine whether the reduced cell number caused by the artemisinin derivatives was associated with changes in the cell cycle progression, an analysis was performed comparing the cell cycle profiles of control (vehicle-only treatment) and compound-treated WHCO1 cells (Figures 2.5 and 2.6). WHCO1 cells were seeded in 100 mm dishes in triplicate and treated with varying concentrations of each compound for 24 and 48 hours. Cells were trypsinised, stained with propidium iodide and analysed by flow cytometry using a FACSCalibur machine together with CELLQuest Pro software and Modfit LT Version 3.2 software for data analysis.

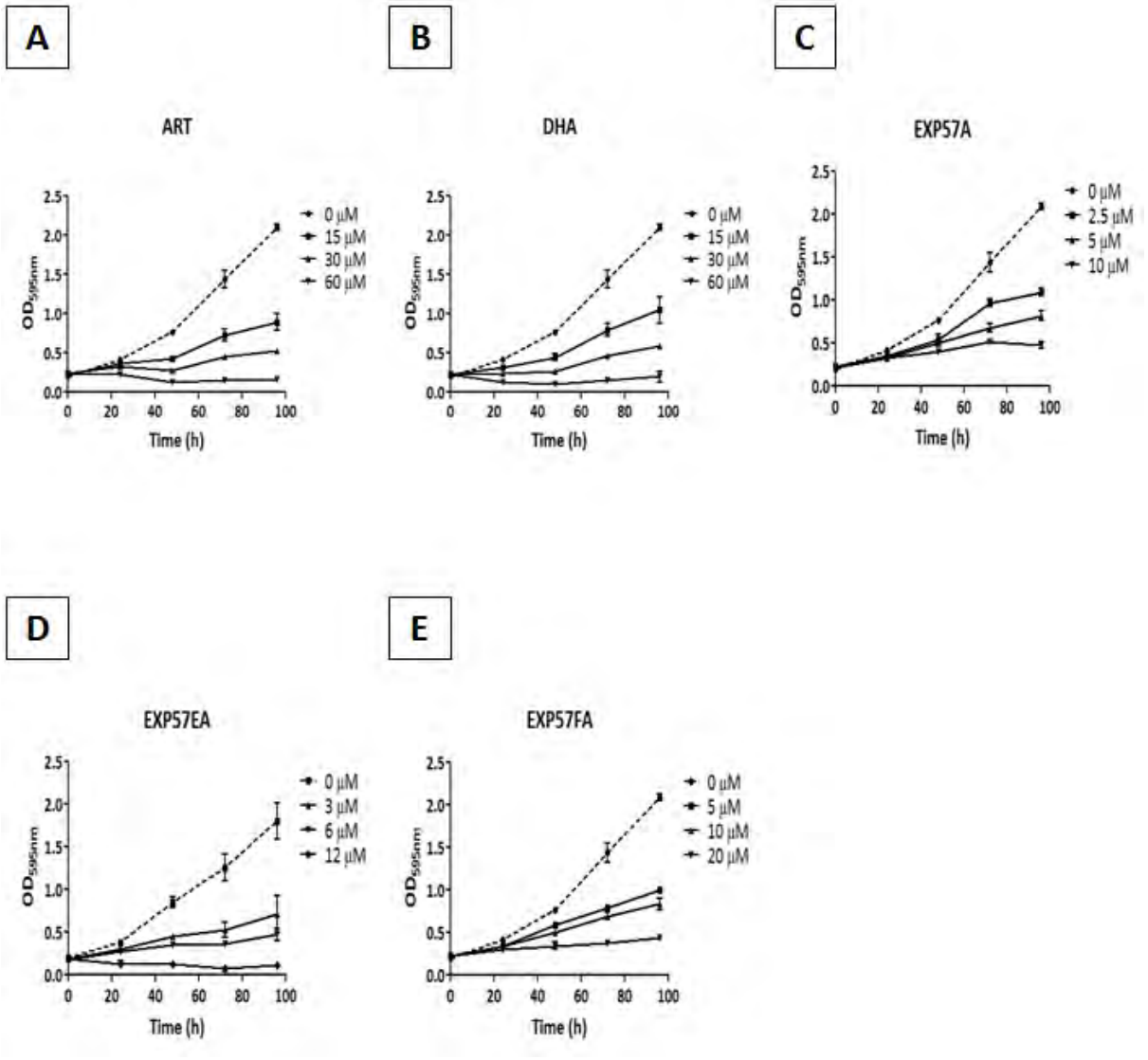

Figure 2.4: Growth curves of WHCO1 cells treated with artemisinin derivatives. Cells were seeded at a density of 1500 cells per well in quadruplicate and allowed to settle overnight before treatment with the artemisinin derivatives. Once the relevant time points had elapsed the MTT assay was performed. Each point represents the mean of 4 wells, with standard deviation, and this is representative of at least two independent experiments.

Treatment of WHCO1 cells with the artemisinin hybrid compounds was associated with an increase in the G0/G1 population at the 24-hour time point, and this was apparent at the lowest concentration of all hybrids tested. However, after 48 hours, EXP57A and EXP57EA

had no obvious effect on the G0/G1 pool size (relative to control), whereas EXP57FA still induced an increase in the G0/G1 pool size at 10 μM (Figure 2.5). These results are quite different from those observed for ART and DHA, which resulted in an increased G2/M pool size after treatment for 24 hours, which was sustained after 48 hours (Figure 2.6).

The results obtained from the cell cycle analysis indicated that first generation artemisinin derivatives and the novel artemisinin-isatin hybrid compounds exerted a biological effect on WHCO1 OC cells and that this warranted further investigation. Furthermore, ART and DHA acted in a similar manner by arresting cells in the G2/M phase of the cell cycle while the three hybrid compounds tested arrested cells in the G0/G1 phase of the cell cycle. From these observations it is fair to deduce that the mode of action of the novel compounds may be quite alike due to their close structural similarity. Bearing this in mind, as well as the limited amounts of compounds available it was decided that further investigations would be carried out on DHA and EXP57EA, the most active hybrid compound synthesized by the linkage of DHA to isatin.

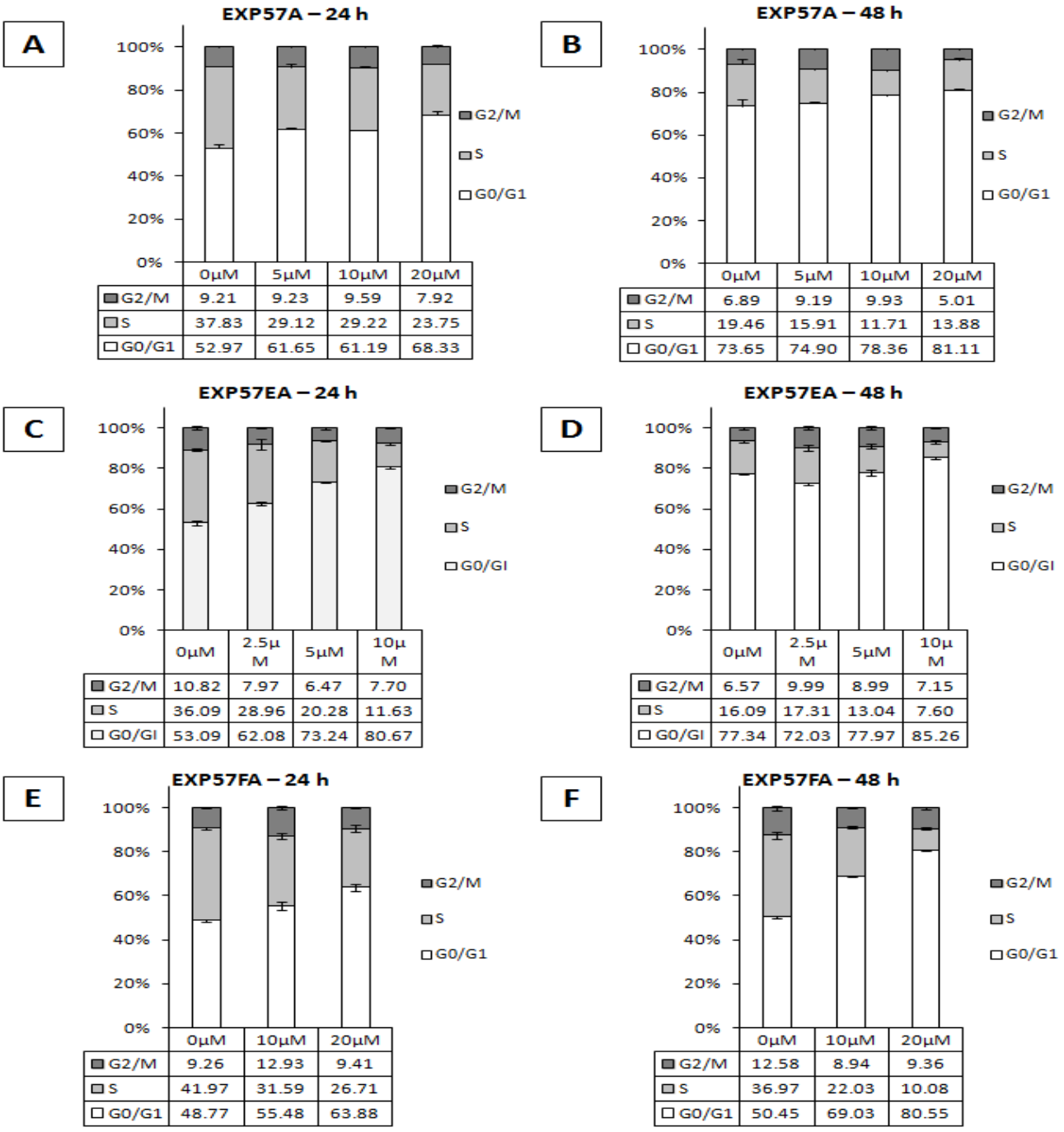

Figure 2.5: Cell cycle profile of WHCO1 cells treated with the artemisinin-isatin hybrids. WHCO1 cells were seeded at a density of 5 x 10^5 cells per 100 mm dish. The next day cells were treated with the indicated concentrations (in triplicate) of EXP57A **(A, B)**, EXP57EA **(C, D)** and EXP57FA **(E, F)** for 24 h **(A, C, E)** and 48 h **(B, D, F)**. Cells were processed for flow cytometry, stained with propidium iodide and analysed on a FACSCalibur machine using CELLQuest Pro software and Modfit LT version 3.2 for data analysis. The results are expressed as a mean of triplicates, with standard deviation indicated by the error bars.

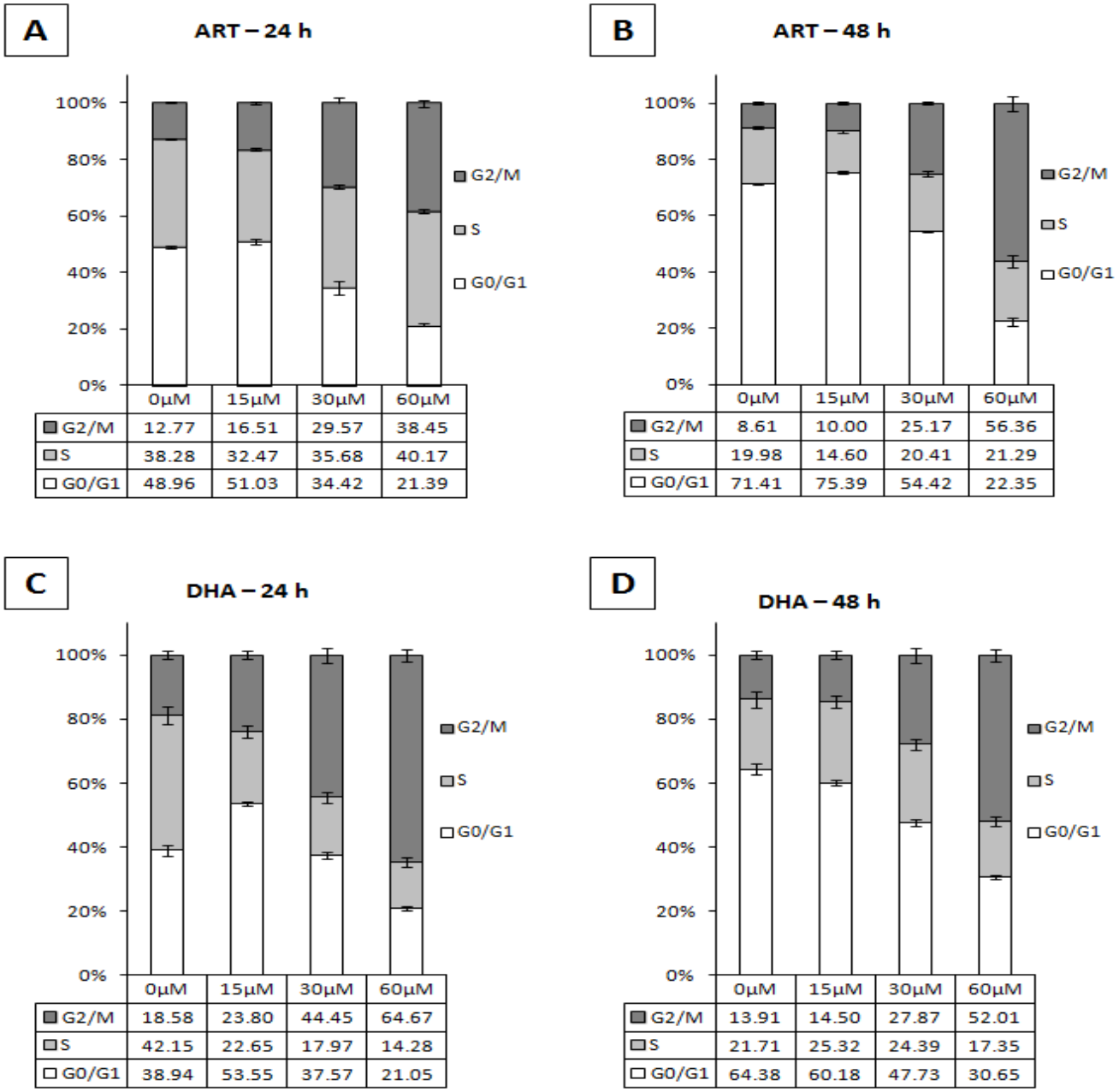

Figure 2.6: Cell cycle profile of WHCO1 cells treated with the first generation artemisinin derivatives. WHCO1 cells were seeded at a density of 5 x 10^5 cells per 100 mm dish in triplicate and cultured for 24 h. Once settled, cells were treated with 0 μM (vehicle-only), 15 μM, 30 μM and 60 μM of ART **(A, B)** and DHA **(C, D)** for 24 h **(A, C)** and 48 h **(B, D)**. Cells were processed for flow cytometry, stained with propidium iodide and analysed on a FACSCalibur machine using CELLQuest Pro software and Modfit LT version 3.2 for data analysis. The results are expressed as a mean of triplicates, with standard deviation indicated by the error bars.

2.2.4 Structure-activity analysis of EXP57EA

The novel artemisinin-isatin hybrid, EXP57EA, was the most active novel compound tested in this study. In addition, we observed that this novel compound displayed activity against cells insensitive to ART and DHA, the first generation artemisinin derivatives. EXP57EA, distinguished from the other novel artemisinin-isatin hybrid compounds by the iodine side chain, was synthesized via covalent linkage of the dihydroartemisinin intermediate compound (IM1, Figure 2.7) to the iodo-isatin azide intermediate compound (IM2, Figure 2.7) using 'click' chemistry (Hans, 2009). Each of the intermediates involved in the synthesis of EXP57EA was tested for activity against WHCO1 and WHCO6 OC cells (Table 2.4).

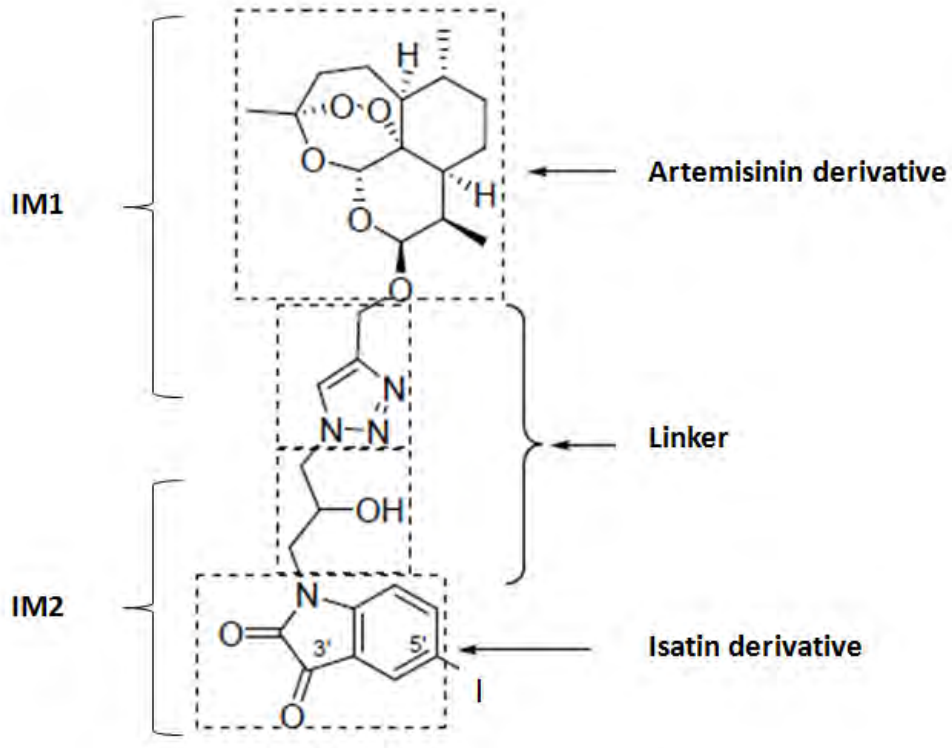

Figure 2.7: General structure showing design of EXP57EA. The chemical structure of EXP57EA illustrating the intermediate compounds that were covalently linked to form the artemisinin-isatin hybrid.

Table 2.4: The effects of the intermediate compounds involved in the synthesis of EXP57EA against WHCO1 and WHCO6 OC cells.

The IC_{50} values (and 95 % CI) obtained for the panel of intermediate compounds including the parent compounds, DHA and EXP57EA, against WHCO1 and WHCO6 oesophageal cancer cells. The MTT assay and GraphPad Prism software were used to calculate IC_{50} values and 95% CI.

	IC_{50} values in µM	
	WHCO1	**WHCO6**
DHA	21.4	23.8
Isatin	NA	NA
Iodoisatin	19.95	17.05
IM1	NA	NA
IM2	20.73	20.70
EXP57EA	4.2	7.6
DHA	21.4	23.8

**NA = Not active at the highest concentration (200µM) tested*

The results obtained after WHCO1 and WHCO6 OC cells were treated with the various chemical moieties involved in the synthesis of EXP57EA showed that isatin had no effect against OC cells (and a variety of other cancer cell lines) and that an IC_{50} value could not be calculated. However, when halogenated with an iodine molecule, forming iodo-isatin, a distinct improvement in activity was observed, demonstrated by IC_{50} values close to those obtained for DHA in WHCO1 and WHCO6 cells (Table 2.4). Interestingly, the intermediate DHA compound synthesized (IM1) for linkage with the isatin intermediate compound was

completely inactive as the cells continued proliferation even at the highest treatment concentration tested (200 μM). On the contrary, the isatin intermediate compound (IM2) was more potent than IM1 with IC_{50} values close to those of DHA and iodoisatin (Table 2.4). The fusion of IM1 and IM2 produced the artemisinin hybrid compound, EXP57EA, with IC_{50} values lower than that of DHA and the intermediate compounds in both OC cell lines tested, which is quite remarkable (Table 2.4).

2.3 Discussion

In this project the effect of ART and DHA (first generation derivatives of artemisinin) together with a panel of novel artemisinin hybrid compounds was assessed on oesophageal cancer cell lines. The novel derivatives were designed and synthesized by the Department of Chemistry at the University of Cape Town. These compounds include the active moiety of DHA (containing the endoperoxide bridge) linked to the active part of other compounds, forming novel hybrid molecules. A series of nineteen artemisinin derivatives were screened for activity against the WHCO1 oesophageal cancer cell line. Active compounds were chosen based on an arbitrary cut off IC_{50} value of 10 μM, which was also used in studies discussed by other authors (Koch et al., 2004; Newman, 2008). Previous reports in our laboratory demonstrated that WHCO1 treated with cisplatin generated an IC_{50} value of 14 μM (Wyk et al., 2008), therefore the aim was to identify novel compounds with better activity against oesophageal cancer cells.

Of the nineteen compounds tested, three represented first generation derivatives (ART, DHA and artemether). Artemether was inactive against WHCO1 cells but ART and DHA displayed IC_{50} values of 13.4 μM and 20.0 μM, respectively, which compared favourably with the IC_{50} value of cisplatin against WHCO1 cells. Hybrid compounds were synthesized by linking the artemisinin derivative, DHA, to compounds such as azidothymidine (Dihyate), chloroquine (AJ19) and isatin (EXPCC). Dihyate was completely inactive in our system and AJ19 generated an IC_{50} value of 14.7 μM, which was similar to that of cisplatin in WHCO1 but did not match the chosen criteria of 10 μM or below. When DHA was hybridized with isatin (a compound that is completely inactive against all cancer cell lines tested) forming

(EXP57CC), an IC_{50} value of 25.9 μM was achieved. However, when DHA-isatin hybrids (referred to as artemisinin-isatin hybrids) were halogenated (EXP57A, EXP57BA, EXP57EA and EXP57FA) a distinct improvement in activity was observed. Isatins represent a class of heterocyclic compounds that is well known for their synthetic versatility and was also found to possess anticancer activity especially when halogenated (Sabet et al., 2010; Vine et al., 2007). Previous studies demonstrated that bromine attached to isatin conferred potent anticancer activity compared to other halogen side chains (Vine et al., 2007). Interestingly, in this study we found that the iodine side chain (EXP57EA) displayed more than two-fold better activity than the bromine side chain (EXP57FA), generating an IC_{50} value of 3.5 μM. When the various intermediate moieties used in the synthesis of EXP57EA were tested, it was shown that none compared to the activity of the whole structure.

In addition to EXP57EA, two other artemisinin-isatin novel hybrid compounds, EXP57A and EXP57FA, displayed IC_{50} values of 10 μM and below, which fell within the pre-specified criteria. Further IC_{50} experiments were carried out against a range of cancer cell lines including oesophageal cancer, cervical cancer, breast cancer, liver cancer and neuroblastoma cell lines, as well as fibroblasts, DMB and FG^0. When tested against the two normal skin fibroblast cells, the first generation artemisinin derivatives, ART and DHA, displayed significantly higher IC_{50} values compared to the values obtained for WHCO1 cells. The novel hybrid artemisinin derivatives displayed decreased activity in the DMB and FG^0 cells compared to WHCO1 cells, although not to the same extent as the first generation derivatives. However, the three novel hybrid compounds were reproducibly more active than the first generation derivatives in all cancer cell lines tested. EXP57A, EXP57EA and EXP57FA generated very similar IC_{50} values in all cell lines with the exception of the two breast cancer cell lines MCF7 and MDA-MB-231 and all the OC cell lines, where EXP57EA

was more active than EXP57A and EXP57FA. Notably, cell lines that frequently display resistance to chemotherapeutic agents, such as SiHa, MDA-MB-231 and T47D (Ciucci et al., 2006; Saxena et al., 2005), also displayed decreased sensitivity to ART and DHA with IC_{50} values well above 50 μM, but these cell lines were quite sensitive to the novel compounds, particularly EXP57EA.

Further biological exploration of the effects of the compounds showed that the novel compounds had an inhibitory effect on WHCO1 growth and proliferation over time, comparable to the first generation derivatives. ART and DHA have been shown by previous investigators to be implicated in cell cycle arrest in various types of cancer cells, particularly the G0/G1 phase of the cell cycle (Hou et al., 2008; Jiang et al., 2012; Lai et al., 2013; Li et al., 2001; Michaelis et al., 2010; Morrissey et al., 2010; Tin et al., 2012; Tran et al., 2013; Wang et al., 2010; Willoughby et al., 2009; Wu et al., 2011). However, other studies have reported that the first generation derivatives induced a G2/M cell cycle arrest in various cancer cells including osteosarcoma, leukaemia, pancreatic, ovarian and non-small cell lung cancer (Ji et al., 2011; Jiao et al., 2007; Zhao et al., 2011; Zhou et al., 2007). In this study, WHCO1 oesophageal cancer cells treated with ART and DHA arrested cells in the G2/M phase of the cell cycle after 24 hours and 48 hours.

In contrast, the novel hybrid compounds (EXP57A, EXP57EA and EXP57FA) arrested cells in the G0/G1 phase of the cell cycle after 24 hours and 48 hours. The results obtained here provided the first indication that the novel halogenated isatin-artemisinin hybrid compounds had a mechanism of action that differs from that of the first generation derivatives ART and DHA. In addition, these results clearly showed that the first generation derivatives ART and

DHA acted similarly (both induced a G2/M cell cycle arrest) in the model cell culture system employed in this study, whereas the hybrid compounds induced a G0/G1 cell cycle arrest. Since compound availability was one of the problems experienced during this project, it was decided that further investigations would be continued on the first generation derivative DHA and the most active novel compound EXP57EA.

The results obtained from this study are consistent with previous reports suggesting the anticancer activity of the first generation derivatives, ART and DHA. The novel artemisinin-isatin hybrid compounds displayed better activity than the first generation derivatives against cancer cell lines tested. The aim of synthesizing hybrid compounds is to produce compounds that have better activity than the parent compounds (Meunier, 2008). The results presented here indicated that this has been achieved where EXP57EA was more active than both DHA and isatin against the cancer cells tested in this study. Hybrid compounds are believed to be pharmacologically different from the parent compounds displaying properties that may differ from parent compounds (Decker, 2011). The initial biological investigation (cell cycle analysis) indicates that the first generation derivatives may have a different molecular mechanism of action compared to the hybrid compounds. Further mechanistic studies are warranted, and due to compound availability, will be continued using DHA and the most active artemisinin-isatin hybrid compound, EXP57EA. It would be valuable to elucidate EXP57EA's biological functions in our oesophageal cancer cell culture model system in comparison with the parental compound, DHA.

CHAPTER 3:

CHARACTERISING THE CYTOTOXIC EFFECTS OF DIHYDROARTEMISININ AND EXP57EA

3.1 Introduction

In the previous chapter, we determined that the novel artemisinin-isatin hybrid compounds were more active than the first generation artemisinin derivatives against oesophageal cancer. Furthermore, the novel compounds were more active than the first generation artemisinin derivatives when tested against previously recognised chemoresistant cell lines. An investigation into the effects of the compounds on the cell cycle revealed that the novel hybrid compounds arrested cells in a different phase of the cell cycle compared to the parental compounds, suggesting that these novel compounds required further investigation in oesophageal cancer.

Since the small panel of novel artemisinin-isatin hybrid compounds displayed similar results and due to compound availability, further studies were performed with the most active artemisinin-hybrid compound, EXP57EA. Furthermore, the parental compounds also displayed similar results therefore DHA was selected for the mechanistic investigation alongside EXP57EA. Previous studies have reported the anticancer effects of DHA, and demonstrated the ability of DHA to induce apoptosis in a number of cancer cell lines (Chen et al., 2010a; Fujita et al., 2008; Hou et al., 2008; Huang et al., 2007; Ji et al., 2011; Jiao et al., 2007; Lu et al., 2008, 2009; Mu et al., 2008; Singh and Lai, 2004, 2001). Therefore, in order

to understand how DHA and EXP57EA caused cell death in oesophageal cancer cells we investigated apoptosis as a possible pathway, using the PARP (poly (ADP-ribose) polymerase) cleavage assay and analysis of activated caspase 3/7 to establish the extent of apoptosis.

Having determined that DHA induced apoptosis in oesophageal cancer cells and that EXP57EA did not, other cell death mechanisms were investigated. Using lactate dehydrogenase (LDH) release to measure necrosis, we showed that both compounds did not induce this type of cell death. Morphological studies confirmed these results but also revealed increased perinuclear vacuoles in EXP57EA-treated cells, indicating that the novel compound may activate autophagy. Quantitative real time reverse transcription polymerase chain reaction (RT-PCR) and western blot analysis were used to investigate the expression of important autophagy regulatory proteins. Furthermore, immunofluorescent analysis and transmission electron microscopy (TEM) were also employed to demonstrate the appearance of autophagosome-bound LC3-II and the perinuclear localisation of autophagosomes, respectively. Furthermore, experiments demonstrating autophagic flux and inhibition of autophagy were performed to establish the importance of this pathway in EXP57EA-induced cytotoxicity.

3.2 Results

3.2.1 Effect of DHA and EXP57EA on morphology of oesophageal squamous carcinoma cells

To determine the effect of DHA and EXP57EA on cell morphology, treated cells were observed under light microscopy. Images were captured with an Olympus CKX42 inverted phase contrast microscope with an Olympus CMOS Colour Camera for Light Microscopy SC30 and analysis® getIT! image software (Centre Valley, USA). After exposure to DHA and EXP57EA for 24 and 48 hours, marked morphological changes were observed in WHCO1 cells (Figure 3.1).

The morphological changes of cells treated with 60 μM DHA (Figure 3.1 C and D) were suggestive of apoptosis. Nuclear condensation and shrinkage of the cytoplasm was observed most clearly at the 48 hour treatment point (Figure 3.1 D). Apoptotic bodies displaying membrane blebbing were also visible. Such apoptotic features were not observed in the control cells. These morphological features strongly suggested that DHA induced apoptosis in WHCO1 oesophageal cancer cells.

Cells treated with 10 μM EXP57EA did not exhibit the same morphological features observed in cells treated with DHA (Figure 3.1 E and F). Instead, after 24 hours and 48 hours of treatment with EXP57EA numerous intracellular, perinuclear vacuoles were observed. The formation of the vacuoles occurred in a dose- (data not shown) and a time-dependent manner.

Also, unlike cells treated with DHA, the cells treated with EXP57EA appeared to maintain nuclear integrity even at the 48 hour treatment point.

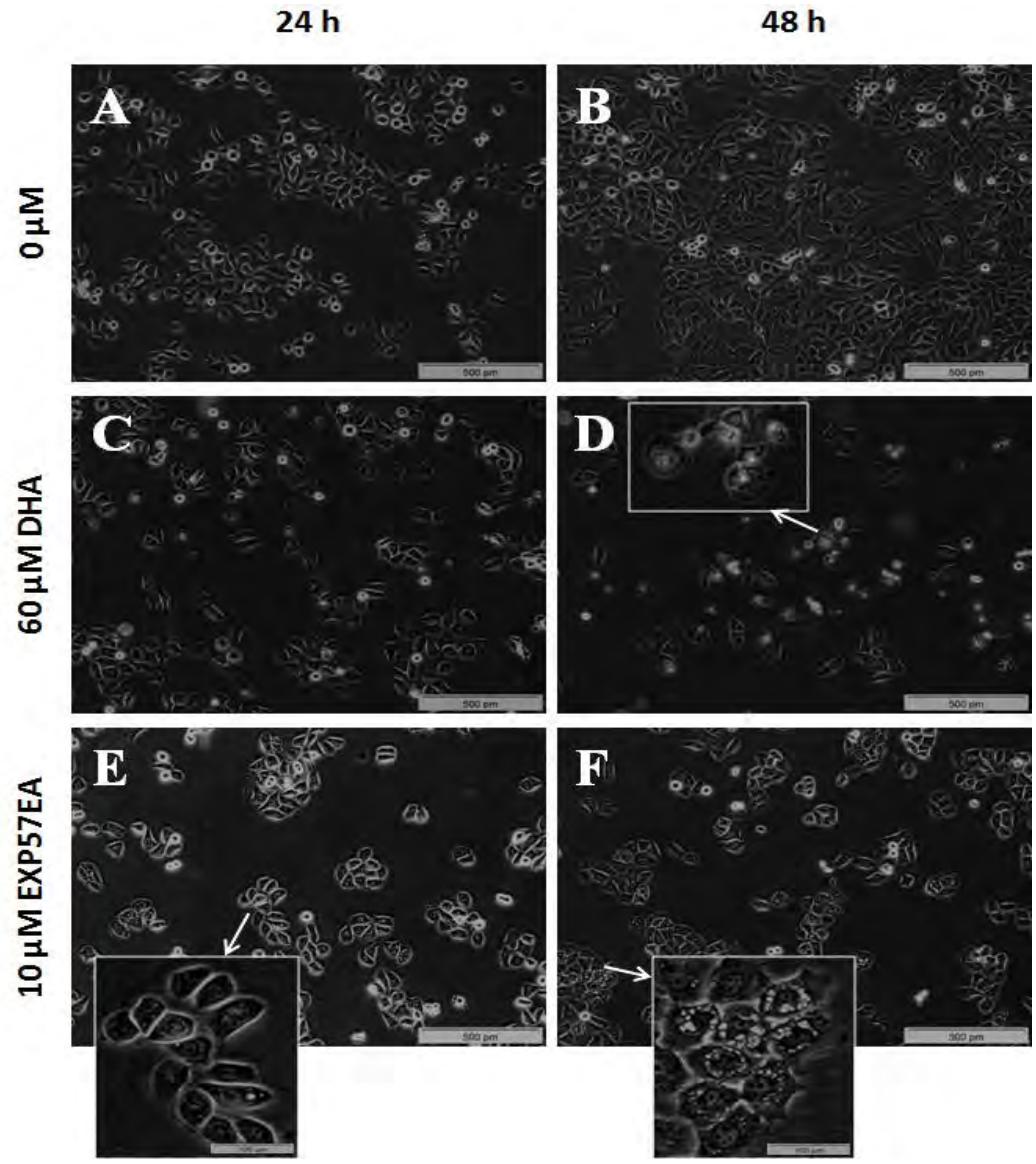

Figure 3.1: Morphology of WHCO1 cells exposed to DMSO only (A-B), DHA (C-D) and EXP57EA (E-F). Cells (300 000) were plated in 60 mm dishes and allowed to settle overnight followed by the addition of 60 µM DHA, 10 µM EXP57EA or DMSO (vehicle). After the indicated time periods, images of the cells were captured using an Olympus CKX41 microscope with an Olympus CMOS Colour Camera for Light Microscopy SC30 and analysis® getIT! image software. DHA-treated cells exhibited features consistent with apoptosis whereas cells treated with EXP57EA did not. Instead, a striking accumulation of perinuclear vacuoles were observed in cells treated with EXP57EA.

3.2.2 Determining the cell death mechanisms engaged by DHA and EXP57EA in oesophageal squamous carcinoma cells

The mechanisms by which cancer chemotherapeutic agents cause cell death is important since there is a common view that apoptosis is the preferred cell death pathway (Fulda and Debatin, 2006; Green and Kroemer, 2005; Lockshin and Zakeri, 2004; Reed, 2003) given that it does not induce an inflammatory response, and is probably most often activated by anticancer drugs (Fischer and Schulze-Osthoff, 2005; Hotchkiss et al., 2009; Kim et al., 2002).

In order to determine whether DHA and EXP57EA induced apoptosis in oesophageal cancer cells, a PARP cleavage assay was performed. PARP is a known caspase substrate and cleavage of PARP into two distinct fragments (116 kDa and 85 kDa) is frequently used as a marker of apoptosis (Boulares et al., 1999; Germain et al., 1999). PARP cleavage was investigated by western blot analysis using WHCO1 and WHCO6 cells treated with 5 μM doxorubicin (DOX) for 24 hours as a positive control and β-Tubulin as a loading control (Figure 3.2 A). WHCO1 cells treated with DHA showed a clear dose-dependent increase in PARP cleavage after 24 and 48 hours, whereas treatment with EXP57EA (57EA) induced very low levels of cleaved PARP after 24 hours which was not observed at the 48 hour treatment point. A similar result was observed in WHCO6 cells. These results were consistent with the morphological changes observed (Figure 3.1) where cells treated with DHA showed clear evidence of apoptosis, which were not observed in EXP57EA-treated cells.

To confirm that EXP57EA does not induce apoptosis in WHCO1 and WHCO6 cells, an assay to measure levels of activated caspase-3 or caspase-7 was performed. The activation of executioner caspases, caspase 3 and 7, are biochemically important and the levels of activated caspase 3/7 are often used to measure apoptosis. This was done using the Caspase-Glo™ 3/7 Assay kit by Promega (Cat#G8090) that detects luminescence after cleavage of a substrate specific for activated caspase-3 or caspase-7. Cells were treated (in triplicate) with varying concentrations of DHA and EXP57EA for 24 hours followed by the addition of the Caspase-Glo reagent. Luminescence was read using a Veritas^{TM} microplate luminometer (Promega) and the results were expressed relative to the caspase-3/7 activity observed in untreated cells, and the data was plotted as shown in Figures 3.2 (B) and 3.2 (C). As observed in the PARP cleavage assay, both cell lines treated with DHA displayed a significant dose-dependent increase in caspase-3/7 activity (Figure 3.2 B - C). The results obtained here further confirmed that EXP57EA does not induce apoptosis in WHCO1 and WHCO6 oesophageal cancer cells at both concentrations tested.

A necrosis assay was performed using the CytoTox-ONE Homogeneous Membrane Integrity assay by Promega (Cat#G7891) to determine whether EXP57EA caused necrosis. As discussed in Chapter 1, necrosis is characterised by swelling of cells that eventually leads to cell lysis, followed by inflammation. The above-mentioned assay measured levels of LDH released by cells as an indication of necrosis. The kit included a reagent which fluoresced in response to cleavage by LDH. This fluorescence was measured using a fluorescence spectrophotometer (Cary Eclipse, Varian, Inc) and the readings represented the levels of necrosis that took place. Cells were plated in quadruplicate and treated with varying concentrations of DHA and EXP57EA. Considering that LDH has a short half-life (Promega, 2009), the cells were treated for 6 hours after which the CytoTox-One reagent was added to

each well. A lysis buffer supplied with the kit served as a positive control, and the results are calculated as the percentage of the fluorescence signal measured for the control (Figures 3.3 A and 3.3 B).

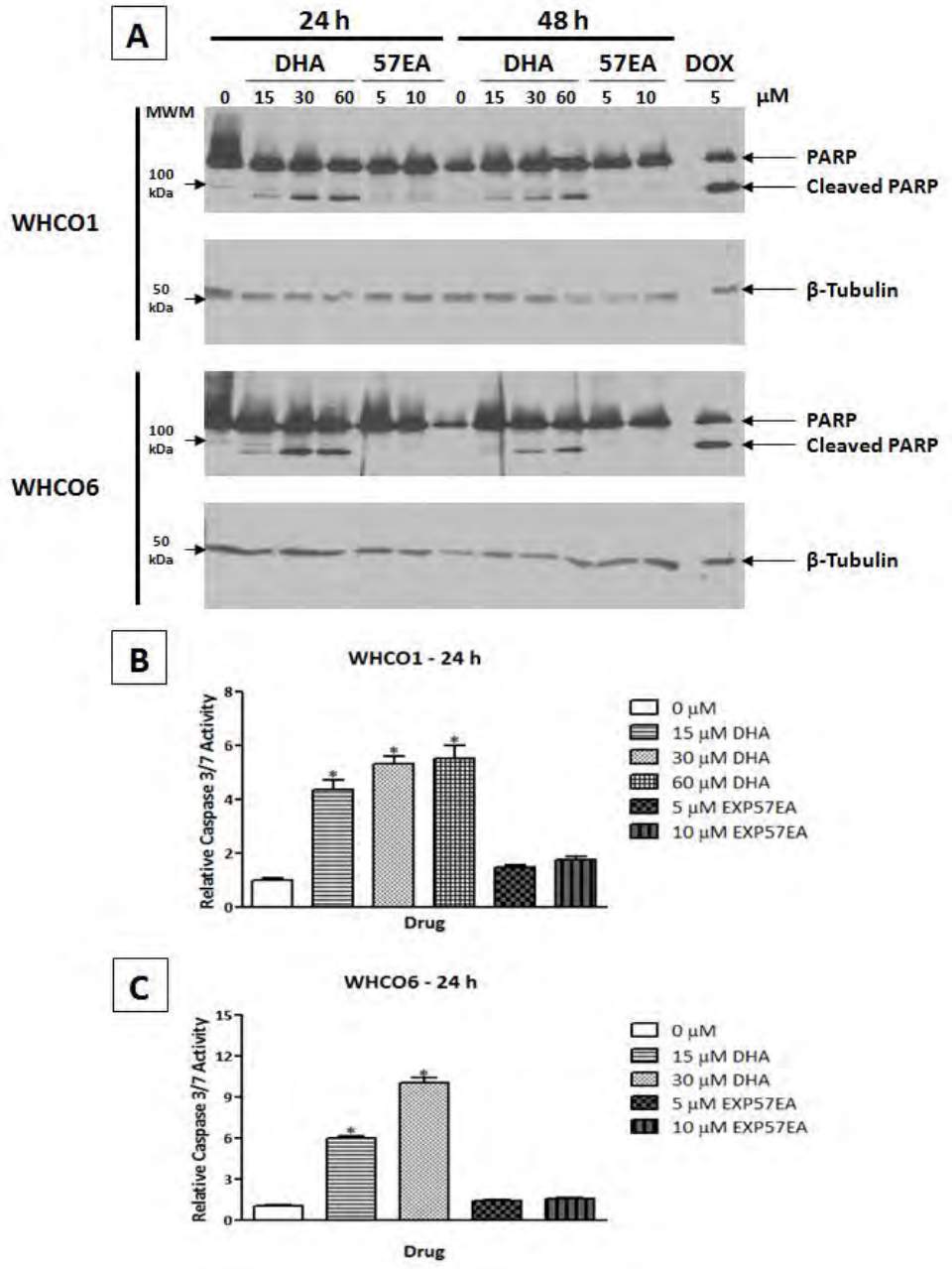

Figure 3.2: Effect of compounds on PARP cleavage (A) and caspase-3/7 activity (B and C). (A), PARP cleavage was used as an indicator of apoptosis. Western blot analysis of WHCO1 and WHCO6 oesophageal cancer cells treated with varying concentrations of DHA and EXP57EA for 24 h and 48 h. Cells treated with 5 µM doxorubicin (DOX) for 24 h were included as a positive control for PARP cleavage. Beta-Tubulin was used as a loading control. To confirm PARP cleavage results, Caspase-3/7 activity was measured in WHCO1 **(B)** and

WHCO6 **(C)** cells treated with the specified concentrations of DHA and EXP57EA for 24 h. Caspase-Glo reagent was added, and the luminescence measured on a Veritas™ microplate Luminometer (Promega). Results are shown relative to Caspase-3/7 activity in control (vehicle-treated) cells, and are represented as the mean ±SD of experiments performed in triplicate and repeated at least two times. *p < 0.05

As shown in Figure 3.3 (A), WHCO1 cells treated with 15 µM and 30 µM DHA for 6 hours displayed no significant increase in LDH activity compared to untreated cells. A similar result was obtained for EXP57EA-treated cells (Figure 3.3 B). Therefore, the results obtained thus far indicate that DHA caused apoptosis and not necrosis in oesophageal cancer cells, whereas EXP57EA caused neither under the described treatment conditions. To characterise the processes associated with the decreased cell number subsequent to EXP57EA treatment, we followed up on the numerous perinuclear vacuoles observed in EXP57EA-treated cells.

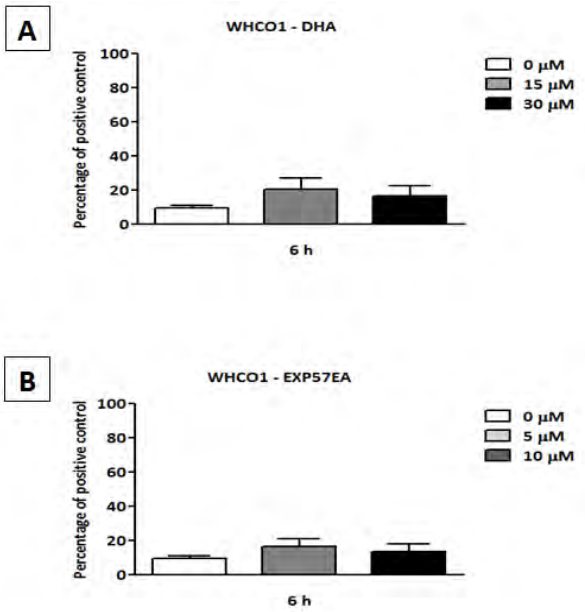

Figure 3.3: Effect of DHA and EXP57EA on LDH release in WHCO1 cells. The ability of DHA **(A)** and EXP57EA **(B)** to induce necrosis was evaluated using LDH release as a marker of necrosis. Cells were treated with the indicated concentrations of DHA or EXP57EA in quadruplicate for 6 h after which CytotoxONE reagent was added. Fluorescence was measured using a fluorescence spectrophotometer. Results are expressed as a percentage of the fluorescent signal obtained for the positive control (lysis buffer) and are represented as the mean ±SD of experiments performed in quadruplicate and repeated at least two times.*p<0.05

As mentioned, treatment of WHCO1 cells with EXP57EA resulted in a substantial increase in perinuclear vacuoles when compared to untreated cells (Figures 3.1 E and 3.1 F) and this was not observed in cells treated with DHA (Figures 3.1 C and 3.1 D). The formation of vacuoles within cells after treatment with chemical compounds could suggest the activation of autophagy (Klionsky et al., 2009). Autophagy is an alternate pathway that could result in cell death (Galluzzi et al., 2012; Kroemer et al., 2009) and a number of markers are available to test for the activation of this pathway. Beclin 1 and Atg5 are essential proteins involved in the formation of the autophagosome (autophagic vacuoles), and LC3-II is another important marker of autophagy. The elongation of the autophagosome requires the conversion of LC3-I to LC3-II which is membrane bound and the only known autophagy protein found on the completed autophagosome. To investigate whether EXP57EA induced autophagy in oesophageal cancer cells, the mRNA levels of Beclin 1 and Atg5 were analysed using quantitative real time RT-PCR. Western blot analysis and immunofluorescence analysis were employed to examine the changes in LC3-II expression levels after treatment with EXP57EA.

Figure 3.4 shows the expression levels of Beclin 1 (Figure 3.4 A) and Atg5 (Figure 3.4 B) corrected to the housekeeping gene GusB (*β-glucoronidase*) after WHCO1 cells were treated with 5 μM and 10 μM EXP57EA for 24 hours. Cells treated with the vehicle only (0 μM) served as the control, and all the values were expressed relative to the control value. A significant increase in Beclin 1 expression levels was observed in cells treated with both 5 μM and 10 μM EXP57EA (Figure 3.4 A) compared to vehicle-treated cells. A 1.8-fold increase in Atg5 expression levels was observed in cells treated with 10 μM EXP57EA (Figure 3.4 B). These results suggested that EXP57EA played a role in the induction of autophagy in oesophageal cancer cells but to confirm this, the expression levels of LC3-II was also evaluated.

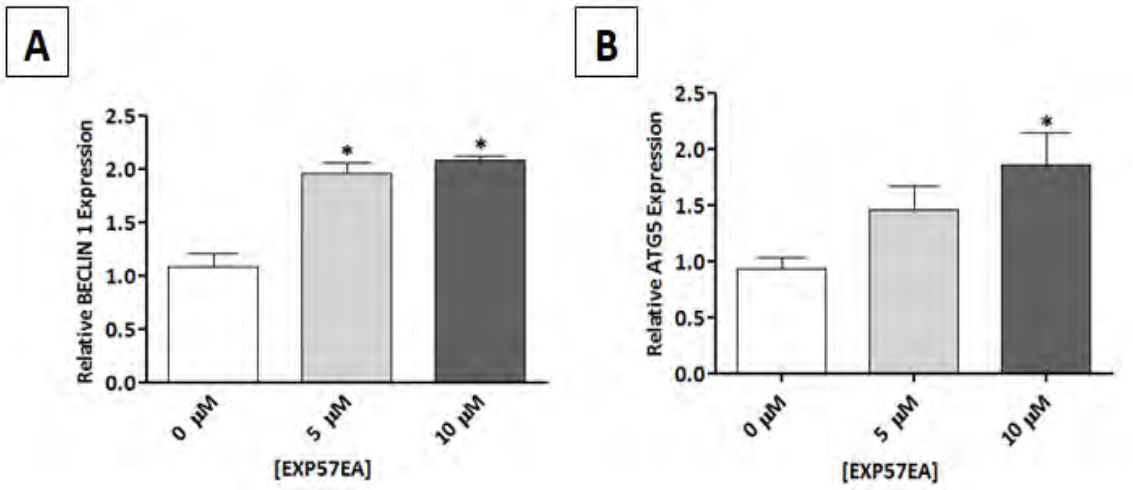

Figure 3.4: Evaluation of mRNA levels of Beclin 1 (A) and Atg5 (B) using quantitative real time RT-PCR. Messenger RNA from cells treated with specified concentrations of EXP57EA for 24 h was analysed by quantitative real-time RT-PCR for the genes encoding Beclin 1 **(A)** and Atg5 **(B)**. Results (corrected to GusB) are shown relative to control (vehicle-treated) cells, and are represented as the mean ±SD of experiments performed in triplicate and repeated at least two times. *$p < 0.05$

Western blot analysis was performed to determine whether LC3-II and Beclin 1 expression levels were increased after WHCO1 cells were treated with varying concentrations of EXP57EA (Figure 3.5). Figure 3.5 (A) and (B) shows a dose-dependent increase in LC3-II expression and Beclin 1 expression, respectively, in response to EXP57EA treatment. Considering that LC3-II is only found on autophagosomes which are formed during the process of autophagy, these results clearly indicate that EXP57EA induces autophagy in WHCO1 cells. Furthermore, immunofluorescence microscopy was also used to determine the expression level and localisation of LC3-II in cells treated with EXP57EA (Figure 3.6 and 3.7). Figure 3.6 (A) shows representative confocal microscopy (Zeiss LSM 510 Meta) images of WHCO1 cells treated with 10 µM EXP57EA compared to vehicle-treated (0 µM) cells. Consistent with the western blot results, a clear increase in punctate staining of LC3-II is observed in cells treated with EXP57EA compared to vehicle-treated cells. LC3-II expression

was mainly perinuclear which was not clear in Figure 3.6 (A) as it represents the merged image planes of a series of images (z-stacked) from different focal planes covering the entire structure of the cells; Figure 3.6 (B) represents one of the image planes.

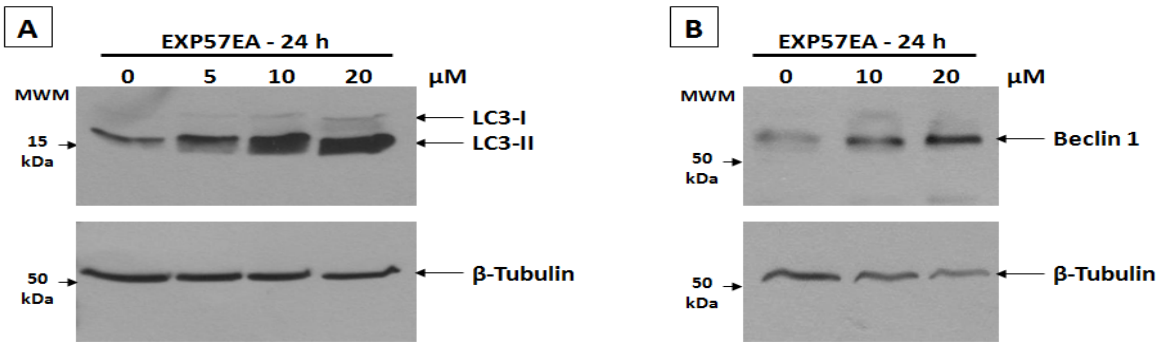

Figure 3.5: LC3-II (A) and Beclin 1 (B) expression in WHCO1 cells after treatment with EXP57EA. WHCO1 cells (300 000) were plated in 60 mm dishes and treated with varying concentrations of EXP57EA for 24 h. Protein was harvested and quantified so that 40 µg could be separated by SDS-PAGE and transferred on to a nitrocellulose membrane. The membrane was probed with antibodies recognising LC3-I and LC3-II **(A)** and Beclin 1 **(B)**. Beta-tubulin was used as a loading control and this figure is representative of two experiments.

The perinuclear localisation of LC3-II was more clearly observed in Figure 3.7, where WHCO6 cells in the presence (10 µM) and absence of EXP57EA (0 µM) were examined under high power magnification using an Axiovert 200M fluorescent microscope (Zeiss).

Taken together, these results confirm that EXP57EA increased the expression levels of LC3-II, an important autophagy regulator involved in formation of the autophagosomes. Another method that is often used to assess autophagy in mammalian cells is transmission electron microscopy (TEM). This method is useful in demonstrating the inclusion of cytoplasmic material within the autophagosomes and autolysosomes.

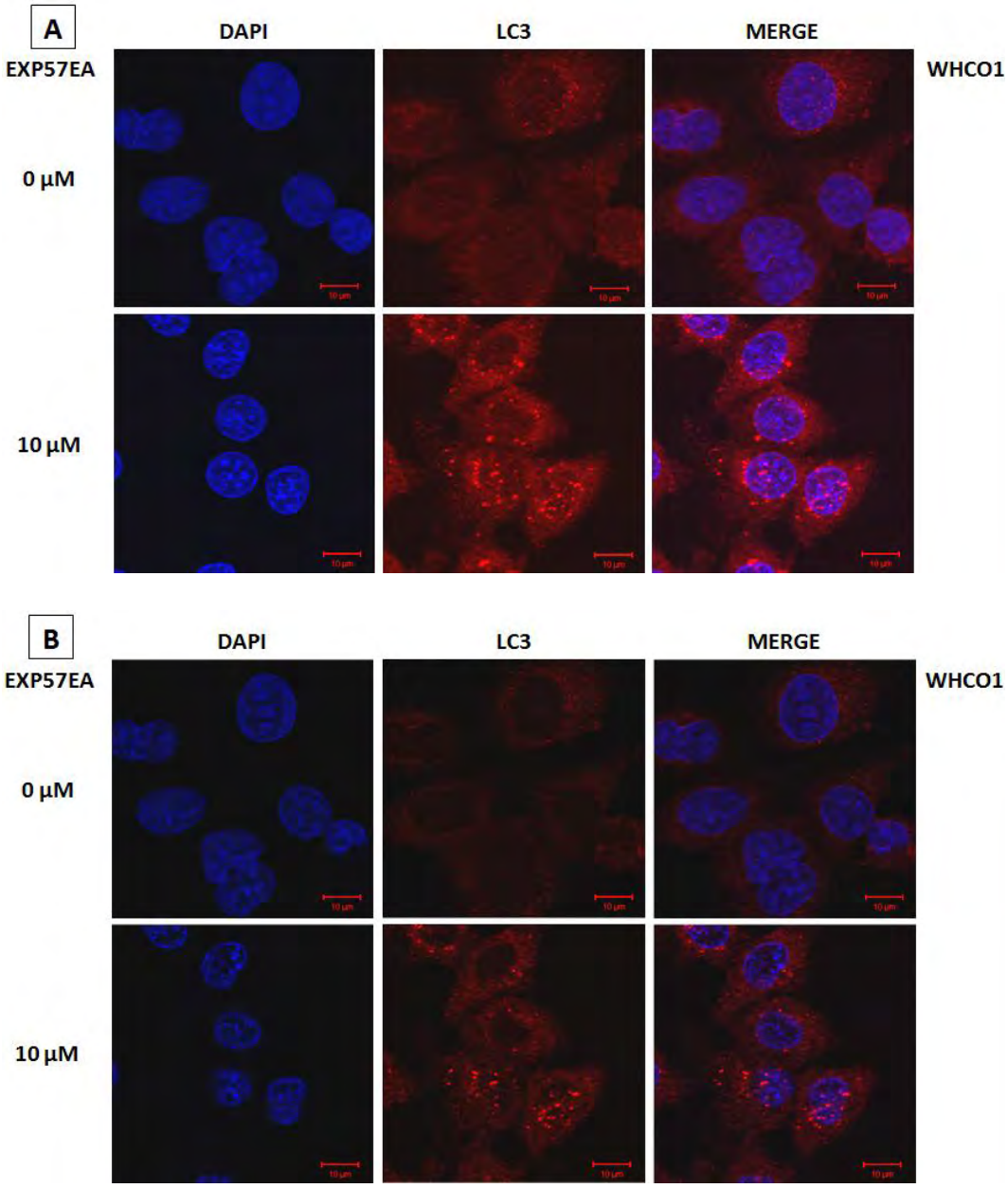

Figure 3.6: Immunofluorescent localisation of LC3-II in WHCO1 cells by confocal microscopy. A total of 80 000 WHCO1 cells were seeded in 6-well plates and treated with 10 µM EXP57EA for 24 h. Vehicle-treated cells (0 µM) were included as a negative control. Following treatment for 24 h, cells were fixed and prepared for immunofluorescence microscopy to determine LC3-II localisation using an anti-LC3 antibody. Cells were viewed under 100x magnification on a Zeiss LSM 510 Meta confocal microscope and images were captured, **(A)** represents z-stacked images and **(B)** represents one of the respective image planes at each treatment point. DAPI staining for nuclei is shown.

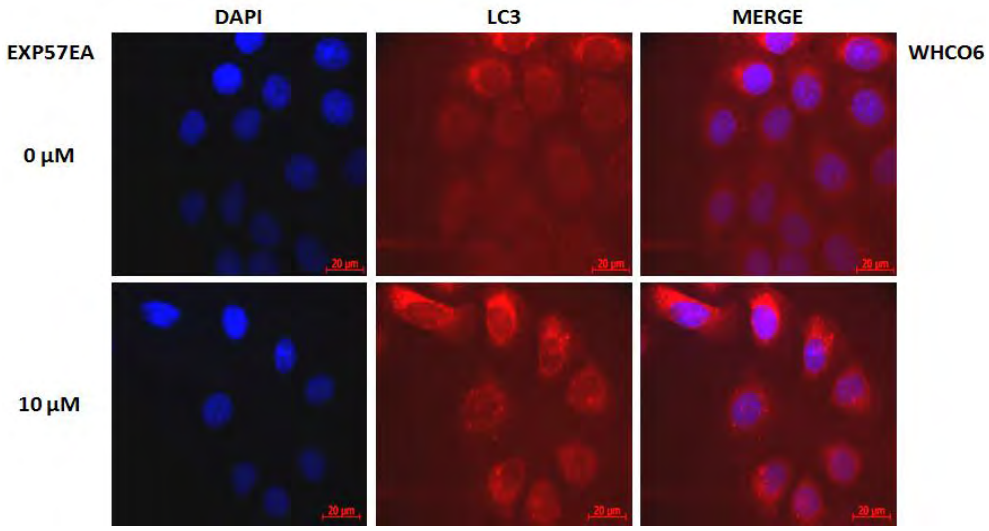

Figure 3.7: Immunofluorescent localisation of LC3-II in WHCO6 cells. A total of 80 000 WHCO1 cells were seeded in 6-well plates and treated with 10 µM EXP57EA for 24 h. Vehicle-treated cells (0 µM) were included as a negative control. Following treatment for 24 h, cells were fixed and prepared for immunofluorescence microscopy to determine LC3-II localisation using an anti-LC3 antibody. Cells were viewed under 100x magnification using a Zeiss Axiovert 200M fluorescent microscope and images were captured. DAPI staining for nuclei is shown.

TEM was performed using WHCO1 cells treated with 5 µM and 10 µM EXP57EA. Control (vehicle-treated) cells were included and the results (Figure 3.8 A) show that these cells contained very few vacuoles. In addition, normal mitochondria (black arrowheads) were observed. In contrast, cells treated with 5 µM EXP57EA demonstrated a high number of vacuoles (Figure 3.8 B) that appeared to increase with dose (Figure 3.8 C).

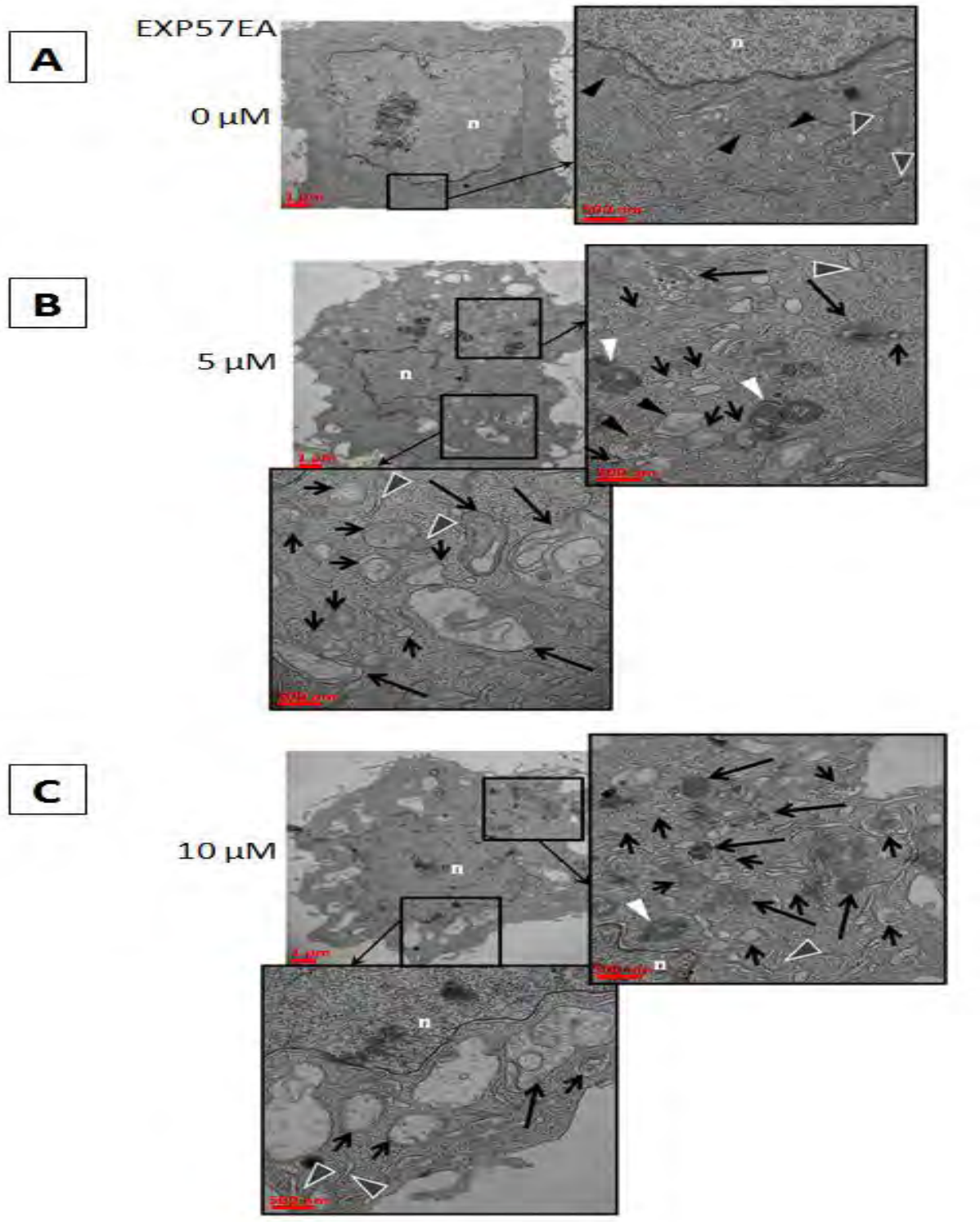

Figure 3.8: Transmission electron photomicrographs of WHCO1 cells treated with EXP57EA. WHCO1 cells (1 x 10^6) were plated in 100 mm dishes and treated with 5 µM **(B)** and 10 µM **(C)** EXP57EA for 24 h. Untreated cells (0 µM) were included as a negative control **(A)**. After treatment samples were fixed in 2.5% glutaraldehyde and prepared for TEM. Representative transmission electron photomicrographs of WHCO1 cells treated with vehicle **(A)** or EXP57EA **(B,C)** indicate autophagosomes containing cytoplasmic material (short arrows); long arrows indicate typical autolysosomes; black arrowheads indicate mitochondria; grey arrowheads indicate ER and white arrowheads indicate multilamellar structures.

Autophagosomes (short arrows) are double-membraned structures containing cytoplasmic material. They can vary in size and shape, and sometimes due to sample preparation it is difficult to see the double-membrane clearly. However, an important criterion for the identification of autophagosomes is that cytoplasmic material (electron dense) is enclosed. Figure 3.8 (B) and (C) clearly shows autophagosomes (short arrows) containing cytoplasmic constituents.

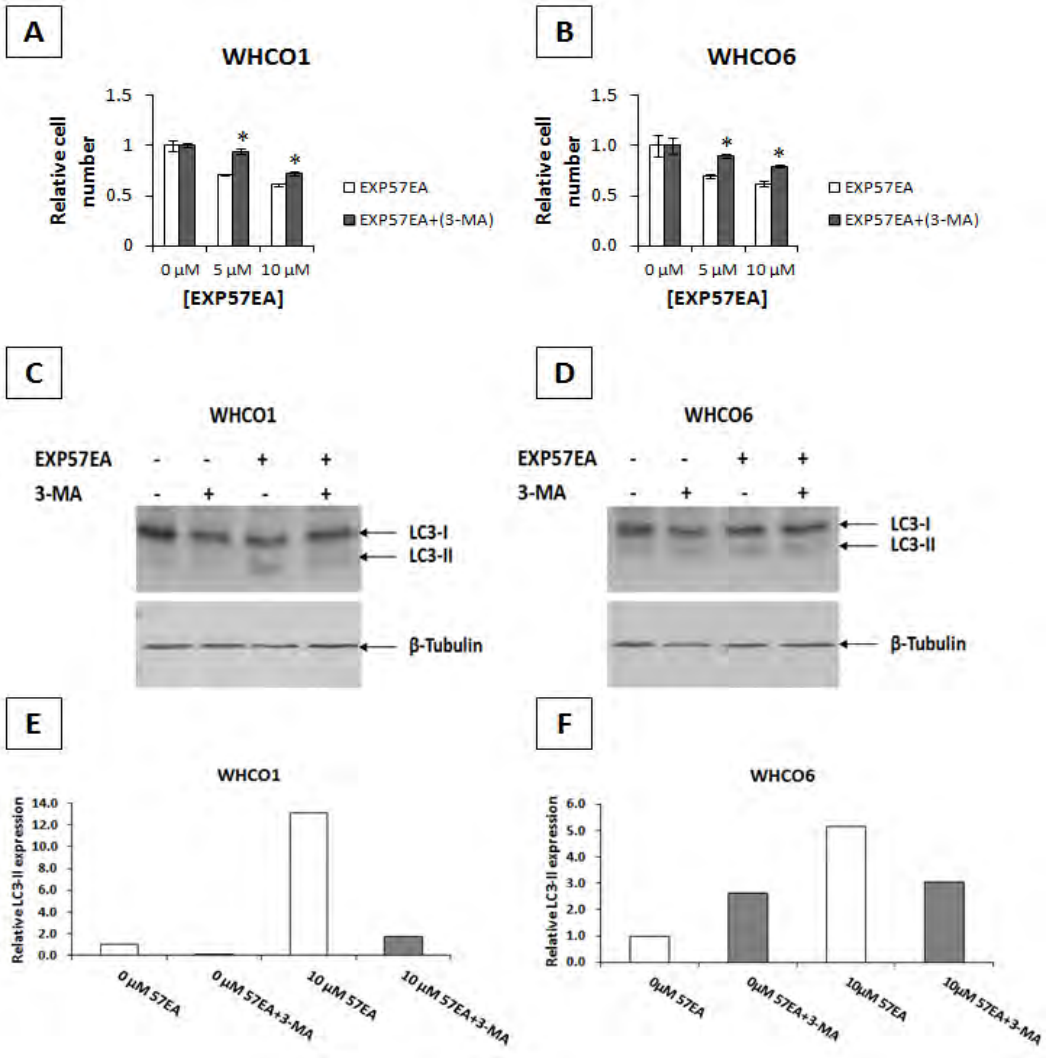

Figure 3.9: Effect of autophagy inhibitor, 3-MA, on WHCO1 and WHCO6 cells treated with EXP57EA. **(A)** WHCO1 and **(B)** WHCO6 cells were seeded in 96-well plates at a density of 3000 cells per well. Cells were pretreated 5 mM 3-MA for 1 h before treatment with 5 µM and 10 µM EXP57EA for 24 h. Vehicle-treated cells (0 µM) were included as a control. The MTT assay was performed and absorbance read on a BioTek plate reader. Results are shown relative to control (vehicle-treated) cells and are represented as the mean ±SD of

experiments performed in triplicate and repeated at least two times. *p < 0.05, **(C)** WHCO1 and **(D)** WHCO6 cells were treated with and without 3-MA, in the absence or presence of EXP57EA, for 24 h. Protein was extracted and processed so that 40 µg lysate could be separated by SDS-PAGE and transferred on to a nitrocellulose membrane before probing with an anti-LC3 antibody. Beta-tubulin was used as a loading control, and densitometry bar graphs (obtained using ImageJ software) shown in **(E)** and **(F)** show LC3-II relative to β-tubulin in WHCO1 and WHCO6 cells, respectively. This result is representative of two independent experiments.

Autolysosomes (autophagosomes fused with lysosomes) containing organelles at various stages of degradation are visible in EXP57EA-treated cells and are indicated by the long black arrows. Consistent with the immunofluorescence analysis results, the autophagic vacuoles displayed perinuclear localisation. Electron-lucent vacuoles and multilamellar structures (white arrowheads) were also visible but these do not represent autophagic vacuoles (Eskelinen, 2008; Ylä-Anttila et al., 2009).

The results represented here provide a clear indication that EXP57EA induced autophagy in oesophageal cancer cells under the treatment conditions described. This compound displayed a cytotoxic effect yet biochemical assays assessing for the presence of apoptosis and necrosis were negative. Thus, these results point to autophagy as the pathway that leads to cell death in cells treated with EXP57EA in oesophageal cancer cells. In order to understand this process a bit better, the autophagy inhibitor, 3-methyladenine (3-MA) was used. Cells were treated with EXP57EA in the presence and absence of 3-MA for 24 hours and the number of live cells was measured using the MTT assay. Figure 3.9 (A) and (B) show a significant increase in WHCO1 and WHCO6 cell number, respectively, when treated with 5 µM and 10 µM EXP57EA in the presence of 3-MA. These results suggested that preventing autophagy

in EXP57EA-treated cells significantly reduced the cell loss associated with EXP57EA treatment. The results in panel C, D, E and F provided evidence that treatment with 3-MA (5 mM) reduced autophagy, based on the decreased levels of LC3-II expression observed in cells treated with EXP57EA in the presence of 3-MA (Figure 3.9). A decrease in LC3-II expression levels was observed in EXP57EA-treated cells in the presence of 3-MA (densitometry demonstrated by Figure 3.9 E and F).

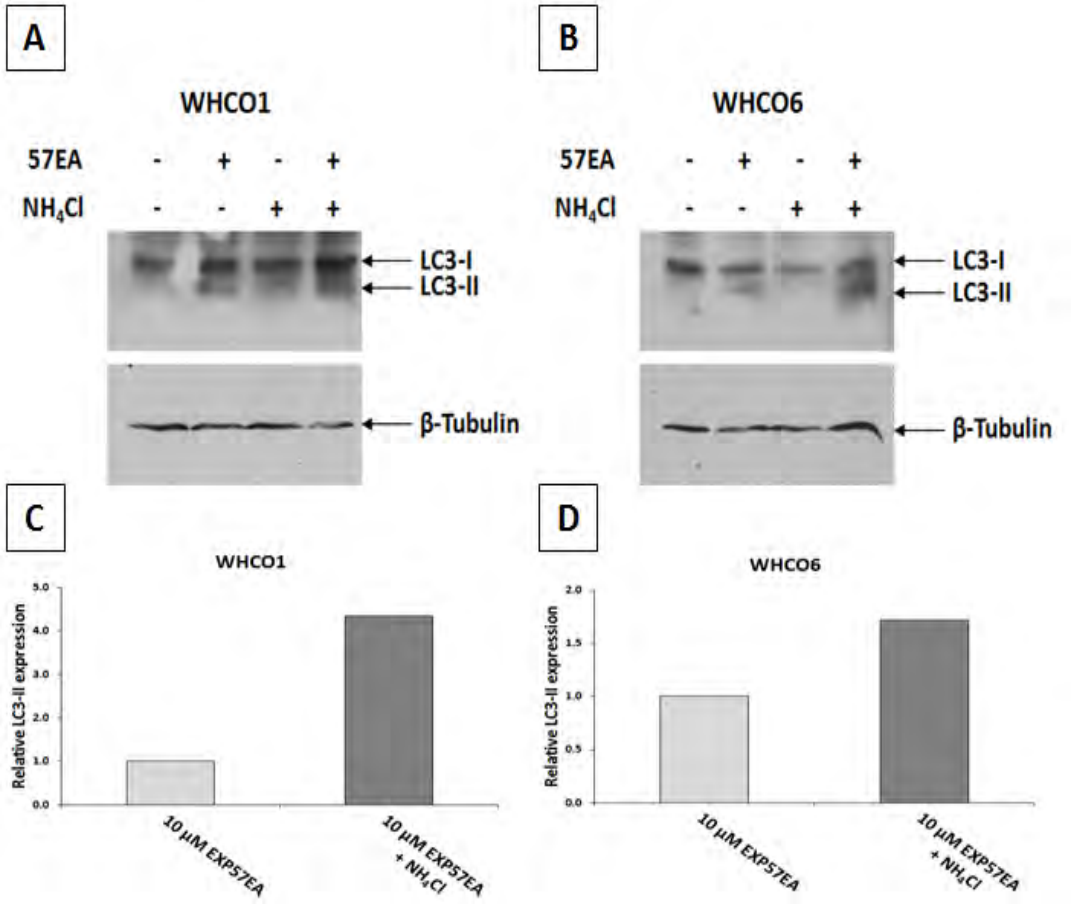

Figure 3.10: Monitoring autophagic flux using ammonium chloride in WHCO1 and WHCO6 cells treated with EXP57EA. (A) WHCO1 and **(B)** WHCO6 cells were seeded in 60 mm dishes at a density of 300 000 cells per dish. Cells were pretreated with 15 mM NH_4Cl for 1 h followed by treatment with 10 µM EXP57EA for 24 h. Protein was extracted, processed and loaded (40 µg) for separation via SDS-PAGE. The protein was transferred onto a nitrocellulose membrane which was probed with an antibody specific for LC3-I and LC3-II. Beta-tubulin was used as loading control. ImageJ software was used to determine LC3-II expression levels relative to β-tubulin expression levels for WHCO1 **(C)** and WHCO6 **(D)** cells treated with EXP57EA in the presence and absence of 15 mM NH_4Cl. This result is representative of two independent experiments.

Autophagy is a complex mechanism that is reliant on a variety of proteins and processes to reach completion, which includes fusion of autophagosomes to lysosomes, forming autolysosomes. Autolysosomes containing cytoplasmic material and organelles result in the degradation of the contents via lysosomal hydrolases. Excessive autophagy can result in cell death by continuous degradation of vital organelles (Maiuri et al., 2007). In order to ascertain whether EXP57EA-treated cells were undergoing the complete autophagic process, it was important that we monitored autophagy flux. An increase in LC3-II expression was insufficient to show that the complete process of autophagy, including formation of the autolysosome, was taking place. If the fusion of the autophagosome to the lysosome was inhibited or acidification of the lysosome is prevented there should be an accumulation of autophagosomes as they are degraded in the autolysosomes. Ammonium chloride (NH_4Cl), a lysosomotropic agent, was used to monitor autophagy flux in this way. Cells were pretreated with 15 mM NH_4Cl for 1 hour before treatment with EXP57EA for 24 hours. Figure 3.10 shows that WHCO1 cells (Figures 3.10 A and C) and WHCO6 cells (Figures 3.10 B and D) treated with 10 μM EXP57EA in the presence of NH_4Cl have increased levels of LC3-II compared to cells without NH_4Cl, indicating that EXP57EA induces the complete autophagic process and not just the accumulation of autophagosomes.

3.3 Discussion

DHA, the in vivo metabolite of some artemisinin derivatives, was investigated together with a novel artemisinin-isatin derivative, EXP57EA, to understand how these compounds exerted their anticancer activity against oesophageal cancer cells. Previous studies in the literature have shown that DHA induces apoptosis in a wide variety of cancer cell lines but since the hybrid compound, EXP57EA, is a novel compound, it is not known whether this compound induces apoptosis or not. The aim of this study was to investigate the cytotoxic effects of DHA and EXP57EA in the oesophageal cell culture model system used here.

The initial part of this study involved the selection of treatment conditions for the WHCO1 cell line (Chapter 2). In order to determine these, time- and dose-dependent experiments were performed. Having established the treatment conditions, the effects of these compounds on the morphology of WHCO1 cells were examined. The results showed that the morphology of DHA-treated cells was distinctly different from that of untreated cells (Figure 3.1). The morphological features observed such as cell shrinkage, nuclear condensation and plasma membrane blebbing are consistent with apoptosis (Lockshin and Zakeri, 2004). Based on the evidence generated in this study, particularly PARP cleavage and caspase-3/7 activation, it can be concluded that DHA induces apoptosis in OC cells. This is similar to reports by other authors, for example Hou et al. found that DHA and ART induced apoptosis in HepG2 liver cancer cell as measured by increased caspase 3 activity and cleaved PARP expression (Hou et al., 2008). In addition, they reported an increased Bax/Bcl-2 ratio in treated cells compared to untreated cells, however DHA and ART arrested HepG2 cells in the G0/G1 phase of the cell cycle (Hou et al., 2008), whereas we reported a G2/M block of the cell cycle induced by

DHA and ART in OC cells (Chapter 2). A similar result was obtained by Ji and colleagues, who demonstrated the ability of DHA to induce apoptosis (detected by flow cytometry using Annexin V-FITC and PI staining, increased Bax/Bcl-2 ratio as well as increased caspase-3 activity) in osteosarcoma cells, which were arrested in the G2/M phase of the cell cycle after DHA treatment for 48 hours (Ji et al., 2011).

Unlike DHA, EXP57EA did not induce apoptosis in WHCO1 and WHCO6 OC cells based on PARP cleavage and caspase-3/7 activation. Furthermore, EXP57EA also did not induce necrosis (Figure 3.3). However, using a wide variety of experimental approaches, we have shown that EXP57EA instead induced autophagy in OC cells. This includes Beclin 1, LC3-II and Atg5 induction in response to EXP57EA treatment, as well as the appearance of double membraned vesicles as visualised by TEM. A significant increase in the expression of critical proteins involved in the formation of the autophagosome, Beclin 1 and Atg5, was observed by quantitative real time RT-PCR. In addition, an increase in Beclin 1 expression after treatment with EXP57EA was shown by western blot analysis. A widely used method to show induction of autophagy is the expression of LC3-II by western blot analysis. When autophagy occurs, LC3 (or Atg8) is conjugated to PE, thus allowing LC3 to recruit the lipid molecules to lengthen the autophagosomal membranes during autophagosome formation. Lipid conjugation is achieved via an amide bond to a glycine residue, exposed by cleavage of LC3 by Atg4. During this process, the 18 kDa LC3-I is converted to 16 kDa LC3-II, which is directly associated with the autophagosomes (Kabeya et al., 2004). Thus, LC3-II expression is a good measure of autophagic activity.

In this study we showed, using two different experimental approaches, that treatment with EXP57EA increases the expression of LC3-II. Firstly the ability of EXP57EA to dose-dependently increase LC3-II expression in oesophageal cancer cells was demonstrated by western blot analysis. This was followed by immunofluorescence microscopy illustrating an increase in punctate staining of LC3-II in cells treated with EXP57EA compared to vehicle-only treated cells, confirming increased expression of LC3-II by EXP57EA. These experiments provided clear evidence that EXP57EA increased autophagy in oesophageal cancer cells; however according to guidelines published by Klionsky and colleagues (Klionsky et al., 2009), it is insufficient to demonstrate an increase in LC3-II (or autophagosome formation) when implicating the process of autophagy in cell death. The complete process of autophagy includes fusion of the autophagosome to the lysosome, forming the autolysosomes, resulting in degradation of its contents. Thus, in order to report that EXP57EA induces the complete autophagic process and not only an increase in autophagosome formation, an autophagic flux experiment was performed.

When WHCO1 and WHCO6 cells were treated with EXP57EA in the presence of the lysosomotropic agent, ammonium chloride (NH_4Cl), an increase LC3-II expression was observed when compared to cells treated with EXP57EA in the absence of NH_4Cl. NH_4Cl inhibits acidification within the autolysosome preventing degradation of its contents, including LC3-II, and can be used to measure autophagic flux (Mizushima et al., 2010). Other experimental approaches to show autophagic flux include pretreatment with the lysosomotropic agent bafilomycin A or lysosomal proteases such as E64d and leupeptin (Mizushima et al., 2010). The use of NH_4Cl to inhibit the complete autophagic process has been demonstrated by other authors studying autophagy (Boland et al., 2008; Kaushik et al., 2008; Singh et al., 2009), and the data obtained in this study showed an increase in LC3-II

expression in cells treated with EXP57EA in the presence of NH_4Cl, compared to EXP57EA-treated cells in the absence of NH_4Cl, suggesting that the complete process of autophagy was induced by EXP57EA, and not merely an increase in autophagosome formation. Furthermore, the micrographs obtained following TEM correlated with these results as an increase in autolysosomes was seen in cells treated with EXP57EA compared to vehicle-only treated cells.

In order to connect autophagy induced by EXP57EA with cell death, 3-methyladenine (3-MA) was employed. The nucleotide derivative inhibits class III PI3K activity which is important for autophagy to take place (Wu et al., 2010). Essential class III PI3K complexes that include Beclin 1 are involved in the formation of the autophagosome (Chen and Klionsky, 2011). When PI3K activity is blocked using 3-MA, autophagy is inhibited and this has been demonstrated by a number of studies (Aoki et al., 2007; Bursch et al., 1996; Chen et al., 2010b, 2008; Cui et al., 2007; Donadelli et al., 2011; Eom et al., 2010; Kanzawa et al., 2004; Li et al., 2009b, 2013; Ling et al., 2011; Seglen and Gordon, 1982; Shimizu et al., 2010; Son et al., 2011). WHCO1 and WHCO6 cells treated with EXP57EA in the presence of 3-MA displayed a significant increase in cell viability at both treatment concentrations tested, compared to EXP57EA-treated cells in the absence of 3-MA. Western blot analysis demonstrated a decrease in LC3-II expression when WHCO1 and WHCO6 cells were treated with EXP57EA in the presence of 3-MA compared to cells treated in the absence of 3-MA. Taken together, these results suggest that autophagy could be the cell death pathway employed by oesophageal cancer cells treated with EXP57EA.

Similarly, curcumin, a natural compound, was shown to be effective against U87-MG and U373-MG glioma cells with very little toxicity against normal cells (Aoki et al., 2007). Further investigation demonstrated that 3-MA inhibited autophagy and reversed the decrease in cell number induced by curcumin treatment, leading the authors to suggest that the natural compound induced autophagic cell death in glioma cells (Aoki et al., 2007). However, Levine and colleagues (Kroemer and Levine, 2008; Levine and Yuan, 2005) proposed that using 3-MA alone to implicate autophagy as a cause of cell death may not be sufficient as 3-MA may have off-target effects, and suggested that using genetic means to inhibit autophagy, such as siRNA technology, should be employed. This was demonstrated by Puissant and colleagues, who suggested that the promising anticancer agent from natural sources, resveratrol, induced autophagic cell death in chronic myelogenous leukaemia cells (Puissant et al., 2010). Elaborate investigations using siRNA directed at Atg5, LC3 and p62 blocked autophagy and cell death, implicating autophagy as the death pathway induced by resveratrol (Puissant et al., 2010). Due to time and budget constraints experienced during this project, experiments that involved silencing of essential autophagy genes in cells treated with EXP57EA could not be performed; though they would be included in future work.

The role of autophagy in cell death is disputed, where some authors have suggested that autophagic cell death is mainly activated in cells where the apoptotic pathway is comprised (Gozuacik and Kimchi, 2004, 2007; Kroemer and Levine, 2008; Levine and Yuan, 2005; Lockshin and Zakeri, 2004). However, in this study we have clearly shown that DHA induced apoptosis in WHCO1 and WHCO6 oesophageal cancer cells lines, and that EXP57EA induced autophagy in the same cell lines. In addition, there was no increase in expression of apoptotic markers after EXP57EA treatment which correlated with morphological studies where no morphological features of apoptosis were observed in cells

treated with EXP57EA. Furthermore, cell number increased when cells were simultaneously treated with EXP57EA and 3-MA suggesting involvement of only autophagy and not apoptosis in cell death. Moreover, experiments conducted with DHA in the same cell lines as EXP57EA provided clear evidence that the apoptotic machinery in these cell lines were intact.

The results presented here reinforces earlier evidence that DHA and EXP57EA exerts their cytotoxic activity against oesophageal cancer cells via different molecular mechanisms. The novel artemisinin-isatin hybrid was shown to kill cells at a lower concentration than DHA and to activate autophagy and not apoptosis. In contrast, cells treated with DHA displayed classical morphological features of apoptosis and strongly increased the expression of apoptotic markers used in this study. Considering that apoptosis is believed to be the preferred cell death pathway employed by cells, it is interesting that EXP57EA induced an alternative pathway in oesophageal cancer that resulted in more effective (lower IC_{50} value) cell death than the parental compound, DHA. Bearing this in mind, another study was embarked upon to identify the signalling pathways involved in DHA-induced apoptosis and EXP57EA-induced autophagy.

CHAPTER 4:

THE SIGNALLING PATHWAYS ACTIVATED BY DHA AND EXP57EA IN OESOPHAGEAL CANCER CELLS

4.1 Introduction

In the previous two chapters we showed that DHA and the novel artemisinin-isatin hybrid, EXP57EA, induced cytotoxicity in oesophageal cancer cells, and that EXP57EA was more active than DHA in several cancer cell lines tested. Further investigations demonstrated that DHA strongly induced apoptosis in oesophageal cancer cell lines whereas EXP57EA induced autophagy, and not apoptosis. A number of studies have been performed to investigate the anticancer effects of artemisinin derivatives in a variety of cancer cell lines, however very little information is available regarding their effects in oesophageal cancer. In this chapter, we sought to elucidate the cellular processes activated by DHA and EXP57EA that contributed to their mechanism of action in oesophageal cancer cells.

Artemisinin derivatives have been shown to exert their cytotoxic effects in several cancer cell lines via reactive oxygen species (ROS)-dependent pathways (Aghaei and Ashtiani, 2012; Berdelle et al., 2011; Du et al., 2010; Efferth et al., 2007; Handrick et al., 2010; Lu et al., 2010; Michaelis et al., 2010; Zhang et al., 2010). Efferth and colleagues found that ART induced ROS-dependent apoptosis via the intrinsic pathway in four different leukaemic T cell lines, including one that was doxorubicin resistant (Efferth et al., 2007). DHA was shown to

induce ROS-dependent apoptosis in the A-431 skin cancer cell line (Aghaei and Ashtiani, 2012) as well as in ASTC-a-1 lung cancer cells (Lu et al., 2010). These studies also showed that ROS played a causal role in the induction of apoptosis since treatment with ROS scavengers inhibited apoptosis. Furthermore, the generation of ROS is associated with DNA damage (Circu and Aw, 2010). In this study, we explored the generation of ROS in cells treated with DHA and the requirement of ROS to induce apoptosis.

The evidence generated in Chapter 3 clearly showed that EXP57EA acts very differently from DHA, where EXP57EA induced autophagy. Considering that EXP57EA is an artemisinin hybrid compound, we wanted to determine the effects of EXP57EA on ROS production. Numerous studies have reported that increased ROS production can lead to the induction of autophagy (Chen et al., 2008; Donadelli et al., 2011; Khan et al., 2012; Ling et al., 2011; Son et al., 2011; Xie et al., 2011), providing a context for investigating ROS production in cells treated with EXP57EA and determining the effects thereof on autophagy. Furthermore, increased ROS production was shown to activate signalling pathways that led to the induction autophagy such as the JNK and ERK signalling pathway as well as the ER stress pathway (Wong et al., 2010; Xavier et al., 2013; Xie et al., 2011). This prompted an investigation of the effects of EXP57EA on ROS-induced pathways that led to the induction of autophagy using western blot analysis to measure protein expression in the presence and absence of EXP57EA.

The results presented in this chapter attempted to characterise the signalling pathways involved in DHA- and EXP57EA-induced cytotoxicity in oesophageal cancer cells, and implicated ROS in the signalling pathways investigated. We have previously shown that

DHA and EXP57EA displayed different mechanisms of action in oesophageal cancer cells, and the results discussed below suggested that the compounds may activate different signalling pathways in oesophageal cancer cells that are ROS dependent.

4.2 Results

4.2.1 Investigating the cellular processes activated by DHA in oesophageal squamous carcinoma cells

4.2.1.1 The effect of DHA on ROS production

To the best of our knowledge, the effect of DHA on ROS production in oesophageal cancer has not been investigated. Therefore we sought to determine the effect of DHA on ROS production in oesophageal cancer cells. The ROS sensitive probe, DCFDA, was used to measure ROS production in cells treated with DHA. DCFDA is a nonfluorescent cell permeable molecule. However, intracellular esterases cleave DCFDA into 2'-7'dichlorodihydrofluorescein ($DCFH_2$) which remains trapped within the cell and which can be oxidised to the fluorescent 2'-7'-dichlorofluorescein (DCF) in the presence of hydrogen peroxide. Although this method is widely used to measure hydrogen peroxide concentration in cells, other types of ROS can also be detected (Curtin et al., 2002).

A number of protocols to measure ROS production using DCFDA were investigated, and after extensive optimisation a 96-well format assay was found to be optimal. A time course was initially performed to determine the optimal time point to measure ROS production in response to DHA treatment (Figure 4.1 A). Cells were seeded in opaque white 96-well plates and pretreated with DCFDA in Krebs-Ringer (KR) buffer for 15 minutes followed by treatment with DHA. Immediately after the treatment times, the fluorescence was measured using a Cary Eclipse fluorescence spectrophotometer (Varian, Inc.). As shown in Figure 4.1 (A), the time course of ROS production in WHCO1 cells treated with DHA showed an

increase up to the 24 hour time point measured. Therefore, the 24 hour DHA treatment time was used for further experiments. Next, cells were treated with different concentrations of DHA for 24 hours (Figure 4.1 B), and a dose-dependent increase in ROS production was observed.

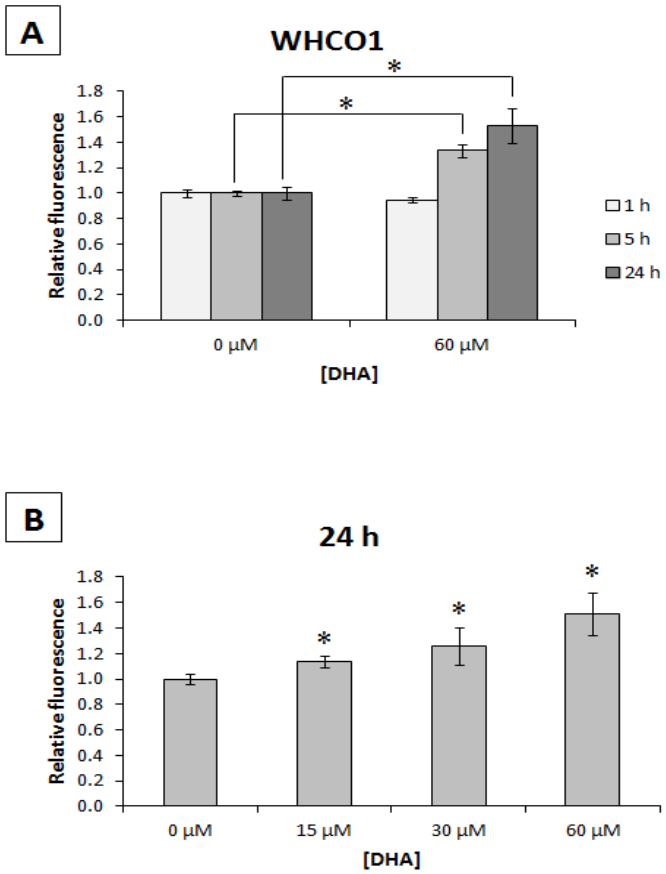

Figure 4.1: ROS production in WHCO1 cells after treatment with DHA. (A.), To determine if WHCO1 cells treated with DHA increased ROS production, a time course experiment was performed. Cells ($1x10^4$) were plated in 96-well white plates and pretreated with 50 µM DCFDA for 15 min followed by the addition of 60 µM DHA. Following the indicated treatment points, fluorescence was measured using a Cary Eclipse fluorescence spectrophotometer (484 nm excitation; 530 nm emission). **(B.),** A concentration course experiment was performed at 24 h. Cells ($1x10^4$) were plated in 96-well white plates and pretreated with 50 µM DCFDA for 15 min followed by the addition of the indicated concentrations of DHA. After 24 h, fluorescence was measured using a Cary Eclipse fluorescence spectrophotometer (484 nm excitation; 530 nm emission). Results are shown relative to fluorescence readings in control (vehicle-treated) cells, and are represented as the mean ±SD of two experiments performed in triplicate. *$p < 0.05$

Previous studies performed to characterise artemisinin derivatives as anticancer agents have linked the increased ROS production observed after treatment with these compounds with DNA damage (Li et al., 2008). H2AX is a member of the histone family of proteins that functions in organising DNA in nucleosomes, the basic unit of chromatin, and is rapidly phosphorylated when DNA double-strand breaks occur (Fernandez-Capetillo et al., 2004). Phosphorylated H2AX (represented as γ-H2AX) is widely used as a sensitive marker of DNA damage, specifically double-strand breaks (Fernandez-Capetillo et al., 2004). Many endogenous and exogenous factors are known to cause double-strand breaks, including ROS which can be produced by intracellular processes such as the electron transport chain and by external causes such as exposure to ionizing radiation and chemical compounds (Podhorecka et al., 2010). We sought to determine the effect of DHA on the expression levels of γ-H2AX by western blot analysis (Figure 4.2). WHCO1 cells treated with DHA displayed a dose-dependent increase in γ-H2AX levels after 24 hours and 48 hours (Figure 4.2), which correlated with the increase in ROS production observed previously (Figure 4.1). The results in Figure 4.2 also suggested that most of the H2AX phosphorylation had taken place after 24 hours of treatment with DHA at 30 μM and 60 μM. However, there was still an increase in H2AX phosphorylation at the 48 hour time point compared to the 24 hour time point for cells treated with 15 μM DHA.

Double-strand breaks resulting in phosphorylation of H2AX leads to the recruitment of important proteins involved in the DNA damage response (Barzilai and Yamamoto, 2004). Should efforts to repair the damaged DNA fail, cell cycle arrest and cell death may follow (Fragkos et al., 2009; Hartwell and Kastan, 1994). Figure 2.6 (Chapter 2) showed the ability of DHA to arrest cells in the G2/M phase of the cell cycle. Figure 4.3 confirmed these results, and included an analysis of the sub-G1 phase of the cell cycle. A dose-dependent increase of

cells arrested at the G2/M phase of the cell cycle was observed, illustrated by the dark grey bars in Figure 4.3. This experiment included the analysis of the sub-G1 population, shown by the black bars in Figure 4.3. A significant increase in the sub-G1 population was revealed indicating an increase in death in cells treated with increasing DHA concentrations. This correlated with the increase in the expression of cleaved PARP, a marker of apoptosis, in oesophageal cancer cells treated with DHA after 24 hours and 48 hours, shown in Figure 3.2 (A) (Chapter 3).

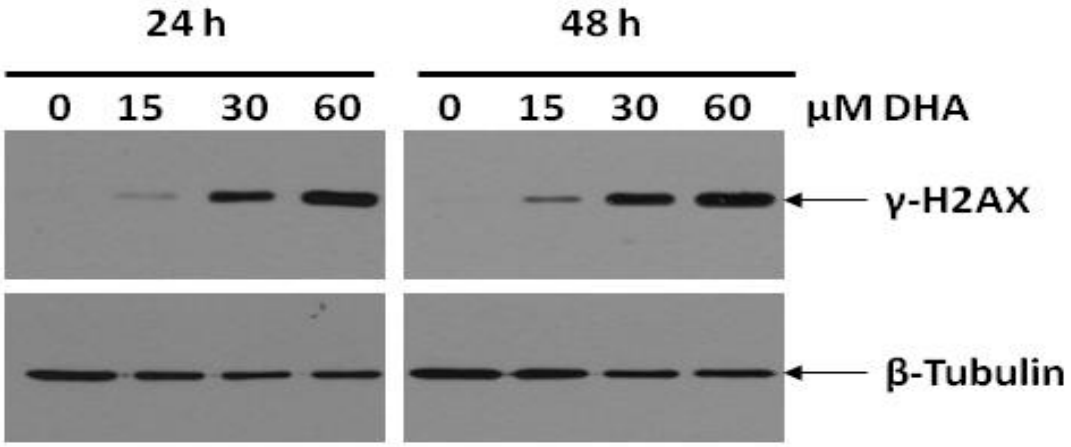

Figure 4.2: Effects of DHA on the expression levels of the DNA damage marker, γ-H2AX, in WHCO1 cells after treatment for 24 h and 48 h. WHCO1 cells were seeded in 60 mm dishes (3 x 10^5 cells per dish) and treated with varying concentrations of DHA for 24 h and 48 h. Protein was extracted and quantified allowing 20 μg to be separated by SDS-PAGE and transferred onto a nitrocellulose membrane. The membrane was probed with antibodies against γ-H2AX and β-Tubulin, which was used as a loading control. This figure is representative of at least two experiments.

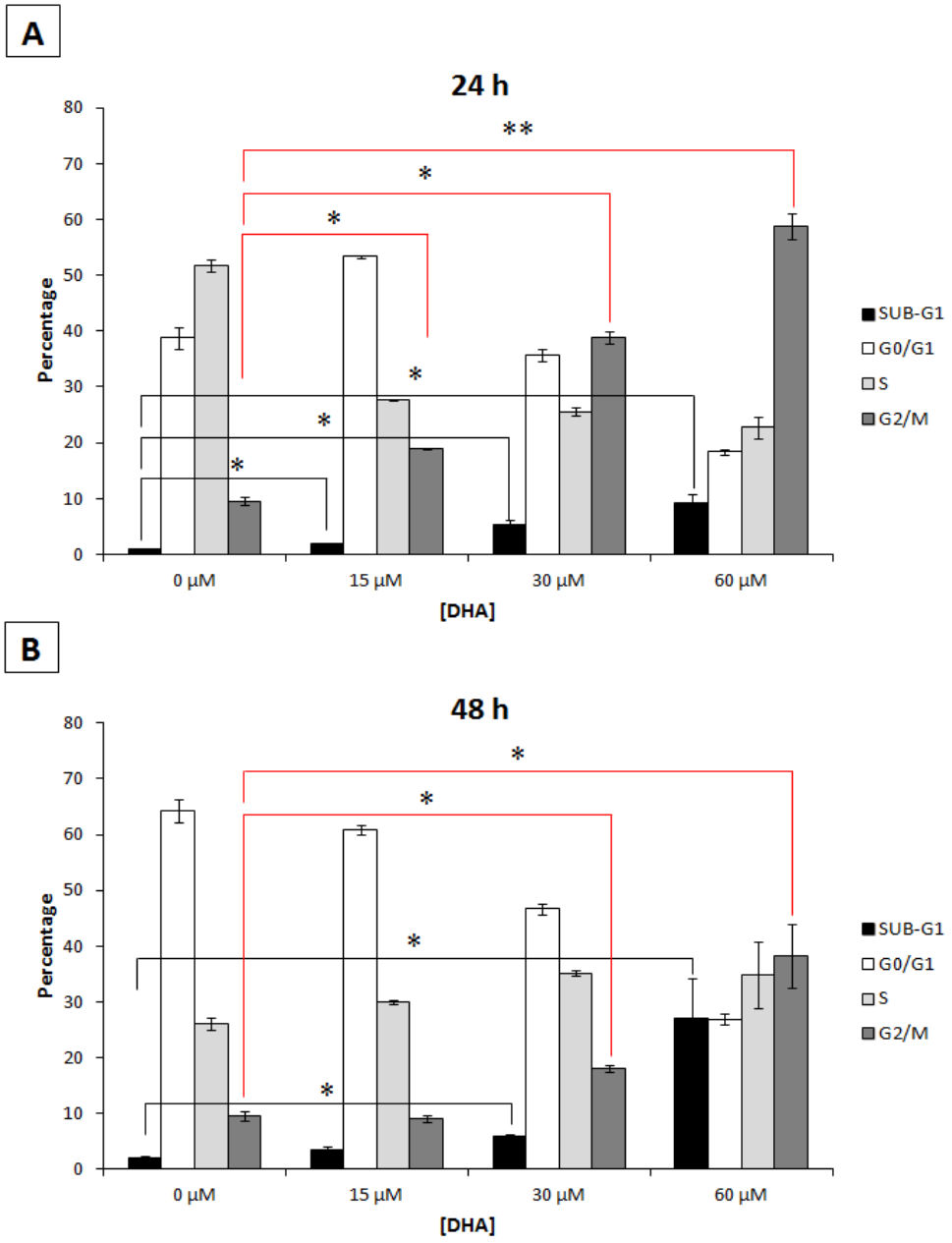

Figure 4.3: Cell cycle profile, including sub-G1 analysis of WHCO1 oesophageal cancer cells treated with DHA for 24 h and 48 h. WHCO1 cells (5 x 10^5) were plated in 100 mm dishes and allowed to settle overnight. The next day cells were treated with the indicated concentrations of DHA (in triplicate) for 24 h **(A)** and 48 h **(B)**. Cells were processed for flow cytometry, stained with propidium iodide and analysed on a FACSCalibur machine using CELLQuest Pro Software and Modfit LT version 3.2 for data analysis. The results are expressed as a mean of triplicates with ±SD indicated by the error bars, and experiments were repeated at least two times. *, $p < 0.05$; ** $p<0.001$

4.2.1.2 The effects of the ROS scavenger, N-acetyl -L-cysteine (NAC), on ROS production and cytotoxicity caused by DHA

To examine the role of ROS production in DHA-induced cytotoxicity in oesophageal cancer cells, we evaluated the effects of the antioxidant, *N*-acetyl-L-cysteine (NAC) on DHA treatment. NAC is an acetylated derivative of the amino acid L-cysteine that is a precursor of reduced glutathione, a tripeptide that protects cells from oxidative stress. NAC functions by supplying important precursors for the synthesis of glutathione, such as sulfhydryl groups, and is also able to scavenge ROS directly (Zhang et al., 2011). In order to investigate whether NAC had the ability to reduce DHA-induced cytotoxicity by decreasing induced-ROS levels, oesophageal cancer cells were treated with DHA in the presence and absence of NAC.

WHCO1 cells treated with 15 μM, 30 μM and 60 μM DHA showed a significant increase in ROS production, as observed previously, however in the presence of NAC the levels of ROS generated in DHA-treated cells remained close to that of the vehicle-only treated cells (Figure 4.4 A). A similar result was obtained with WHCO6 cells treated with 30 μM DHA (Figure 4.4 B). A greater fold increase in ROS production was observed in WHCO6 cells treated with 30 μM DHA (3-fold) than WHCO1 cells treated with the same concentration (1.2-fold), however when co-treated with NAC the ROS levels were reduced to that of vehicle-only treated cells. These results indicate that 10 mM NAC, a concentration widely used in the literature, successfully scavenged the ROS induced by treatment of oesophageal cancer cells with DHA. Therefore, we proceeded to investigate whether NAC was able to rescue cells from DHA-induced cell death.

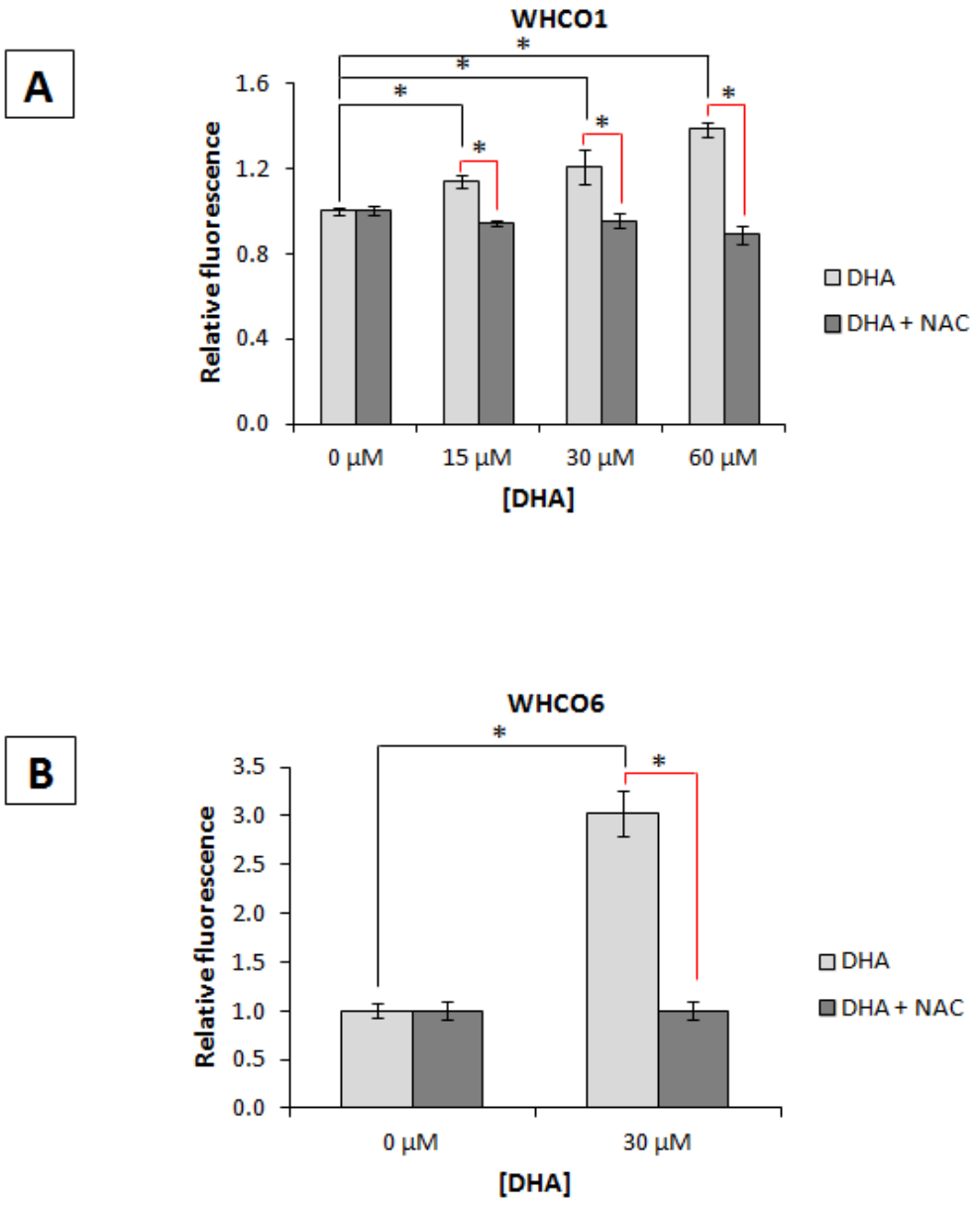

Figure 4.4: Inhibition of DHA-induced ROS by a ROS scavenger, NAC, after 24 h in WHCO1 (A) and WHCO6 (B) cells. Cells ($1x10^4$) were plated in 96-well white plates and allowed to settle overnight. The next day cells were pretreated with 10 mM NAC (+NAC) or KR buffer only for 1 h, followed by pretreatment with 50 µM DCFDA for 15 min. The indicated concentrations of DHA was added and incubated for 24 h. Fluorescence was measured using a Cary Eclipse fluorescence spectrophotometer (484 nm excitation; 530 nm emission). Results are shown relative to fluorescence readings in control (vehicle-treated) cells, and are represented as the mean ±SD of experiments performed in triplicate and repeated at least two times. *$p < 0.05$

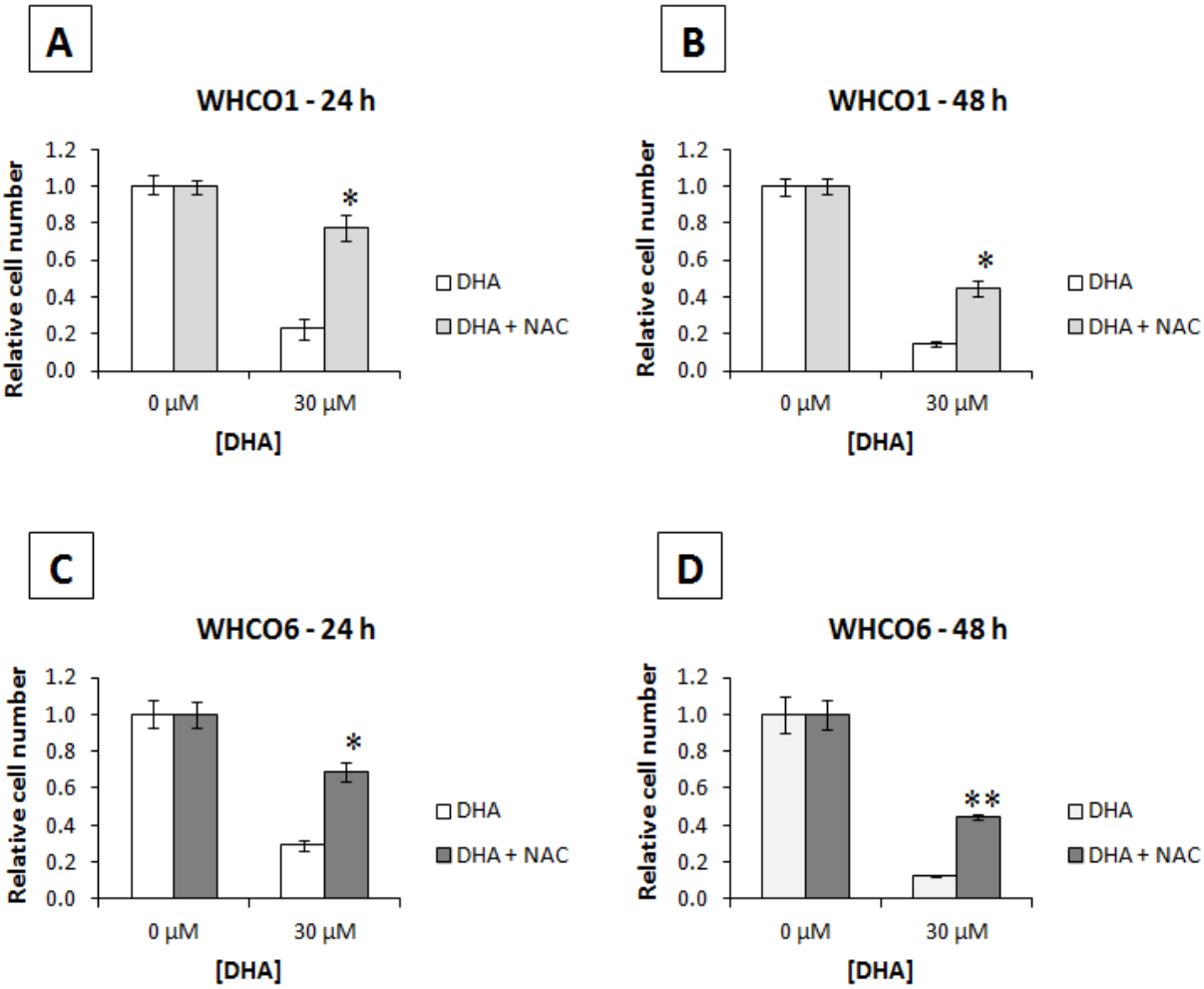

Figure 4.5: Effect of NAC on WHCO1 (A and B) and WHCO6 (C and D) cell number (OD_{595nm}) after treatment with DHA for 24 h (A and C) and 48 h (B and D). Cells were plated in 96-well plates at a density of 3000 cells per well and allowed to settle overnight. Cells were either pretreated with 10 mM NAC (+NAC) or media only for 1 h, followed by treatment with 30 µM DHA for 24 and 48 h. The media was removed and MTT reagent was added to fresh media and incubated for 4 h followed by the addition of solubilisation solution. The next day the absorbance was measured at 595 nm using a BioTek plate reader. Results are shown relative to absorbance readings in vehicle-only treated cells (0 µM) and are represented as the mean ±SD of experiments performed in triplicate and repeated at least two times. *$p < 0.05$, **$p < 0.001$

Using the MTT assay the effect of NAC on WHCO1 and WHCO6 cell number after treatment with 30 µM DHA for 24 hours and 48 hours was evaluated (Figure 4.5). Cell number of both cell lines were significantly reduced after DHA treatment (white bars, Figure

4.5 A-D), but co-treatment with NAC resulted in an attenuation of the effect of DHA on cell number, as measured by absorbance readings at 595 nm. However, NAC did not completely block the effects of DHA since there was still a 20 - 30% reduction in cell number in DHA-treated cells in the presence of NAC compared to untreated cells after 24 hours (Figure 4.5 A and C), and ~55% reduction in cell number after 48 hours (Figure 4.5 B and D). Considering that NAC interacted with the MTT reagent by increasing the absorbance readings on its own (data not shown), the protocol was adjusted to remove the media containing NAC and replace with fresh media containing the MTT reagent. The experiment shown in Figure 4.5 was carried out using the modified protocol. These results were confirmed using a different assay to measure the effects on cell number, the Neutral red uptake (NRU) assay, where similar results were obtained (data not shown). Visual inspection of the cells treated with DHA in the presence of NAC, using a phase-contrast microscope, further confirmed the ability of NAC to rescue DHA-treated cells from cell death as illustrated by Figure 4.6. Cells treated with DHA alone displayed a dose-dependent decrease in cell number and this effect was inhibited in the presence of NAC, where the number of cells in the DHA-treated samples resembled the vehicle-only treated sample.

Having previously shown that DHA treatment increased the expression of the DNA damage marker, γ-H2AX, in oesophageal cancer cells (Figure 4.2), we next investigated the effects of NAC on the expression level of γ-H2AX when WHCO1 and WHCO6 cells were treated with DHA (Figure 4.7). A dose-dependent increase in γ-H2AX expression levels was observed in both WHCO1 and WHCO6 cells treated with DHA for 24 hours, and this was effectively attenuated in the presence of 10 mM NAC. A large decrease in γ-H2AX expression at the 30 μM treatment point correlated with the increase in cell number observed in Figure 4.5, when WHCO1 and WHCO6 cells were co-treated with DHA and NAC. In addition, NAC caused a

minimal increase in γ-H2AX expression in the absence of DHA. However, in the presence of NAC and DHA the levels of γ-H2AX were lower than that of γ-H2AX levels in the presence of DHA alone. This data suggested that DHA-induced ROS was responsible for the DNA damage and cytotoxicity observed in WHCO1 and WHCO6 cells treated with DHA.

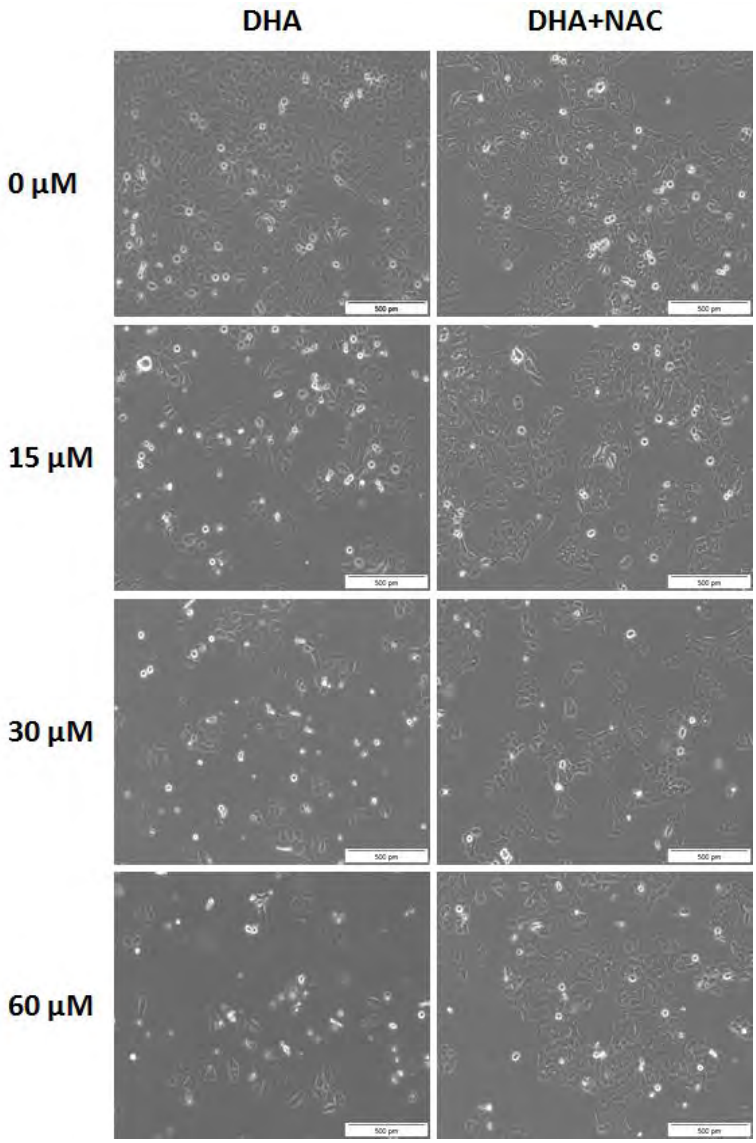

Figure 4.6: Morphology of WHCO1 cells treated with DHA in the presence and absence of NAC for 48 h. Cells were plated in 60 mm dishes at a density of 3 x 10^5 cells per dish and allowed to settle overnight. Cells were either pretreated with 10 mM NAC (+NAC) or media only for 1 h, followed by treatment with the indicated concentrations of DHA for 48 h. Images of the cells were captured using a Olympus CKX42 phase contrast microscope with an Olympus CMOS Colour Camera for Light Microscopy SC30 and analysis® getIT! image software.

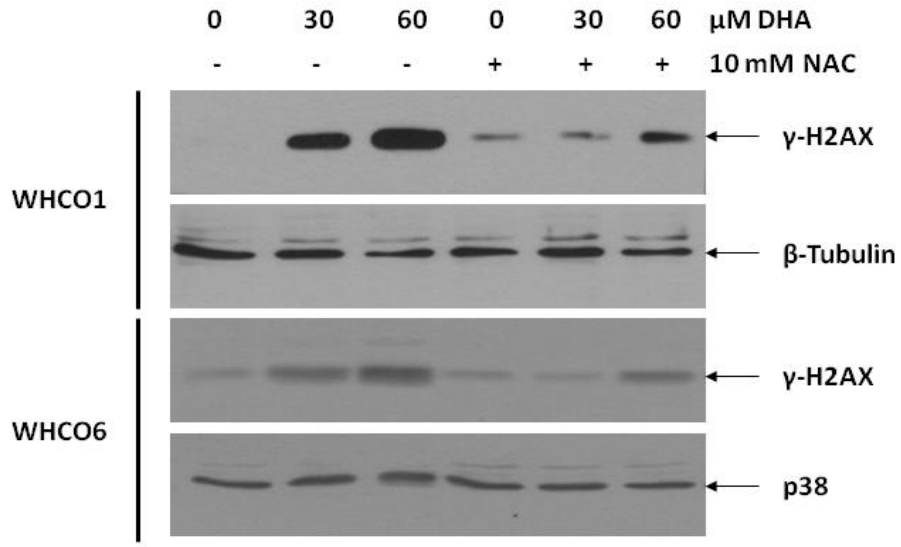

Figure 4.7: Western blot analysis demonstrating the effects of NAC on γ-H2AX expression in WHCO1 and WHCO6 cells treated with DHA. WHCO1 and WHCO6 cells (3 x 10^5) were plated in 60 mm dishes and incubated overnight. Cells were pretreated with 10 mM NAC (+) or media only (-) for 1 h followed by treatment with the indicated concentrations of DHA for 24 h. Protein was harvested and quantified so that 20 µg could be separated by SDS-PAGE and transferred onto a nitrocellulose membrane. The membrane was probed with antibodies recognising γ-H2AX. Beta-Tubulin and p38 were used as loading controls. This figure is representative of at least two experiments.

In order to determine whether the ROS production and DNA damage induced by DHA had an effect on the cell cycle profile, cell cycle analysis was performed after WHCO1 and WHCO6 cells were treated with DHA in the presence and absence of NAC for 24 hours (Figure 4.8). As shown by the black bars, there was a significant decrease in the sub-G1 population when cells were treated with 30 µM (~ 60%) and 60 µM (~30%) DHA in the presence of NAC concomitant with a significant decrease in the G2/M population (~55%), represented by the dark grey bars (Figure 4.8 A and B). In accordance with this data, it is evident that DHA-induced ROS played an important role in the G2/M cell cycle arrest observed in oesophageal cancer cells. Cell cycle arrest at the G2/M phase of the cell cycle

may be attributed to DNA damage, which if not repaired can lead to cell death (Hartwell and Kastan, 1994; Kastan et al., 1991; Taylor and Stark, 2001).

We have demonstrated earlier that DHA induced apoptosis in oesophageal cancer cells, and in order to understand the role of DHA-induced ROS production in the activation of the apoptotic pathway we investigated the effect of DHA and NAC co-treatment on the expression of cleaved PARP (Figure 4.9). As seen previously, a clear increase in the expression of cleaved PARP was observed in WHCO1 and WHCO6 cells treated with DHA only, however this effect was abrogated in the presence of NAC at both 30 μM DHA (~ 80% in WHCO1 cells and ~95% in WHCO6 cells) and reduced at 60 μM DHA (~60% in WHCO1 cells and ~30% in WHCO6 cells). These results correlated with the data shown above, and strongly suggested that the generation of ROS by DHA was responsible for the induction of apoptosis in WHCO1 and WHCO6 oesophageal cancer cells.

Taken together, the results presented here provide strong evidence that DHA exerted its cytotoxic effects on oesophageal cancer cells via a ROS-dependent mechanism. The ROS scavenger, NAC, efficiently attenuated the effects of DHA in both WHCO1 and WHCO6 cells and rescued cells from DHA-induced cytotoxicity. Having elucidated the mechanistic effects of DHA in our oesophageal cancer cell culture system, we next sought to explore the effects of the novel artemisinin-hybrid compound, EXP57EA, in the same system.

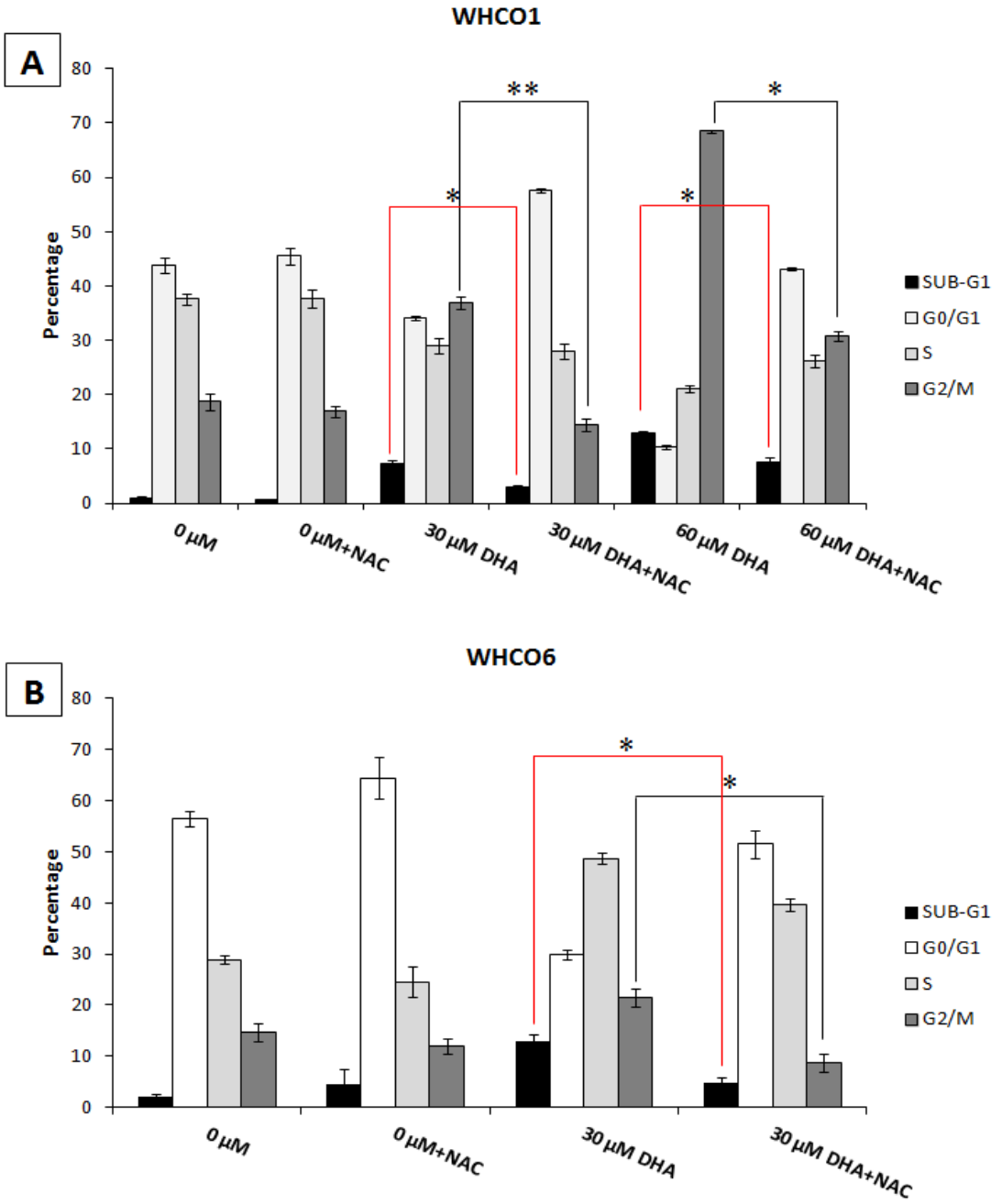

Figure 4.8: Cell cycle profile of WHCO1 (A) and WHCO6 (B) cells treated with DHA in the presence and absence of NAC. Cells were plated at a density of 5 x 10^5 cells per dish in 100 mm dish and incubated overnight. Cells were pretreated with 10 mM NAC (+NAC) or media only for 1 h followed by treatment with the indicated concentrations of DHA for 24 h. Cells were processed for flow cytometry, stained with propidium iodide and analysed on a FACSCalibur machine using CELLQuest Pro software and Modfit LT version 3.2 for data analysis. Results are represented as the mean ±SD of experiments performed in triplicate and repeated at least two times. *$p < 0.05$, **$p < 0.001$

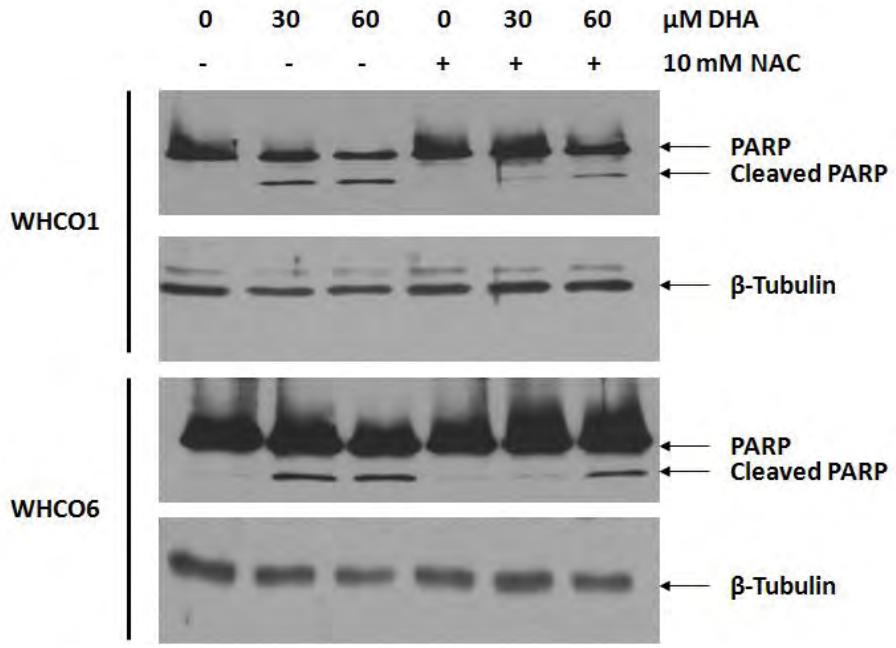

Figure 4.9: The effect of NAC on DHA-induced PARP cleavage. WHCO1 and WHCO6 cells (3 x 10^5) were plated in 60 mm dishes and incubated overnight. Cells were pretreated with 10 mM NAC (+) or media only (-) for 1 h followed by treatment with the indicated concentrations of DHA for 24 h. Protein was harvested and quantified so that 20 µg could be separated by SDS-PAGE and transferred onto a nitrocellulose membrane. The membrane was probed with antibodies recognising PARP and cleaved PARP. Beta-Tubulin was used as a loading control and this figure is representative of at least two experiments.

4.2.2 The molecular mechanisms engaged by EXP57EA in oesophageal squamous carcinoma cells

4.2.2.1 The effect of EXP57EA on ROS production

WHCO1 cells were plated in 96-well white plates, pretreated with DCFDA and treated with EXP57EA for the indicated times. ROS was measured, as done previously, at 530 nm emission when the samples were excited at 484 nm using the Cary Eclipse fluorescence spectrophotometer (Varian, Inc.). A time course experiment measuring ROS production after treatment with EXP57EA up to 18 hours (data not shown) revealed that the optimal time to

measure ROS production was 5 hours therefore all subsequent ROS assays were performed after 5 hours treatment with EXP57EA (Figure 4.10).

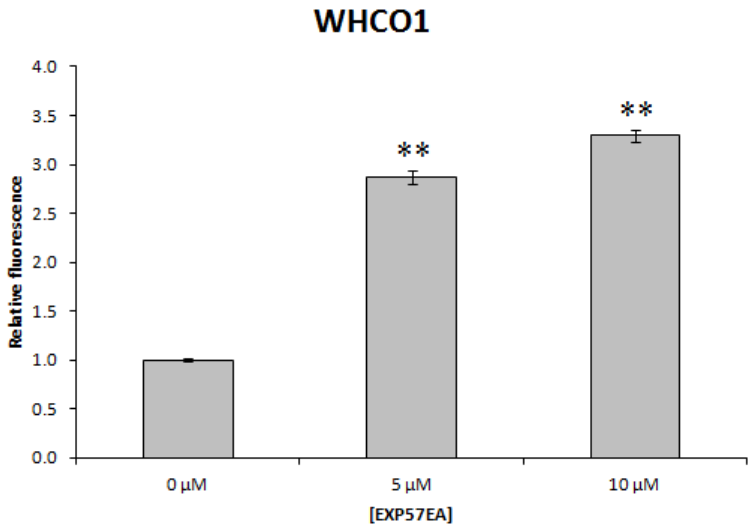

Figure 4.10: ROS production in WHCO1 cells after treatment with EXP57EA. WHCO1 cells ($1x10^4$) were pretreated with 50 µM DCFDA for 15 min followed by the addition of the indicated concentrations of EXP57EA in 96-well white plates for 5 h. Fluorescence was measured using a Cary Eclipse fluorescence spectrophotometer (484 nm excitation; 530 nm emission). Results are shown relative to fluorescence readings in control (vehicle-treated) cells, and are represented as the mean ±SD of experiments performed in triplicate, and repeated at least two times. **$p < 0.001$

The effect of NAC on ROS generation after treatment with EXP57EA was examined, and WHCO1 (Figure 4.11 A) and WHCO6 cells (Figure 4.11 B) cells displayed a significant decrease in ROS generation after treatment with EXP57EA in the presence of 10 mM NAC. However, when the effect on cell number after co-treatment with EXP57EA and NAC was investigated, the results indicated that NAC did not rescue cells from EXP57EA-induced cytotoxicity (Figure 4.12), unlike the results observed in DHA-treated cells (Figure 4.5). Moreover, 5 µM EXP57EA in the presence of NAC appeared more cytotoxic than EXP57EA alone in both WHCO1 and WHCO6 cells, especially after 48 hours (Figure 4.12 B and D).

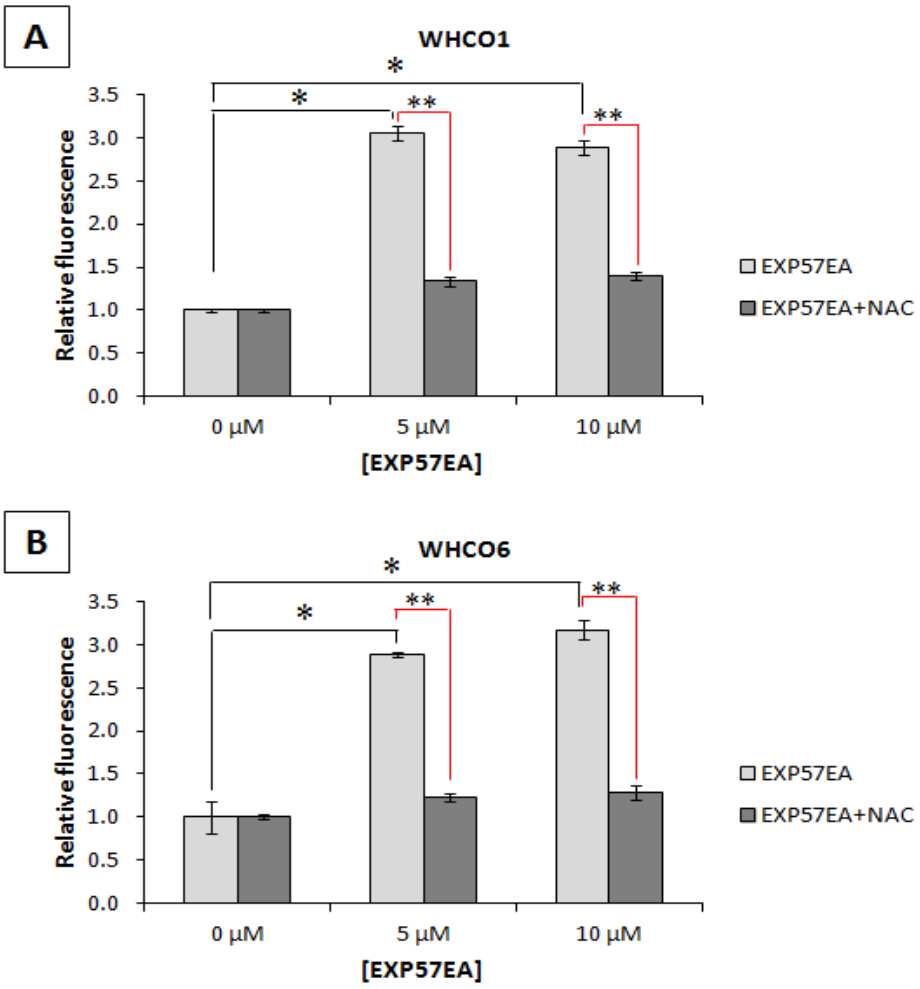

Figure 4.11: ROS production in WHCO1 (A) and WHCO6 (B) cells after treatment with EXP57EA in the presence and absence of NAC for 5 h. Cells ($1x10^4$) were plated in 96-well white plates and pretreated with 10 mM NAC (+NAC) or KR buffer only for 1 h, followed by pretreatment with 50 µM DCFDA for 15 min. EXP57EA was added and incubated for 5 h. Fluorescence was measured using a Cary Eclipse fluorescence spectrophotometer (484 nm excitation; 530 nm emission). Results are shown relative to fluorescence readings in control (vehicle-treated) cells, and are represented as the mean ±SD of experiments performed in triplicate and repeated at least two times. *$p<0.05$, **$p < 0.001$

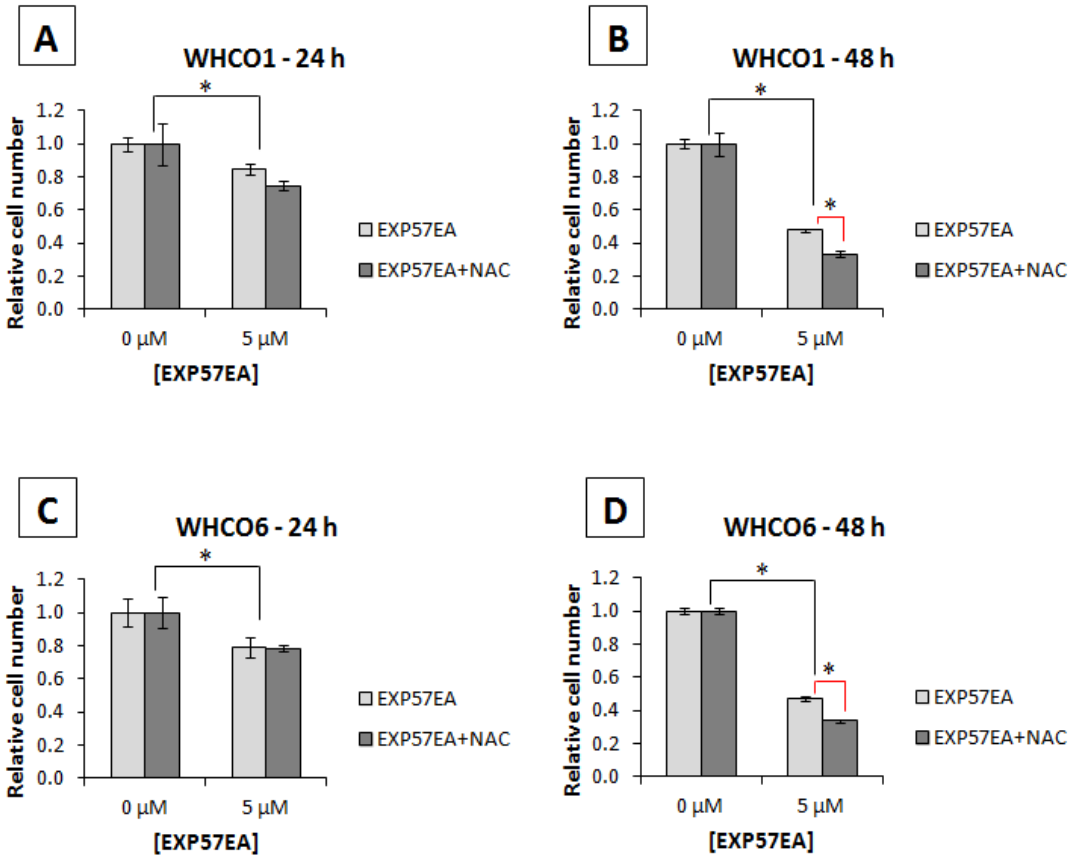

Figure 4.12: Effect of NAC on WHCO1 (A and B) and WHCO6 (C and D) cell number (OD_{595nm}) after treatment with EXP57EA for 24 h (A and C) and 48 h (B and D). Cells were plated in 96-well plates at a density of 3000 cells per well and allowed to settle overnight. Cells were either pretreated with 10 mM NAC (+NAC) or media only for 1 h, followed by treatment with 5 µM EXP57EA for 24 and 48 h. MTT reagent was added to fresh media and incubated for 4 h followed by the addition of solubilisation solution. The next day the absorbance was measured at 595 nm using a BioTek plate reader. Results are shown relative to absorbance readings in vehicle-only treated cells (0 µM) and are represented as the mean ±SD of experiments performed in triplicate and repeated at least two times. *$p < 0.05$

The concentration of NAC used in the literature varies, and studies have used concentrations ranging from 1 mM to 20 mM NAC to inhibit ROS production (Alexandre et al., 2006; Donadelli et al., 2011; Park et al., 2011; Spagnuolo et al., 2006). We wanted to investigate whether lowering the NAC concentration may have an effect on rescuing oesophageal cancer

cells from EXP57EA-induced cytotoxicity (considering the apparent increase in toxicity observed in the presence of EXP57EA and NAC (Figure 4.12). Figure 4.13 (A) demonstrated that in addition to 10 mM NAC, 2.5 mM and 5 mM NAC were also effective in scavenging ROS generated in WHCO1 cells treated with EXP57EA for 5 hours. However, 10 mM NAC was the most effective, maintaining ROS levels close to the baseline levels or that of the vehicle-only treated cells. Cells treated with 5 µM EXP57EA for 24 hours in the absence of NAC caused a small but significant reduction in cell number (Figure 4.13 B).

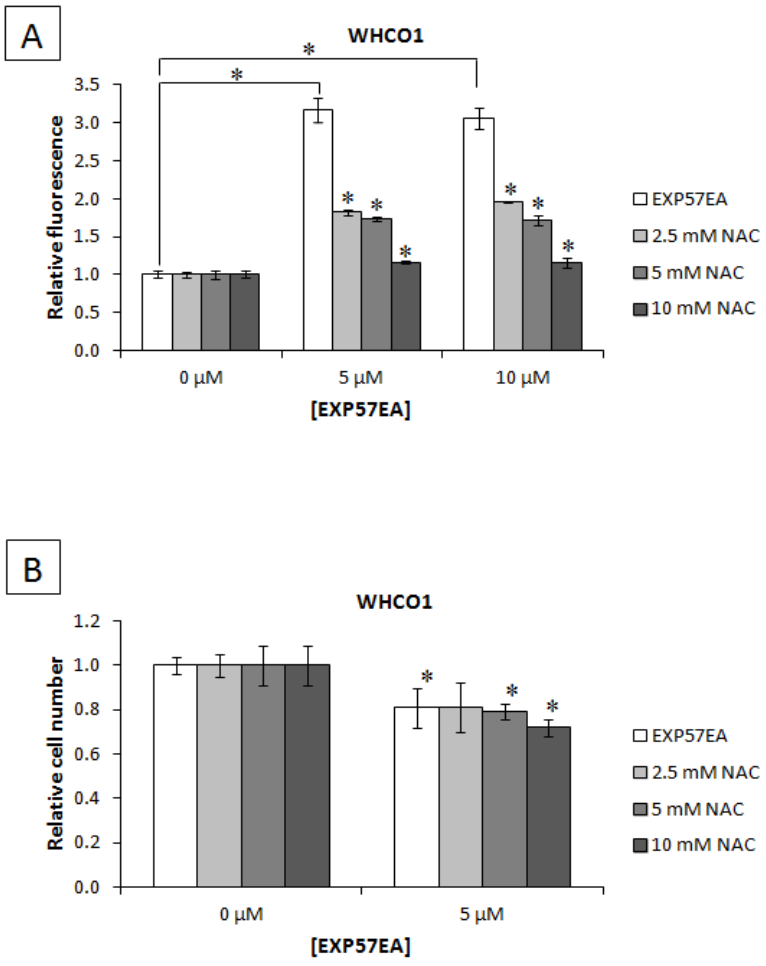

Figure 4.13: Effect of varying concentrations of NAC on ROS production (A) and cell number (OD_{595nm}) (B) in WHCO1 cells were treated with EXP57EA. (A), Cells ($1x10^4$) were seeded in 96-well white plates and pretreated with 2.5 mM, 5mM and 10 mM NAC or KR buffer only for 1 h, followed by treatment with 50 µM DCFDA for 15 min. The indicated concentrations of EXP57EA was added and incubated for 5 h. Fluorescence was measured using a Cary Eclipse fluorescence spectrophotometer (484 nm excitation; 530 nm emission).

Results are shown relative to fluorescence readings in control (vehicle-treated) cells. **(B)**, Cells (3000 per well) seeded in 96-well plates and were pretreated with 2.5 mM, 5mM and 10 mM NAC or media only for 1 h, followed by treatment with 5 μM EXP57EA for 24 h. MTT reagent was added to fresh media and incubated for 4 h followed by the addition of solubilisation solution. The next day the absorbance was measured at 595 nm using a BioTek plate reader. Results are shown relative to absorbance readings in vehicle-only treated cells (0 μM) and are represented as the mean ±SD of experiments performed in triplicate and repeated at least two times. *$p < 0.05$ compared to vehicle-only treated cells (0 μM).

As observed before (in Figure 4.12), there was no effect on cell number when WHCO1 cells were treated with 5 μM EXP57EA in the presence of the 2.5 mM and 5 mM NAC for 24 hours in comparison with cells treated with EXP57EA in the absence of NAC (Figure 4.13 B). Nevertheless, an assay to measure cell number was performed using higher concentrations of NAC (15 mM and 20 mM – similar to concentrations used by other authors (Donadelli et al., 2011; Kim et al., 2012) together with 5 μM EXP57EA (Figure 4.14). The results revealed that 15 mM NAC was ineffective in rescuing WHCO1 cells from EXP57EA-induced cytotoxicity and 20 mM NAC was very cytotoxic resulting in a 2.5 fold decrease in cell viability compared to vehicle-only treated cells. Subsequent experiments used 10 mM NAC to determine the effect of NAC in EXP57EA-treated cells.

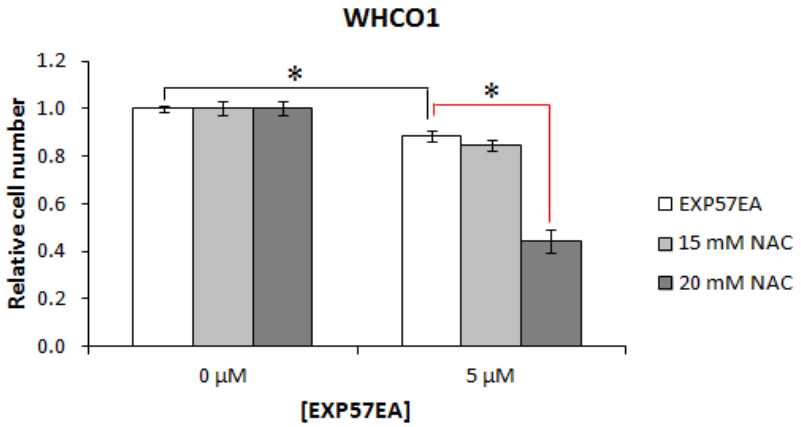

Figure 4.14: Effect of high NAC concentrations on WHCO1 cells after treatment with EXP57EA. Cells (3000 per well) seeded in 96-well plates and were pretreated with 15 mM, and 20 mM NAC or media only for 1 h, followed by treatment with 5 µM EXP57EA for 24 h. MTT reagent was added to fresh media and incubated for 4 h followed by the addition of solubilisation solution. The next day the absorbance was measured at 595 nm using a BioTek plate reader. Results are shown relative to absorbance readings in vehicle-only treated cells (0 µM) and are represented as the mean ±SD of experiments performed in triplicate and repeated at least two times. *$p < 0.05$

Furthermore, western blot analysis was performed to assess the expression of LC3-II, a marker of autophagy, in WHCO1 cells treated with EXP57EA in the presence and absence of 10 mM NAC. Illustrated in Figure 4.15 it was evident that the expression of LC3-II was unaffected in EXP57EA-treated WHCO1 cells in the presence of NAC. In addition, there was no change in the expression of cleaved PARP in cells treated with EXP57EA and NAC (Figure 4.16). In addition, to determine the effect of NAC on DNA damage in cells treated with EXP57EA, the expression levels of the DNA damage marker, γ-H2AX, was examined (Figure 4.17). In the absence of NAC, a dose-dependent increase in γ-H2AX expression was observed that was exacerbated by the presence of NAC, unlike the results observed for DHA-treated cells in the presence of NAC where γ-H2AX expression was decreased compared to γ-H2AX expression in DHA-treated cells in the absence of NAC.

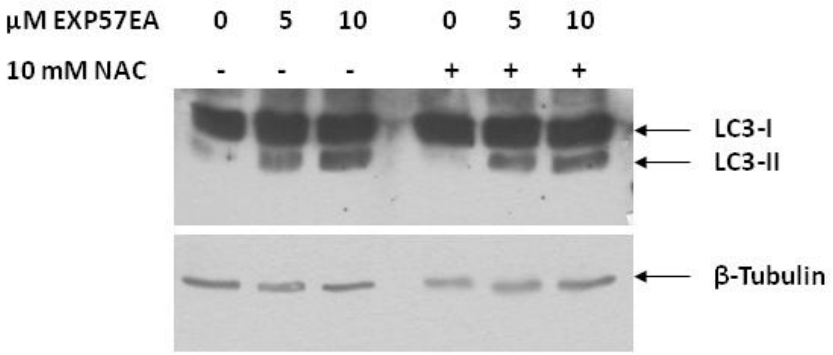

Figure 4.15: Western blot analysis illustrating the effect of NAC on the expression levels of LC3-II in WHCO1 cells treated with EXP57EA. WHCO1 cells (3 x 10^5) were plated in 60 mm dishes and incubated overnight. Cells were pretreated with 10 mM NAC (+) or media only (-) for 1 h followed by treatment with the indicated concentrations of EXP57EA for 24 h. Protein was harvested and quantified so that 40 µg could be separated by SDS-PAGE and transferred onto a nitrocellulose membrane. The membrane was probed with antibodies recognising LC3-I and LC3-II. Beta-Tubulin was used as a loading control and this figure is representative of at least two experiments.

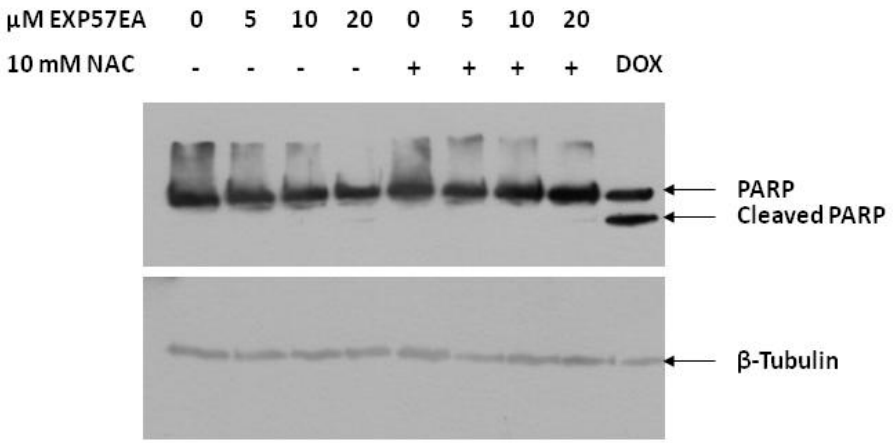

Figure 4.16: Western blot analysis illustrating the effect of NAC on expression levels of cleaved PARP in WHCO1 cells treated with EXP57EA for 24 h. WHCO1 cells (3 x 10^5) were plated in 60 mm dishes and incubated overnight. Cells were pretreated with 10 mM NAC (+) or media only (-) for 1 h followed by treatment with the indicated concentrations of EXP57EA for 24 h. Protein was harvested and quantified so that 20 µg could be separated by SDS-PAGE and transferred onto a nitrocellulose membrane. The membrane was probed with antibodies recognising PARP and cleaved PARP. The last lane contained WHCO1 cells treated with 5 µM DOX for 24 has a positive control to show PARP cleavage. Beta-Tubulin was used as a loading control and this figure is representative of at least two experiments.

Given that NAC was ineffective in rescuing oesophageal cancer cells from cytotoxicity induced by EXP57EA, and considering that EXP57EA significantly increased ROS production it was worthwhile investigating whether using alternative ROS scavengers may be effective. Therefore, L-ascorbic acid (LAA) and 6-hydroxy-2,5,7,8-tetramethylchroman-2-carboxylic acid (Trolox) were employed. LAA, more commonly known as vitamin C, and Trolox, a water-soluble analogue of vitamin E, are known to scavenge a wide array of ROS (Schlieve et al., 2006).

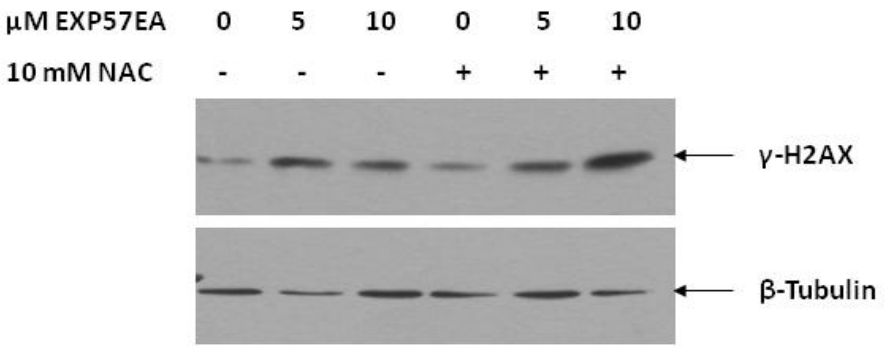

Figure 4.17: The effect of NAC on γ-H2AX expression in cells treated with EXP57EA. WHCO1 cells (3 x 10^5) were plated in 60 mm dishes and incubated overnight. Cells were pretreated with 10 mM NAC (+) or media only (-) for 1 h followed by treatment with the indicated concentrations of EXP57EA for 24 h. Protein was harvested and quantified so that 20 μg could be separated by SDS-PAGE and transferred onto a nitrocellulose membrane. The membrane was probed with antibodies recognising γ-H2AX. Beta-Tubulin was used as a loading control. This figure is representative of at least two experiments.

The DCFDA ROS assay was suitable to use for these experiments because it detects a broad range of ROS. As shown in Figure 4.18 A, both LAA and Trolox significantly reduced ROS generated by WHCO1 cells treated with EXP57EA for 5 hours. However, both scavengers had minimal effect on cell number in cells treated with EXP57EA after 24 hours and 48 hours. A report published by Chen and colleagues described superoxide as the main type of ROS that is associated with the induction of autophagy (Chen et al., 2009b). None of the

scavengers used above specifically quenched superoxide, thus TEMPOL (4-hydroxy-2,2,6,6-tetra-ethylpiperidine 1-oxyl), a superoxide-specific scavenger (Yamada et al., 2003), was used.

WHCO1 and WHCO6 cells treated with EXP57EA in the presence of 0.25 mM TEMPOL displayed a significant reduction in ROS (grey bars) compared to cells treated with EXP57EA in the absence of TEMPOL (white bars) (Figure 4.19 A and B, respectively). Interestingly, a significant increase in cell number was observed in cells treated with EXP57EA in the presence of TEMPOL (grey bars) in WHCO1 (Figure 4.19 C) and WHCO6 (Figure 4.19 D) cells for 24 hours when compared to EXP57EA-treated cells in the absence of TEMPOL (white bars). Thus, these results suggested that superoxide is the main type of ROS involved in EXP57EA-induced cytotoxicity.

MnSOD, an endogenous scavenger of superoxide, functions by catalysing the reaction of superoxide to hydrogen peroxide and oxygen (Li et al., 2010). When cells are exposed to high concentrations of superoxide, SOD genes are transcribed in order to prevent oxidative stress. In order to substantiate the effect of EXP57EA on superoxide levels in oesophageal cancer cells, the expression of MnSOD (manganese superoxide dismutase) was investigated after treatment with EXP57EA after 8 hours and 24 hours (Figure 4.20). A dose-dependent increase in the expression of MnSOD was observed after the 8 hour treatment point that was not sustained until the 24 hour treatment point (Figure 4.20).

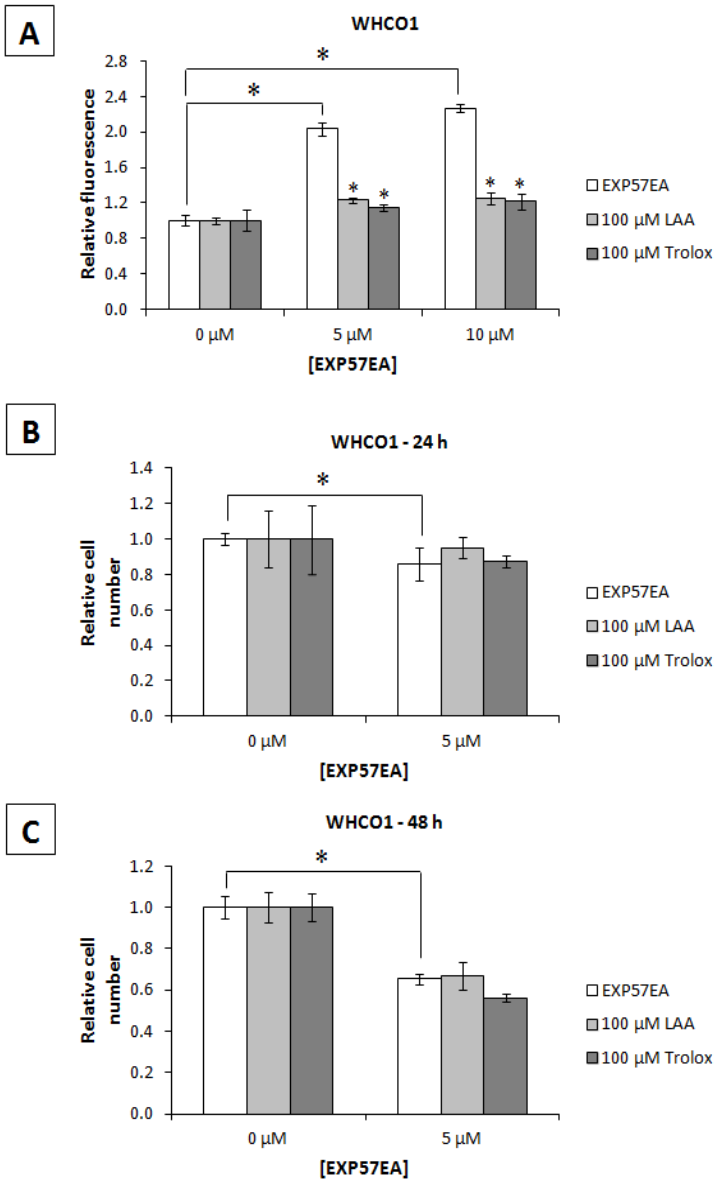

Figure 4.18: Effect of LAA and Trolox on ROS production (A) and cell number after 24 h (B) and 48 h (C) in WHCO1 cells treated with EXP57EA (A), Cells ($1x10^4$) were seeded in 96-well white plates and pretreated with 100 µM LAA, 100 µM Trolox or Krebs Ringer's buffer only for 1 h, followed by treatment with 50 µM DCFDA for 15 min. The indicated concentrations of EXP57EA was added and incubated for 5 h. Fluorescence was measured using a Cary Eclipse fluorescence spectrophotometer (484 nm excitation; 530 nm emission). Results are shown relative to fluorescence readings in control (vehicle-treated) cells. **(B, C),** Cells (3000 per well) seeded in 96-well plates and were pretreated with 100 µM LAA, 100 µM Trolox or media only for 1 h, followed by treatment with 5 µM EXP57EA for 24 h **(B)** and 48 h **(C)**. MTT reagent was added to fresh media and incubated for 4 h followed by the addition of solubilisation solution. The next day the absorbance was measured at 595 nm using a BioTek plate reader. Results are shown relative to absorbance readings in vehicle-only treated cells (0 µM) and are represented as the mean ±SD of experiments performed in triplicate and repeated at least two times. *$p < 0.05$

This result correlated with the ROS assay data where a significant increase in ROS production was observed after cells were treated with EXP57EA for 5 hours (Figure 4.10), suggesting that EXP57EA-induced cytotoxicity was mediated by early oxidative stress events. Furthermore, it is evident from these results that oesophageal cancer cells treated with EXP57EA responded to excessive superoxide levels by increasing the transcription of MnSOD.

Having established that superoxide was the main type of ROS involved in EXP57EA-induced cytotoxicity, we next wanted to determine the effect of this type of ROS on EXP57EA-induced autophagy. Thus, the effect of TEMPOL on EXP57EA-induced LC3-II expression was examined. WHCO1 cells treated with 10 μM EXP57EA in the presence of 0.25 mM TEMPOL displayed decreased expression of LC3-II compared to cells treated with EXP57EA in the absence of TEMPOL (Figure 4.21). The results presented here is consistent with the hypothesis that EXP57EA-induced superoxide plays a role in the activation of the autophagic pathway.

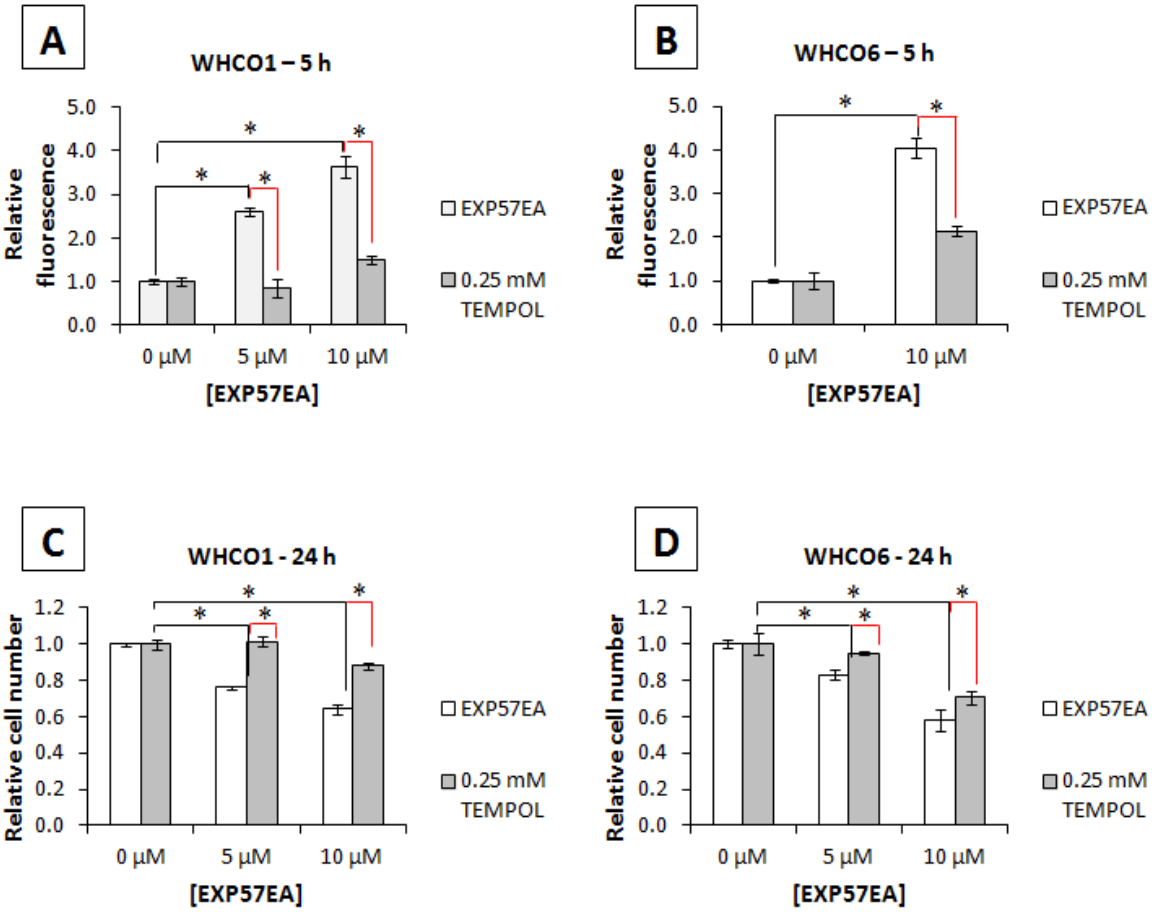

Figure 4.19: Effect of TEMPOL on ROS production (A and B) and cell number (OD_{490nm}) (C and D) in WHCO1 and WHCO6 cells after treatment with EXP57EA. (A, B), Cells ($1x10^4$) were seeded in 96-well white plates and pretreated with 0.25 mM TEMPOL or KR buffer only for 1 h, followed by treatment with 50 µM DCFDA for 15 min. The indicated concentrations of EXP57EA were added and incubated for 5 h. Fluorescence was measured using a Cary Eclipse fluorescence spectrophotometer (484 nm excitation; 530 nm emission). Results are shown relative to fluorescence readings in control (vehicle-treated) cells. **(C, D),** Cells (3000 per well) seeded in 96-well plates and were pretreated with 0.25 mM TEMPOL or media only for 1 h, followed by treatment with the indicated concentrations of EXP57EA for 24 h. NR (Neutral Red) reagent was added to fresh media and incubated for 3 h. Cells were washed with 1 x phosphate buffered saline (PBS) and incubated with NR desorb reagent for 45 min with rotation. Following 5 min incubation at RT (room temperature), absorbance was measured at 490 nm using a BioTek plate reader. Results are shown relative to absorbance readings in vehicle-only treated cells (0 µM) and are represented as the mean ±SD of experiments performed in triplicate and repeated at least two times. *$p < 0.05$

To further confirm the role of EXP57EA-generated superoxide in the induction of autophagy, the expression of phosphorylated p70S6 kinase (p-p70S6K) was assessed. The activation of this downstream target of mTOR, a negative regulator of autophagy, is known to be inhibited when autophagy occurs (Son et al., 2011; Sridharan et al., 2011). When WHCO1 and WHCO6 cells were treated with EXP57EA in the absence of TEMPOL, a decrease in p-p70S6K expression was observed after the 8 hour treatment point (Figure 4.24 A) and the 24 hour treatment point (Figure 4.24 B).

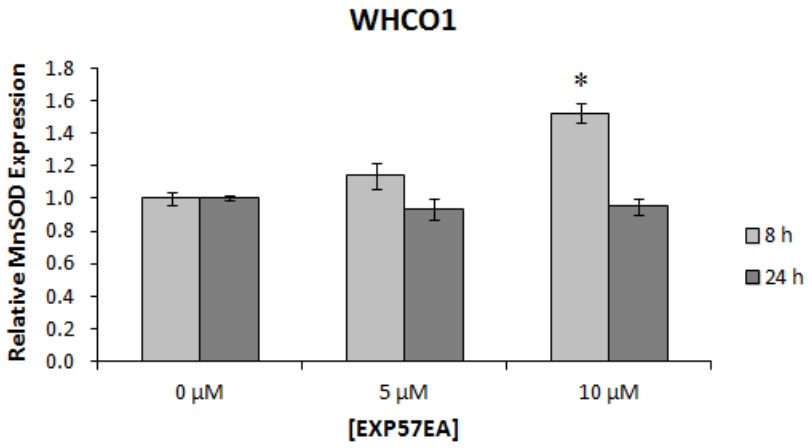

Figure 4.20: Evaluation of mRNA levels of MnSOD in WHCO1 cells treated with EXP57EA for 8 h and 24 h .WHCO1 cells were seeded at a density of 3 x10^5 per dish in 60 mm dishes. Cells were treated with 5 µM and 10 µM EXP57EA for 8 h and 24 h, after which RNA was extracted and processed. mRNA was analysed by quantitative real-time RT-PCR for the genes encoding MnSOD and GusB. Results (corrected using GusB expression levels) are shown relative to 0 µM (vehicle-treated) cells and are represented as the mean ±SD of experiments performed in triplicate and repeated at least two times. *$p < 0.05$

This observation is consistent with the induction of autophagy. TEMPOL (0.25 mM) increased p-p70S6K expression levels by ~10% in WHCO1 cells and ~5% in WHCO6 cells at the 8 hour treatment point, and ~8% in WHCO6 cells at the 24 hour treatment point in the absence of EXP57EA. However, in the presence of EXP57EA and TEMPOL, elevated levels of p-p70S6K expression is detected in WHCO1 and WHCO6 cells after 8 hours (1.3 fold and 3 fold, respectively) and 24 hours (8 fold and 11 fold, respectively), relative to p-p70S6K levels in EXP57EA-treated cells in the absence of TEMPOL (normalised to β-Tubulin) (Figure 4.22). These results implicated EXP57EA-induced superoxide in the inhibition of the mTOR pathway which correlates with the activation of the autophagic pathway.

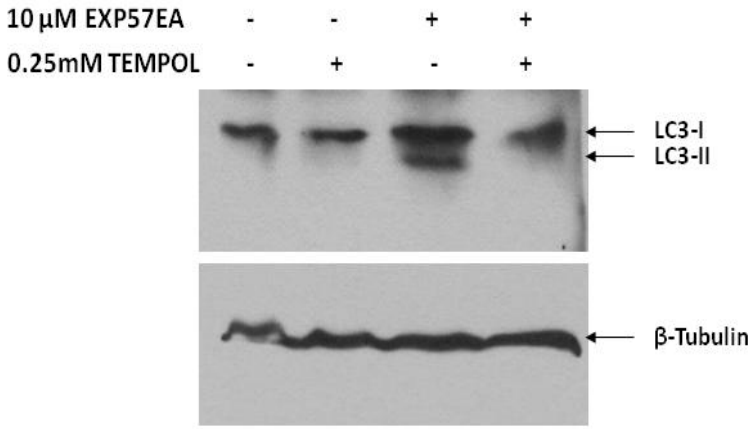

Figure 4.21: Western blot analysis demonstrating the effect of TEMPOL on expression levels of LC3-II in WHCO1 cells treated with EXP57EA. WHCO1 cells (3 x 10^5) were plated in 60 mm dishes and incubated overnight. Cells were pretreated with 0.25 mM TEMPOL or media only for 1 h followed by treatment with the 10 µM EXP57EA for 24 h. Protein was harvested and quantified so that 40 µg could be separated by SDS-PAGE and transferred onto a nitrocellulose membrane. The membrane was probed with antibodies recognising LC3-I and LC3-II and β-Tubulin, the loading control. This figure is representative of at least two experiments

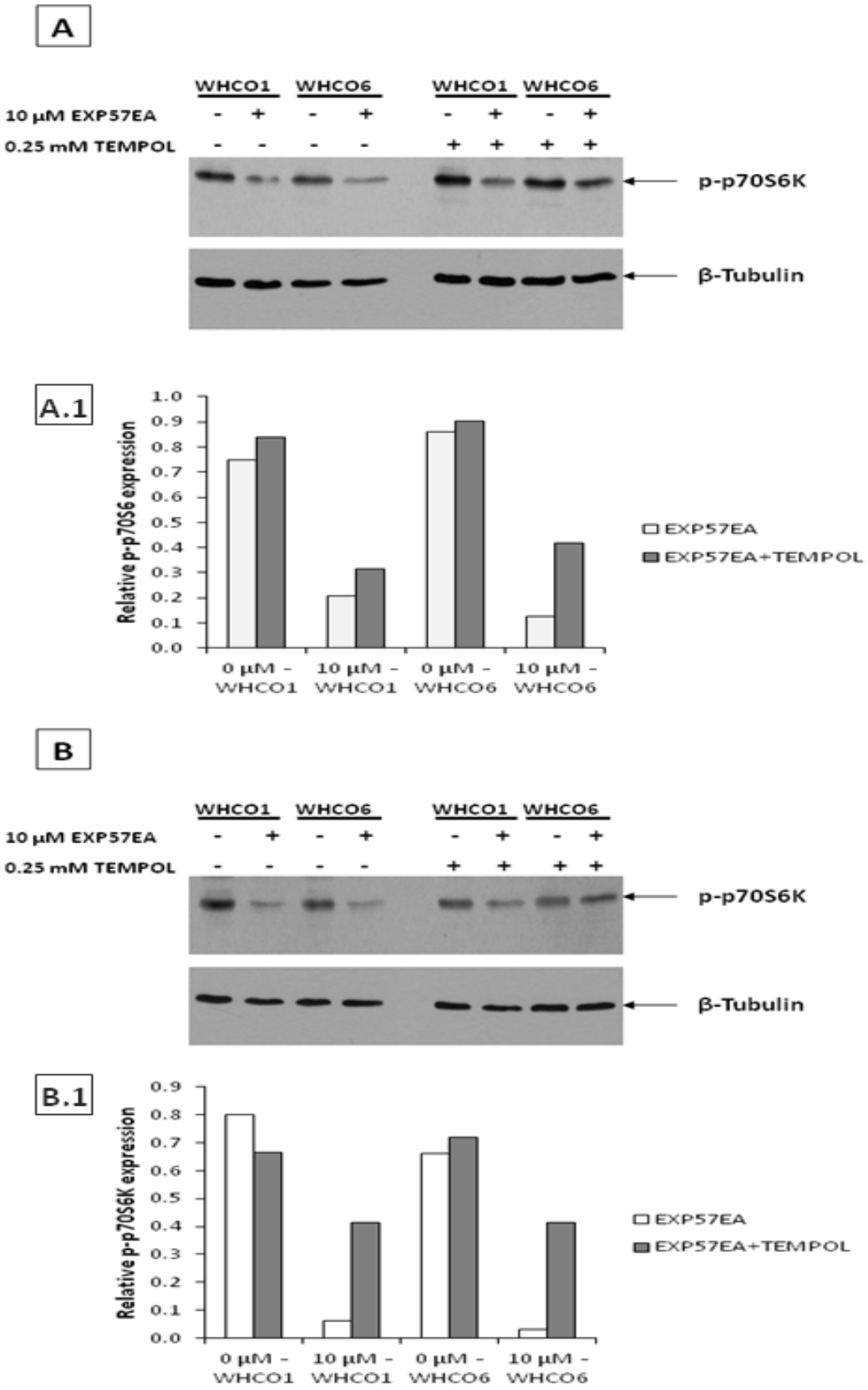

Figure 4.22: The effect of TEMPOL on expression of p-p70S6K in WHCO1 and WHCO6 cells treated with EXP57EA for 8 h (A) and 24 h (B). WHCO1 and WHCO6 cells (3 x 10^5) were plated in 60 mm dishes, and pretreated with 0.25 mM TEMPOL or media only for 1 h followed by treatment with the 10 µM EXP57EA

for 8 h **(A)** and 24 h **(B)**. Protein was harvested and quantified so that 40 µg could be separated by SDS-PAGE and transferred onto a nitrocellulose membrane. The membrane was probed with antibodies recognising p-p70S6K and β-Tubulin, the loading control. ImageJ software was used to determine p-p70S6K expression levels relative to β-Tubulin expression levels for WHCO1 **(A.1)** and WHCO6 **(B.1)** cells treated with EXP57EA in the presence and absence of 0.25 mM TEMPOL. This figure is representative of at least two experiments.

4.2.2.2 The effect of EXP57EA-induced ROS on signalling pathways involved in the activation of autophagy

Considering previous reports implicating mitogen activated protein kinases (MAPK) in the induction of autophagy via ROS-dependent mechanisms (Eom et al., 2010; Wong et al., 2010; Xavier et al., 2013), we were curious to learn whether EXP57EA-induced ROS had an effect on the MAPK pathways involved in autophagy. Therefore, the next step was to elucidate the role of EXP57EA on the activation of c-Jun-N-terminal kinase (JNK), extracellular-signal-related kinase (ERK) and p38 MAPK using western blot analysis.

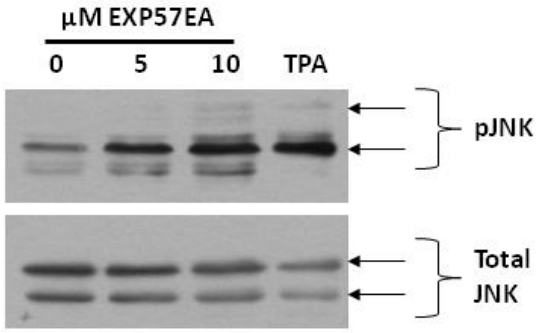

Figure 4.23: The effect of EXP57EA after 24 h on the expression levels of phosphorylated JNK (pJNK) in WHCO1. WHCO1 cells (3 x 10^5) were plated in 60 mm dishes and incubated overnight. Cells were treated with the indicated concentrations of EXP57EA for 24 h. Cells treated with 20 nM TPA for 1 h served as a positive control. Protein was harvested and quantified so that 40 µg could be separated by SDS-PAGE and transferred onto a nitrocellulose membrane. The membrane was probed with antibodies recognising pJNK and total JNK. This figure is representative of at least two experiments

WHCO1 cells treated with EXP57EA for 24 hours induced a dose-dependent increase in JNK activation (pJNK) (Figure 4.23). Bearing in mind that the increase in ROS measured by the ROS assay and the increase in MnSOD expression was observed after cells were treated with EXP57EA for short time points (5 hours and 8 hours, respectively), the effect of EXP57EA on pJNK expression levels was monitored after 8 hours (Figure 4.24). The strong activation of JNK after the 8 hour treatment with EXP57EA was clearly evident in both WHCO1 and WHCO6 cell lines, and this effect was reduced (by ~50% in WHCO1 cells and ~30% in WHCO6 cells) by co-treatment with SP600125, an inhibitor of JNK activity. Interestingly, EXP57EA had minimal effects on the activation of ERK over a period of time (Figure 4.25) and p38 after 8 hours (Figure 4.26) in oesophageal cancer cells.

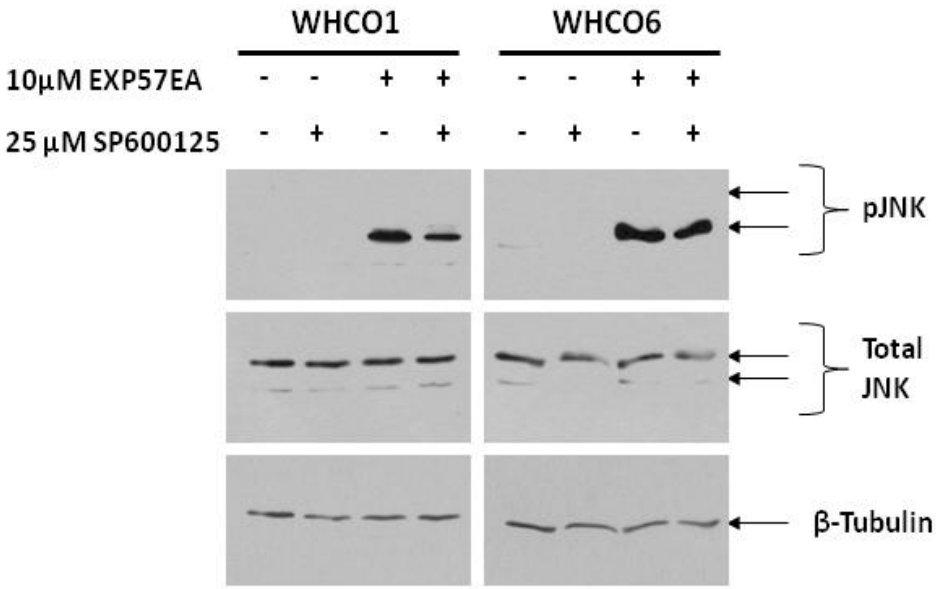

Figure 4.24: The effect of EXP57EA after 8 h on the expression levels of pJNK in WHCO1 and WHCO6 in the presence and absence of SP600125. WHCO1 and WHCO6 cells (3 x 10^5) were plated in 60 mm dishes and incubated overnight. Cells were pretreated with 25 μM SP600125 or media only for 1 h followed by treatment with 10 μM EXP57EA for 8 h. Protein was harvested and quantified so that 40 μg could be separated by SDS-PAGE and transferred onto a nitrocellulose membrane. The membrane was probed with antibodies recognising pJNK, total JNK and the loading control, β-Tubulin. This figure is representative of at least two experiments.

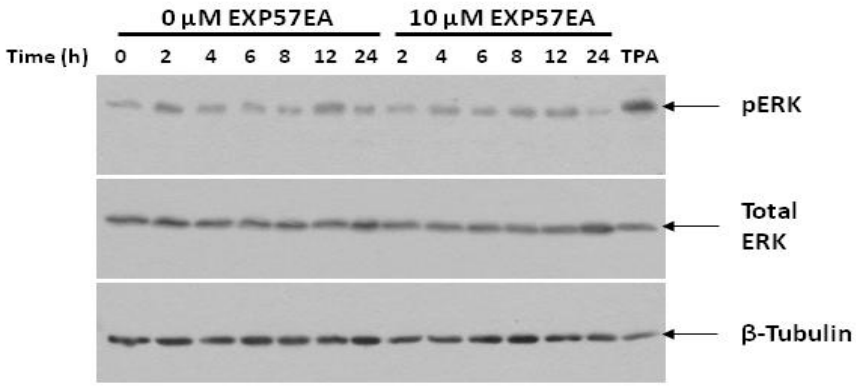

Figure 4.25: The effect of EXP57EA on the expression levels of phosphorylated ERK (pERK) in WHCO1 cells over time. WHCO1 cells (3 x 10^5) were plated in 60 mm dishes and incubated overnight. Cells were treated with 10 µM EXP57EA for the indicated time points. Cells treated with vehicle-only (0 µM) served as a control. Protein was harvested and quantified so that 40 µg could be separated by SDS-PAGE and transferred onto a nitrocellulose membrane. The membrane was probed with antibodies recognising pERK, total ERK and the loading control, β-Tubulin. This figure is representative of at least two experiments.

It is possible that the production of superoxide by oesophageal cancer cells treated with EXP57EA could be attributed to the metabolism of the compound by p450 enzymes in the endoplasmic reticulum (ER), which is also one of the major producers of ROS. The ER can produce different types of ROS, particularly superoxide, during metabolism of exogenous compounds (Curtin et al., 2002; Kim et al., 2009), which is associated with ER stress concomitant with increased calcium release from the ER (Malhotra and Kaufman, 2007). Since ER stress is closely associated with calcium release, an assay to monitor calcium signalling was used. NFAT (nuclear factor of activated T cells) activity is directly linked to an increase in intracellular calcium. Briefly, a sustained increase in intracellular calcium activates calcineurin, which dephosphorylates cytoplasmic NFAT transcription factors allowing rapid translocation to the nucleus (Wilkins et al., 2004). NFAT luciferase reporter activity was assessed by transient transfection of WHCO1 cells with a NFAT luciferase reporter plasmid containing three tandem repeats of a 30 bp fragment of the IL-2 promoter known to bind NFAT.

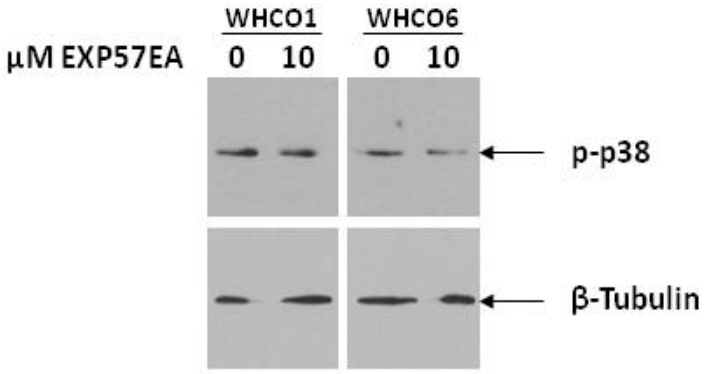

Figure 4.26: The effect of EXP57EA after 8 h on the expression levels of phosphorylated p38 (p-p38) in WHCO1 and WHCO6 cells. WHCO1 and WHCO6 cells (3 x 10^5) were plated in 60 mm dishes, and treated with 10 μM EXP57EA for 8 h. Protein was harvested and quantified so that 40 μg could be separated by SDS-PAGE and transferred onto a nitrocellulose membrane. The membrane was probed with antibodies recognising p-p38 and the loading control, β-Tubulin.

NFAT transactivation was measured in the presence and absence of TEMPOL, and after treatment with 10 μM EXP57EA for 24 hours, WHCO1 and WHCO6 cells (Figure 4.27 A and B, respectively) displayed ~ 1.5-fold increase in NFAT luciferase activity in the absence of TEMPOL; this effect was attenuated in the presence of 0.25 mM TEMPOL. Given that the increase in ROS production and that activation of JNK was observed at earlier time points, the experiment was repeated after a 6-hour treatment with EXP57EA (Figure 4.27 C and D). Although a similar result was seen after 6 hours, a smaller fold-increase (~1.2-fold) was observed in the absence of TEMPOL. These results indicate the EXP57EA-induced superoxide may increase intracellular calcium, which could be a result of ER stress. A further experiment was performed to determine the expression levels of CHOP, a marker of ER stress, in EXP57EA-treated cells (data not shown). The results revealed a strong increase in CHOP expression in WHCO1 and WHCO6 cells treated with 10 μM EXP57EA, however this represented preliminary results that must be repeated.

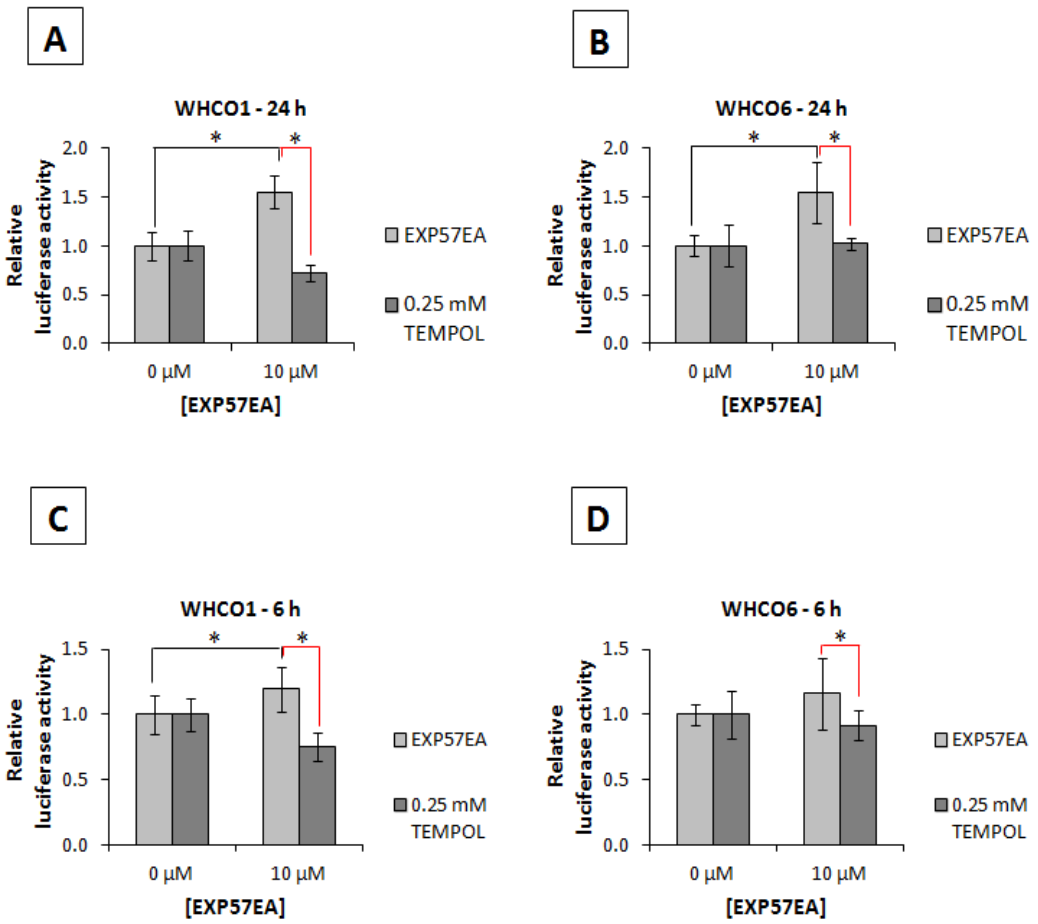

Figure 4.27: NFAT luciferase activity in WHCO1 and WHCO6 cells treated with EXP57EA for 24 h (A and B) and 6 h (C and D) in the presence and absence of TEMPOL.WHCO1 cells (3 x 10^4 per well) were plated in 24-well plates, and transfected with 50 ng GFP-NFAT plasmid, 50 ng NFAT-luciferase and 5 ng pRL-TK, using Genecellin™ Transfection Reagent. The following day cells were pretreated with 0.25 mM TEMPOL for 1 h then treated with 10 µM EXP57EA for 24 h **(A, B)** and 6 h **(B, C)**. After the relevant time points passed, cells were stimulated with 100 nM TPA and 1.3 µM Ionomycin for 5 h, following which luciferase activity was measured using the Veritas™ microplate luminometer. Luciferase readings were normalised to Renilla luciferase in the same extract. Results are shown relative to readings in vehicle-only treated cells (0 µM) and are represented as the mean ±SD of experiments performed in triplicate and repeated at least two times. *$p < 0.05$

4.3 Discussion

One of the objectives of this study was to characterise the effects of the artemisinin derivative, DHA, in our oesophageal cancer cell culture model together with the novel artemisinin-isatin hybrid, EXP57EA. The artemisinin derivatives, including DHA, have been investigated extensively in a large number of cancer cell lines as potential anticancer agents, but very little is known regarding the mechanistic effects of these compounds in oesophageal cancer. However, in the course of the finalisation of this thesis, a recent paper was published that reported the induction of apoptosis and autophagy by DHA in an OC cell culture model (Du et al., 2013). This paper is inconsistent with the observations made in this study, since we have never seen the induction of autophagy-associated vesicles in OC cells treated with DHA.

Artemisinin derivatives have been shown to induce apoptosis in a wide variety of cancer cell lines, and increased ROS production has been implicated as one of the important events leading to cell death, as mentioned earlier. In this study, we have conclusively shown that DHA induced both ROS and apoptosis. Furthermore, a ROS scavenger effectively blocked ROS production and also blocked apoptosis, highlighting a causal link between ROS production and the induction of apoptosis.

Different types of ROS (superoxide, hydroxyl radicals, hydrogen peroxide, singlet oxygen, nitric oxide and peroxynitrite) exist, of which most are produced at low concentrations in cells in order to participate in normal metabolic processes or are the byproducts thereof

(Barzilai and Yamamoto, 2004). Endogenous antioxidants such as superoxide dismutase, glutathione peroxidase, catalase, vitamins C and E are employed to maintain cellular homeostasis. Oxidative stress occurs when these scavenger mechanisms of the cell are overwhelmed by excessive ROS production, for example when cells are exposed to ionising radiation or exogenous compounds (Circu and Aw, 2010). Cancer cells have higher concentrations of ROS, compared to normal cells, due to increased metabolic activity as well as reduced levels of antioxidants due to tumourigenesis (Pelicano et al., 2004; Szatrowski and Nathan, 1991). This characteristic is often exploited by chemotherapeutic agents, which further increase the ROS concentration in cancer cells thus inducing cell death.

ROS can cause cancer cell death by apoptosis by direct stimulation of the sensors in the death receptor pathway, by promoting MOMP resulting in cytochrome c release or by causing DNA damage resulting in a cell cycle arrest (Circu and Aw, 2010). In this study, we showed that DHA significantly increased ROS production in oesophageal cancer cells. Very high concentrations of ROS within cells are frequently associated with DNA damage. In fact, DNA damage induced by ROS contributes to most of the DNA damage events observed in cells of the human body and can activate signalling pathways that participate in the "DNA damage response" (Barzilai and Yamamoto, 2004). Double-strand breaks (DSB) inflicted by ROS are a type of DNA damage that can cause apoptosis (Rich et al., 2000).

H2AX phosphorylation occurs on DSB during DNA damage and is often used as a marker for this process. The effect of DHA on the expression of phosphorylated H2AX (γ-H2AX) in WHCO1 and WHCO6 cells was determined. OC cells displayed a dose-dependent increase in γ-H2AX expression levels. The ROS scavenger, NAC, abrogated the effect of DHA on the

expression of γ-H2AX confirming that DHA-induced ROS production increased DNA damage in OC cells. A similar result was obtained by Berdelle and colleagues who reported the ROS-dependent DNA damaging effects of artesunate in LN-229 glioblastoma cells (Berdelle et al., 2011). Furthermore, ROS scavengers, including NAC, effectively inhibited the production of ROS and DNA damage and prevented cell death (Berdelle et al., 2011). Therefore, our study further substantiates reports in the literature of the ability of DHA to cause ROS-dependent DNA damage.

DNA damage can arrest cells in the various phases of the cell cycle. DNA repair mechanisms are activated during the G1/S or G2/M checkpoints of the cell cycle and success of these mechanisms result in the release of the block on arrested cells and allow the progression to the next stage of the cell cycle (Hartwell and Kastan, 1994). However, if repair is not possible or DNA damage is too extensive, programmed cell death results (Fragkos et al., 2009; Hartwell and Kastan, 1994). We have previously shown that OC cells treated with DHA arrested cells in the G2/M phase of the cell cycle, which was effectively blocked by treatment with NAC, reflecting the role of ROS in the G2/M arrest observed. Lu and colleagues demonstrated a similar effect in lung adenocarcinoma using the ASTC-a-1 cell line. Cells treated with DHA for 24 hours and 48 hours caused a significant increase in cells arrested in the G2/M phase of the cell cycle and this effect was abrogated in the presence of NAC (Lu et al., 2010). In addition, NAC also prevented DHA induced ROS-dependent Bax translocation, cytochrome c release, caspase-9, caspase-8, and caspase-3 activation, confirming the importance of ROS in the apoptotic pathway (Lu et al., 2010).

In this study, WHCO1 and WHCO6 cells treated with DHA resulted in a dose-dependent increase in the sub-G1 phase of the cell cycle. This effect was significantly reduced when cells were treated with DHA in the presence of NAC. Further substantiating this observation, cells co-treated with NAC and DHA displayed a reduction in the expression of cleaved PARP compared to cells treated with DHA alone. Moreover, NAC effectively rescued cells from DHA-induced cytotoxicity, measured using the MTT assay. These results are consistent with previous reports in the literature demonstrating the ROS-dependent induction of cancer cell death by artemisinin derivatives.

Interestingly, NAC was not able to rescue OC cells treated with the novel artemisinin-isatin hybrid compound, EXP57EA, despite being able to abrogate ROS production by EXP57EA-treated cells, at different concentrations of NAC tested. Furthermore, cells treated with EXP57EA in the presence of NAC displayed no change in LC3-II or cleaved PARP expression. Two different types of ROS scavengers, LAA and Trolox, were also tested and found to be ineffective in rescuing cells from EXP57EA-induced cytotoxicity. Indeed, ROS produced by treatment of cells with EXP57EA was measured after 5 hours since that was the time point during which the largest increase in ROS production was observed. Therefore, the broad ROS scavengers were effective at reducing ROS at that time point, but could not rescue cells from EXP57EA-induced cytotoxicity after the 24-hour treatment point. This could have been as a result of the scavengers not effectively reducing all types of ROS induced by EXP57EA treatment, and this reasoning was validated by work published by Chen and colleagues, implicating superoxide as the main type of ROS involved in the induction of autophagy (Chen et al., 2009b). The effect of a superoxide specific-scavenger, TEMPOL, was tested in cells treated with EXP57EA, and it was found that TEMPOL abrogated the effect of EXP57EA on ROS production and was able to rescue cells from EXP57EA-induced

cytotoxicity, unlike NAC. Further corroborating the cytotoxic effects of EXP57EA-induced superoxide, OC cells treated with EXP57EA in the presence of TEMPOL displayed a reduction of LC3-II and an increase in p-p70S6K (downstream target of mTOR, a key negative regulator of autophagy) expression, compared to cells treated with EXP57EA alone. This observation verified the role of superoxide in the induction of the autophagic pathway.

Superoxide can be produced by a variety of methods within the cells, and one method is via the microsomal monooxygenase (MMO) system of the ER. The MMO system is made up of cytochrome P450, NADPH-P450 reductase (NPR) and phospholipids. The cytochrome P450 family, especially, P4502E1 plays an important role in the detoxification of exogenous compounds, producing large amounts of ROS, especially superoxide and hydrogen peroxide (Kim et al., 2009; Meunier et al., 2004). Large amounts of ROS production in the ER can lead to ER stress, and increased release of calcium into the cytoplasm is one of the hallmarks of ER stress (Malhotra and Kaufman, 2007). A substantial increase in cytoplasmic calcium is essential to maintain NFAT activity in the nucleus of cells (Wilkins et al., 2004), and such high concentrations of calcium release into the cytoplasm is usually attributed to ER stress. In cells treated with EXP57EA in the absence of TEMPOL a significant increase in NFAT activity was observed, and this effect was attenuated in the presence of TEMPOL, suggesting that superoxide is required for the increase in calcium concentrations and thus ER stress. Supporting the concept of ER-induced superoxide production by EXP57EA, OC cells treated with EXP57EA revealed a large increase in CHOP (ER stress marker) expression (data not shown); however the experiment was performed once in two cell lines and represents preliminary results that must be repeated.

Superoxide can be quickly converted to hydrogen peroxide by SOD in the cell (Li et al., 2010). It is interesting to note that hydrogen peroxide can be rapidly converted to the hydroxyl radical when in contact with iron, via the Fenton reaction (Curtin et al., 2002). Cancer cells are known to have high concentrations of iron due to increased metabolism. One possibility could be that EXP57EA-induced superoxide is rapidly converted to hydrogen peroxide within the cell, increasing hydroxyl radicals in the cells leading to cytotoxicity, considering that the ROS scavenger mechanisms cannot truly scavenge hydroxyl radicals (Palmieri and Sblendorio, 2006). In addition, superoxide can also produce other types of ROS such as peroxynitrile, hypochlorous acid and singlet oxygen, which may play a role in the signalling events within the cell. Therefore, EXP57EA-induced superoxide could result in autophagic cell death via signalling pathways mediated by different types of ROS compared to those produced by DHA, supporting the improved activity observed by EXP57EA in oesophageal cancer cells compared to DHA. Furthermore, our hypothesis that EXP57EA-induced superoxide could be produced as a result of metabolism by cytochrome P450 enzymes in the ER is supported by the fact that DHA is the in vivo active metabolite of artesunate, artemether and arteether, therefore requires no metabolism by the cytochrome P450 enzymes (Ilett et al., 2002; Sertel et al., 2010). Therefore, the type of ROS induced by DHA could be a direct result from the reaction of the characteristic artemisinin-endoperoxide bridge with intracellular iron, known to be increased in cancer cells compared to normal cells.

The activation of JNK is frequently associated with increased ROS production (Circu and Aw, 2010), and cells treated with EXP57EA displayed increased phosphorylated JNK (pJNK) expression compared to vehicle-only treated cells. JNK activation is involved in the induction of autophagy by two ways: a.) pJNK can inhibit the Beclin 1-Bcl-2 complex freeing Beclin 1 to function in autophagosome formation, and b.) pJNK activates

transcription factors, cJun and AP-1, which are responsible for the transcription of Beclin 1 (Li et al., 2009a; Park et al., 2009). Furthermore, JNK can be activated by different types of ROS, including superoxide (Bai et al., 2012). A number of studies have showed that compounds (such as bufalin , resveratrol and calyxin Y) were able to induce autophagy in cancer cells (including colorectal cancer, chronic myelogenous leukemia and lung cancer) via ROS-mediated JNK activation (Puissant et al., 2010; Wong et al., 2010; Xie et al., 2011; Zhang et al., 2013). Whilst we have shown that EXP57EA treatment results in the increased expression of pJNK, we have not been able to show the effects of TEMPOL on pJNK expression in cells treated with EXP57EA, due to time constraints.

The results presented in this chapter provided strong evidence that DHA induced apoptosis in oesophageal cancer cells, mediated by ROS-induced DNA damage and cell cycle arrest. ROS-mediated apoptosis has been demonstrated in studies performed on various cancer cell lines treated with currently used anticancer drugs including paclitaxel (Alexandre et al., 2006), etoposide (Oh et al., 2007), doxorubicin (Tsang et al., 2003) and cisplatin (Berndtsson et al., 2007; Miyajima et al., 1997). EXP57EA also increased ROS production in oesophageal cancer cells but our data suggested that superoxide produced by EXP57EA resulted in cytotoxicity. In accordance with our data, superoxide is the main type of ROS involved in EXP57EA-induced autophagy which maybe be mediated by ER stress and JNK signalling pathways; however this requires further investigation.

CHAPTER 5:

CONCLUSION

Oesophageal cancer represents a significant health challenge in South Africa, which is a high risk area for the disease. Considering that OC is usually asymptomatic and as a result, diagnosed at a very late stage, the prognosis for patients with OC is very poor. The morbidity and mortality associated with this disease could be reduced if improved chemotherapeutic options for these patients could be developed. Effective chemotherapy includes agents that are capable of targeting and killing cancer cells without affecting normal cells; and there is an ongoing search for such agents, especially from natural sources. Natural products have made a significant contribution to currently used chemotherapeutic agents, therefore the aim of this project was to investigate the effects of novel compounds derived from natural products against oesophageal cancer cells.

This project focussed on artemisinins, compounds derived from a plant used in Traditional Chinese Medicine, and hybrids thereof. Novel hybrid compounds, which were synthesized by combining the artemisinin derivative, DHA, with the natural product scaffold, isatin, were investigated for their anticancer effects. In this study, it was demonstrated that the first generation artemisinin derivatives, ART and DHA, were active against oesophageal cancer cells, and that the novel hybrid compounds were more active than the first generation derivatives. Furthermore, this effect was demonstrated in a number of cancer cell lines, including cervical cancer and breast cancer cell lines. Both the first generation and the novel

compounds displayed selectivity to cancer cells versus normal cells; however the first generation derivatives were more selective for cancer cells over normal cells than the artemisinin-isatin hybrids. Importantly, lower concentrations of the novel compounds were required to kill cancer cells after the same treatment time as the first generation derivatives and the novel hybrid compounds were reproducibly more active than the first generation derivatives in all cancer cell lines tested. The observation that the novel compounds were more active than the parental compounds against cell lines that were considered chemoresistant, such as SiHa and MDA-MB-231, was very promising and warrants further investigation.

This study examined the mechanistic effects of the artemisinin derivatives, focussing on DHA and the novel artemisinin-isatin hybrid, EXP57EA, which was the most active novel hybrid compound tested. The initial biological investigations suggested that the first generation derivatives may have a different molecular mechanism of action compared to the hybrid compounds (G2/M cell cycle arrest versus G0/G1 cell cycle arrest, respectively), and upon further investigations we demonstrated that the parent compound, DHA, strongly induced apoptosis in OC cell lines whereas the novel hybrid, EXP57EA, induced autophagy. The role of autophagy in tumourigenesis is quite controversial considering conflicting evidence for its role in cell survival and cell death. A number of reports have demonstrated the ability of potential anticancer compounds to induce autophagic cell death in a variety of cancer cell lines (Ling et al., 2011; Puissant et al., 2010; Xie et al., 2011; Zhang et al., 2013). In this study, our results suggested that EXP57EA induces autophagy as a cell death pathway since there was no evidence of either apoptosis or necrosis. Using 3-MA, a chemical inhibitor of autophagy that is widely used in the literature, in cells treated with EXP57EA we were able to show the inhibition of autophagy with a concomitant increase in cell number,

compared to cells treated in the absence of 3-MA. Furthermore, autophagic flux was demonstrated using ammonium chloride, indicating that the complete autophagic pathway was activated by EXP57EA. Together this suggests that EXP57EA induces autophagic cell death in treated cells. However, to fully implicate EXP57EA-induced autophagy as the cause of cell death, it would be important to determine the effects of genetically inhibiting essential autophagy regulators such as Beclin 1 and Atg5 on expression of essential autophagy markers such as LC3-II, and then to determine the effects on cell number in OC cells treated with EXP57EA. This is in line with the criteria recommended by the NCCD (Galluzzi et al., 2012) in order to implicate autophagy as the cell death pathway in EXP57EA-treated cells. Therefore the future work on this project will include genetically inhibiting two or more essential regulators of autophagy and determining the effect on LC3-II expression as well as the effect on cell number after treatment with EXP57EA. We have already met the other two criteria outlined: a.) showing that 3-MA suppresses cell death and decreases expression of LC3-II in EXP57EA-treated cells, and b.) demonstrating that EXP57EA does not activate apoptosis or necrosis in OC cells.

The results obtained in this project demonstrated for the first time, to the best of our knowledge, that DHA induced ROS-dependent apoptosis in OC cells. DHA-treated OC cells displayed an increase in ROS production, γ-H2AX expression, G2/M cell cycle arrest, caspase3/7 activation and cleaved PARP expression. In the presence of the ROS scavenger, NAC, OC cells treated with DHA demonstrated a significant decrease in ROS production, γ-H2AX expression, G2/M cell cycle arrest, cleaved PARP expression and cell number compared to DHA-treated cells in the absence of NAC, implicating DHA-induced ROS production as the main signalling event leading to apoptotic cell death. Whilst similar results

were obtained in other cancer cell lines (Berdelle et al., 2011; Lu et al., 2010), this has not been reported in oesophageal cancer.

EXP57EA, on the other hand, was more active than DHA in our cell culture models and OC cells treated with EXP57EA in the presence of NAC did not respond in the same manner as OC cells treated with DHA in the presence of NAC. The results obtained in this study demonstrated a large increase in ROS production in cells treated with EXP57EA. Whilst NAC apparently scavenged the ROS generated by EXP57EA, it could not rescue the cells from the cytotoxicity associated with EXP57EA, unlike TEMPOL which scavenged the ROS and reduced the EXP57EA induced cytotoxicity. Consequently, we demonstrated that superoxide was the main type of ROS produced by OC cells treated with EXP57EA. The results obtained thereafter implicated EXP57EA-induced superoxide production in the activation of the autophagic pathway when TEMPOL, a superoxide-specific scavenger, abrogated the effects of EXP57EA on the expression of LC3-II and other markers of the autophagic pathway. Furthermore, we hypothesized that the superoxide produced after treatment with EXP57EA could be as a result of its metabolism by the cytochrome P450 enzyme family in the ER. Our preliminary results suggested that ER stress pathway may be activated by EXP57EA in OC cells, and this requires further investigation. In addition, our results suggested that another important stress pathway, the JNK pathway, may have a role in EXP57EA-induced autophagy.

Future work on this project will be done to confirm the effect of EXP57EA on ER stress by confirming the increased expression of CHOP as well as other proteins involved in the ER stress pathway such as GRP78. Furthermore, the expression levels of these proteins will be

evaluated in the presence and absence of TEMPOL to confirm that EXP57EA-induced superoxide is directly associated with ER stress. It will also be a valuable exercise to confirm the EXP57EA-ER stress-induced release of calcium, as calcium can exacerbate ROS production via interaction with the mitochondria (Malhotra and Kaufman, 2007). In addition, calcium can also activate autophagy through CaMKKβ activation leading to the activation of the AMPK pathway. Furthermore, apart from calcium signalling, the ER stress pathway is involved in the induction of autophagy via multiple mechanisms (discussed in Chapter1.2.3.4), including the JNK pathway. ER stress activates a variety of proteins including IRE1 that leads to the activation of JNK (Maholtra and Kaufman). Therefore, this investigation will also be included in the future work planned for this project. It will be important to characterise the effects of EXP57EA on the JNK pathway considering that JNK activation can induce autophagy and that the JNK pathway can be regulated by ROS and ER stress, both associated with EXP57EA treatment of oesophageal cancer cells.

There is a need for new chemotherapeutic agents to treat oesophageal cancer. Artemisinins represent a new class of drugs that possess anticancer properties and in this study novel artemisinin hybrid compounds were investigated for their effects against oesophageal cancer. These compounds have not been studied, to the best of our knowledge, in oesophageal cancer. We have demonstrated that the novel compounds were more active than the first generation artemisinin derivatives and that DHA induced ROS-dependent apoptosis whereas the most active novel hybrid compound, EXP57EA, activated autophagy. Our results suggest that superoxide plays an important role in the cytotoxic effects observed in cells treated with EXP57EA. This certainly requires further investigation to answer important mechanistic questions pertaining to oesophageal cancer cells treated with EXP57EA, a promising drug lead for the treatment of cancer.

The hybrid compounds were synthesized with the intention of improving the activity of the parental compounds and this study provides evidence that this has been achieved. Furthermore, the EXP57EA displayed a molecular mechanism of action different to the parental compound. This has an important implication in the treatment of cancer where the development of resistance to anticancer drugs is a common occurrence. Therefore, characterising chemotherapeutic agents capable of activating alternate cell death and signalling pathways, compared those frequently induced by most currently used chemotherapeutic agents, may provide a valuable contribution to anticancer drug discovery.

CHAPTER 6:

MATERIALS AND METHODS

6.1 Cell Culture

6.1.1 Cell lines

The three oesophageal cancer cell lines, WHCO1, WHCO5 and WHCO6, were derived from biopsies of primary oesophageal squamous cell carcinomas (Veale and Thornley, 1989) and kindly provided by Professor Rob Veale (University of Witwatersrand, South Africa). The KYSE oesophageal squamous cell carcinoma cell lines (KYSE30, KYSE150 and KYSE180) previously established by Shimada and co-workers (Shimada et al., 1992), were purchased from the German Resource Centre for Biological Material (http://www.dsmz.de). The CaSki, HeLa and SiHa cervical cancer cell lines, MCF7, MDA-MB-231 and T47D breast cancer cell lines, HepG2 liver cancer cell line and the SK-N-SH neuroblastoma cell line were purchased from the American Type Culture Collection (Rockville, MD, USA). Two primary fibroblast control cell cultures prepared from human skin, DMB and FG^0, were used as a normal cell types and were developed and kindly donated by Sheena Jones, University of Cape Town, South Africa.

6.1.2 Cell culture

All cell lines were maintained at 70 - 80% confluency in Gibco® Dulbecco's Modified Eagle Medium (DMEM) (Invitrogen, USA) containing 10% heat-inactivated foetal bovine serum (FBS) (Gibco, Paisley, Scotland), penicillin (100 U/ml) and streptomycin (100 µg/ml). DMEM prepared in this way is referred to as complete DMEM. All cell lines used were cultured at 37°C in a humidified atmosphere which was supplied with 5% carbon dioxide.

6.1.3 Sub-culturing cells

Cells cultured in a 100 mm culture dish to a confluency of 70 – 80% were washed once with a 0.05% trypsin-EDTA (Difco, USA) solution (hereafter referred to as trypsin), followed by the addition of 3 ml fresh trypsin. The trypsinisation of cells was monitored with a light microscope (Telaval 31, Zeiss, Germany) for up to 5 min, or until 80 – 90% of cells had lifted off the culture dish. The trypsin was neutralised with 3 ml complete DMEM. The cell suspension was transferred to a 10 ml Falcon tube and centrifuged at 1000 rpm (revolutions per minute) for 5 min. The solution of media and trypsin was aspirated off and the pelleted cells were resuspended in 1 ml complete DMEM. A fresh 100 mm culture dish was prepared containing 10 ml fresh DMEM to which 500 µl of the cell suspension was inoculated.

6.1.4 Freezing and thawing cells

In order to prepare cell stocks, cells were grown to 80% confluency, sub-cultured with trypsin and neutralized with complete DMEM. This was followed by centrifugation at 1000 rpm to pellet the cells. The cells were resuspended in cell freezing medium (70% complete DMEM, 20% FBS and 10% DMSO) and 1 ml was aliquotted per cryotube. The cells were placed at -

80°C for a maximum of one week before submergence in liquid nitrogen for long term storage.

Cells removed from liquid nitrogen were swirled gently in a 37°C waterbath until a small ball of ice remained. The cells were transferred, drop-wise, to 5 ml pre-warmed complete DMEM and pelleted by centrifugation. The cells were resuspended in 1 ml complete DMEM and transferred to 60 mm dish containing 3 ml complete DMEM

6.1.5 Test for mycoplasma

Mycoplasma tests were routinely performed on all cell lines to rule out contamination. Mycoplasma are microbes that are invisible under normal tissue culture light microscopy. Cells were cultured in media free of penicillin and streptomycin for at least four days before plating onto coverslips. After a further incubation for up to 48 h, cells were fixed with fixing solution followed by staining with the fluorescent DNA-binding Hoechst 33258 fluorochrome stain (Sigma-Aldrich® Co.). The coverslip was mounted after a brief wash with water and cells were visualised on the Zeiss Axiovert 200 Fluorescent microscope (Carl Zeiss, Germany). Stained nuclei appeared bright green and tiny green spots in the cytoplasm between nuclei were indicative of mycoplasma. The absence of the spots in the cytoplasm indicated cell cultures that were free of mycoplasma.

6.2 Compounds and inhibitors

All compounds received from the Department of Chemistry (UCT) were dissolved in tissue culture grade DMSO (Sigma-Aldrich® Co), unless otherwise stated. Doxorubicin (DOX), 3-methyladeninine (3-MA), ammonium chloride (NH_4Cl), *N*-acetyl-L-cysteine (NAC), L-ascorbic acid (LAA), 6-hydroxy-2,5,7,8-tetramethylchroman-2-carboxylic acid (Trolox), 4-hydroxy-2,2,6,6- tetra-ethylpiperidine 1-oxyl (TEMPOL), 12-*o*-tetradecanoylphorbol-13-acetate (TPA), JNK inhibitor (SP600125) and Ionomycin (ION) were purchased from Sigma-Aldrich® Co and dissolved in tissue culture grade DMSO with the exception of NAC, LAA , 3-MA and NH_4Cl, which were dissolved in sterile dH_2O.

6.3 Compound sensitivity testing

The 3-[4,5-Dimethylthiazol-2-yl]-2,5-diphenyltetrazolium bromide (MTT) (Sigma-Aldrich® Co) assay was employed to test compound sensitivity. The IC_{50} values were determined using a range of concentrations (0, 0.1, 1, 5, 10, 50, 100 and 200 µM). Cells were plated at a density of 3000 cells per well in triplicate in 90 µl of media in 96-well plates and incubated O/N at 37°C. The cells were treated with 10 µl of compound diluted in media and DMSO to give a final DMSO concentration of 0.2%. The cells were incubated for 48 h after which 10 µl MTT solution was added to each well and incubated for a further 4 h. MTT reagent consists of yellow tetrazolium salt that is reduced to purple formazan crystals in the mitochondria of living cells. After the 4 h incubation period the formazan crystals were solubilised by the addition of 100 µl solubilisation reagent (10% w/v SDS, 0.01 M HCl)

followed by an O/N incubation. The absorbance was subsequently measured at 595 nm on a BioTek EL800 (BioTek, Winooski, VT, USA) 96-well microplate reader. The absorbance of media plus compound was subtracted from the absorbance of the compound-treated cells in media to account for background absorbance. The IC_{50} values were calculated using GraphPad Prism version 5.00 for Windows (GraphPad Software, USA, www.graphpad.com). The dose-response curves were generated by non-linear regression analysis (Non-linear regression (Sigmoidal dose response with variable slope)) to yield an IC_{50} value. The following formula was used: $Y = bottom + (top-bottom)/ (1+10^{(\log IC50 - x)\ (hill\ slope)})$.

6.4 Cell proliferation and viability assays

6.4.1 MTT assays

6.4.1.1 Time-course experiments

Time-course experiments were performed whereby cells were treated with the indicated concentrations of the compounds over a period of 4 days, and cell proliferation was measured. Cells were seeded at a density of 1500 cells in 90 µl media per well, in quadruplicate and allowed to settle O/N. This was followed by treatment (10 µl) with the various concentrations of each compound. After each time point elapsed, 10 µl MTT reagent was added and incubated for 4 h 37ºC followed by an O/N incubation with 100 µl solubilisation reagent at 37ºC. Absorbance was read at an OD of 595 nm using a BioTek microplate reader and a growth curve was generated using GraphPad Prism version 5.00 for Windows, GraphPad Prism Software.

6.4.1.2 Viability assays using chemical inhibitors

The effect of the indicated concentrations of the compounds in the presence and absence of the respective chemical inhibitors on cell viability was determined using the MTT assay. Briefly, 3000 cells per well were seeded into 96-well plates, pretreated with the inhibitors for 1 h, followed by treatment with the indicated compounds for 24 h and/or 48 h. MTT reagent was added and incubated for 4 h at 37ºC followed by an O/N incubation with 100 µl solubilisation reagent at 37ºC. Absorbance was read at an OD of 595 nm using a BioTek microplate reader. Microsoft Excel was used to analyse data and generate bar graphs.

6.4.2 Neutral red uptake assays

The neutral red uptake (NRU) assay was used when the MTT assay could not be employed due to reaction with certain inhibitors. This assay, based on the ability of viable cells to take up and bind neutral red, was also used to confirm the results of the MTT viability assays. In short, 3000 cells per well were seeded into 96-well plates, pretreated with the inhibitors for 1 h, followed by treatment with the indicated compounds for 24 h and/or 48 h. Media was removed from each well, 200 µl neutral red (NR) media was added and incubated for 3 h. The NR media was removed and cells were washed once with 200 µl prewarmed 1 x PBS. One hundred microlitres NR desorb was added to each well. The plate was covered with foil and incubated at RT for 45 min with rotation. This was followed by a RT incubation with rotation for 5 min. Absorbance was read at 490 nm using BioTek microplate reader. Microsoft Excel was used to analyse data and generate bar graphs.

6.5 Western blot analysis

6.5.1 Extraction, processing and quantification of total cell protein

Cells (3 x 10^5) were plated in 60 mm dishes and incubated for 24 h, after which cells were exposed to the indicated concentrations of each compound for the relevant time points. Media was removed and cells were washed twice with ice cold 1 x PBS. All rinses and media were collected in 12 ml tubes and subjected to centrifugation (1000 rpm for 5 min) to pellet cells that may have detached from the tissue culture dish during compound treatment. The adherent cells in the tissue culture dish were harvested (on ice) using a cell scraper (rubber policeman) and 60 µl of ice cold radioimmunoprecipitation assay (RIPA) buffer containing 1 x protease inhibitor cocktail (Roche, Switzerland), 1 mM sodium orthovanadate and 20 mM sodium fluoride (to inhibit phosphatase activity). This lysis solution was used to resuspend the pelleted non-adherent cells, and the resulting lysates were subjected to sonication (on ice) for 10 s with a probe sonicator (Heat System-Ultrasonics). This was followed by centrifugation for 15 min at 11,000 x *g* (at 4°C), to remove cell debris. The supernatant containing the total protein was transferred to a fresh, chilled eppendorf tube and kept on ice. The protein concentration was determined using the Bicinchoninic Acid (BCA) Protein Assay Kit (Pierce, Thermo Scientific, USA) according to the manufacturer's instructions, and either stored at -80°C or prepared for separation by sodium dodecyl sulphate polyacrylamide gel electrophoresis (SDS-PAGE).

6.5.2 SDS-PAGE, immunoblotting and immunodetection

The BioRad Mini-Protean II gel system (BioRad, USA) was used to separate proteins using either a 10% or 15% acrylamide (Sigma-Aldrich® Co) separating gel. A 4% acrylamide stacking gel was consistently used, and the SDS-polyacrylamide gels were cast in either 1 mm or 1.5 mm glass plates. Protein samples (20 - 40 μg) were suspended in 1 x Laemmli buffer and denatured at 80°C for 5 min prior to loading into the wells of the SDS-polyacrylamide gels. The protein molecular weight marker, Spectra Multicolour Broad Range Protein Ladder (Fermentas), was used to determine the size of the proteins. Proteins were subjected to electrophoresis at 100-150 volts for the appropriate time.

Following electrophoresis, proteins were transferred to Hybond™-ECL™ nitrocellulose membranes (Amersham Biosciences, UK) using a buffered tank transfer system (BioRad), at 100 volts for 1 h. Membranes were rinsed briefly using TBS with 0.1% Tween 20 (Sigma-Aldrich® Co.) (TBS-T) and incubated for 1 h with 5% fat-free dry milk in TBS-T (blocking solution) to block nonspecific binding sites, then incubated with the primary antibody to the protein of interest at 4 °C O/N, with rotation. Antibody concentrations and incubation conditions were optimised for each individual antibody, and are shown in Table 6.1.The membrane was washed three times with TBS-T for 10 min each and incubated with secondary antibody for 1 h at RT, with rotation. The membrane was washed a further three times for 10 min each with TBS-T.

Table 6.1. Antibody concentrations and incubation conditions

Primary Antibody	Company & Catalogue No.	Primary Antibody Conditions	Secondary Antibody	Secondary Antibody Conditions	Substrate	Size (kDa)
PARP	Santa Cruz sc-7150	1:2000 5% milk	GαR Biorad	1:5000 5% milk	Super Signal West Pico	116 89
LC3	Cell Signaling #2775	1:1000 TBS-T	GαR Biorad	1:5000 5% milk	LumiGlo Reserve	18 16
β-Tubulin	Santa Cruz sc-9104	1:1000 TBS-T	GαR Biorad	1:5000 5% milk	Super Signal West Pico	55
Beclin 1	Santa Cruz sc-48341	1:1000 5% milk	GαM Biorad	1:5000 5% milk	Super Signal West Dura	58
γ-H2AX (Ser139)	Cell Signaling #9718	1:1000 TBS-T	GαR Biorad	1:5000 5% milk	Super Signal West Dura	15
p-p70S6K (Thr389)	Cell Signaling #9205	1:1000 5% BSA	GαR Biorad	1:5000 5% milk	LumiGlo Reserve	70
p-SAPK/JNK (Thr183/Tyr185)	Cell Signaling #9251	1:1000 5% BSA	GαR Biorad	1:5000 5% milk	Super Signal West Dura	46 54
SAPK/JNK	Cell Signaling #9258	1:1000 5% BSA	GαR Biorad	1:5000 5% milk	Super Signal West Pico	46 54
p-p38	Cell Signaling #9211	1:1000 TBS-T	GαR Biorad	1:1000 5% milk	Super Signal West Dura	38
p38	SIGMA MO800	1:1000 3% milk	GαR Biorad	1:5000 5% milk	LumiGlo	38
pERK ½ (Thr202/Tyr204)	Cell Signaling #9106	1:500 1% BSA	GαM Biorad	1:1000 2.5% milk	Super Signal West Dura	42 44
ERK 2 (C-14)	Santa Cruz sc-154	1:1000 1% milk	GαR Biorad	1:1000 2.5% milk	Super Signal West Pico	42
CHOP	Cell Signaling #55545	1:1000 5% milk	GαR Biorad	1:2000 5% milk	LumiGlo Reserve	27
GAPDH	Cell Signaling #2118	1:1000 5% BSA	GαR Biorad	1:5000 5% milk	LumiGlo	37

The immunoreactivity was detected by enhanced chemiluminescence and depending on the strength of the signal one of the following chemiluminescent substrates were used: SuperSignal West Pico or West Dura kits (Pierce, Thermo Scientific, USA) or Lumiglo or Lumiglo Reserve (KPL Inc., USA). Chemiluminescent light emission was detected manually using developer (AGFA G128) and fixative (AGFA G333C). Protein bands were visualised by developing AGFA X-ray film in developer, washing with water, and then fixing using the fixative, for the appropriate times according to manufacturer's instructions.

6.5.3 Stripping and reprobing membranes

In order to reprobe membranes, the primary antibody was stripped off by incubation in 1M glycine at pH 2.5 for 7 min per side. This was followed by neutralisation with 1/10 volume 1 M Tris-Cl, pH 8.0, after which the membranes were washed three times for 10 min each with TBS-T. Subsequently, the membranes were incubated in blocking solution for 30 - 45 min prior to O/N incubation with the primary antibody.

6.6 RNA extraction, quantification and preparation for quantitative real-time RT-PCR

6.6.1 RNA extraction from cultured cells

Cells (80 000) were plated in 35 mm dishes in triplicate and incubated for 24 h, after which cells were exposed to the indicated concentrations of each compound for the relevant times. RNA was harvested from treated cells with QIAzol (Qiagen, Germany) according to the manufacturer's instructions. Briefly, cells were rinsed twice with ice cold 1 x PBS, after

which QIAzol was added to cells and incubated for 5 min at RT. With the aid of a rubber policeman the homogenate was scraped off the tissue culture dish and transferred to a chilled eppendorf tube. Subsequently, 0.2 ml chloroform per 1 ml of QIAzol was added to each sample, mixed vigorously for 15 s followed by a 2 min incubation at RT. The samples were centrifuged at 12 000 x *g* at 4°C for 15 min in order to separate the phases. The upper aqueous phase was transferred to a fresh eppendorf tube, and RNA was precipitated using 0.5 ml isopropanol per 1 ml QIAzol. Following a thorough mix using a vortex and 10 min incubation at RT, samples were subjected to centrifugation at 12 000 x *g* at 4°C for 10 min. The supernatant was discarded and RNA pellets were washed with ice cold 75% ethanol (centrifugation at 7500 x *g* at 4°C for 5 min). RNA pellets were air-dried (for a maximum of 10 min) and resuspended in 30 µl diethylpyrocarbonate (DEPC)-treated dH_2O.

RNA was quantified using the Nanodrop™ 2000c spectrophotometer (Thermo Scientific, USA) and 1 µg of RNA was mixed with RNA loading dye and electrophoresed on a 1.5% MOPS/formaldehyde agarose gel (containing 0.5 µg/µl ethidium bromide) to determine the integrity of the extracted RNA.

6.6.2 Quantitative real time RT-PCR

cDNA was prepared by reverse transcribing 2 µg of the total RNA by hybridization with 0.5 µg oligo $(dT)_{20}$ primer (Promega, USA) or 0.5 µg random hexamer primers (Oligonucleotides Synthesis Facility, UCT) in a final volume of 8 µl at 70°C for 10 min. Subsequently, 1 µl ImPromII Reverse Transcriptase II, 40 units of RNAsin RNase inhibitor, 2 mM $MgCl_2$, 1 mM dNTPs and 1 x ImPromII reaction buffer (all reagents from Promega, USA) were added

to each sample yielding a final volume of 20 µl. The samples were incubated at RT for 10 min, 42°C for 30 min, 80°C for 2 min and the resultant cDNA were placed on ice until use or aliquotted and stored at -80°C for later use.

Quantitative real time reverse transcription polymerase chain reaction (RT-PCR) was performed using the StepOne Real-time PCR System (Applied Biosystems, USA), and the comparative threshold cycle (C_T) method was used for the calculation of expression fold change between samples. Real time RT-PCR was performed using triplicate samples with 2 µl of cDNA (~200 ng), or dH_2O as a negative control, using the KAPA SYBR qPCR Master Mix (KAPA Biosystems, South Africa), and 200 nM of the primer pairs listed in Table 6.2. The PCR cycling conditions were an enzyme activation step at 95°C for 3 min followed by 40 cycles of denaturation at 95°C for 1 s and annealing at T_a for 20 s. C_T values were calculated using StepOne Version 2.0 software (Applied Biosystems) and the $\Delta\Delta C_T$ method was used to calculate the expression of target mRNA relative to that of a known housekeeping gene, *β-glucuronidase* (GusB). PCR products were electrophoresed on a 2% agarose gel containing ethidium bromide in order to ensure that a single, specific PCR product was amplified and that there was no contamination or primer dimer formation. Samples were prepared in 6 x loading dye (Fermentas) and electrophoresed at 65 V for 1 h. A DNA ladder (O' GeneRuler DNA Ladder Mix, Thermo Scientific) was used to approximate target gene size.

Table 6.2. Sequences of primers used for real-time RT-PCR

Gene	Sequence	PCR product size (bp)	T_a (°C)
Beclin1 Forward	5'AGGAACTCACAGCTCCATTAC 3'	88	55
Beclin1 Reverse	5' AATGGCTCCTCTCCTGAGTT 3'		
Atg5 Forward	5' GGAGTAGGTTTGGCTTTGGTTGA 3'	191	55
Atg5 Reverse	5' TCGTCCAAACCACACATCTCG 3'		
MnSOD Forward	5' GCACTAGCAGCATGTTGAGC 3'	142	60
MnSOD Reverse	5' GCGTTGATGTGAGGTTCCAG 3'		
GusB Forward	5' CTCATTTGGAATTTTGCCGATT 3'	81	55
GusB Reverse	5' CCGAGTGAAGATCCCCTTTTTA 3'		

T_a refers to the annealing temperature

6.7 Caspase-Glo® Assay

Caspases are important mediators of the apoptotic pathway and their activity is often used to measure apoptosis by using a luminogenic substrate, where the luminescence produced is proportional to caspase activity. To assay for Caspase-3/7 activity, the Caspase-Glo® 3/7 Assay (Promega Cat#G8090) was performed, according to the manufacturer's instructions. Briefly, cells (3000 per well) were seeded in 96 well plates in a final volume of 90 µl, in triplicate. The next day cells were treated with the indicated concentration of the compounds bringing the final volume in the wells to 100 µl. An equal volume of Caspase-Glo® reagent was added to each well, mixed carefully by rotation at 300 rpm for 30 s and subsequently

incubated at RT for 1 h. Thereafter, 100 µl of the mixture in each well was tranferred to a white 96-well plate and luminescence was measured using the Glomax 96 Microplate Luminometer (Promega, USA).

6.8 Necrosis Assay

The CytoTox-ONE™ Homogeneous Membrane Integrity Assay (Promega Cat#G7891) was used to analyse the levels of necrosis by detection of lactate dehydrogenase (LDH) released from cells. Cells (3000 per well) were plated in 96 well plates in a final volume of 90 µl, in quadruplicate, and allowed to settle O/N. Thereafter, cells were treated with compounds (10 µl) bringing the final volume in the wells to 100 µl. After the indicated time points elapsed, 100 µl of CytoTox ONE reagent was added for 10 min followed by the addition of 50 µl of Stop solution. At each time point a lysis buffer, supplied with the kit, was added to a set of wells and served as the positive control. The fluorescence was measured using a Cary Eclipse fluorescent spectrophotometer, and the results were expressed as a percentage of the positive control.

6.9 Phase-Contrast Microscopy

Eighty thousand cells were plated on ethanol-flamed coverslips in 35 mm dishes and allowed settle O/N. The cells were then treated with different concentrations of the compounds and incubated for 24 h and 48 h at 37ºC. The cells were washed with 1 x PBS and fixed in 4%

paraformaldehyde in1 x PBS for 20 min at RT. Cells were washed once more with 1 x PBS and the coverslip was lifted carefully using tweezers and placed briefly in a beaker containing dH_20. The excess dH_20 was removed by touching the tip of the coverslip with paper towel and the cells were mounted onto slides in Mowiol 4-88 (Calbiochem #475904) and allowed to dry for at least 15 min before being visualised on the phase-contrast microscope (Axiovert 200M microscope (Zeiss)). Images were captured using an AxioCamHR camera with Axiovision software, version 4.7 (Zeiss).

6.10 Immunofluorescent analysis

Cells were seeded at a density of 80 000 cells per well, on ethanol-flamed coverslips, in a 6-well plate for immunofluorescent analysis of protein expression and localisation. The cells were treated with the indicated concentrations of the compounds for the relevant time points in a total volume of 1.5 ml media. Thereafter, 1 ml ice cold methanol was added to the cells and media and mixed briefly. The methanol/media mixture was discarded and 1 ml ice cold media was added to the cells and incubated at -20°C for 10 min. The methanol was discarded and the cells were rinsed 3 times with cold 1 x PBS. Cold 3% BSA prepared in 1 x PBS was added to the cells and incubated for 1 h, with rotation. Coverslips were incubated with 50 µl primary antibody (rabbit α-LC3, 1:500 in 3% BSA) in a humidified chamber for 1 h. Subsequently, the primary antibody was removed by three 5 min washes in 1 x PBS, and 50 µl secondary antibody (Cy3-conjugated goat anti-rabbit, 1:1000 in 3% BSA) was placed on the coverslips. After a 1 h incubation in a darkened humidified chamber, coverslips were washed 3 times for 5 min in 1 x PBS. Nuclei of the cells were stained using 0.5 µg/ml Hoechst prepared in 1 x PBS for 30 s, and this was followed by 2 washes with 1 x PBS. The

coverslips were mounted on slides with Mowiol 4-88, and viewed under an Axiovert 200M microscope (Zeiss) and images were captured using AxioCamHR camera with Axiovision software, version 4.7 (Zeiss). Confocal images were taken using a Zeiss LSM 510 Meta confocal microscope with a Mai Tai two photon laser and ZEN 2009 software.

6.11 Cell cycle profile analysis

Cells were seeded in 100 mm dishes at a density of 0.5 x 10^6 cells per dish, in triplicate. The indicated concentrations of each compound was added and incubated for the relevant times. The media and washes (once with 2 ml trypsin) were collected on 50 ml Falcon tube and the cells were harvested using 3 ml 0.05% trypsin-EDTA. Complete DMEM (3 ml) was added to neutralise the trypsin, and the cell suspension was transferred to the tube containing the media and initial wash. This was followed by centrifugation at 1000 rpm for 5 min. The pelleted cells were resuspended in 1 ml 1 x PBS and cells were counted. Thereafter, 9 ml ice cold 95% ethanol was added to each sample which were stored at -20ºC for up to 2 weeks. The samples were centrifuged at 1000 rpm for 5 min, the pellets resuspended in 1 ml 1 x PBS and centrifuged at 1000 rpm for 5min, once more. The cell pellets were resuspended in 1 ml 1 x PBS and transferred to a fresh eppendorf and subjected to a final centrifugation at 1000 rpm for 5 min. A total of 1 x 10^6 cells were incubated in 50 µg/ml RNAse A (in 1 x PBS) for 30 min at RT. The cell cycle staining solution was added to each sample and incubated in the dark for 30 min. Cells were analysed on a Beckman Coulter FACScalibur flow cytometer (Becton Dickinson, USA) using CellQuest Pro Software (Becton Dickinson). The cell cycle profiles were analysed using ModFit 3.2 (Verity Software House, USA).

6.12 Reactive oxygen species (ROS) assay

Cells were seeded in an opaque white 96-well plate at a density of 1 x 10^4 cells per well (in triplicate) in a final volume of 100 µl media. The next day media was removed and cells were rinsed once with pre-warmed KR buffer. This was followed by the addition of 100 µl 50 µM DCFDA in KR buffer, and a 15 min incubation at 37ºC in the dark. The cells were treated with the indicated concentrations of the compounds for the relevant time points, and the fluorescence was read at 484 nm excitation and 530 nm emission using a Cary Eclipse fluorescence spectrophotometer (Varian, Inc.). For the scavenging of ROS, the cells were pretreated with the scavengers (NAC, LAA, Trolox or TEMPOL) for 1 h before the DCFDA was added to the cells.

6.13 Transmission electron microscopy (TEM)

Ultrastructural analysis was performed to detect the induction of autophagy morphologically in compound-treated cells using transmission electron microscopy (TEM). Cells were seeded in 100 mm dishes at 1 x 10^6 cells per dish and incubated O/N. The cells were then treated with the indicated concentrations of the compound and incubated for 6 h and 24 h. Following treatment, cells (detached using 0.05% trypsin-EDTA) and media were collected and centrifuged at 1000 rpm for 5 min to pellet cells. Supernatant was discarded and the pelleted cells were washed with 1 ml ice cold 1 x PBS by centrifugation at 1000 rpm for 5 min at 4ºC. Cells were fixed with 2.5% glutaraldehyde in 0.1 M Sorenson's phosphate buffer pH 7.4 for at least 1 h and then washed twice with the same buffer. The cells were post-fixed in 1%

OsO4 (Osmium tetroxide) in 0.1 M Sorenson's phosphate buffer pH 7.4 for 1 h at RT followed by washing once with the same buffer and twice with dH_2O. Cells were then pre-stained with 1% uranyl acetate for 1 h at RT. This was followed by one dH_2O wash before the dehydration process, which entailed multiple centrifugation (cell pelleting) and resuspension steps in increasing ethanol concentrations. Each centrifugation was 5 min long at 1000 rpm until 100% ethanol concentration was reached, in which cells were centrifuged twice for 10 min each at 1000 rpm (100% ethanol discarded and fresh 100% ethanol added after first 10 min elapsed). This was followed by two 10 min centrifugation steps in 100% acetone (following same procedure as with 100% ethanol), leading to the resin infiltration steps beginning with an O/N incubation at RT in a 1:1 ratio of resin:acetone. The next day the cells were pelleted by centrifugation (5 min at 1000 rpm), resuspended in a 3:1 ratio of resin: acetone and incubated for 6 h at RT. The cells were pelleted, resuspended in 100% resin and incubated O/N at RT. The next day the cells were pelleted, resuspended in 100% resin and incubated for 1 h. This was followed by the final embedding of the cells in resin by an O/N incubation at 60ºC in 100% resin. After the cells were embedded in the resin, ultrathin sections of 120 nm were cut using a Reichert Ultracut S ultramicrotome and collected in a boat of distilled water. Using a fine pair of tweezers, a copper grid was used to collect the ultrathin sections from the boat of water. The grids were placed on filter paper in a Petri dish which was inverted. The sections were then stained with 2% uranyl acetate for 10 min at RT followed by 5 washes with dH_2O. The final 5 min staining with lead citrate culminated the sample preparation process allowing the sections to be analysed using a FEI Tecnai F20 transmission electron microscope (Apollo Scientific).

6.14 NFAT luciferase assay

An assay to monitor NFAT luciferase activity was employed using a NFAT-luciferase report plasmid, containing three tandem repeats of a 30 bp fragment of the IL-2 promoter known to bind NFAT. Thirty thousand cells were plated per well in 24-well plates, and transfected with 50 ng GFP-NFAT plasmid (Addgene plasmid # 24219, gift of Jerry Crabtree (Beals et al., 1997), 50 ng NFAT-luciferase (Addgene plasmid # 10959, gift of Toren Finkel (Ichida and Finkel, 2001), and 5 ng pRL-TK, using 0.4 µl Genecellin™ Transfection Reagent (Celtic Molecular Diagnostics, South Africa). The following day cells were treated with the indicated concentrations of the compound and after an O/N incubation, stimulated with 100 nM TPA (Sigma-Aldrich® Co) and 1.3 µM Ionomycin (Sigma-Aldrich® Co) for 5 h, following which luciferase activity was measured using the Veritas™ microplate luminometer (Promega, USA). Luciferase readings were normalised to Renilla luciferase in the same extract.

6.15 Statistical analysis

Microsoft Excel or GraphPad Prism software was used for statistical analyses. Experiments were performed in triplicate or quadruplicate and represented as the mean ± standard deviation (SD), or the mean ± standard error of the mean (SEM), as indicated. Experiments were repeated at least two times. For data comparisons between untreated (vehicle-only treated) and treated (compound-treated) groups, the Student's two-tailed paired t-tests were performed with a p value of <0.05 considered statistically significant.

6.16 Solutions

Cell culture solutions

Complete DMEM

450 ml DMEM

50 ml FBS

5 ml Penicillin (100 U/ml) and streptomycin (100 µg/ml)

Stored at 4°C.

10 x Phosphate buffered saline (PBS), pH 7.4

40 g NaCl

1 g KCl

5.75 g Na_2HPO_4.7H2O

1 g KH_2PO_4

Made up to 500 ml with dH_2O.

1 x Phosphate buffered saline (PBS), pH 7.4

100 ml 10 x PBS

900 ml dH_2O

0.5 M EDTA, pH 8.0

37.22 g EDTA

140 ml dH_2O

Adjusted to pH 8.0 using 10 M NaOH.

Made up to 200 ml with dH_2O.

Trypsin-EDTA solution

0.5 g Trypsin

8 g NaCl

1.45 g $Na_2HPO_4.2H_2O$

0.2 g KCl

0.2 g KH_2PO_4

10 mM EDTA pH 8.0

Made up to 1000 ml with 1 X PBS, and stored at 4°C.

Cell freezing medium

70% DMEM

20% FBS

10% DMSO

Mycoplasma detection solutions

Hank's balanced salt solution, pH 7.4

5.4 mM KCl

0.3 mM Na_2HPO_4

0.4 mM KH_2PO_4

1.3 mM $CaCl_2$

0.5 mM $MgCl_2$

0.6 mM $MgSO_4$

137 mM NaCl

5.6 mM D-glucose

Made up to 1000 ml with dH_2O, and stored at 4°C.

Mycoplasma fixing solution

1 part glacial acetic acid to 3 parts methanol

Hoechst stain (0.5µg/ml)

5 mg Hoechst No. 33258

100 ml Hank's balanced salt solution

Stored at -20°C.

Mounting fluid

1.05 g citric acid

1.41 g $Na_2HPO_4.2H_2O$

50 ml glycerol

pH 5.5

Stored at 4°C.

Drug sensitivity testing solutions

MTT reagent (5 mg/ml)

100 mg MTT

20 ml 1 x PBS

Vortexed briefly, incubated at 37°C for 15 min then filtered through a 0.2 µm filter.

Wrapped in foil and stored at 4°C for up to one month.

Solubilisation reagent

25 g Sodium lauryl sulphate

Made up to 250 ml with dH_2O, then added 76.6µl concentrated HCl.

Neutral red (NR) stock solution (3.3 mg/ml)

0.33 g Neutral Red H_2O

10 ml dH_2O

Filtered using a 0.2 μm filter, wrapped in foil and stored at RT for up to 2 months.

NR media (33 μg/ml)

1 ml Neutral red stock solution

99 ml Complete media

Made fresh, and maintained at 37°C before use.

Used within 30 min of preparation.

NR desorb

1% Glacial acetic acid

50% Ethanol

49% dH_2O

Western Blot Analysis Solutions

RIPA buffer

150 mM Sodium chloride

1 % Triton X-100

1 % Sodium deoxycholate

0.1 % SDS

10 mM Tris-Cl, pH 7.4

10% Acrylamide separating gel (10 ml)

4 ml dH_2O

2.5 ml 1.5 M Tris-Cl, pH 8.8

100 µl 10% SDS

3.3 ml 30% Acrylamide

100 µl 10% Ammonium persulphate

10 µl TEMED

15% Acrylamide separating gel (10 ml)

2.3 ml dH_2O

2.5 ml 1.5 M Tris-Cl, pH 8.8

100 µl 10% SDS

5 ml 30% Acrylamide

100 µl 10% Ammonium persulphate

10 µl TEMED

4% Acrylamide stacking gel (5 ml)

3 ml dH_2O

1.25 ml 0.5 M Tris-Cl, pH 6.8

50 µl 10% SDS

670 µl 30% Acrylamide

50 µl 10% Ammonium persulphate

5 µl TEMED

4 x Laemmli loading dye

250 mM Tris-Cl, pH 6.8

6 % SDS

0.005 % Bromophenol Blue

40 % Glycerol

10 % β-mercaptoethanol

10 x Running buffer

30.2 g Tris

144 g Glycine

10 g SDS

Made up to 1000 ml with dH_2O.

1 x Running buffer

100 ml 10 x running buffer

900 ml dH_2O

10 x Transfer buffer

144 g Glycine

30.3 g Tris

Made up to 1000 ml with dH_2O.

1 x Transfer buffer (1000 ml)

In this order:

100 ml 10 x Transfer buffer

700 ml dH_2O

200 ml methanol

Made fresh before use, and kept ice cold until use.

10 x Tris buffered saline (TBS), pH 7.5

60.5 g Tris

87.6 g NaCl

Dissolved in 700 ml dH_2O,

Adjusted pH using 1 N HCL or 10 M NaOH, then made up to 1000 ml with dH_2O.

1 x TBS-T

100 ml 10 x TBS

900 ml dH_2O

1 ml Tween-20

Mixed well.

Blocking solution

0.5 g fat free milk powder (Elite)

10 ml 1 x TBS-T

Rapid Coomassie staining solution

0.024 % Coomassie Brilliant Blue

10 % Acetic acid

90 % dH_2O

Destain

10 % Glacial Acetic Acid; 10% Methanol

Real-time RT-PCR solutions

DEPC-treated- dH_2O

0.1% DEPC in dH_2O; autoclaved

10 x MOPS

41.86 g MOPS (0.2 M)

16.6 ml 3 M NaAcetate (0.05 M)

20 ml 0.5 M EDTA (0.01 M)

Made up to 1000 ml with dH_2O, and diluted to 1 x with dH_2O as required.

RNA Loading Buffer (1.5 ml)

720 µl Formamide

160 µl 10 x MOPS Buffer

260 µl 37 % Formaldehyde

80 µl dH_2O

100 µl 80 % Glycerol

200 µl 0.25 % Bromophenol Blue

1.5 % MOPS/formaldehyde agarose gel

0.75 g Agarose

5 ml 10 x MOPS

42 ml dH_2O

2.7 ml 37 % Formaldehyde

2.5 µl (10 mg/ml) Ethidium Bromide

Mixed agarose, 10 x MOPS and dH_2O together; heated to dissolve, and then cooled to ~50°C.

In fumehood, added formaldehyde and mixed well, then added ethidium bromide.

10 x Tris borate EDTA (TBE)

108 g Tris

55 g Boric Acid

7.4 g EDTA

Made up to 1000 ml with dH2O

2% agarose gel (100ml)

2 g Agarose

10 ml 10 x TBE

90 ml dH_2O

2.5µl (10 mg/ml) ethidium bromide

Microscopy

16% paraformaldehyde

16g paraformaldehyde

80 ml dH_2O

Covered with foil and stirred for 1 h on a heated magnetic stirrer, with temperature kept below 60°C. Added 10M NaOH until solution appeared clear, then filtered using a 0.45 µM filter. Adjusted pH to pH 7 using HCl. For long term storage: 2.5 ml aliquots kept at -20°C.

4% paraformaldehyde

Thawed 16% paraformaldehyde, than added 7.5 ml 1 x PBS and mixed well

Mowiol 4-88

12 g Mowiol 4-88

30 ml glycerol

30 ml dH_2O

60 ml 0.2 M Tris-Cl pH 8.5

Stirred at RT O/N, and then stirred at 50°C for 1 h. Centrifuged at 5000 x *g* for 15 min.

Stored supernatant in 2ml aliquots at -20°C. Added 2.5 % anti-fading agent (N-propyl gallate) prior to use. Centrifuged at 1200 x *g* for 5 min to remove insoluble particles and air bubbles.

Cell cycle analysis solutions

RNase A (50 µg/ml)

300µl 1 mg/ml RNase A

5.7 ml 1 x PBS

0.1 M PIPES pH 6.8

3.02 g PIPES

100 ml dH_2O

Cell cycle staining solution

0.1% Triton X-100

2mM $MgCl_2$

100 mM NaCl

10 mM PIPES pH 6.8

10 µg/ml Propidium Iodide

ROS assay solutions

Krebs-Ringer (KR) Buffer pH 7.4

110 mM NaCl

2.6 mM KCl

1.2 mM $MgSO_4$

1.2 mM KH_2PO_4

25 mM $NaHCO_3$

11 mM glucose

Made up to final volume using sterile dH_2O, filter sterilised and stored at 4°C.

DCFDA stock (50 mM)

0.0074 g DCFDA

303.7 µl DMSO

Prepared 15 µl aliquots

Covered with foil and stored at -20°C

TEM solutions

In order to prepare 0.2 M Sorenson's Phosphate buffer and 0.1 M Sorenson's buffer, Solution A and Solution B (shown in Table 6.3) were initially prepared:

Table 6.3: Preparation of Solution A and Solution B

	Solution	**Reagent**	**MW**	**Mass**	**dH_2O**
A	0.2 M dibasic sodium phosphate	$Na_2HPO_4 \bullet 2H_2O$	178.05 g/mol	35.61 g	1000 ml
B	0.2 M monobasic sodium phosphate	$NaH_2PO_4 \bullet H_2O$	138.01 g/mol	27.6 g	1000 ml

The volumes of Solution A and B were added, as shown in the Table 6.4 and 6.5, to achieve 0.2 M Sorenson's Phosphate buffer and 0.1 M Sorenson's buffer, respectively.

Table 6.4: 0.2 M Sorenson's Phosphate buffer pH7.4:

Solution A	**Solution B**	**Total**
40.5 ml	9.5 ml	50 ml
81 ml	19 ml	100 ml

Table 6.5: 0.1M Sorenson's Phosphate buffer, pH7.4

Solution A	Solution B	dH_2O	Total
40.5 ml	9.5 ml	50 ml	100 ml
81 ml	19 ml	100 ml	200 ml

0.2 M Sorenson's phosphate buffer, pH 7.4 was used to prepare 2.5% Glutaraldehyde fixative, as shown in Table 6.6.

Table 6.6: 2.5% Glutaraldehyde fixative

Solution	Volume
0.2 M Sorenson's Phosphate buffer pH7.4 (stock)	25 ml
25% Glutaraldehyde	5 ml
dH_2O	20 ml

APPENDIX A

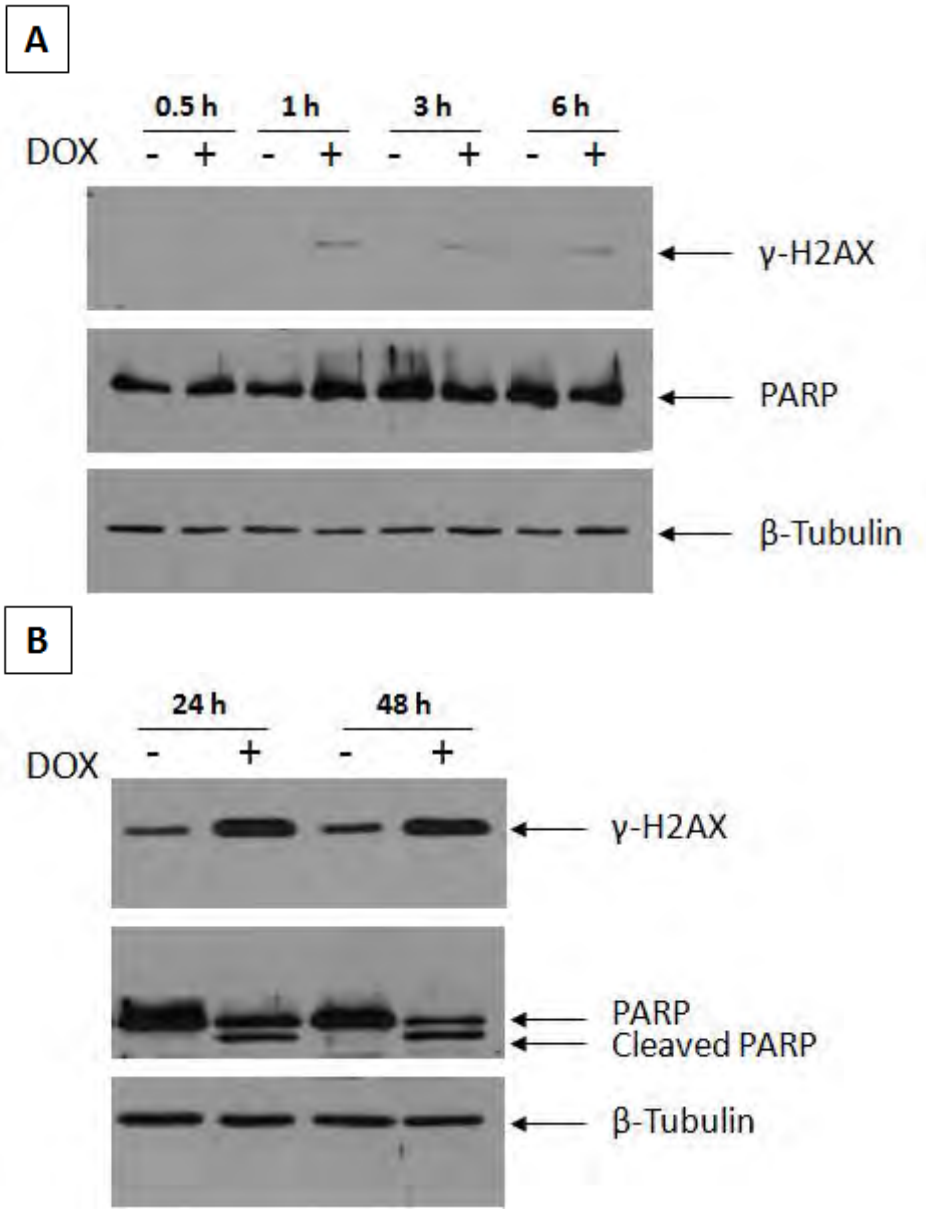

Figure A.1: Western blot analysis demonstrating the increased expression levels of γ-H2AX and cleaved PARP in WHCO1 treated with doxorubicin (DOX) over time. WHCO1 (3 x 10^5) were seeded in 60 mm dishes and incubated overnight. Cells were treated with vehicle only (0 µM) and 5 µM DOX for 0.5, 1, 3 and 6 h **(A)** and 24 and 48 h **(B)**. Protein was harvested and quantified so that 20 µg could be separated by SDS-PAGE and transferred onto a nitrocellulose membrane. The membrane was probed with antibodies recognising γ-H2AX, PARP and cleaved PARP. Beta-tubulin was used as a loading control.

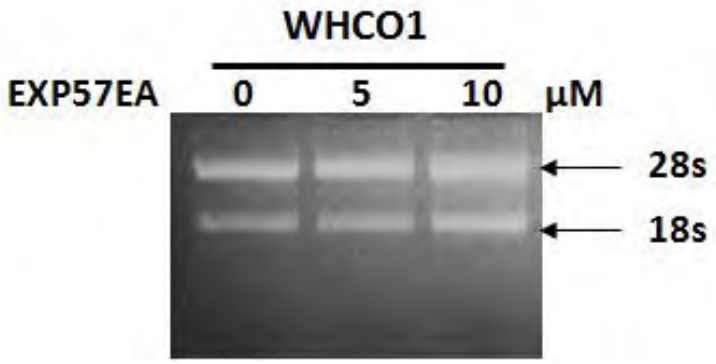

Figure A.2: MOPS/formaldehyde agarose gel electrophoresis of RNA samples prepared using Qiazol. RNA prepared from WHCO1 cells treated with the indicated concentrations of EXP57EA for 24 h and subjected to electrophoresis on a MOPS/formaldehyde agarose gel to assess RNA quality. Positions of 28s and 18s rRNA are indicated.

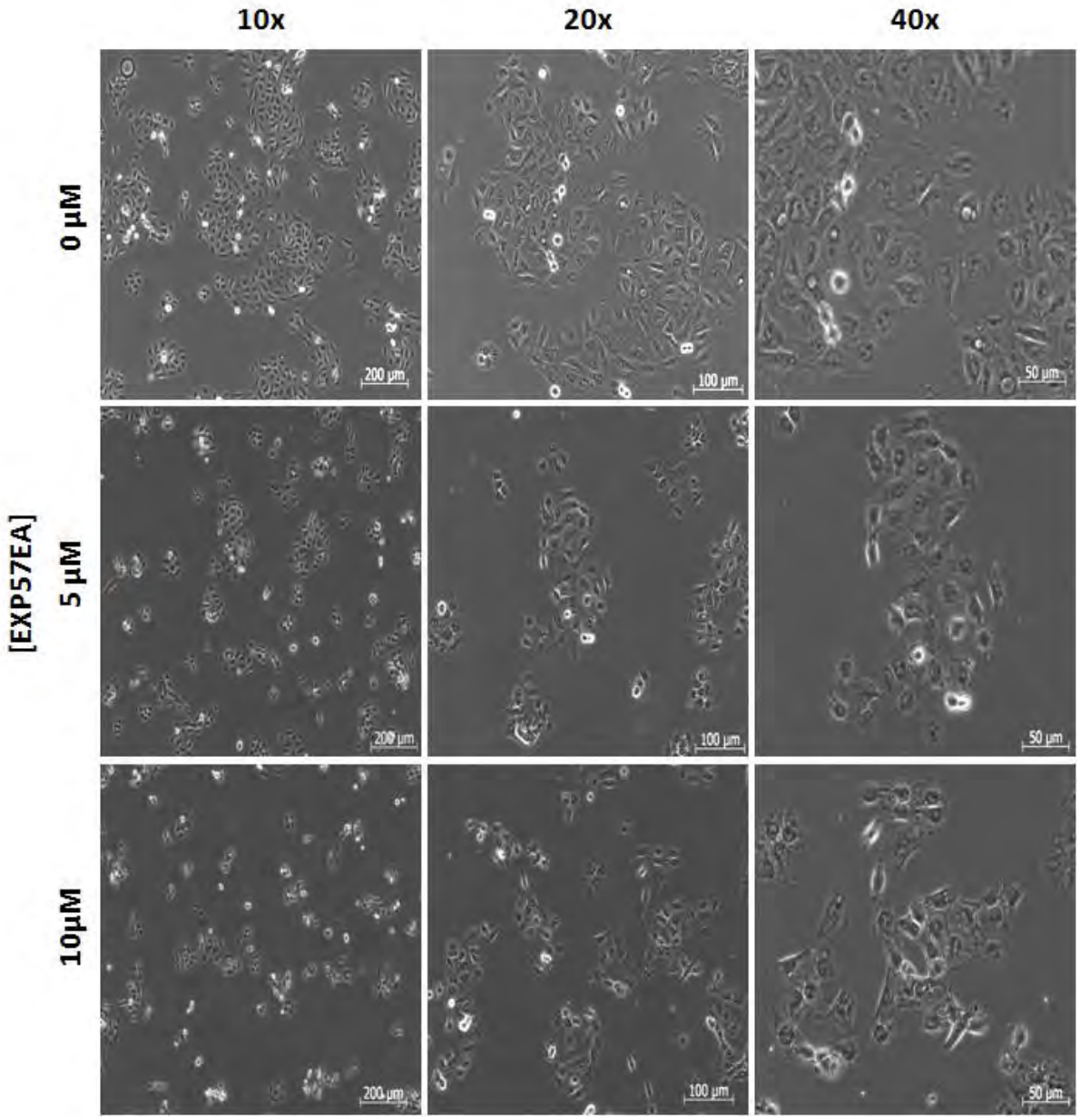

Figure A.3: Phase-contrast microscopy images of WHCO1 cells treated with EXP57EA for 24 h.

Eighty thousand cells were seeded on ethanol-flamed coverslips in 35 mm dishes. The next day cells were treated 5 µM and 10 µM EXP57EA and incubated for 24 h. Cells treated with vehicle-only (0 µM) served as the untreated control group. Subsequently, cells were fixed with 4% paraformaldehyde and mounted onto slides in Mowiol 4-88 prior to viewing using an Axiovert 200M microscope (Zeiss). Images were captured using an AxioCamHR camera with Axiovision software, version 4.7 (Zeiss).

APPENDIX B

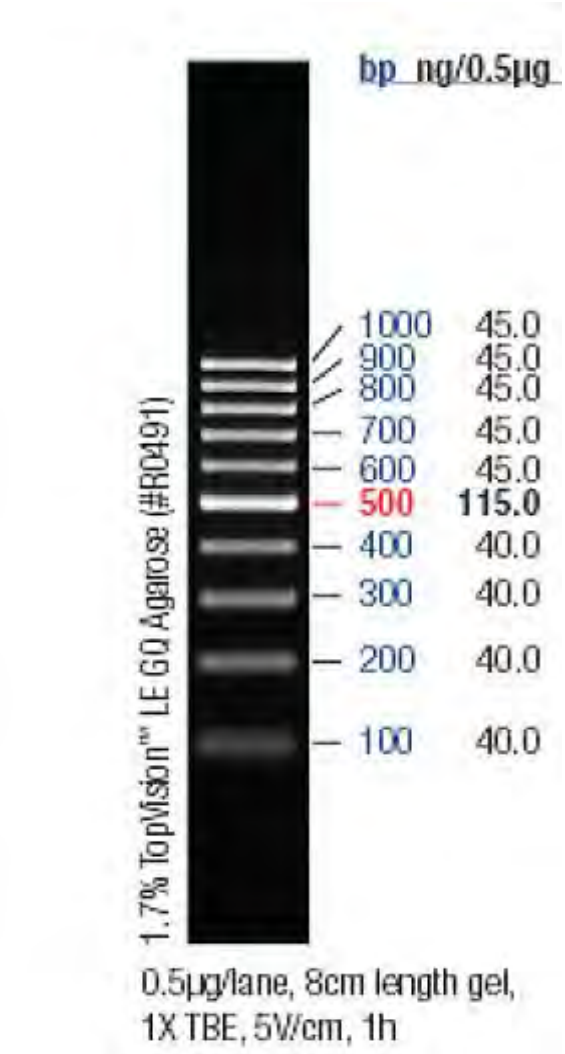

Figure B.1: Fermentas O'GeneRuler™ 100 bp DNA Ladder, ready-to-use

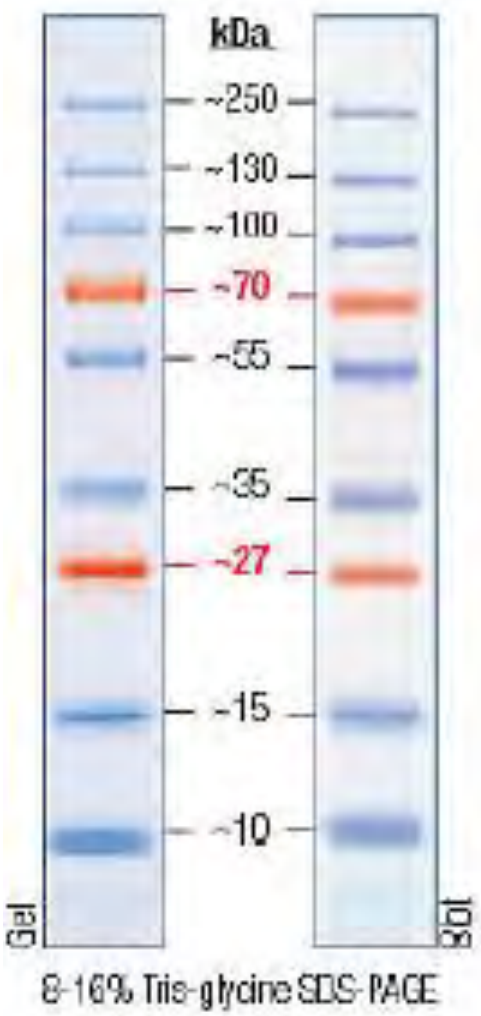

Figure B.2: Spectra Multicolor Broad Range Protein Ladder

REFERENCES

Aghaei, M., and Ashtiani, H.A. (2012). Dihydroartemisinin induces apoptosis in skin cancer cell line A-431 via ROS pathway. J. Pharm. *2*, 49–54.

Alexandre, J., Batteux, F., Nicco, C., Chéreau, C., Laurent, A., Guillevin, L., Weill, B., and Goldwasser, F. (2006). Accumulation of hydrogen peroxide is an early and crucial step for paclitaxel-induced cancer cell death both in vitro and in vivo. Int. J. Cancer *119*, 41–48.

Allen, D.D., Caviedes, R., Cárdenas, A.M., Shimahara, T., Segura-Aguilar, J., and Caviedes, P. (2005). Cell lines as in vitro models for drug screening and toxicity studies. Drug Dev. Ind. Pharm. *31*, 757–768.

Aoki, H., Takada, Y., Kondo, S., Sawaya, R., and Aggarwal, B.B. (2007). Evidence that curcumin suppresses the growth of malignant gliomas in vitro and in vivo through induction of autophagy : role of Akt and Extracellular Signal-Regulated Kinase signaling pathways. Mol. Pharmacol. *72*, 29–39.

Apel, A., Zentgraf, H., Büchler, M.W., and Herr, I. (2009). Autophagy-A double-edged sword in oncology. Int. J. Cancer *125*, 991–995.

Ashburn, T.T., and Thor, K.B. (2004). Drug repositioning: identifying and developing new uses for existing drugs. Nat. Rev. Drug Discov. *3*, 673–683.

Assunção Guimarães, C., and Linden, R. (2004). Programmed cell deaths. Apoptosis and alternative deathstyles. Eur. J. Biochem. *271*, 1638–1650.

Baehrecke, E.H. (2003). Autophagic programmed cell death in Drosophila. Cell Death Differ. *10*, 940–945.

Bai, L., Xu, X., Wang, Q., Xu, S., Ju, W., Wang, X., Chen, W., He, W., Tang, H., and Lin, Y. (2012). A superoxide-mediated mitogen-activated protein kinase phosphatase-1 degradation and c-Jun NH(2)-terminal kinase activation pathway for luteolin-induced lung cancer cytotoxicity. Mol. Pharmacol. *81*, 549–555.

Bandla, S., Pennathur, A., Luketich, J.D., Beer, D.G., Lin, L., Bass, A.J., Godfrey, T.E., and Litle, V.R. (2012). Comparative genomics of esophageal adenocarcinoma and squamous cell carcinoma. *93*, 1101–1106.

Bang, Y.-J., Kang, Y.-K., Kang, W.K., Boku, N., Chung, H.C., Chen, J.-S., Doi, T., Sun, Y., Shen, L., Qin, S., et al. (2011). Phase II study of sunitinib as second-line treatment for advanced gastric cancer. Invest. New Drugs *29*, 1449–1458.

Barzilai, A., and Yamamoto, K.-I. (2004). DNA damage responses to oxidative stress. DNA Repair (Amst). *3*, 1109–1115.

Beals, C.R., Clipstone, N.A., Ho, S.N., and Crabtree, G.R. (1997). Nuclear localization of NF-ATc by a calcineurin-dependent, cyclosporin-sensitive intramolecular interaction. Genes Dev. *11*, 824–834.

Berdelle, N., Nikolova, T., Quiros, S., Efferth, T., and Kaina, B. (2011). Artesunate induces oxidative DNA damage, sustained DNA double-strand breaks, and the ATM/ATR damage response in cancer cells. Mol. Cancer Ther. *10*, 2224–2233.

Berndtsson, M., Hägg, M., Panaretakis, T., Havelka, A.M., Shoshan, M.C., and Linder, S. (2007). Acute apoptosis by cisplatin requires induction of reactive oxygen species but is not associated with damage to nuclear DNA. Int. J. Cancer *120*, 175–180.

Bidabadi, E., and Mashouf, M. (2010). A randomized trial of propranolol versus sodium valproate for the prophylaxis of migraine in pediatric patients. Paediatr. Drugs *12*, 269–275.

Boatright, K.M., and Salvesen, G.S. (2003). Mechanisms of caspase activation. Curr. Opin. Cell Biol. *15*, 725–731.

Boguski, M.S., Mandl, K.D., and Sukhatme, V.P. (2009). Repurposing with a difference. Science (80-.). *324*, 1394–1395.

Boland, P.M., and Burtness, B. (2013). Esophageal carcinoma: are modern targeted therapies shaking the rock? Curr. Opin. Oncol. *25*, 417–424.

Boland, B., Kumar, A., Lee, S., Platt, F.M., Wegiel, J., Yu, W.H., and Nixon, R. a (2008). Autophagy induction and autophagosome clearance in neurons: relationship to autophagic pathology in Alzheimer's disease. J. Neurosci. *28*, 6926–6937.

Boone, J., Ten Kate, F.J.W., Offerhaus, G.J. a, van Diest, P.J., Rinkes, I.H.M.B., and van Hillegersberg, R. (2008). mTOR in squamous cell carcinoma of the oesophagus: a potential target for molecular therapy? J. Clin. Pathol. *61*, 909–913.

Boulares, A.H., Yakovlev, A.G., Ivanova, V., Stoica, B.A., Wang, G., Iyer, S., Smulson, M., and Chem, M.J.B. (1999). Role of poly (ADP-ribose) polymerase (PARP) cleavage in apoptosis. J. Biol. Chem. *274*, 22932–22940.

Bursch, W., Ellinger, a, Kienzl, H., Török, L., Pandey, S., Sikorska, M., Walker, R., and Hermann, R.S. (1996). Active cell death induced by the anti-estrogens tamoxifen and ICI 164 384 in human mammary carcinoma cells (MCF-7) in culture: the role of autophagy. Carcinogenesis *17*, 1595–1607.

Cagnol, S., and Chambard, J.-C. (2010). ERK and cell death: mechanisms of ERK-induced cell death--apoptosis, autophagy and senescence. FEBS J. *277*, 2–21.

Campbell, N.P. (2010). Neoadjuvant treatment of esophageal cancer. World J. Gastroenterol. *16*, 3793.

Chai, J., and Jamal, M.M. (2012). Esophageal malignancy: a growing concern. World J. Gastroenterol. *18*, 6521–6526.

Chen, N., and Debnath, J. (2010). Autophagy and tumorigenesis. FEBS Lett. *584*, 1427–1435.

Chen, N., and Karantza, V. (2011). Autophagy as a therapeutic target in cancer. Cancer Biol. Ther. *11*, 157–168.

Chen, N., and Karantza-Wadsworth, V. (2009). Role and regulation of autophagy in cancer. Biochim. Biophys. Acta *1793*, 1516–1523.

Chen, Y., and Klionsky, D.J. (2011). The regulation of autophagy - unanswered questions. J. Cell Sci. *124*, 161–170.

Chen, H., Zhou, J., and Fang, X. (2003). Inhibition of human cancer cell line growth and human umbilical vein endothelial cell angiogenesis by artemisinin derivatives in vitro. Pharmacol. Res. *48*, 231–236.

Chen, H., Sun, B., Wang, S., Pan, S., Gao, Y., Bai, X., and Xue, D. (2010a). Growth inhibitory effects of dihydroartemisinin on pancreatic cancer cells: involvement of cell cycle arrest and inactivation of nuclear factor-kappaB. J. Cancer Res. Clin. Oncol. *136*, 897–903.

Chen, R.-J., Ho, C.-T., and Wang, Y.-J. (2010b). Pterostilbene induces autophagy and apoptosis in sensitive and chemoresistant human bladder cancer cells. Mol. Nutr. Food Res. *54*, 1819–1832.

Chen, T., Li, M., Zhang, R., and Wang, H. (2009a). Dihydroartemisinin induces apoptosis and sensitizes human ovarian cancer cells to carboplatin therapy. J. Cell. Mol. Med. *13*, 1358–1370.

Chen, Y., McMillan-Ward, E., Kong, J., Israels, S.J., and Gibson, S.B. (2008). Oxidative stress induces autophagic cell death independent of apoptosis in transformed and cancer cells. Cell Death Differ. *15*, 171–182.

Chen, Y., Azad, M.B., and Gibson, S.B. (2009b). Superoxide is the major reactive oxygen species regulating autophagy. Cell Death Differ. *16*, 1040–1052.

Chipuk, J.E., Moldoveanu, T., Llambi, F., Parsons, M.J., and Green, D.R. (2010). The BCL-2 family reunion. Mol. Cell *37*, 299–310.

Christofferson, D.E., and Yuan, J. (2010). Necroptosis as an alternative form of programmed cell death. Curr. Opin. Cell Biol. *22*, 263–268.

Circu, M.L., and Aw, T.Y. (2010). Reactive oxygen species, cellular redox systems, and apoptosis. Free Radic. Biol. Med. *48*, 749–762.

Ciucci, A., Gianferretti, P., Piva, R., Guyot, T., Snape, T.J., Roberts, S.M., and Santoro, M.G. (2006). Induction of apoptosis in estrogen receptor-negative breast cancer cells by natural and synthetic cyclopentenones : role of the IkB Kinase/Nuclear Factor-kB pathway. Mol. Pharmacol. *70*, 1812–1821.

Clarke, P.G.H. (1990). Developmental cell death: morphological diversity and multiple mechanism. Anat. Embryol. (Berl). *181*, 195–213.

Clarke, P.G.H., and Puyal, J. (2012). Autophagic cell death exists. Autophagy *8*, 867–869.

Codogno, P., and Meijer, A.J. (2005). Autophagy and signaling: their role in cell survival and cell death. Cell Death Differ. *12 Suppl 2*, 1509–1518.

Cragg, G.M., and Newman, D.J. (2013). Natural products: a continuing source of novel drug leads. Biochim. Biophys. Acta *1830*, 3670–3695.

Crazzolara, R., Bradstock, K.F., and Bendall, L.J. (2009). RAD001 (everolimus) induces autophagy in acute lymphoblastic leukemia. Autophagy *5*, 727–728.

Crespo-Ortiz, M.P., and Wei, M.Q. (2012). Antitumor activity of artemisinin and its derivatives: from a well-known antimalarial agent to a potential anticancer drug. J. Biomed. Biotechnol. *2012*, 247597.

Crighton, D., Wilkinson, S., and Ryan, K.M. (2007). DRAM links autophagy to p53 and programmed cell death. Autophagy *3*, 72–74.

Cui, Q., Tashiro, S., Onodera, S., Minami, M., and Ikejima, T. (2007). Oridonin induced autophagy in human cervical carcinoma HeLa cells. J. Pharmacol. Sci. *105*, 317–325.

Curtin, J.F., Donovan, M., and Cotter, T.G. (2002). Regulation and measurement of oxidative stress in apoptosis. J. Immunol. Methods *265*, 49–72.

Decker, M. (2011). Hybrid molecules incorporating natural products: applications in cancer therapy, neurodegenerative disorders and beyond. Curr. Med. Chem. *18*, 1464–1475.

Degterev, A., Huang, Z., Boyce, M., Li, Y., Jagtap, P., Mizushima, N., Cuny, G.D., Mitchison, T.J., Moskowitz, M. a, and Yuan, J. (2005). Chemical inhibitor of nonapoptotic cell death with therapeutic potential for ischemic brain injury. Nat. Chem. Biol. *1*, 112–119.

Degterev, A., Hitomi, J., Germscheid, M., Ch'en, I.L., Korkina, O., Teng, X., Abbott, D., Cuny, G.D., Yuan, C., Wagner, G., et al. (2008). Identification of RIP1 kinase as a specific cellular target of necrostatins. Nat. Chem. Biol. *4*, 313–321.

Dell'Eva, R., Pfeffer, U., Vené, R., Anfosso, L., Forlani, A., Albini, A., and Efferth, T. (2004). Inhibition of angiogenesis in vivo and growth of Kaposi's sarcoma xenograft tumors by the anti-malarial artesunate. Biochem. Pharmacol. *68*, 2359–2366.

Demeester, S.R. (2009). Epidemiology and biology of esophageal cancer. Gastrointest. Cancer Res. *3*, 2–5.

Desoize, B., and Madoulet, C. (2002). Particular aspects of platinum compounds used at present in cancer treatment. Crit. Rev. Oncol. Hematol. *42*, 317–325.

Dice, J.F. (2007). Chaperone-Mediated Autophagy. Autophagy *3*, 295–299.

Donadelli, M., Dando, I., Zaniboni, T., Costanzo, C., Dalla Pozza, E., Scupoli, M.T., Scarpa, A., Zappavigna, S., Marra, M., Abbruzzese, A., et al. (2011). Gemcitabine/cannabinoid combination triggers autophagy in pancreatic cancer cells through a ROS-mediated mechanism. Cell Death Dis. *2*, e152.

Du, J.-H., Zhang, H.-D., Ma, Z.-J., and Ji, K.-M. (2010). Artesunate induces oncosis-like cell death in vitro and has antitumor activity against pancreatic cancer xenografts in vivo. Cancer Chemother. Pharmacol. *65*, 895–902.

Du, X.-X., Li, Y.-J., Wu, C.-L., Zhou, J.-H., Han, Y., Sui, H., Wei, X.-L., Liu, L., Huang, P., Yuan, H.-H., et al. (2013). Initiation of apoptosis, cell cycle arrest and autophagy of esophageal cancer cells by dihydroartemisinin. Biomed. Pharmacother. *67*, 417–424.

Duan, W.-J., Li, Q.-S., Xia, M.-Y., Tashiro, S.-I., Onodera, S., and Ikejima, T. (2011). Silibinin activated p53 and induced autophagic death in human fibrosarcoma HT1080 cells via reactive oxygen species - p38 and c-Jun N-terminal kinase pathways. Biol. Pharm. Bull. *34*, 47–53.

Duprez, L., Wirawan, E., Vanden Berghe, T., and Vandenabeele, P. (2009). Major cell death pathways at a glance. Microbes Infect. *11*, 1050–1062.

De Duve, C., and Wattiaux, R. (1966). Functions of lysosomes. Annu. Rev. Physiol. *28*, 435–492.

Eccles, D.M., Cranston, G., Steel, C.M., Nakamura, Y., and Leonard, R.C. (1990). Allele losses on chromosome 17 in human epithelial ovarian carcinoma. Oncogene *5*, 1599–1601.

Edinger, A.L., and Thompson, C.B. (2004). Death by design: apoptosis, necrosis and autophagy. Curr. Opin. Cell Biol. *16*, 663–669.

Efferth, T., Dunstan, H., Sauerbrey, A., Miyachi, H., and Chitambar, C.R. (2001). The anti-malarial artesunate is also active against cancer. Int. J. Oncol. *18*, 767–773.

Efferth, T., Benakis, A., Romero, M.R., Tomicic, M., Rauh, R., Steinbach, D., Häfer, R., Stamminger, T., Oesch, F., Kaina, B., et al. (2004). Enhancement of cytotoxicity of artemisinins toward cancer cells by ferrous iron. Free Radic. Biol. Med. *37*, 998–1009.

Efferth, T., Giaisi, M., Merling, A., Krammer, P.H., and Li-Weber, M. (2007). Artesunate induces ROS-mediated apoptosis in doxorubicin-resistant T leukemia cells. PLoS One *2*, e693.

Efferth, T., Romero, M.R., Wolf, D.G., Stamminger, T., Marin, J.J.G., and Marschall, M. (2008). The antiviral activities of artemisinin and artesunate. Clin. Infect. Dis. *47*, 804–811.

Ellington, A., Berhow, M., and Singletary, K.W. (2006). Inhibition of Akt signaling and enhanced ERK1/2 activity are involved in induction of macroautophagy by triterpenoid B-group soyasaponins in colon cancer cells. Carcinogenesis *27*, 298–306.

Elmore, S. (2007). Apoptosis: a review of programmed cell death. Toxicol. Pathol. *35*, 495–516.

Elton, E. (2005). Esophageal cancer. Dis. Mon. *51*, 664–684.

Eom, J.-M., Seo, M.-J., Baek, J.-Y., Chu, H., Han, S.H., Min, T.S., Cho, C., and Yun, C.-H. (2010). Alpha-eleostearic acid induces autophagy-dependent cell death through targeting AKT/mTOR and ERK1/2 signal together with the generation of reactive oxygen species. Biochem. Biophys. Res. Commun. *391*, 903–908.

Esclatine, A., Chaumorcel, M., and Codogno, P. (2009). Macroautophagy signaling and regulation. In Autophagy in Infection and Immunity, pp. 33–70.

Eskelinen, E. (2008). Fine Structure of the Autophagosome. Methods Mol. Biol. *445*, 11–28.

Eskelinen, E.-L. (2011). The dual role of autophagy in cancer. Curr. Opin. Pharmacol. *11*, 294–300.

Eslick, G.D. (2010). Infectious causes of esophageal cancer. Infect. Dis. Clin. North Am. *24*, 845–52, vii.

Fels, D.R., Ye, J., Segan, A.T., Kridel, S.J., Spiotto, M., Olson, M., Koong, A.C., and Koumenis, C. (2008). Preferential cytotoxicity of bortezomib toward hypoxic tumor cells via overactivation of endoplasmic reticulum stress pathways. Cancer Res. *68*, 9323–9330.

Fenton, J.I., and Hord, N.G. (2006). Stage matters: choosing relevant model systems to address hypotheses in diet and cancer chemoprevention research. Carcinogenesis *27*, 893–902.

Ferlay, J., Shin, H.-R., Bray, F., Forman, D., Mathers, C., and Parkin, D.M. (2010). Estimates of worldwide burden of cancer in 2008: GLOBOCAN 2008. Int. J. Cancer *127*, 2893–2917.

Fernandez-Capetillo, O., Lee, A., Nussenzweig, M., and Nussenzweig, A. (2004). H2AX: the histone guardian of the genome. DNA Repair (Amst). *3*, 959–967.

Fischer, U., and Schulze-Osthoff, K. (2005). Apoptosis-based therapies and drug targets. Cell Death Differ. *12*, 942–961.

Fragkos, M., Jurvansuu, J., and Beard, P. (2009). H2AX is required for cell cycle arrest via the p53/p21 pathway. Mol. Cell. Biol. *29*, 2828–2840.

Fuchs, Y., and Steller, H. (2011). Programmed cell death in animal development and disease. Cell *147*, 742–758.

Fujita, T., Felix, K., Pinkaew, D., Hutadilok-Towatana, N., Liu, Z., and Fujise, K. (2008). Human fortilin is a molecular target of dihydroartemisinin. FEBS Lett. *582*, 1055–1060.

Fulda, S., and Debatin, K.-M. (2006). Extrinsic versus intrinsic apoptosis pathways in anticancer chemotherapy. Oncogene *25*, 4798–4811.

Fung, C., Lock, R., Gao, S., Salas, E., Debnath, J., Francisco, S., and Biology, C. (2008). Induction of autophagy during extracellular matrix detachment promotes cell survival. Mol. Biol. Cell *19*, 797–806.

Futreal, P.A., Söderkvist, P., Marks, J.R., Sã, P., Iglehart, J.D., Cochran, C., Barrett, J.C., and Wiseman, R.W. (1992). Detection of frequent allelic loss on proximal chromosome 17q in sporadic breast carcinoma using microsatellite length polymorphisms. Cancer Res. *52*, 2624–2627.

Galal, A.M., Ross, S.A., Jacob, M., and ElSohly, M.A. (2005). Antifungal activity of artemisinin derivatives. J. Nat. Prod. *68*, 1274–1276.

Galluzzi, L., and Kroemer, G. (2008). Necroptosis: a specialized pathway of programmed necrosis. Cell *135*, 1161–1163.

Galluzzi, L., Vitale, I., Abrams, J.M., Alnemri, E.S., Baehrecke, E.H., Blagosklonny, M. V, Dawson, T.M., Dawson, V.L., El-Deiry, W.S., Fulda, S., et al. (2012). Molecular definitions of cell death subroutines: recommendations of the Nomenclature Committee on Cell Death 2012. Cell Death Differ. *19*, 107–120.

Gao, X., Zacharek, A., Salkowski, A., Grignon, J., Sakr, W., and Porter, T. (1995). Loss of heterozygosity of the BRCA1 and other loci on chromosome 17q in human prostate cancer. Cancer Res. *55*, 1002–1005.

Germain, M., Affar, E.B., Amours, D.D., Dixit, V.M., Salvesen, G.S., and Poirier, G.G. (1999). Cleavage of automodified poly (ADP-ribose) polymerase during apoptosis. J. Biol. Chem. *274*, 28379–28384.

Glucksman, A. (1951). Cell death in normal vertebrate ontogeny. Biol. Rev. *26*, 59–86.

Golstein, P., and Kroemer, G. (2007). Cell death by necrosis: towards a molecular definition. Trends Biochem. Sci. *32*, 37–43.

Gong, K., Chen, C., Zhan, Y., Chen, Y., Huang, Z., and Li, W. (2012). Autophagy-related gene 7 (ATG7) and reactive oxygen species/extracellular signal-regulated kinase regulate tetrandrine-induced autophagy in human hepatocellular carcinoma. J. Biol. Chem. *287*, 35576–35588.

Gozuacik, D., and Kimchi, A. (2004). Autophagy as a cell death and tumor suppressor mechanism. Oncogene *23*, 2891–2906.

Gozuacik, D., and Kimchi, A. (2007). Autophagy and cell death. Curr. Top. Dev. Biol. *78*, 217–245.

Green, D.R. (2000). Apoptotic pathways: paper wraps stone blunts scissors. Cell *102*, 1–4.

Green, D.R., and Evan, G.I. (2002). A matter of life and death. Cancer Cell *1*, 19–30.

Green, D.R., and Kroemer, G. (2005). Pharmacological manipulation of cell death : clinical applications in sight? J. Clin. Invest. *115*, 2610–2617.

Griffin, S.M., and Wahed, S. (2011). Oesophageal cancer. Surg. *29*, 557–562.

Guertin, D.A., and Sabatini, D.M. (2007). Defining the role of mTOR in cancer. Cancer Cell *12*, 9–22.

Gupta, S.C., Sung, B., Prasad, S., Webb, L.J., and Aggarwal, B.B. (2013). Cancer drug discovery by repurposing: teaching new tricks to old dogs. Trends Pharmacol. Sci. *34*, 508–517.

Haglund, C., Aleskog, A., Nygren, P., Gullbo, J., Höglund, M., Wickström, M., Larsson, R., and Lindhagen, E. (2012). In vitro evaluation of clinical activity and toxicity of anticancer drugs using tumor cells from patients and cells representing normal tissues. Cancer Chemother. Pharmacol. *69*, 697–707.

Hanahan, D., and Weinberg, R.A. (2000). The Hallmarks of Cancer. Cell *100*, 57–70.

Hanahan, D., and Weinberg, R.A. (2011). Hallmarks of cancer: the next generation. Cell *144*, 646–674.

Handrick, R., Ontikatze, T., Bauer, K.-D., Freier, F., Rübel, A., Dürig, J., Belka, C., and Jendrossek, V. (2010). Dihydroartemisinin induces apoptosis by a Bak-dependent intrinsic pathway. Mol. Cancer Ther. *9*, 2497–2510.

Hans, R.H. (2009). Thesis: Novel antimalarial and antitubercular agents based on natural products. University of Cape Town.

Hartwell, L.H., and Kastan, M.B. (1994). Cell cycle control and cancer. Science *266*, 1821–1828.

Hayashi, T., Saito, A., Okuno, S., and Ferrand-drake, M. (2005). Damage to the endoplasmic reticulum and activation of apoptotic machinery by oxidative stress in ischemic neurons. 41–53.

Haynes, R.K., and Krishna, S. (2004). Artemisinins: activities and actions. Microbes Infect. *6*, 1339–1346.

He, C., and Klionsky, D.J. (2009). Regulation mechanisms and signaling pathways of autophagy. Annu. Rev. Genet. *43*, 67–93.

He, C., and Levine, B. (2010). The Beclin 1 interactome. Curr. Opin. Cell Biol. *22*, 140–149.

Hendricks, D., and Parker, M.I. (2002). Oesophageal Cancer in Africa. 263–268.

Hengartner, M.O. (2000). The biochemistry of apoptosis. Nature *407*, 770–776.

Herrero-Martín, G., Høyer-Hansen, M., García-García, C., Fumarola, C., Farkas, T., López-Rivas, A., and Jäättelä, M. (2009). TAK1 activates AMPK-dependent cytoprotective autophagy in TRAIL-treated epithelial cells. EMBO J. *28*, 677–685.

Hitomi, J., Christofferson, D.E., Ng, A., Yao, J., Degterev, A., Xavier, R.J., and Yuan, J. (2008). Identification of a molecular signaling network that regulates a cellular necrotic cell death pathway. Cell *135*, 1311–1323.

Hockenbery, D. (1995). Defining apoptosis. Am. J. Pathol. *146*, 16–19.

Holler, N., Zaru, R., Micheau, O., Thome, M., Attinger, A., Valitutti, S., Bodmer, J.L., Schneider, P., Seed, B., and Tschopp, J. (2000). Fas triggers an alternative, caspase-8-independent cell death pathway using the kinase RIP as effector molecule. Nat. Immunol. *1*, 489–495.

Hosokawa, N., Hara, T., Kaizuka, T., Kishi, C., Takamura, A., Miura, Y., Iemura, S., Natsume, T., Takehana, K., Yamada, N., et al. (2009). Nutrient-dependent mTORC1 association with the ULK1 – Atg13 – FIP200 complex required for autophagy. Mol. Cell. Biol. *20*, 1981–1991.

Hotchkiss, R.S., Strasser, A., McDunn, J.E., and Swanson, P.E. (2009). Cell death. N. Engl. J. Med. *361*, 1570–1583.

Hou, J., Wang, D., Zhang, R., and Wang, H. (2008). Experimental therapy of hepatoma with artemisinin and its derivatives: in vitro and in vivo activity, chemosensitization, and mechanisms of action. Clin. Cancer Res. *14*, 5519–5530.

Høyer-Hansen, M., and Jäättelä, M. (2007). Connecting endoplasmic reticulum stress to autophagy by unfolded protein response and calcium. Cell Death Differ. *14*, 1576–1582.

Høyer-Hansen, M., Bastholm, L., Szyniarowski, P., Campanella, M., Szabadkai, G., Farkas, T., Bianchi, K., Fehrenbacher, N., Elling, F., Rizzuto, R., et al. (2007). Control of macroautophagy by calcium, calmodulin-dependent kinase kinase-beta, and Bcl-2. Mol. Cell *25*, 193–205.

Huang, J., Lam, G.Y., and Brumell, J.H. (2011a). Autophagy signaling through reactive oxygen species. Antioxid. Redox Signal. *14*, 2215–2231.

Huang, X., Yuan, D., Zhang, C., and Zhang, X. (2008). Artesunate induces prostate cancer cell line PC-3 differentiation and cell cycle arrest. J. Chinese Integr. Med. *6*, 591–594.

Huang, X., Bai, H.-M., Chen, L., Li, B., and Lu, Y.-C. (2010). Reduced expression of LC3B-II and Beclin 1 in glioblastoma multiforme indicates a down-regulated autophagic capacity that relates to the progression of astrocytic tumors. J. Clin. Neurosci. *17*, 1515–1519.

Huang, X.-J., Ma, Z.-Q., Zhang, W.-P., Lu, Y.-B., and Wei, E.-Q. (2007). Dihydroartemisinin exerts cytotoxic effects and inhibits hypoxia inducible factor-1alpha activation in C6 glioma cells. J. Pharm. Pharmacol. *59*, 849–856.

Huang, Y.-C., Hung, W.-C., Chye, S.-M., Chen, W.-T., and Chai, C.-Y. (2011b). para-Phenylenediamine-induced autophagy in human uroepithelial cell line mediated mutant p53 and activation of ERK signaling pathway. Toxicol. Vitr. *25*, 1630–1637.

Ichida, M., and Finkel, T. (2001). Ras regulates NFAT3 activity in cardiac myocytes. J. Biol. Chem. *276*, 3524–3530.

Ilett, K.F., Ethell, B.T., Maggs, J.L., Davis, T.M.E., Batty, K.T., Burchell, B., Binh, T.Q., Thi, L.E., Thu, A.N.H., Hung, N.C., et al. (2002). Glucuronidation of dihydroartemisinin in

vivo and by human liver microsomes and expressed UDP-glucuronosyltransferases. Drug Metab. *30*, 1005–1012.

Ilson, D.H. (2008). Esophageal cancer chemotherapy: recent advances. Gastrointest. Cancer Res. *2*, 85–92.

Ixe, L.X., Hai, X.Z., En, L.R., Eng, H.M., Iu, C.L., Hu, W.Z., and Hao, Y.Z. (2011). Design, synthesis and antitumor activity of novel artemisinin. Chem. Pharmacol. Bull. *59*, 984–990.

Jacobson, M.D., Weil, M., and Raff, M.C. (1997). Programmed cell death in animal development. Cell *88*, 347–354.

Jäger, S., Bucci, C., Tanida, I., Ueno, T., Kominami, E., Saftig, P., and Eskelinen, E.-L. (2004). Role for Rab7 in maturation of late autophagic vacuoles. J. Cell Sci. *117*, 4837–4848.

Jahreiss, L., Menzies, F.M., and Rubinsztein, D.C. (2008). The itinerary of autophagosomes: from peripheral formation to kiss-and-run fusion with lysosomes. Traffic *9*, 574–587.

Jemal, A., Bray, F., and Center, M. (2011). Global cancer statistics. CA a Cancer J. … *61*, 69–90.

Ji, Y., Zhang, Y.-C., Pei, L.-B., Shi, L.-L., Yan, J.-L., and Ma, X.-H. (2011). Anti-tumor effects of dihydroartemisinin on human osteosarcoma. Mol. Cell. Biochem. 99–108.

Jiang, P., Zhao, Y., Shi, W., Deng, X., Xie, G., Mao, Y., Li, Z., Zheng, Y., and Yang, S. (2008). Cell growth inhibition, G2/M cell cycle arrest, and apoptosis induced by chloroquine in human breast cancer cell line Bcap-37. Cell. Physiol. Biochem. 431–440.

Jiang, Z., Chai, J., Chuang, H.H.F., Li, S., Wang, T., Cheng, Y., Chen, W., and Zhou, D. (2012). Artesunate induces G0/G1 cell cycle arrest and iron-mediated mitochondrial apoptosis in A431 human epidermoid carcinoma cells. Anticancer. Drugs *23*, 606–613.

Jiao, Y., Ge, C., Meng, Q., Cao, J., Tong, J., and Fan, S. (2007). Dihydroartemisinin is an inhibitor of ovarian cancer cell growth. Acta Pharmacol. Sin. *28*, 1045–1056.

Jin, S. (2006). Autophagy, mitochondrial quality control, and oncogenesis. Autophagy *2*, 80–84.

Juhasz, G., and Neufeld, T.P. (2006). Autophagy: a forty-year search for a missing membrane source. PLoS Biol. *4*, e36.

Jung, C.H., Jun, C.B., Ro, S., Kim, Y., Otto, N.M., Cao, J., Kundu, M., and Kim, D. (2009). ULK-Atg13-FIP200 complexes mediate mTOR signaling to the autophagy machinery. Mol. Biol. Cell *20*, 1992–2003.

Jung, C.H., Ro, S.-H., Cao, J., Otto, N.M., and Kim, D.-H. (2010). mTOR regulation of autophagy. FEBS Lett. *584*, 1287–1295.

Kabeya, Y., Mizushima, N., Ueno, T., Yamamoto, a, Kirisako, T., Noda, T., Kominami, E., Ohsumi, Y., and Yoshimori, T. (2000). LC3, a mammalian homologue of yeast Apg8p, is localized in autophagosome membranes after processing. EMBO J. *19*, 5720–5728.

Kabeya, Y., Mizushima, N., Yamamoto, A., Oshitani-Okamoto, S., Ohsumi, Y., and Yoshimori, T. (2004). LC3, GABARAP and GATE16 localize to autophagosomal membrane depending on form-II formation. J. Cell Sci. *117*, 2805–2812.

Kanzawa, T., Germano, I.M., Komata, T., Ito, H., Kondo, Y., and Kondo, S. (2004). Role of autophagy in temozolomide-induced cytotoxicity for malignant glioma cells. Cell Death Differ. *11*, 448–457.

Karantza-Wadsworth, V., Patel, S., Kravchuk, O., Chen, G., Mathew, R., Jin, S., and White, E. (2007). Autophagy mitigates metabolic stress and genome damage in mammary tumorigenesis. Genes Dev. *21*, 1621–1635.

Kastan, M.B., Onyekwere, O., Sidransky, D., Vogelstein, B., and Craig, R.W. (1991). Participation of p53 protein in the cellular response to DNA damage participation of p53 protein in the cellular response to DNA damage. Cancer Res. *51*, 6304–6311.

Kaufmann, S.H., and Hengartner, M.O. (2001). Programmed cell death: alive and well in the new millennium. Trends Cell Biol. *11*, 526–534.

Kaushik, S., Massey, A.C., Mizushima, N., and Cuervo, A.M. (2008). Constitutive activation of chaperone-mediated autophagy in cells with impaired macroautophagy. Mol. Biol. Cell *19*, 2179–2192.

Kenific, C.M., Thorburn, A., and Debnath, J. (2010). Autophagy and metastasis: another double-edged sword. Curr. Opin. Cell Biol. *22*, 241–245.

Kerr, J.F., Wyllie, A.H., and Currie, A.R. (1972). Apoptosis: A basic biological phenomenon with wide ranging implications in tissue kinetics. Br. J. Cancer *26*, 239.

Khan, M.I., Mohammad, A., Patil, G., Naqvi, S. a H., Chauhan, L.K.S., and Ahmad, I. (2012). Induction of ROS, mitochondrial damage and autophagy in lung epithelial cancer cells by iron oxide nanoparticles. Biomaterials *33*, 1477–1488.

Kim, H.-R., Lee, G.-H., Cho, E.Y., Chae, S.-W., Ahn, T., and Chae, H.-J. (2009). Bax inhibitor 1 regulates ER-stress-induced ROS accumulation through the regulation of cytochrome P450 2E1. J. Cell Sci. *122*, 1126–1133.

Kim, J.Y., Cho, T.J., Woo, B.H., Choi, K.U., Lee, C.H., Ryu, M.H., and Park, H.R. (2012). Curcumin-induced autophagy contributes to the decreased survival of oral cancer cells. Arch. Oral Biol. *57*, 1018–1025.

Kim, R., Tanabe, K., Uchida, Y., Emi, M., Inoue, H., and Toge, T. (2002). Current status of the molecular mechanisms of anticancer drug-induced apoptosis. The contribution of molecular-level analysis to cancer chemotherapy. Cancer Chemother. Pharmacol. *50*, 343–352.

Klayman, D.L. (1985). Qinghaosu (Artemisinin): An antimalarial drug from China. Science (80-.). *228*, 1049–1055.

Klionsky, D.J. (2008). Autophagy revisited: A conversation with Christian de Duve. Autophagy *4*, 740–743.

Klionsky, D.J., and Emr, S.D. (2000). Autophagy as a regulated pathway of cellular degradation. Science *290*, 1717–1721.

Klionsky, D.J., Berry, D.L., Baehrecke, E.H., Abeliovich, H., Agostinis, P., Agrawal, D.K., Aliev, G., Askew, D.S., Baba, M., Bahr, B.A., et al. (2009). Guidelines for the use and interpretation of assays monitoring autophagy in higher eukaryotes. Autophagy *4*, 151–175.

Knævelsrud, H., and Simonsen, A. (2012). Lipids in autophagy: constituents, signaling molecules and cargo with relevance to disease. Biochim. Biophys. Acta *1821*, 1133–1145.

Koch, M. a, Wittenberg, L.-O., Basu, S., Jeyaraj, D. a, Gourzoulidou, E., Reinecke, K., Odermatt, A., and Waldmann, H. (2004). Compound library development guided by protein structure similarity clustering and natural product structure. Proc. Natl. Acad. Sci. U. S. A. *101*, 16721–16726.

Kokwaro, G., Mwai, L., and Nzila, A. (2007). Artemether/lumefantrine in the treatment of uncomplicated falciparum malaria. Expert Opin. Pharmacother. *8*, 75–94.

Konkimalla, V.B., Mccubrey, J.A., and Efferth, T. (2009). The role of downstream signaling pathways of the epidermal growth factor receptor for artesunate's activity in cancer cells. Curr. Cancer Drug Targets *9*, 72–80.

Kouroku, Y., Fujita, E., Tanida, I., Ueno, T., Isoai, a, Kumagai, H., Ogawa, S., Kaufman, R.J., Kominami, E., and Momoi, T. (2007). ER stress (PERK/eIF2alpha phosphorylation) mediates the polyglutamine-induced LC3 conversion, an essential step for autophagy formation. Cell Death Differ. *14*, 230–239.

Kranzfelder, M., Büchler, P., Lange, K., and Friess, H. (2010). Treatment options for squamous cell cancer of the esophagus: a systematic review of the literature. J. Am. Coll. Surg. *210*, 351–359.

Kreuzaler, P., and Watson, C.J. (2012). Killing a cancer: what are the alternatives? Nat. Rev. Cancer *12*, 411–424.

Kroemer, G., and Levine, B. (2008). Autophagic cell death: the story of a misnomer. Nat. Rev. Mol. Cell Biol. *9*, 1004–1010.

Kroemer, G., Dallaporta, B., and Resche-Rigon, M. (1998). The mitochondrial death/life regulator in apoptosis and necrosis. Annu. Rev. Physiol. *60*, 619–642.

Kroemer, G., Galluzzi, L., Vandenabeele, P., Abrams, J., Alnemri, E.S., Baehrecke, E.H., Blagosklonny, M. V, El-Deiry, W.S., Golstein, P., Green, D.R., et al. (2009). Classification of cell death: recommendations of the Nomenclature Committee on Cell Death 2009. Cell Death Differ. *16*, 3–11.

Kunz, C., Focke, F., Saito, Y., Schuermann, D., Lettieri, T., Selfridge, J., and Schär, P. (2009). Base excision by thymine DNA glycosylase mediates DNA-directed cytotoxicity of 5-fluorouracil. PLoS Biol. *7*, e91.

Kuppusamy, M., Sylvester, J., and Low, D.E. (2011). In an era of health reform: defining cost differences in current esophageal cancer management strategies and assessing the cost of complications. J. Thorac. Cardiovasc. Surg. *141*, 16–21.

Lai, H., and Singh, N.P. (1995). Selective cancer cell cytotoxicity from exposure to dihydroartemisinin and holotransferrin. Cancer Lett. *91*, 41–46.

Lai, H., and Singh, N.P. (2006). Oral artemisinin prevents and delays the development of 7,12-dimethylbenz[a]anthracene (DMBA)-induced breast cancer in the rat. Cancer Lett. *231*, 43–48.

Lai, H., Sasaki, T., and Singh, N.P. (2005). Targeted treatment of cancer with artemisinin and artemisinin-tagged iron-carrying compounds. Expert Opin. Ther. Targets *9*, 995–1007.

Lai, H.C., Singh, N.P., and Sasaki, T. (2013). Development of artemisinin compounds for cancer treatment. Invest. New Drugs *31*, 230–246.

Lao-Sirieix, P., Caldas, C., and Fitzgerald, R.C. (2010). Genetic predisposition to gastro-oesophageal cancer. Curr. Opin. Genet. Dev. *20*, 210–217.

Layke, J.C., and Lopez, P.P. (2006). Esophageal cancer: a review and update. Am. Fam. Physician *73*, 2187–2194.

Lee, J.W., Park, S., Takahashi, Y., and Wang, H.-G. (2010). The association of AMPK with ULK1 regulates autophagy. PLoS One *5*, e15394.

Levine, B., and Yuan, J. (2005). Autophagy in cell death : an innocent convict ? J. Clin. Invest. *115*, 2679–2688.

Li, C., and Johnson, D.E. (2012). Bortezomib induces autophagy in head and neck squamous cell carcinoma cells via JNK activation. Cancer Lett. *314*, 102–107.

Li, D.-D., Wang, L.-L., Deng, R., Tang, J., Shen, Y., Guo, J.-F., Wang, Y., Xia, L.-P., Feng, G.-K., Liu, Q.Q., et al. (2009a). The pivotal role of c-Jun NH2-terminal kinase-mediated Beclin 1 expression during anticancer agents-induced autophagy in cancer cells. Oncogene *28*, 886–898.

Li, J., Hou, N., Faried, A., Tsutsumi, S., Takeuchi, T., and Kuwano, H. (2009b). Inhibition of autophagy by 3-MA enhances the effect of 5-FU-induced apoptosis in colon cancer cells. Ann. Surg. Oncol. *16*, 761–771.

Li, L., Ishdorj, G., and Gibson, S.B. (2012). Reactive oxygen species regulation of autophagy in cancer: Implications for cancer treatment. Free Radic. Biol. Med. *53*, 1399–1410.

Li, L.-N., Zhang, H.-D., Yuan, S.-J., Tian, Z.-Y., Wang, L., and Sun, Z.-X. (2007). Artesunate attenuates the growth of human colorectal carcinoma and inhibits hyperactive Wnt/beta-catenin pathway. Int. J. Cancer *121*, 1360–1365.

Li, P.C.H., Lam, E., Roos, W.P., Zdzienicka, M.Z., Kaina, B., and Efferth, T. (2008). Artesunate derived from traditional Chinese medicine induces DNA damage and repair. Cancer Res. *68*, 4347–4351.

Li, T., Su, L., Zhong, N., Hao, X., Zhong, D., Singhal, S., and Liu, X. (2013). Salinomycin induces cell death with autophagy through activation of endoplasmic reticulum stress in human cancer cells. Autophagy *9*, 1057–1068.

Li, Y., Shan, F., Wu, J.M., Wu, G.S., Ding, J., Xiao, D., Yang, W.Y., Atassi, G., Léonce, S., Caignard, D.H., et al. (2001). Novel antitumor artemisinin derivatives targeting G1 phase of the cell cycle. Bioorg. Med. Chem. Lett. *11*, 5–8.

Li, Y., Reuter, N.P., Li, X., Liu, Q., Zhang, J., and Martin, R.C.G. (2010). Colocalization of MnSOD expression in response to oxidative stress. Mol. Carcinog. *49*, 44–53.

Liang, C., Feng, P., Ku, B., Dotan, I., Canaani, D., Oh, B.-H., and Jung, J.U. (2006). Autophagic and tumour suppressor activity of a novel Beclin1-binding protein UVRAG. Nat. Cell Biol. *8*, 688–699.

Liang, J., Shao, S.H., Xu, Z.-X., Hennessy, B., Ding, Z., Larrea, M., Kondo, S., Dumont, D.J., Gutterman, J.U., Walker, C.L., et al. (2007). The energy sensing LKB1-AMPK pathway regulates p27(kip1) phosphorylation mediating the decision to enter autophagy or apoptosis. Nat. Cell Biol. *9*, 218–224.

Liang, X.H., Jackson, S., Seaman, M., Brown, K., Kempkes, B., Hibshoosh, H., and Levine, B. (1999). Induction of autophagy and inhibition of tumorigenesis by beclin 1. Nature *402*, 672–676.

Lin, C.-C., and Papadopoulos, K.P. (2007). Novel targeted therapies for advanced esophageal cancer. Dis. Esophagus *20*, 365–371.

Ling, L.-U., Tan, K.-B., Lin, H., and Chiu, G.N.C. (2011). The role of reactive oxygen species and autophagy in safingol-induced cell death. Cell Death Dis. *2*, e129.

Liu, E.Y., and Ryan, K.M. (2012). Autophagy and cancer--issues we need to digest. J. Cell Sci. *125*, 2349–2358.

Liu, D., Yang, Y., Liu, Q., and Wang, J. (2011). Inhibition of autophagy by 3-MA potentiates cisplatin-induced apoptosis in esophageal squamous cell carcinoma cells. Med. Oncol. *28*, 105–111.

Lockshin, R. a, and Zakeri, Z. (2004). Apoptosis, autophagy, and more. Int. J. Biochem. Cell Biol. *36*, 2405–2419.

Lockshin, R.A., and Williams, C.M. (1964). Programmed cell death—II. Endocrine potentiation of the breakdown of the intersegmental muscles of silkmoths. J. Insect Physiol. *10*, 643–649.

Lockshin, R.A., and Zakeri, Z. (2001). Apoptosis : origins of the theory. Nat. Rev. Mol. Cell Biol. *2*, 5–10.

Löfdahl, H.E., Du, J., Näsman, A., Andersson, E., Rubio, C. a, Lu, Y., Ramqvist, T., Dalianis, T., Lagergren, J., and Dahlstrand, H. (2012). Prevalence of human papillomavirus (HPV) in oesophageal squamous cell carcinoma in relation to anatomical site of the tumour. PLoS One *7*, e46538.

Longley, D.B., Harkin, D.P., and Johnston, P.G. (2003). 5-Fluorouracil: mechanisms of action and clinical strategies. Nat. Rev. Cancer *3*, 330–338.

Lorin, S., Borges, A., Ribeiro Dos Santos, L., Souquère, S., Pierron, G., Ryan, K.M., Codogno, P., and Djavaheri-Mergny, M. (2009). c-Jun NH2-terminal kinase activation is essential for DRAM-dependent induction of autophagy and apoptosis in 2-methoxyestradiol-treated Ewing sarcoma cells. Cancer Res. *69*, 6924–6931.

Lu, J.-J., Meng, L.-H., Cai, Y.-J., Chen, Q., Tong, L.-J., Lin, L.-P., and Ding, J. (2008). Dihydroartemisinin induces apoptosis in HL-60 leukemia cells dependent of iron and p38 mitogen-activated protein kinase activation but independent of reactive oxygen species. Cancer Biol. Ther. *7*, 1017–1023.

Lu, Y.-Y., Chen, T.-S., Qu, J.-L., Pan, W.-L., Sun, L., and Wei, X.-B. (2009). Dihydroartemisinin (DHA) induces caspase-3-dependent apoptosis in human lung adenocarcinoma ASTC-a-1 cells. J. Biomed. Sci. *16*, 16.

Lu, Y.-Y., Chen, T.-S., Wang, X.-P., and Li, L. (2010). Single-cell analysis of dihydroartemisinin-induced apoptosis through reactive oxygen species-mediated caspase-8 activation and mitochondrial pathway in ASTC-a-1 cells using fluorescence imaging techniques. J. Biomed. Opt. *15*, 046028:1–16.

Lv, J. (2009). Effect of neoadjuvant chemoradiotherapy on prognosis and surgery for esophageal carcinoma. World J. Gastroenterol. *15*, 4962.

Maiuri, M.C., Zalckvar, E., Kimchi, A., and Kroemer, G. (2007). Self-eating and self-killing: crosstalk between autophagy and apoptosis. Nat. Rev. Mol. Cell Biol. *8*, 741–752.

Malhotra, J.D., and Kaufman, R.J. (2007). Endoplasmic reticulum stress and oxidative stress: a vicious cycle or a double-edged sword? Antioxid. Redox Signal. *9*, 2277–2293.

Manning, B.D., Tee, A.R., Logsdon, M.N., Blenis, J., and Cantley, L.C. (2002). Identification of the tuberous sclerosis complex-2 tumor suppressor gene product tuberin as a target of the phosphoinositide 3-kinase/akt pathway. Mol. Cell *10*, 151–162.

Mathew, R., Karantza-wadsworth, V., and White, E. (2007). Role of autophagy in cancer. Nat. Rev. *7*, 961–968.

Mathew, R., Karp, C.M., Beaudoin, B., Vuong, N., Chen, G., Chen, H.-Y., Bray, K., Reddy, A., Bhanot, G., Gelinas, C., et al. (2009). Autophagy suppresses tumorigenesis through elimination of p62. Cell *137*, 1062–1075.

Matsha, T., Erasmus, R., Kafuko, a B., Mugwanya, D., Stepien, a, and Parker, M.I. (2002). Human papillomavirus associated with oesophageal cancer. J. Clin. Pathol. *55*, 587–590.

Matsha, T., Donninger, H., Erasmus, R.T., Hendricks, D., Stepien, a, and Parker, M.I. (2007). Expression of p53 and its homolog, p73, in HPV DNA positive oesophageal squamous cell carcinomas. Virology *369*, 182–190.

Matsunaga, K., Saitoh, T., Tabata, K., Omori, H., Satoh, T., Kurotori, N., Maejima, I., Shirahama-Noda, K., Ichimura, T., Isobe, T., et al. (2009). Two Beclin 1-binding proteins, Atg14L and Rubicon, reciprocally regulate autophagy at different stages. Nat. Cell Biol. *11*, 385–396.

Matsuura, a, Tsukada, M., Wada, Y., and Ohsumi, Y. (1997). Apg1p, a novel protein kinase required for the autophagic process in Saccharomyces cerevisiae. Gene *192*, 245–250.

Mawhinney, M.R., and Glasgow, R.E. (2012). Current treatment options for the management of esophageal cancer. Cancer Manag. Res. *4*, 367–377.

Mayosi, B.M., Flisher, A.J., Lalloo, U.G., Sitas, F., Tollman, S.M., and Bradshaw, D. (2009). The burden of non-communicable diseases in South Africa. Lancet *374*, 934–947.

Mcbride, W.G. (1961). Thalidomide and congential abnormalities. Lancet *278*.

McCall, K. (2010). Genetic control of necrosis - another type of programmed cell death. Curr. Opin. Cell Biol. *22*, 882–888.

McCormack, V. a, and Schüz, J. (2012). Africa's growing cancer burden: environmental and occupational contributions. Cancer Epidemiol. *36*, 1–7.

Meijer, A.J., and Codogno, P. (2004). Regulation and role of autophagy in mammalian cells. Int. J. Biochem. Cell Biol. *36*, 2445–2462.

Meley, D., Bauvy, C., Houben-Weerts, J.H.P.M., Dubbelhuis, P.F., Helmond, M.T.J., Codogno, P., and Meijer, A.J. (2006). AMP-activated protein kinase and the regulation of autophagic proteolysis. J. Biol. Chem. *281*, 34870–34879.

Mercer, C. a, Kaliappan, A., and Dennis, P.B. (2009). A novel, human Atg13 binding protein, Atg101, interacts with ULK1 and is essential for macroautophagy. Autophagy *5*, 649–662.

Meshnick, S.R. (2002). Artemisinin: mechanisms of action, resistance and toxicity. Int. J. Parasitol. *32*, 1655–1660.

Meunier, B. (2008). Hybrid molecules with a dual mode of action: dream or reality? Acc. Chem. Res. *41*, 69–77.

Meunier, B., de Visser, S.P., and Shaik, S. (2004). Mechanism of oxidation reactions catalyzed by cytochrome p450 enzymes. Chem. Rev. *104*, 3947–3980.

Michaelis, M., Kleinschmidt, M.C., Barth, S., Rothweiler, F., Geiler, J., Breitling, R., Mayer, B., Deubzer, H., Witt, O., Kreuter, J., et al. (2010). Anti-cancer effects of artesunate in a panel of chemoresistant neuroblastoma cell lines. Biochem. Pharmacol. *79*, 130–136.

Miyajima, a, Nakashima, J., Yoshioka, K., Tachibana, M., Tazaki, H., and Murai, M. (1997). Role of reactive oxygen species in cis-dichlorodiammineplatinum-induced cytotoxicity on bladder cancer cells. Br. J. Cancer *76*, 206–210.

Mizushima, N., Yoshimori, T., and Levine, B. (2010). Methods in mammalian autophagy research. Cell *140*, 313–326.

Morrissey, C., Gallis, B., Solazzi, J.W., Kim, B.J., Gulati, R., Vakar-Lopez, F., Goodlett, D.R., Vessella, R.L., and Sasaki, T. (2010). Effect of artemisinin derivatives on apoptosis and cell cycle in prostate cancer cells. Anticancer. Drugs *21*, 423–432.

Mortimore, G.E., Lardeuxt, B.R., and Adams, E. (1988). Regulation of microautophagy and basal protein turnover in rat liver. J. Biol. Chem. *263*, 2506–2512.

Moscat, J., and Diaz-Meco, M.T. (2009). P62 at the crossroads of autophagy, apoptosis, and cancer. Cell *137*, 1001–1004.

Mu, D., Zhang, W., Chu, D., Liu, T., Xie, Y., Fu, E., and Jin, F. (2008). The role of calcium, P38 MAPK in dihydroartemisinin-induced apoptosis of lung cancer PC-14 cells. Cancer Chemother. Pharmacol. *61*, 639–645.

Müller, O., Sattler, T., Flötenmeyer, M., Schwarz, H., Plattner, H., and Mayer, a (2000). Autophagic tubes: vacuolar invaginations involved in lateral membrane sorting and inverse vesicle budding. J. Cell Biol. *151*, 519–528.

Nakase, I., Lai, H., Singh, N.P., and Sasaki, T. (2008). Anticancer properties of artemisinin derivatives and their targeted delivery by transferrin conjugation. Int. J. Pharm. *354*, 28–33.

Nakase, I., Gallis, B., Takatani-Nakase, T., Oh, S., Lacoste, E., Singh, N.P., Goodlett, D.R., Tanaka, S., Futaki, S., Lai, H., et al. (2009). Transferrin receptor-dependent cytotoxicity of artemisinin-transferrin conjugates on prostate cancer cells and induction of apoptosis. Cancer Lett. *274*, 290–298.

Neill, P.M.O., and Posner, G.H. (2004). A medicinal chemistry perspective on artemisinin and related endoperoxides. J. Med. Chem. *47*, 2945–2964.

Newman, D.J. (2008). Natural products as leads to potential drugs : an old process or the new hope for drug discovery? J. Med. Chem. *51*, 2589–2599.

Nicholson, D.W. (2000). From bench to clinic with apoptosis-based therapeutic agents. Nature *407*, 810–816.

Novac, N. (2013). Challenges and opportunities of drug repositioning. Trends Pharmacol. Sci. *34*, 267–272.

Ogata, M., Hino, S., Saito, A., Morikawa, K., Kondo, S., Kanemoto, S., Murakami, T., Taniguchi, M., Tanii, I., Yoshinaga, K., et al. (2006). Autophagy is activated for cell survival after endoplasmic reticulum stress. Mol. Cell. Biol. *26*, 9220–9231.

Oh, S., Kim, B.J., Singh, N.P., Lai, H., and Sasaki, T. (2009). Synthesis and anti-cancer activity of covalent conjugates of artemisinin and a transferrin-receptor targeting peptide. Cancer Lett. *274*, 33–39.

Oh, S.-Y., Sohn, Y.-W., Park, J.-W., Park, H.-J., Jeon, H.-M., Kim, T.-K., Lee, J.-S.J.-B., Jung, J.-E., Jin, X., Chung, Y.G., et al. (2007). Selective cell death of oncogenic Akt-transduced brain cancer cells by etoposide through reactive oxygen species mediated damage. Mol. Cancer Ther. *6*, 2178–2187.

Ohsumi, Y. (2001). Molecular dissection of autophagy: two ubiquitin-like systems. Nat. Rev. Mol. Cell Biol. *2*, 211–216.

Olliaro, P.L., Haynes, R.K., Meunier, B., and Yuthavong, Y. (2001). Possible modes of action of the artemisinin-type compounds. TRENDS Parasitol. *17*, 122–126.

Pacella-Norman, R., Urban, M., Sitas, F., Carrara, H., Sur, R., Hale, M., Ruff, P., Patel, M., Newton, R., Bull, D., et al. (2002). Risk factors for oesophageal, lung, oral and laryngeal cancers in black South Africans. Br. J. Cancer *86*, 1751–1756.

Padhy, B.M., and Gupta, Y.K. (2011). Drug repositioning: re-investigating existing drugs for new therapeutic indications. J. Postgrad. Med. *57*, 153–160.

Palmieri, B., and Sblendorio, V. (2006). Oxidative stress detection: what for? Part I. Eur. Rev. Med. Pharmacol. Sci. *10*, 291–317.

Park, K.-J., Lee, S.-H., Lee, C.-H., Jang, J.-Y., Chung, J., Kwon, M.-H., and Kim, Y.-S. (2009). Upregulation of Beclin-1 expression and phosphorylation of Bcl-2 and p53 are involved in the JNK-mediated autophagic cell death. Biochem. Biophys. Res. Commun. *382*, 726–729.

Park, M.-T., Song, M.-J., Lee, H., Oh, E.-T., Choi, B.-H., Jeong, S.-Y., Choi, E.-K., and Park, H.J. (2011). β-lapachone significantly increases the effect of ionizing radiation to cause mitochondrial apoptosis via JNK activation in cancer cells. PLoS One *6*, e25976.

Pelicano, H., Carney, D., and Huang, P. (2004). ROS stress in cancer cells and therapeutic implications. Drug Resist. Updat. *7*, 97–110.

Pennathur, A., Luketich, J.D., Landreneau, R.J., Ward, J., Christie, N. a, Gibson, M.K., Schuchert, M., Cooper, K., Land, S.R., and Belani, C.P. (2008). Long-term results of a phase II trial of neoadjuvant chemotherapy followed by esophagectomy for locally advanced esophageal neoplasm. Ann. Thorac. Surg. *85*, 1930–6; discussion 1936–7.

Podhorecka, M., Skladanowski, A., and Bozko, P. (2010). H2AX phosphorylation: its role in DNA damage response and cancer therapy. J. Nucleic Acids *2011*, 1–9.

Promega (2009). CytoTox-ONE ^{TM} Homogeneous Membrane Integrity Assay.

Proskuryakov, S.Y.., Konoplyannikov, A.G., and Gabai, V.L. (2003). Necrosis: a specific form of programmed cell death? Exp. Cell Res. *283*, 1–16.

Puissant, A., Robert, G., Fenouille, N., Luciano, F., Cassuto, J.-P., Raynaud, S., and Auberger, P. (2010). Resveratrol promotes autophagic cell death in chronic myelogenous leukemia cells via JNK-mediated p62/SQSTM1 expression and AMPK activation. Cancer Res. *70*, 1042–1052.

Qu, X., Yu, J., Bhagat, G., Furuya, N., Hibshoosh, H., Troxel, A., Rosen, J., Eskelinen, E., Mizushima, N., Ohsumi, Y., et al. (2003). Promotion of tumorigenesis by heterozygous disruption of the beclin 1 autophagy gene. J. Clin. Invest. *112*, 1809–1820.

Rajagopalan, S., Politi, P.M., Sinha, B.K., and Myers, C.E. (1988). Adriamycin-induced free radical formation in the perfused rat heart: implications for cardiotoxicity. Cancer Res. *48*, 4766–4769.

Reed, J.C. (2003). Apoptosis-targeted therapies for cancer. Cancer Cell *3*, 17–22.

Rich, T., Allen, R.L., and Wyllie, a H. (2000). Defying death after DNA damage. Nature *407*, 777–783.

Romero, M.R., Efferth, T., Serrano, M. a, Castaño, B., Macias, R.I.R., Briz, O., and Marin, J.J.G. (2005). Effect of artemisinin/artesunate as inhibitors of hepatitis B virus production in an “in vitro” replicative system. Antiviral Res. *68*, 75–83.

Russell, S.E., Hickey, G.I., Lowry, W.S., White, P., and Atkinson, R.J. (1990). Allele loss from chromosome 17 in ovarian cancer. Oncogene *5*, 1581–1583.

Rutkowski, D.T., and Kaufman, R.J. (2004). A trip to the ER: coping with stress. Trends Cell Biol. *14*, 20–28.

Rutkowski, D.T., and Kaufman, R.J. (2007). That which does not kill me makes me stronger: adapting to chronic ER stress. Trends Biochem. Sci. *32*, 469–476.

Sabet, R., Mohammadpour, M., Sadeghi, A., and Fassihi, A. (2010). QSAR study of isatin analogues as in vitro anti-cancer agents. Eur. J. Med. Chem. *45*, 1113–1118.

Sadava, D., Phillips, T., Lin, C., and Kane, S.E. (2002). Transferrin overcomes drug resistance to artemisinin in human small-cell lung carcinoma cells. Cancer Lett. *179*, 151–156.

Saikumar, P., Dong, Z., Mikhailov, V., Denton, M., Weinberg, J.M., and Venkatachalam, M. (1999). Apoptosis: definition, mechanisms, and relevance to disease. Am. J. Med. *107*, 489–506.

Saito, H., Inazawa, J., and Saito, S. (1993). Detailed deletion mapping of chromosome 17q in ovarian and breast cancers: 2-cM region on 17q21 . 3 often and commonly eeleted in tumors. Cancer Res. *53*, 3382–3385.

SAMF (2010). South African Medicines Formulary produced by the Division of Clinical Pharmacology, Faculty of Health Sciences, University of Cape Town, 9th Edition (Cape Town: Health and Medical Publishing Group of the South African Medical Association).

Saxena, A., Yashar, C., Taylor, D.D., and Gercel-Taylor, C. (2005). Cellular response to chemotherapy and radiation in cervical cancer. Am. J. Obstet. Gynecol. *192*, 1399–1403.

Scarpa, M., Valente, S., Alfieri, R., Cagol, M., Diamantis, G., Ancona, E., and Castoro, C. (2011). Systematic review of health-related quality of life after esophagectomy for esophageal cancer. World J. Gastroenterol. *17*, 4660–4674.

Scherz-Shouval, R., and Elazar, Z. (2007). ROS, mitochondria and the regulation of autophagy. Trends Cell Biol. *17*, 422–427.

Scherz-Shouval, R., and Elazar, Z. (2011). Regulation of autophagy by ROS: physiology and pathology. Trends Biochem. Sci. *36*, 30–38.

Schlieve, C.R., Lieven, C.J., and Levin, L. a (2006). Biochemical activity of reactive oxygen species scavengers do not predict retinal ganglion cell survival. Invest. Ophthalmol. Vis. Sci. *47*, 3878–3886.

Schmitt, J.M., Robin, E., Tong, Y., and Hanna, N. (2012). Sunitinib Plus Paclitaxel in Patients with Advanced Esophageal Cancer. *7*, 760–763.

Schoenlein, P. V, Periyasamy-thandavan, S., Samaddar, J.S., Jackson, W.H., and Barrett, J.T. (2009). Autophagy facilitates the progression of ER alpha-positive breast cancer cells to antiestrogen resistance. Autophagy *5*, 400–403.

Seglen, P.O., and Gordon, P.B. (1982). 3-Methyladenine: specific inhibitor of autophagic/lysosomal protein degradation in isolated rat hepatocytes. Proc. Natl. Acad. Sci. U. S. A. *79*, 1889–1892.

Sertel, S., Plinkert, P.K., and Efferth, T. (2010). Novel developments on artemisinin and its derivatives for cancer therapy. In Supportive Cancer Care with Chinese Medicine, pp. 227–251.

Sewram, V., Stefani, E. De, Brennan, P., and Boffetta, P. (2003). Maté consumption and the risk of squamous cell esophageal cancer in Uruguay. Cancer Epidemiol. Biomarkers Prev. *12*, 508–513.

Shao, Y., Gao, Z., Marks, P. a, and Jiang, X. (2004). Apoptotic and autophagic cell death induced by histone deacetylase inhibitors. Proc. Natl. Acad. Sci. U. S. A. *101*, 18030–18035.

Shaw, R.J., Kosmatka, M., Bardeesy, N., Hurley, R.L., Witters, L., DePinho, R., and Cantley, L.C. (2004). The tumor suppressor LKB1 kinase directly activates AMP-activated kinase and

regulates apoptosis in response to energy stress. Proc. Natl. Acad. Sci. U. S. A. *101*, 3329–3335.

Shen, S., Kepp, O., and Kroemer, G. (2012). The end of autophagic cell death? Autophagy *8*, 1–3.

Shi, Y. (2002). Mechanisms of caspase activation and inhibition during apoptosis. Mol. Cell *9*, 459–470.

Shimada, Y., Imamura, M., Wagata, T., Yamaguchi, N., and Tobe, T. (1992). Characterization of 21 newly established esophageal cancer cell lines. Cancer *69*, 277–284.

Shimizu, S., Kanaseki, T., Mizushima, N., Mizuta, T., Arakawa-Kobayashi, S., Thompson, C.B., and Tsujimoto, Y. (2004). Role of Bcl-2 family proteins in a non-apoptotic programmed cell death dependent on autophagy genes. Nat. Cell Biol. *6*, 1221–1228.

Shimizu, S., Konishi, a, Nishida, Y., Mizuta, T., Nishina, H., Yamamoto, a, and Tsujimoto, Y. (2010). Involvement of JNK in the regulation of autophagic cell death. Oncogene *29*, 2070–2082.

Shinojima, N., Yokoyama, T., Kondo, Y., and Kondo, S. (2007). Roles of the Akt/mTOR/p70S6K and ERK1/2 signaling pathways in curcumin-induced autophagy. Autophagy *3*, 635–637.

Shintani, T., and Klionsky, D.J. (2004). Autophagy in health and disease: a double-edged sword. Science *306*, 990–995.

Simard, E.P., Ward, E.M., Siegel, R., and Jemal, A. (2012). Cancers with increasing incidence trends in the United States: 1999 through 2008. CA. Cancer J. Clin.

Singh, N.P., and Lai, H. (2001). Selective toxicity of dihydroartemisinin and holotransferrin toward human breast cancer cells. Life Sci. *70*, 49–56.

Singh, N.P., and Lai, H.C. (2004). Artemisinin induces apoptosis in human cancer cells. Anticancer Res. *24*, 2277–2280.

Singh, R., Xiang, Y., Wang, Y., Baikati, K., Cuervo, A.M., Luu, Y.K., Tang, Y., Pessin, J.E., Schwartz, G.J., and Czaja, M.J. (2009). Autophagy regulates adipose mass and differentiation in mice. J. Clin. Invest. *119*, 3329–3339.

Solomon, V.R., and Lee, H. (2009). Chloroquine and its analogs: a new promise of an old drug for effective and safe cancer therapies. Eur. J. Pharmacol. *625*, 220–233.

Somdyala, N.I.M., Marasas, W.F.O., Venter, F.S., Vismer, H.F., and Africa, S. (2003). Cancer patterns in four districts of the Transkei region. South African Med. J. *93*.

Son, Y.-O., Wang, X., Hitron, J.A., Zhang, Z., Cheng, S., Budhraja, A., Ding, S., Lee, J.-C., and Shi, X. (2011). Cadmium induces autophagy through ROS-dependent activation of the LKB1-AMPK signaling in skin epidermal cells. Toxicol. Appl. Pharmacol. *255*, 287–296.

Spagnuolo, G., D'Antò, V., Cosentino, C., Schmalz, G., Schweikl, H., and Rengo, S. (2006). Effect of N-acetyl-L-cysteine on ROS production and cell death caused by HEMA in human primary gingival fibroblasts. Biomaterials *27*, 1803–1809.

Sridharan, S., Jain, K., and Basu, A. (2011). Regulation of Autophagy by Kinases. Cancers (Basel). *3*, 2630–2654.

Stein, H.J., Feith, M., Bruecher, B.L.D.M., Naehrig, J., Sarbia, M., and Siewert, J.R. (2005). Early Esophageal Cancer. Ann. Surg. *242*, 566–575.

Stoner, G.D., and Gupta, a (2001). Etiology and chemoprevention of esophageal squamous cell carcinoma. Carcinogenesis *22*, 1737–1746.

Stringer, T., Taylor, D., de Kock, C., Guzgay, H., Au, A., An, S.H., Sanchez, B., O'Connor, R., Patel, N., Land, K.M., et al. (2013). Synthesis, characterization, antiparasitic and cytotoxic evaluation of thioureas conjugated to polyamine scaffolds. Eur. J. Med. Chem. *69*, 90–98.

Sunassee, S.N., Veale, C.G.L., Shunmoogam-Gounden, N., Osoniyi, O., Hendricks, D.T., Caira, M.R., de la Mare, J.-A., Edkins, A.L., Pinto, A. V, da Silva Júnior, E.N., et al. (2013). Cytotoxicity of lapachol, β-lapachone and related synthetic 1,4-naphthoquinones against oesophageal cancer cells. Eur. J. Med. Chem. *62*, 98–110.

Syntichaki, P., and Tavernarakis, N. (2002). Death by necrosis. Uncontrollable catastrophe, or is there order behind the chaos? EMBO Rep. *3*, 604–609.

Syrigos, K.N., Zalonis, a, Kotteas, E., and Saif, M.W. (2008). Targeted therapy for oesophageal cancer: an overview. Cancer Metastasis Rev. *27*, 273–288.

Szatrowski, T.P., and Nathan, C.F. (1991). Production of large amounts of hydrogen peroxide by human tumor cells. Cancer Res. *51*, 794–798.

Takahashi, Y., Coppola, D., Matsushita, N., Cualing, H.D., Sun, M., Sato, Y., Liang, C., Jung, J.U., Cheng, J.Q., Mulé, J.J., et al. (2007). Bif-1 interacts with Beclin 1 through UVRAG and regulates autophagy and tumorigenesis. Nat. Cell Biol. *9*, 1142–1151.

Tanaka, Y., Guhde, G., Suter, a, Eskelinen, E.L., Hartmann, D., Lüllmann-Rauch, R., Janssen, P.M., Blanz, J., von Figura, K., and Saftig, P. (2000). Accumulation of autophagic vacuoles and cardiomyopathy in LAMP-2-deficient mice. Nature *406*, 902–906.

Tanemura, M., Saga, a, Kawamoto, K., Machida, T., Deguchi, T., Nishida, T., Sawa, Y., Doki, Y., Mori, M., and Ito, T. (2009). Rapamycin induces autophagy in islets: relevance in islet transplantation. Transplant. Proc. *41*, 334–338.

Tanida, I., Minematsu-Ikeguchi, N., Ueno, T., and Kominami, E. (2005). Lysosomal turnover, but not a cellular level, of endogenous LC3 is a marker for autophagy. Autophagy *1*, 84–91.

Tata, J.R. (1966). Requirement for RNA and protein synthesis for induced regression of the tadpole tail in organ culture. Dev. Biol. *13*, 77–94.

Taylor, W.R., and Stark, G.R. (2001). Regulation of the G2/M transition by p53. Oncogene *20*, 1803–1815.

Tew, W.P., Kelsen, D.P., and Ilson, D.H. (2005). Therapies for esophageal cancer. Oncologist *10*, 590–601.

Thornberry, N.A., Rano, T.A., Peterson, E.P., Rasper, D.M., Timkey, T., Garcia-Calvo, M., Houtzager, V.M., Nordstrom, P.A., Roy, S., Vaillancourt, J.P., et al. (1997). A combinatorial approach defines specificities of members of the caspase family and granzyme B: functional relationships established for key mediators of apoptosis. J. Biol. Chem. *272*, 17907–17911.

Tietze, L.F., Bell, H.P., and Chandrasekhar, S. (2003). Natural product hybrids as new leads for drug discovery. Angew. Chem. Int. Ed. Engl. *42*, 3996–4028.

Tin, A.S., Sundar, S.N., Tran, K.Q., Park, A.H., Poindexter, K.M., and Firestone, G.L. (2012). Antiproliferative effects of artemisinin on human breast cancer cells requires the downregulated expression of the E2F1 transcription factor and loss of E2F1-target cell cycle genes. Anticancer. Drugs *23*, 370–379.

Tobinick, E.L. (2009). Repurposing should be a primary strategy in durg discovery for every broadly, focused, research-based pharmaceutical company. Drug News Perspect. *22*, 119.

Togawa, K., Jaskiewicz, K., Takahashi, H., Meltzer, S.J., and Rustgi, A.K. (1994). Human papillomavirus DNA sequences in esophagus squamous cell carcinoma. Gastroenterology *107*, 128–136.

Tran, K.Q., Tin, A.S., and Firestone, G.L. (2013). Artemisinin triggers a G1 cell cycle arrest of human Ishikawa endometrial cancer cells and inhibits cyclin-dependent kinase-4 promoter activity and expression by disrupting nuclear factor-κB transcriptional signaling. Anticancer. Drugs *25*, 270–281.

Tsang, W.., Chau, S.P.., Kong, S.., Fung, K.., and Kwok, T.. (2003). Reactive oxygen species mediate doxorubicin induced p53-independent apoptosis. Life Sci. *73*, 2047–2058.

Tsujimoto, Y., and Shimizu, S. (2005). Another way to die: autophagic programmed cell death. Cell Death Differ. *12 Suppl 2*, 1528–1534.

Varfolomeev, E.E., Schuchmann, M., Luria, V., Chiannilkulchai, N., Beckmann, J.S., Mett, I.L., Rebrikov, D., Brodianski, V.M., Kemper, O.C., Kollet, O., et al. (1998). Targeted disruption of the mouse Caspase 8 gene ablates cell death induction by the TNF receptors, Fas/Apo1, and DR3 and is lethal prenatally. Immunity *9*, 267–276.

Vaux, D.L., Cory, S., and Adams, J.M. (1988). Bcl-2 gene promotes haemopoietic cell survival and cooperates with c-myc to immortalize pre-B cells. Nature *335*, 440–442.

Veale, R.B., and Thornley, A.L. (1989). Increased single class low-affinity Egf receptors expressed by human esophageal squamous carcinoma cell-lines. S. Afr. J. Sci. *85*, 375–379.

Vercammen, D., Brouckaert, G., Denecker, G., Van de Craen, M., Declercq, W., Fiers, W., and Vandenabeele, P. (1998). Dual signaling of the Fas receptor: initiation of both apoptotic and necrotic cell death pathways. J. Exp. Med. *188*, 919–930.

Verfaillie, T., Salazar, M., Velasco, G., and Agostinis, P. (2009). Linking ER stress to autophagy: potential implications for cancer therapy. Int. J. Cell Biol. *2010*, 1–19.

Villaflor, V.M., Allaix, M.E., Minsky, B., Herbella, F. a, and Patti, M.G. (2012). Multidisciplinary approach for patients with esophageal cancer. World J. Gastroenterol. *18*, 6737–6746.

Vine, K.L., Locke, J.M., Ranson, M., Benkendorff, K., Pyne, S.G., and Bremner, J.B. (2007). In vitro cytotoxicity evaluation of some substituted isatin derivatives. Bioorg. Med. Chem. *15*, 931–938.

Wainberg, Z. a, Lin, L.-S., DiCarlo, B., Dao, K.M., Patel, R., Park, D.J., Wang, H.-J., Elashoff, R., Ryba, N., and Hecht, J.R. (2011). Phase II trial of modified FOLFOX6 and erlotinib in patients with metastatic or advanced adenocarcinoma of the oesophagus and gastro-oesophageal junction. Br. J. Cancer *105*, 760–765.

Walsh, J.J., Coughlan, D., Heneghan, N., Gaynor, C., and Bell, A. (2007). A novel artemisinin-quinine hybrid with potent antimalarial activity. Bioorg. Med. Chem. Lett. *17*, 3599–3602.

Wang, S.-J., Gao, Y., Chen, H., Kong, R., Jiang, H.-C., Pan, S.-H., Xue, D.-B., Bai, X.-W., and Sun, B. (2010). Dihydroartemisinin inactivates NF-kappaB and potentiates the anti-tumor effect of gemcitabine on pancreatic cancer both in vitro and in vivo. Cancer Lett. *293*, 99–108.

Wang, Y., Qiu, Q., Shen, J.-J., Li, D.-D., Jiang, X.-J., Si, S.-Y., Shao, R.-G., and Wang, Z. (2012). Cardiac glycosides induce autophagy in human non-small cell lung cancer cells through regulation of dual signaling pathways. Int. J. Biochem. Cell Biol. *44*, 1813–1824.

Whibley, C.E., Keyzers, R.A., Soper, A.G., Davies-coleman, M.T., Samaai, T., and Hendricks, D.T. (2005). Antiesophageal cancer activity from Southern African marine organisms. Ann. New York Acad. Sci. *1056*, 405–412.

Whibley, C.E., McPhail, K.L., Keyzers, R. a, Maritz, M.F., Leaner, V.D., Birrer, M.J., Davies-Coleman, M.T., and Hendricks, D.T. (2007). Reactive oxygen species mediated apoptosis of esophageal cancer cells induced by marine triprenyl toluquinones and toluhydroquinones. Mol. Cancer Ther. *6*, 2535–2543.

WHO (2013). World Health Statistics 2013, Part III: Global health indications.

Wilkins, B.J., Dai, Y.-S., Bueno, O.F., Parsons, S. a, Xu, J., Plank, D.M., Jones, F., Kimball, T.R., and Molkentin, J.D. (2004). Calcineurin/NFAT coupling participates in pathological, but not physiological, cardiac hypertrophy. Circ. Res. *94*, 110–118.

Willoughby, J. a, Sundar, S.N., Cheung, M., Tin, A.S., Modiano, J., and Firestone, G.L. (2009). Artemisinin blocks prostate cancer growth and cell cycle progression by disrupting

Sp1 interactions with the cyclin-dependent kinase-4 (CDK4) promoter and inhibiting CDK4 gene expression. J. Biol. Chem. *284*, 2203–2213.

Wirawan, E., Vanden Berghe, T., Lippens, S., Agostinis, P., and Vandenabeele, P. (2012). Autophagy: for better or for worse. Cell Res. *22*, 43–61.

Wong, C.H., Iskandar, K.B., Yadav, S.K., Hirpara, J.L., Loh, T., and Pervaiz, S. (2010). Simultaneous induction of non-canonical autophagy and apoptosis in cancer cells by ROS-dependent ERK and JNK activation. PLoS One *5*, 1–12.

Woods, A., Johnstone, S.R., Dickerson, K., Leiper, F.C., Fryer, L.G.D., Neumann, D., Schlattner, U., Wallimann, T., Carlson, M., and Carling, D. (2003). LKB1 is the upstream kinase in the AMP-activated protein kinase cascade. Curr. Biol. *13*, 2004–2008.

Wu, J., Hu, D., Yang, G., Zhou, J., Yang, C., Gao, Y., and Zhu, Z. (2011). Down-regulation of BMI-1 cooperates with artemisinin on growth inhibition of nasopharyngeal carcinoma cells. J. Cell. Biochem. *112*, 1938–1948.

Wu, Y.-T., Tan, H.-L., Shui, G., Bauvy, C., Huang, Q., Wenk, M.R., Ong, C.-N., Codogno, P., and Shen, H.-M. (2010). Dual role of 3-methyladenine in modulation of autophagy via different temporal patterns of inhibition on class I and III phosphoinositide 3-kinase. J. Biol. Chem. *285*, 10850–10861.

Wyk, A.W.W. Van, Gray, C.A., Whibley, C.E., Osoniyi, O., Hendricks, D.T., Caira, M.R., and Davies-coleman, M.T. (2008). Bioactive metabolites from the South African marine mollusk Trimusculus costatus. J. Nat. Prod. *71*, 420–425.

Wyllie, A.H. (1980). Glucocorticoid-induced thymocyte apoptosis is associated with endogenous endonuclease activation. Nature *284*, 555–556.

Xavier, C.P.R., Lima, C.F., Pedro, D.F.N., Wilson, J.M., Kristiansen, K., and Pereira-Wilson, C. (2013). Ursolic acid induces cell death and modulates autophagy through JNK pathway in apoptosis-resistant colorectal cancer cells. J. Nutr. Biochem. *24*, 706–712.

Xie, Z., and Klionsky, D.J. (2007). Autophagosome formation: core machinery and adaptations. Nat. Cell Biol. *9*, 1102–1109.

Xie, C.-M., Chan, W.Y., Yu, S., Zhao, J., and Cheng, C.H.K. (2011). Bufalin induces autophagy-mediated cell death in human colon cancer cells through reactive oxygen species generation and JNK activation. Free Radic. Biol. Med. *51*, 1365–1375.

Xie, Z., Nair, U., and Klionsky, D.J. (2008). Atg8 Controls Phagophore Expansion during Autophagosome Formation. Mol. Biol. Cell *19*, 3290–3298.

Yamada, J., Yoshimura, S., Yamakawa, H., Sawada, M., Nakagawa, M., Hara, S., Kaku, Y., Iwama, T., Naganawa, T., Banno, Y., et al. (2003). Cell permeable ROS scavengers, Tiron and Tempol, rescue PC12 cell death caused by pyrogallol or hypoxia/reoxygenation. Neurosci. Res. *45*, 1–8.

Yang, Z., and Klionsky, D.J. (2010a). Mammalian autophagy: core molecular machinery and signaling regulation. Curr. Opin. Cell Biol. *22*, 124–131.

Yang, Z., and Klionsky, D.J. (2010b). Eaten alive: a history of macroautophagy. Nat. Cell Biol. *12*, 814–822.

Yang, X., Wang, W., Tan, J., Song, D., Li, M., Liu, D., Jing, Y., and Zhao, L. (2009). Synthesis of a series of novel dihydroartemisinin derivatives containing a substituted chalcone with greater cytotoxic effects in leukemia cells. Bioorg. Med. Chem. Lett. *19*, 4385–4388.

Ylä-Anttila, P., Vihinen, H., Jokitalo, E., and Eskelinen, E.-L. (2009). Monitoring autophagy by electron microscopy in mammalian cells. Methods Enzymol. *452*, 143–164.

Yorimitsu, T., and Klionsky, D.J. (2005). Autophagy: molecular machinery for self-eating. Cell Death Differ. *12 Suppl 2*, 1542–1552.

Yu, L., Alva, A., Su, H., Dutt, P., Freundt, E., Welsh, S., Baehrecke, E.H., and Lenardo, M.J. (2004). Regulation of an ATG7-beclin 1 program of autophagic cell death by caspase-8. Science *304*, 1500–1502.

Yuan, J., and Kroemer, G. (2010). Alternative cell death mechanisms in development and beyond. Genes Dev. *24*, 2592–2602.

Yuan, J., Shaham, S., Ledoux, S., Ellis, H.M., and Horvitz, H.R. (1993). The C. elegans cell death gene ced-3 encodes a protein similar to mammalian interleukin-1 beta-converting enzyme. Cell *75*, 641–652.

Yue, Z., Jin, S., Yang, C., Levine, A.J., and Heintz, N. (2003). Beclin 1, an autophagy gene essential for early embryonic development, is a haploinsufficient tumor suppressor. Proc. Natl. Acad. Sci. U. S. A. *100*, 15077–15082.

Zalckvar, E., Berissi, H., Eisenstein, M., and Kimchi, A. (2009). Phosphorylation of Beclin 1 by DAP-kinase promotes autophagy by weakening its interactions with Bcl-2 and Bcl-X L. Autophagy *5*, 720–722.

Zang, R., Li, D., Tang, I., Wang, J., and Yang, S. (2012). Cell-Based Assays in High-Throughput Screening for Drug Discovery. Int. J. Biotechnol. Wellness Ind. 31–51.

Zhang, C., Yang, L., Wang, X., Wang, J., Geng, Y., Yang, C., and Kong, L. (2013). Calyxin Y induces hydrogen peroxide-dependent autophagy and apoptosis via JNK activation in human non-small cell lung cancer NCI-H460 cells. Cancer Lett. *340*, 51–62.

Zhang, D.-W., Shao, J., Lin, J., Zhang, N., Lu, B.-J., Lin, S.-C., Dong, M.-Q., and Han, J. (2009). RIP3, an energy metabolism regulator that switches TNF-induced cell death from apoptosis to necrosis. Science *325*, 332–336.

Zhang, F., Lau, S.S., and Monks, T.J. (2011). The cytoprotective effect of N-acetyl-L-cysteine against ROS-induced cytotoxicity is independent of its ability to enhance glutathione synthesis. Toxicol. Sci. *120*, 87–97.

Zhang, S., Chen, H., and Gerhard, G.S. (2010). Heme synthesis increases artemisinin-induced radical formation and cytotoxicity that can be suppressed by superoxide scavengers. Chem. Biol. Interact. *186*, 30–35.

Zhao, Y., Jiang, W., Li, B., Yao, Q., Dong, J., Cen, Y., Pan, X., Li, J., Zheng, J., Pang, X., et al. (2011). Artesunate enhances radiosensitivity of human non-small cell lung cancer A549 cells via increasing NO production to induce cell cycle arrest at G2/M phase. Int. Immunopharmacol. *11*, 2039–2046.

Zheng, Y., Zhao, Y.-L., Deng, X., Yang, S., Mao, Y., Li, Z., Jiang, P., Zhao, X., and Wei, Y. (2009). Chloroquine inhibits colon cancer cell growth in vitro and tumor growth in vivo via induction of apoptosis. Cancer Invest. *27*, 286–292.

Zhou, H.-J., Wang, W.-Q., Wu, G.-D., Lee, J., and Li, A. (2007). Artesunate inhibits angiogenesis and downregulates vascular endothelial growth factor expression in chronic myeloid leukemia K562 cells. Vascul. Pharmacol. *47*, 131–138.

Zimmermann, K.C., and Green, D.R. (2001). How cells die: Apoptosis pathways. J. Allergy Clin. Immunol. *108*, S99–S103.